Design, synthesis, and evaluation of bioactive molecules; Chiral polyvinylpyrrolidones supported Cu/Au nanoclusters catalyzed cyclization of 5-substituted nona-1,8-dien-5-ols

by

Man Zhang

B.S., Anhui University, 2011

AN ABSTRACT OF A DISSERTATION

submitted in partial fulfillment of the requirements for the degree

DOCTOR OF PHILOSOPHY

Department of Chemistry
College of Arts and Sciences

KANSAS STATE UNIVERSITY
Manhattan, Kansas

2017

Abstract

Small molecules are of great importance in drug discovery currently. The first three chapters discussed the design, synthesis and bio-evaluation of three different classes of small molecules and exploration of their biological targets. Triacsin C analogs were designed as long chain fatty acyl-CoA synthetase (ACSL) inhibitors for attenuating ischemia and reperfusion (I/R) injury. Oxadiazole derivatives were designed as T-type calcium channel inhibitors, which have potential application in the treatment of seizure and epilepsy. Tricyclic pyrone derivatives were reported as anti-Alzheimer lead compounds in previous research done by the Hua group. TP70 and CP2 were synthesized to explore their pharmacokinetics properties.

Chapter 4 described chiral-substituted poly-*N*-vinylpyrrolidones (CSPVP) supported Cu/Au nanoclusters mediation of cyclization reaction of 5-substituted nona-1,8-dien-5-ols. A five-member cyclized lactone possessing a stereogenic tetrasubstituted carbon center was formed in a one-step Cu/Au nanoclusters-hydrogen peroxide oxidation reaction. This developed a novel and simple method to synthesize tetrasubstituted carbon stereogenic center. Drawbacks of the method in my initial study were low reaction yield and moderate enantioselectivity. The chemical yield and enantioselectivity have been significantly improved by introducing bulkier substitution in C3 and C4 positions of CSPVP according to the updates of ongoing research.

Design, synthesis, and evaluation of bioactive molecules; Chiral polyvinylpyrrolidones supported Cu/Au nanoclusters catalyzed cyclization of 5-substituted nona-1,8-dien-5-ols

by

Man Zhang

B.S., Anhui University, 2011

A DISSERTATION

submitted in partial fulfillment of the requirements for the degree

DOCTOR OF PHILOSOPHY

Department of Chemistry
College of Arts and Sciences

KANSAS STATE UNIVERSITY
Manhattan, Kansas

2017

Approved by:

Major Professor
Dr. Duy H. Hua

Copyright

Abstract

Small molecules are of great importance in drug discovery currently. The first three chapters discussed the design, synthesis and bio-evaluation of three different classes of small molecules and exploration of their biological targets. Triacsin C analogs were designed as long chain fatty acyl-CoA synthetase (ACSL) inhibitors for attenuating ischemia and reperfusion (I/R) injury. Oxadiazole derivatives were designed as T-type calcium channel inhibitors, which have potential application in the treatment of seizure and epilepsy. Tricyclic pyrone derivatives were reported as anti-Alzheimer lead compounds in previous research done by the Hua group. TP70 and CP2 were synthesized to explore their pharmacokinetics properties.

Chapter 4 described chiral-substituted poly-*N*-vinylpyrrolidones (CSPVP) supported Cu/Au nanoclusters mediation of cyclization reaction of 5-substituted nona-1,8-dien-5-ols. A five-member cyclized lactone possessing a stereogenic tetrasubstituted carbon center was formed in a one-step Cu/Au nanoclusters-hydrogen peroxide oxidation reaction. This developed a novel and simple method to synthesize tetrasubstituted carbon stereogenic center. Drawbacks of the method in my initial study were low reaction yield and moderate enantioselectivity. The chemical yield and enantioselectivity have been significantly improved by introducing bulkier substitution in C3 and C4 positions of CSPVP according to the updates of ongoing research.

Table of Contents

List of Figures xi
List of Tables xiii
List of Schemes xiv
List of Symbols xv
List of Abbreviations xvi
Acknowledgements xvii
Dedication xix
Chapter 1 - Design, synthesis and bio-evaluation of triacsin C analogs as long chain fatty acyl-CoA synthetase inhibitors attenuating ischemia and reperfusion injury 1
1.1 Background and significance 1
1.1.1 Long chain fatty acyl-CoA synthetase (ACSL) 1
1.1.2 Ischemia and reperfusion (I/R) injury 2
1.1.3 Inhibition of ACSL and I/R injury 2
1.1.4 Triacsin C 3
1.2 Research objectives 4
1.3 Molecular design and synthetic routes 5
1.3.1 Molecular design: Lipinski rules and Veber rules 5
1.3.2 Bioisosteric replacement strategy 5
1.3.3 Synthetic routes 8
1.4 Bio-evaluaion 10
1.4.1 Methods 10
1.4.1.1 The *in vitro* ACSL inhibition 10
1.4.1.2 The *in situ* ACSL inhibition 11
1.4.1.3 Inhibition of leukocyte recruitment 12
1.4.2 Results 13
1.4.2.1 The *in vitro* ACSL inhibitory activity 13
1.4.2.2 The *in situ* ACSL inhibitory activity 14
1.4.2.3 Leukocyte recruitment inhibition 16

1.4.3 Discussion 17
1.4.3.1 Structure-activity relationship of the synthesized triacsin C analogs towards *in vitro* ACSL inhibitory ability 17
1.4.3.2 Concerns 18
1.5 Conclusion 19
1.6 Synthetic experimental procedures 19
1.6.1 General 19
1.6.2 Representative synthesis 20
1.6.2.1 *(2E,4E,7E)-N*-Undeca-2,4,7-trienylhydroxylamine (Compound 1-10). 20
1.6.2.2 *N*-((4-Hydroxycarbonyl)pheynlazo)-*N-(2E,4E,7E)*-(undeca-2,4,7-trienyl) hydroxylamine (Compound 1-6) 20
1.6.2.3 2-((*2E,4E,7E*)-Undeca-2,4,7-trienylamino)-1,1-dioxo-1-isothiazolidine (Compound 1-8) 21
1.6.2.4 2-((*2E,4E,7E*)-Undeca-2,4,7-trienyl)-(1,2,4)oxadiazolidine-3,5-dione (Compound 1-12) 21
1.6.2.5 *N*-((4-Hydroxycarbonyl)phenylazo)-*N*-(nona-*2E,5E*-dienyl) hydroxylamine (Compound 1-7) 22
References 24
Chapter 2 - Design, synthesis and bio-evaluation of 1,3,4-oxadiazole derivatives as T-type calcium channel inhibitors 28
2.1 Background and significance 28
2.1.1 T-type calcium channel 28
2.1.2 Epilepsy and T-type calcium currents influx 29
2.2 Research objectives 30
2.3 Molecular design and synthetic routes 30
2.3.1 Reported T-type calcium channel blockers 30
2.3.2 Oxadiazoles derivatives as T-type Ca^{2+} channel inhibitors 31
2.3.3 Molecular design 32
2.3.4 Synthetic routes 34
2.4 Bio-evaluation 38
2.4.1 Methods 38

2.4.1.1 Patch clamp recordings 38
2.4.1.2 Seizure models 39
2.4.2 Results and discussion 40
2.4.2.1 Inhibition of T-type calcium channel and seizure 40
2.4.2.2 Structure-activity relationship towards inhibition of T-type calcium channel 43
2.4.2.3 Lead compound CI-6 versus reported T-type calcium channel inhibitor Z944 44
2.4.2.4 Concerns 45
2.5 Conclusion 46
2.6 Synthetic experimental procedures 46
2.6.1 General 46
2.6.2 Representative synthesis 46
2.6.2.1 *N*-(Carbamothioylamino)-5-chlorothiophene-2-carboxamide (Compound 2-2) 46
2.6.2.2 1-Benzoyl-3-thiosemicarbazide (Compound 2-3) 47
2.6.2.3 5-(5-Chlorothiophen-2-yl)-1,3,4-oxadiazol-2-amine (Compound 2-4) 48
2.6.2.4 5-Phenyl-1,3,4-oxadiazol-2-amine (Compound 2-5) 48
2.6.2.5 5,6-Dichloro-2-(5-(5-chlorothiophen-2-yl)-1,3,4-oxadiazol-2-yl)isoindoline-1,3-dione (Compound CI-1) 48
2.6.2.6 3-(3-Chlorophenyl)-*N*-(5-(5-chlorothiophen-2-yl)-1,3,4-oxadiazol-2-yl)propanamide (Compound CI-2) 49
2.6.2.7 *N*-(5-(5-Chlorothiophen-2-yl)-1,3,4-oxadiazol-2-yl)benzamide (Compound CI-3) 50
2.6.2.8 2-(4-Cyanopiperidin-1-yl)-*N*-phenylacetamide (Compound 2-6-3) 51
2.6.2.9 1-((Phenylcarbamoyl)methyl)-*N*-(5-(5-chlorothiophen-2-yl)-1,3,4-oxadiazol-2-yl)piperidine-4-carboxamide (Compound CI-4) 51
2.6.2.10 5-Chloro-*N*-(5-phenyl-1,3,4-oxadiazol-2-yl)thiophene-2-carboxamide (Compound CI-6) 52
Reference 54
Chapter 3 - Synthesis and bioevaluation of tricyclic pyrone derivatives for the treatment of Alzheimer's disease (AD) 60
3.1 Background and significance 60
3.1.1 Alzheimer's disease (AD) 60

3.1.2 Previous studies on tricyclic pyrone compounds as anti-Alzheimer's disease drugs .. 61
3.2 Research objectives 61
3.3 Syntheses of tricyclic pyrone compounds 62
3.3.1 Synthetic routes 63
3.3.2 Purification of CP2 65
3.3.2.1 Column chromatography 65
3.3.2.2 Crystallization and recrystallization 66
3.3.2.3 Purity determination by HPLC analysis 67
3.4 Bioevaluation and discussion 69
3.4.1 Methods 70
3.4.1.1 Studies on *in vitro* neuronal protective properties 70
3.4.1.2 Studies on pharmacokinetics properties 71
3.4.2 Results and discussion 71
3.4.2.1 Studies on *in vitro* neuronal protecitve properties 71
3.4.2.2 Studies on pharmacokinetics properties 73
3.5 Conclusion 75
Reference 76
Chapter 4 - Chiral-substituted polyvinylpyrrolidones (CSPVP) supported Cu/Au nanoclusters and catalytic cyclization of 5-substituted nona-1,8-dien-5-ols 79
4.1 Background and significance 79
4.2 Research objectives 80
4.3. Syntheses and characterizations of chiral-substituted polyvinylpyrrolidones (CSPVP) for stabilization of Cu/Au nanoclusters in catalytic asymmetric oxidation reactions 80
4.3.1 Syntheses of different C-5 chiral-substituted PVP precursors. 80
4.3.2 Synthesis of chiral-substituted polyvinylpyrrolidones (CSPVP) 83
4.4 CSPVP supported Cu/Au nanoclusters catalyzed cyclization reaction of diene 86
4.4.1 Syntheses of different 5-substituted nona-1,8-dien-5-ols 86
4.4.2 Cyclization experimental procedure 86
4.5 Discussion 88
4.5.1 Results, discussion and product characterization. 88
4.5.2 Concerns 90

4.5.3 Future work 90
4.6 Conclusion 92
4.7 Synthetic experimental procedures 92
4.7.1 General 92
4.7.2 Representative synthesis 93
4.7.2.1 *(S)-tert*-Butyl 3-*tert*-butoxy-1-(2,2-dimethyl-4,6-dioxo-1,3-dioxan-5-yl)-1-oxopropan-2-ylcarbamate (Compound 4-11) 93
4.7.2.2 *(R)-tert*-Butyl 3-*tert*-butoxy-1-(2,2-dimethyl-4,6-dioxo-1,3-dioxan-5-yl)propan-2-ylcarbamate (Compound 4-15) 93
4.7.2.3 *(R)-N*-(*tert*-Butoxycarbonyl)-5-(*tert*-butoxymethyl)-pyrrolidin-2-one (Compound 4-1) 94
4.7.2.4 *(R)-tert*-Butyl 2-isopropyl-5-oxopyrrolidine-1-carboxylate (Compound 4-2) 95
4.7.2.5 *(R)-tert*-Butyl 2-*tert*-butyl-5-oxopyrrolidine-1-carboxylate (Compound 4-3) 95
4.7.2.6 *(R)-tert*-Butyl 2-((naphthalen-1-yl)methyl)-5-oxopyrrolidine-1-carboxylate (Compound 4-5) 95
4.7.2.7 *(5R)-tert*-Butyl 5-isopropyl-2-oxo-3-(phenylselanyl)pyrrolidine-1-carboxylate (Compound 4-19) 96
4.7.2.8 *(S)-tert*-Butyl 2-isopropyl-5-oxo-2H-pyrrole-1(5H)-carboxylate (Compound 4-4) 96
4.7.2.9 5-Methylnona-1,8-dien-5-ol (Compound 4-S1) 97
4.7.2.10 5-Phenylnona-1,8-dien-5-ol (Compound 4-S2) 98
4.7.2.11 5-(But-3-enyl)-dihydro-5-methylfuran-2(3H)-one (Compound 4-L) 98
Reference 99

List of Figures

Figure 1.1. Long chain fatty acyl-CoA synthetase (ACSL) catalyzed formation of fatty acyl CoA. 1
Figure 1.2. General procedure for protein palmitoylation. 2
Figure 1.3. Relationship between inhibition of ACSL and I/R injury. 3
Figure 1.4. Chemical structures of triacsin C and palmitic acid. 5
Figure 1.5. Chemical structures of designed triacsin C analogs. 6
Figure 1.6. General procedure for *in vitro* ACSL inhibition test. 11
Figure 1.7. General procedure for *in situ* ACSL inhibition test 12
Figure 1.8. Concentration effect curves of the inhibition of ACSL activity in solubilized brain endothelial bEND3 cells for each of the analogs, as compared to triacsin C 14
Figure 1.9. The *in situ* inhibition of ACSL by triacsin C and analogs in bEND3 brain cells, as evaluated by the incorporation of [^{14}C]-palmitic acid into extractable lipid (A), aqueous (B), media (C), and recovery (D) 15
Figure 1.10. The L-NAME induced leukocyte recruitment at 120 minutes in the presence of compounds 1-1 and 1-9. 16
Figure 2.1. T-type calcium channels (cartoon presentation) are multi-subunits protein complexes. 29
Figure 2.2. Reported T-type calcium channel blockers 31
Figure 2.3. Chemical structures of compound CID3373841 and compound CID46943243. 32
Figure 2.4. Designed substituted 1,3,4-oxadiazole compounds as T-type calcium channel inhibitors. 33
Figure 2.5. Chemical structures of Z944 and compound CI-6. 44
Figure 2.6. CI-6 blocked the native T-type calcium currents recorded on DRG neurons in dose dependently manner (A). CI-6 slightly inhibited sodium (B) and potassium (C) mediated currents recorded on DRG. The effect was not dose dependently, suggesting the unspecific inhibition. (D) Z944 blocked the voltage dependent sodium currents. Each point represents the averaged data of 3-7 cells 45
Figure 3.1. Chemical structure of (+)-pyripyropene A. 61
Figure 3.2. Chemical structures of tricyclic pyrone compounds 62

Figure 3.3. UV absorption spectrum of CP2 68
Figure 3.4. Purity of obtained CP2 after recrystallization was determined by HPLC 69
Figure 3.5. General procedure for *in vitro* neuronal protective properties test 70
Figure 3.6. The neuroprotective effects of TP70 72
Figure 3.7. Some pharmacokinetics (PK) properties of TP70 74
Figure 4.1. CSPVP supported Cu/Au catalyzed cyclization of 5-substituted nona-1,8-dien-5-ols. 79
Figure 4.2. Chemical structures of various C-5 chiral-substituted PVP precursors. 81
Figure 4.3. Chemical structures of chiral-substuted PVP 4-24, 4-25 and 4-26. 85
Figure 4.4. Chemical structures of synthesized and proposed 5-substituted nona-1,8-dien-5-ols. 86
Figure 4.5. ^{1}H-^{1}H COSY spectrum of compound 4-L. 89
Figure 4.6. Optical purity of obtained compound 4-L was determined by HPLC 90
Figure 4.7. Chem-3D calculated C(4)-C(5)-O(11) and C(6)-C(5)-O(11) bond-angle values on minimized energy models of compounds 4-S1 and 4-S2. 92

List of Tables

Table 1.1. Molecular weights and log P values of designed triacsin C analogs. 8
Table 1.2. ACSL inhibition in solubilized brain endothelial bEND3 cells. 14
Table 1.3. Structure-activity relationship of triacsin C analogs towards ACSL inhibitory ability (*in vitro*). 18
Table 2.1. Molecular weights and log P values of designed 1,3,4-oxadiazole derivatives. 34
Table 2.2. *in vitro* and *in vivo* Bioactivities of synthesized 1,3,4-oxadiazole derivatives. 42
Table 2.3. Compounds CI-6 and CI-7 showed selective T-type calcium channel inhibition. 42
Table 2.4. Inhibition results of seizure induced death in mice models for compounds CI-2 and CI-6 43
Table 2.5. Structure-activity relationship (SAR) summary towards inhibition of T-type calcium channel. 44
Table 3.1. FDA approved drugs for the treatment of Alzheimer's disease. 60
Table 3.2. A gradient mixture of water (solvent A) and methanol (solvent B) was used as HPLC eluent. 68
Table 3.3. Analysis for CP2 HPLC data. 69
Table 3.4. Results for *in vitro* neuronal protective efficacy of screened tricyclic pyrone compounds. 71
Table 4.1. Reaction conditions of CSPVP-Cu/Au nanoclusters catalyzed cyclization of 5-methylnona-1,8-dien-5-ol (compound 4-S1). 88

List of Schemes

Scheme 1.1. Last two steps of the reported total synthesis of triacsin C. 4
Scheme 1.2. Synthesis of compound 1-13. 8
Scheme 1.3. Syntheses of compounds 1-2 and 1-8. 9
Scheme 1.4. Syntheses of compounds 1-6, 1-10 and 1-12. 9
Scheme 1.5. Synthesis of compound 1-7. 10
Scheme 2.1. Syntheses of compounds 2-4 and 2-5. 35
Scheme 2.2. Possible mechanism of formation of 1,3,4-oxadiazole ring. 36
Scheme 2.3. Syntheses of compounds CI-1, CI-2, CI-3 and CI-4. 37
Scheme 2.4. Synthesis of compound 2-6. 37
Scheme 2.5. Synthesis of compound CI-6. 38
Scheme 3.1. Synthesis of isopropenyl-substituted tricyclic pyrone intermediate (compound 3-3). 63
Scheme 3.2. Possible explanation of the stereoselectivity in the synthesis of compound 3-3. 64
Scheme 3.3. Syntheses of compounds TP70 and TP82. 64
Scheme 3.4. Synthesis of compound CP2. 65
Scheme 4.1. Syntheses of compounds 4-1, 4-2, 4-3 and 4-5. 82
Scheme 4.2. Possible mechanism for the cyclization of pyrrolidone ring. 82
Scheme 4.3. Synthesis of compound 4-4. 83
Scheme 4.4. Synthesis of C5-benzhydrol substituted chiral PVP polymer. 84
Scheme 4.5. Syntheses of substrates 4-S1 and 4-S2. 86

List of Symbols

EC_{50}	half maximal effective concentration
ED_{50}	half maximal effective dose
IC_{50}	half maximal inhibitory concentration
TD_{50}	median toxic dose
δ	data, chemical shift
ee	enantiomeric excess
$t_{1/2}$	half time

List of Abbreviations

ACSL	long chain fatty acyl-CoA synthetase
AD	Alzheimer's disease
AIBN	azobisisobutyronitrile
Aβ	Amyloid β-peptides
AβO	β-amyloid oligomer
COSY	NMR correlation spectroscopy
CSPVP	chiral-substituted polyvinylpyrrolidone
DBDMH	1,3-dibromo-5,5-dimethylhydantoin
DCC	*N*,*N*′-dicyclohexylcarbodiimide
DI water	deionized water
DMA	*N*,*N*-dimethyl acetamide
DMAP	4-(dimethylamino)pyridine
DMF	*N*,*N*-dimethyl formamide
DRG	dorsal root ganglion
EDC	*N*-(3-dimethylaminopropyl)-*N*′-ethylcarbodiimide hydrochloride
HPLC	high performance liquid chromatography
I/R	ischemia and reperfusion
LDA	lithium diisopropylamide
MES	maximal electroshock seizure
MS	mass spectrometry
NMR	nuclear magnetic resonance
PTZ	pentylenetetrazole
PVP	polyvinylpyrrolidone
ROS	reactive oxidative species
TC	tetracycline
THF	tetrahydrofuran
TI	therapeutic index
TLC	thin-layer chromatography

Acknowledgements

First of all, many thanks go to my advisor Dr. Duy H. Hua and his beautiful wife Mrs. Sadami Hua. It is really my honor to have a chance to work in the Hua group. From here, I got systematic training of how to be a qualified synthetic chemist. Dr. Hua is the one who told me not to work as a robot, but to think more about what to do and why to do so. Except all of the synthetic techniques, he also taught me the importance to be a reliable and responsible person. Thanks to him, I could have the chances to conduct several projects related with drug discovery and in which I found my enthusiasm and decided to pursue drug discovery as my future career. Mrs. Sadami Hua is a super-nice lady who always cares about the group members and shares delicious home-made cookies with us.

Then, I would like to thank all my committee members, Dr. Stefan H. Bossmann, Dr. Ping Li and Dr. Yunjeong Kim for their generous suggestions, helps and dedications during my Ph. D. study. Really appreciate it.

Thank collaborators in the Hua group, Dr. Allan M. Prior, Dr. Sahani Weerasekara, Ms. Medha J. Gunaratna and Mr. Bo Hao for their excellent teamwork in different projects. Thank Dr. Gaochao Huang in Dr. Li's laboratory at the Chemistry Department, K-State for the help in HPLC analysis of compound CP2. Thank collaborators outside the department, the Weis group from Texas Tech University, the Xie group from AfaSci Research Laboratory, the Jin group from UC Davis for their dedication in the bio-evaluation work.

Thank K-State Chemistry Department for all of the technique support. Thank the department faculties and staff, Mr. Jim Hodgson, Dr. Leila Maurmann, Mr. Ron Jackson, Mr. Tobe Eggers, Dr. Tingting Liu, Ms. Mary Dooley and Ms. Kimberly Ross and others for their kind help in my five years.

Thank my current and previous lab mates, Dr. Jianyu Lu, Dr. Allan M. Prior, Dr. Sahani Weerasekara, Dr. Thi D. T. Nguyen, Dr. Laxman Pokhrel, Ms. Medha J. Gunaratna, Mr. Bo Hao, Mr. Serkan Koldas and others for their friendship and support.

Dedication

My beloved parents: Mr. Guicheng Zhang and Mrs. Guangjun Zhou. They are the ones who always stand by my side and encourage me all the time during my Ph.D. study.

Thank all my friends in and outside the United States for their companion and friendship in my five years abroad study.

Chapter 1 - Design, synthesis and bio-evaluation of triacsin C analogs as long chain fatty acyl-CoA synthetase inhibitors attenuating ischemia and reperfusion injury

1.1 Background and significance

1.1.1 Long chain fatty acyl-CoA synthetase (ACSL)

Long chain fatty acyl-CoA (ACSL) is an enzyme which can catalyze formation of fatty acyl CoA in a two-step process (as shown in Figure 1.1) through a fatty acyl adenyl intermediate.[1] ACSL families are of great importance in the fatty acid metabolism. Palmitoyl-CoA is formed when ACSL catalyzing acylation of palmitic acid and the formed palmitoyl-CoA is an important intermediate in the palmitoylation of protein.[2] During protein palmitoylation (see Figure 1.2), in the presence of palmitoyl-CoA and palmitoyl acyltransferase (PAT), cysteine thiol groups on a substrate protein (usually membrane proteins) are converted to palmitoyl thioesters, which contribute to increased hydrophobicity of the protein.[3]

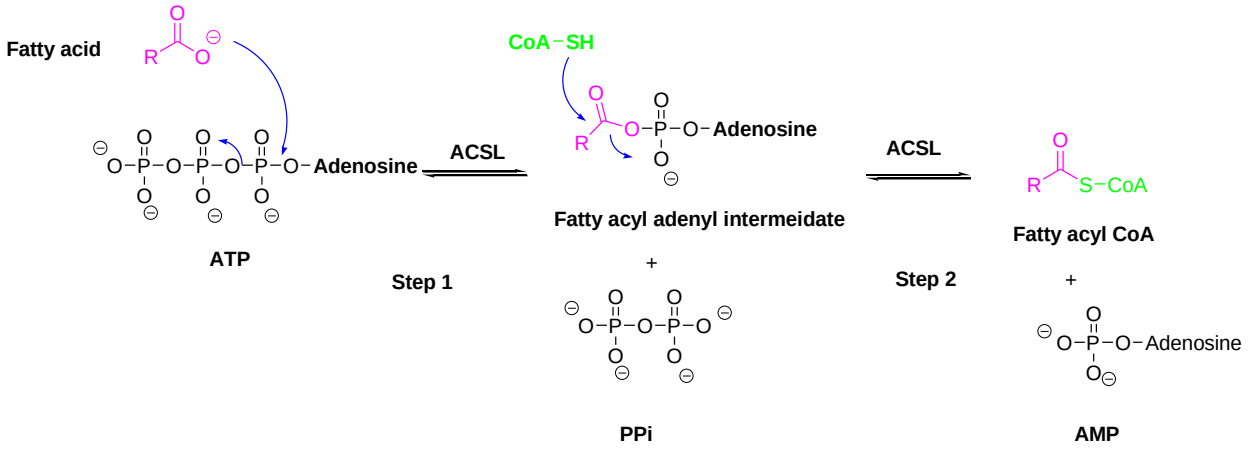

Figure 1.1. Long chain fatty acyl-CoA synthetase (ACSL) catalyzed formation of fatty acyl CoA.

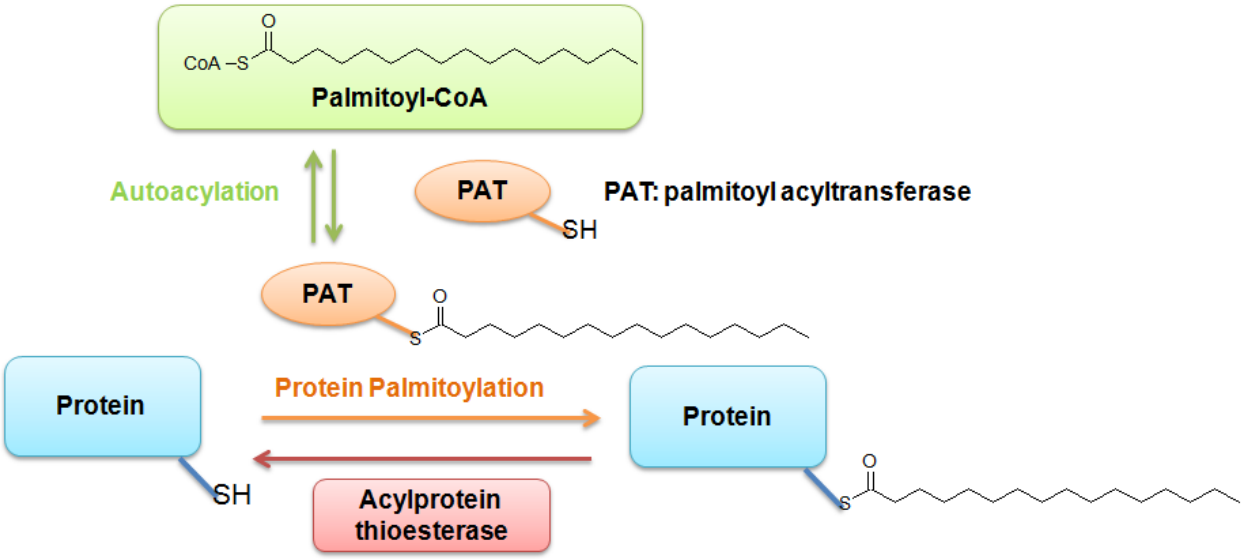

Figure 1.2. General procedure for protein palmitoylation.

1.1.2 Ischemia and reperfusion (I/R) injury

Ischemia is the cutoff of blood supply to a tissue or certain organs from blood vessels. It often leads to the formation of stroke, infarction and other thrombotic events.[3] Prolonged ischemia will lead to cell death.[3] One way to decrease the injury of ischemia is to restore blood to the thrombosis tissue. However, studies have shown that instead of attenuating the injury, usually a higher extent of injury occurs.[4,5] It is believed that ischemia leads to accumulation of aerobic metabolites, which undergo rapid reactions in the presence of reperfused oxygen.[6-8] The injury caused by the reperfusion of blood to ischemia tissue is called ischemia and reperfusion (I/R) injury and it's often featured with cascade of intracellular events, such as reduced nitric oxide level and leukocyte recruitment.[9] Among various intracellular events, the translocation of cell adhesion molecules induced inflammatory response greatly attribute to the I/R injury.[10,11] Thus, inhibiting the inflammation response is found to be a novel strategy towards inhibition of I/R injury.

1.1.3 Inhibition of ACSL and I/R injury

As reported, leukocyte recruitment is the key feature of inflammation responses and it starts with the translocation of cell adhesion molecules.[12] Palmitoylation of membrane proteins (see Figure 1.2 for protein palmitoylation) results in increased hydrophobicity of proteins and activates cell

adhesion molecules by transferring them from blood plasma to endothelia membrane.[2] The presence of palmitoyl-CoA is necessary in protein palmitoylation, thus inhibition of the formation of palmitoyl-CoA will lead to the inhibition of protein palmitoylation, which eventually leads to attenuation of I/R injury as shown in Figure 1.3.

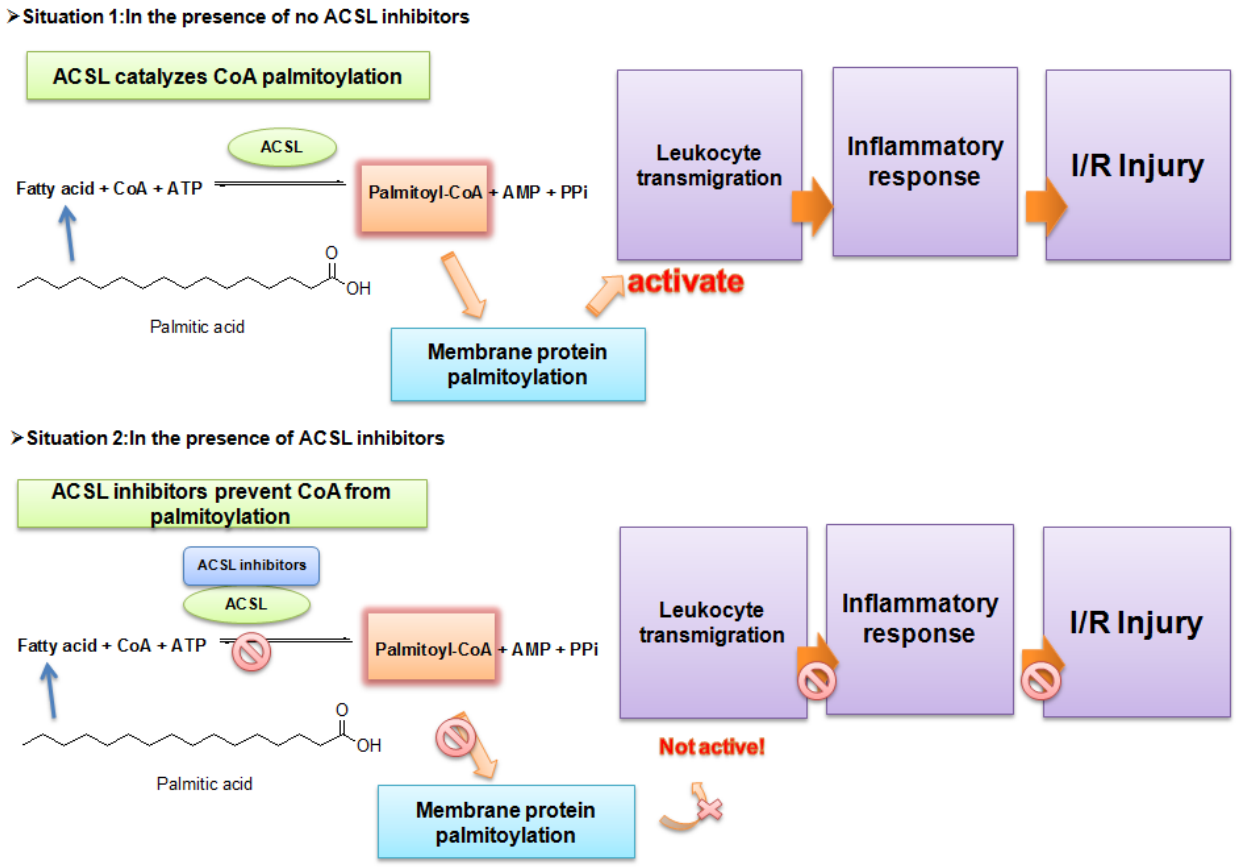

Figure 1.3. Relationship between inhibition of ACSL and I/R injury.

1.1.4 Triacsin C

Triacsin C is a known potent ACSL inhibitor.[13,14] According to previous study done in Hua group[15], its analogs have both ACSL inhibition ability and good anti-rotavirus activity. Studies reported by Blakeman et. al.[16,17] found that triacsin C improved cardiac function after ischemia in rat model, which supported the hypothesis that suppressing ACSL function could reduce I/R injury.

The total synthesis of triacsin C has been reported by Tanaka et al.[18] in 1982, and until now it is the only reported total synthesis method with extremely low yield (0.6%) in the last step (Scheme 1.1). With such a low yield, it is not affordable to prepare tracsin C for further bio-evaluation utilizing this reported total synthesis The hydroxyl triazene is a reactive moiety which makes it difficult to explore synthetic approach. In addition, the unstable hydroxyl triazene structural moiety implies that triacsin C has poor drug like properties. The development of new triacsin C analogs with better drug-like properties and more straight-forward synthetic method is needed.

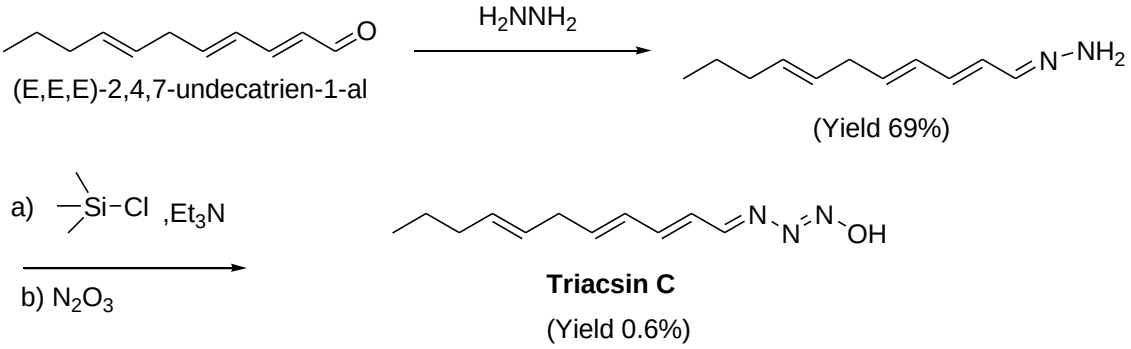

Scheme 1.1. Last two steps of the reported total synthesis of triacsin C (Tanaka et al. 1982[18]).

1.2 Research objectives

Research objective 1: Discover more straight forward approach towards the synthesis of a small library of triacsin C analogs.

Research objective 2: Screen designed small molecules for their ACSL inhibitory activity and study the structure-activity relationship (SAR). (This biological study was performed in our collaborator, Dr. Weis group)

Research objective 3: Study the inhibition of leukocyte recruitment of hit ACSL inhibitors and evaluate the feasibility of using ACSL inhibitor to reduce ischemia and reperfusion injury. (This biological study was performed in our collaborator, Dr. Young group)

1.3 Molecular design and synthetic routes

1.3.1 Molecular design: Lipinski rules and Veber rules

Drug design can not only be focused on the optimization of pharmacodynamics properties, the molecular properties are also of great importance, or with the hit molecules may be very potent but with poor drug-like properties and cannot pass through all the clinical trials. Veber rules and Lipinski rules are summarized based on the discovered drug candidates and are directions to follow to get molecules with good drug-like properties. According to Lipinski rules[19], it is likely that designed molecules (except biological transporters) will have poor absorption or permeation if they possess any of the properties: molecule has more than 5 H-bond donors or more than 10 H-bond acceptor; molecular weight above 500 or log P value above 5. Veber et al.[20] studied the relationship between molecular structures and oral bioavailability in rats. Molecules are likely to have good bioavailability in rats if they have less than 10 rotatable bonds, less than 140 $Å^2$ polar surface area or less than twelve total H-bonds. Generally, Veber rules and Lipinski rules are following as basic guide lines when conducting molecular designs.

1.3.2 Bioisosteric replacement strategy

Bioisosteres were defined as "*groups or molecules which have chemical and physical similarities producing broadly similar biological effects*" by Thornber in 1979[21]. Bioisosteric replacement has effect on changing different molecular properties, such as size, polarity, reactivity, and others, thus lead to improvements towards selectivity, solubility, stability, safety profile and straight forward synthetic approach[22]. Bioisosteric replacement is a useful strategy in the discovery of lead compounds.

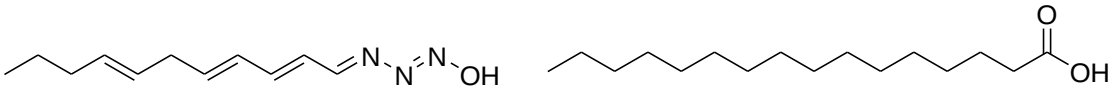

Triacsin C **Palmitic acid**

Figure 1.4. Chemical structures of triacsin C and palmitic acid.

Triacsin (as shown in Figure 1.4) is a known nonspecific long chain fatty acyl CoA synthetase (ACSL) inhibitor.[16,23] Bioisosteric replacement is a replacement of a bioactive group to a

different functional group and this strategy was applied in the design of triacsin C analogs in order to obtain hit molecules with increased stability.

Triacsin C was found to be acting like a substrate binding site blocker when inhibiting ACSL[13]. The availability of palmitoyl-CoA is need for protein to go through palmitoylation.[2] Tracsin C can act as a substrate competitor against palmitic acid and prevent the formation of palmitoyl-CoA. Both triacsin C and palmitic acid have long aliphatic tails and hydrophilic head groups. In the structural analysis of triacsin C, the hydroxyl triazene is mimicking the acid head in palmitic acid, and long C-H chain with conjugated diene moiety is mimicking the long aliphatic chain in palmitic acid. However, it is not clear whether hydrophilic head group or long chain tail that makes triacsin C a potent inhibitor. The general approach for designing triacsin C analogs are changing the unstable hydroxyl triazene head group to other bioactive groups and changing the length and number of double bond of the long alkyl chain.

A small library of triacsin C analogs was designed as shown in Figure 1.5 based on these criteria.

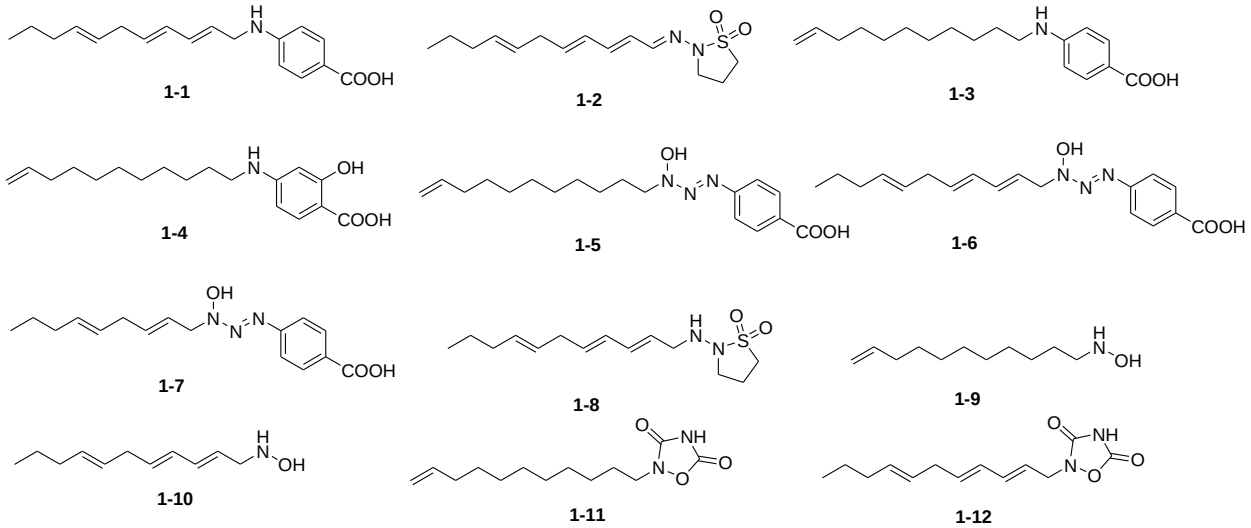

Figure 1.5. Chemical structures of designed triacsin C analogs.

Predicted log P values of the designed small molecules were calculated using interactive log P calculator (© Molinspiration Cheminformatics 2017)[24], which is available online. The calculated results were shown in Table 1.1. Most of the designed molecules have the predicted log P values

less than five, which follows Lipinski rules. Some of the molecules (compounds **1-3**, **1-4** and **1-5**) have predicted log P values as high as 6, meaning that they were supposed to be more hydrophilic and may cause some cell penetration and absorption problems later. Structural optimizations towards increasing hydrophobicity will be performed in the future to solve the problem to optimize the pharmacokinetics (PK) properties.

Compound	Chemical Structure	Molecular Weight	log P value
1-1	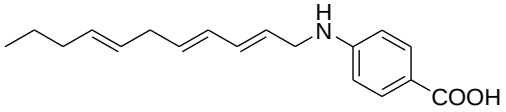	285.39	5.21
1-2	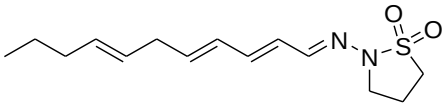	282.41	3.19
1-3	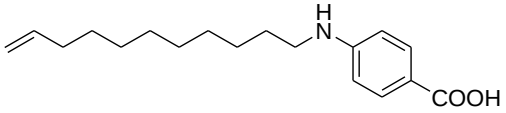	289.42	6.16
1-4	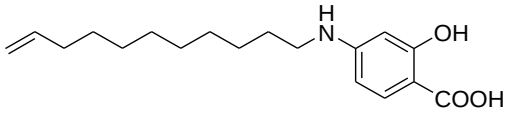	305.42	6.16
1-5	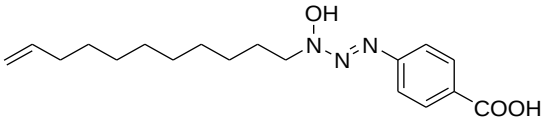	333.436	6.21
1-6	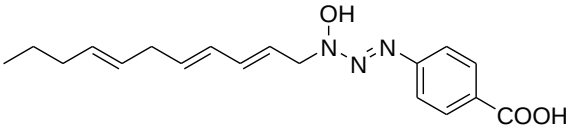	329.40	5.26
1-7	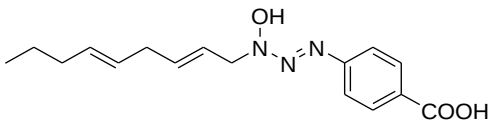	303.36	4.74
1-8	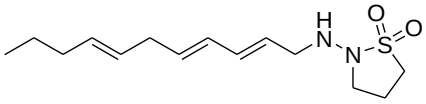	284.43	3.11
1-9	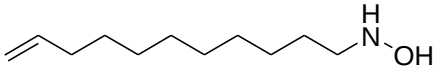	185.31	4.24
1-10	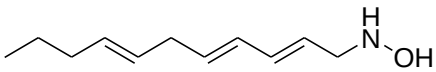	181.28	3.28

1-11	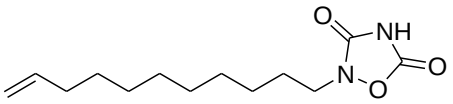	254.33	3.31
1-12	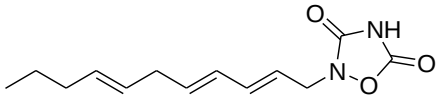	250.30	2.35
Triacsin C	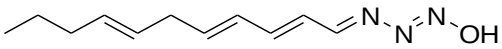	207.28	3.21
Palmitic acid	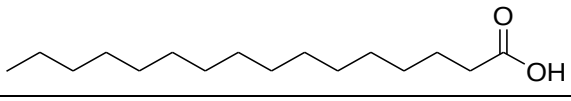	256.43	7.06

Table 1.1. Molecular weights and log P values of designed triacsin C analogs.

1.3.3 Synthetic routes

The synthetic work was collaborated with Dr. Allan M. Prior in Hua group and I carried out the syntheses of compounds **1-2**, **1-6**, **1-7**, **1-8**, **1-10** and **1-12**. The synthetic routes were shown as follows (Scheme 1.2 - Scheme 1.5). Compound *(E,E,E)*-2,4,7-undecatrien-1-al (**1-13**) was allowed to react with various nucleophiles to give designed molecules. The synthesis of aldehyde **1-13** was followed by the reported procedure[15,18] and shown in Scheme 1.2. Commercial available *trans*-2-hexen-1-ol (**1-13-1**) was brominated and displaced to give THP protected compound **1-13-2**, which further deprotected with oxalic acid and underwent a series of reduction, oxidation and carbon extension reactions to give aldehyde **1-13**.

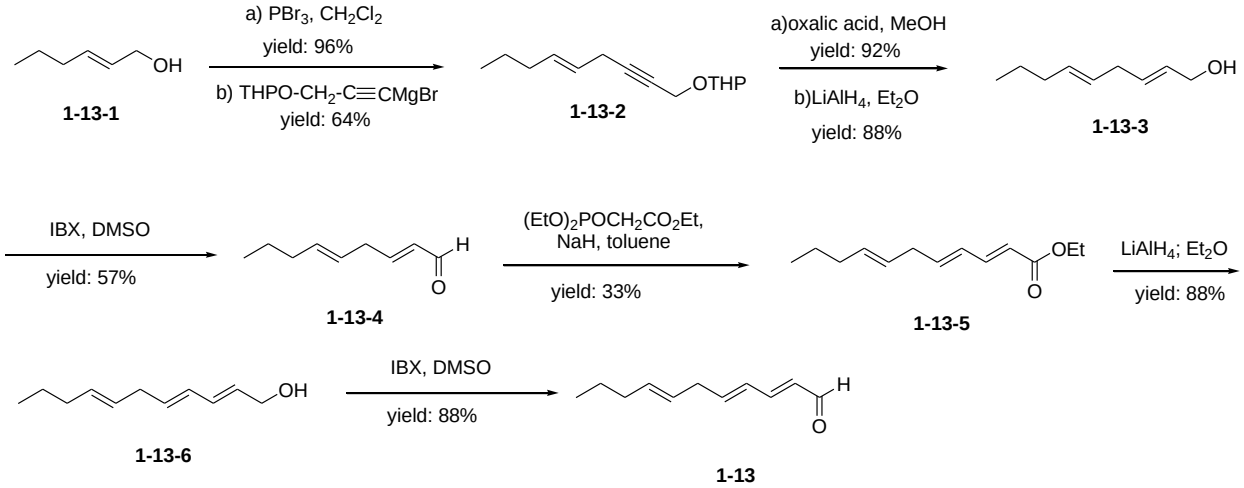

Scheme 1.2. Synthesis of compound 1-13.

Syntheses of compounds **1-2** and **1-8** were shown in Scheme 1.3. The intermediate aldehyde **1-13** went through reductive amination and cyclization to give compound **1-2**. Compound **1-2** was further reduced by $NaCNBH_3$ to give compound **1-8**.

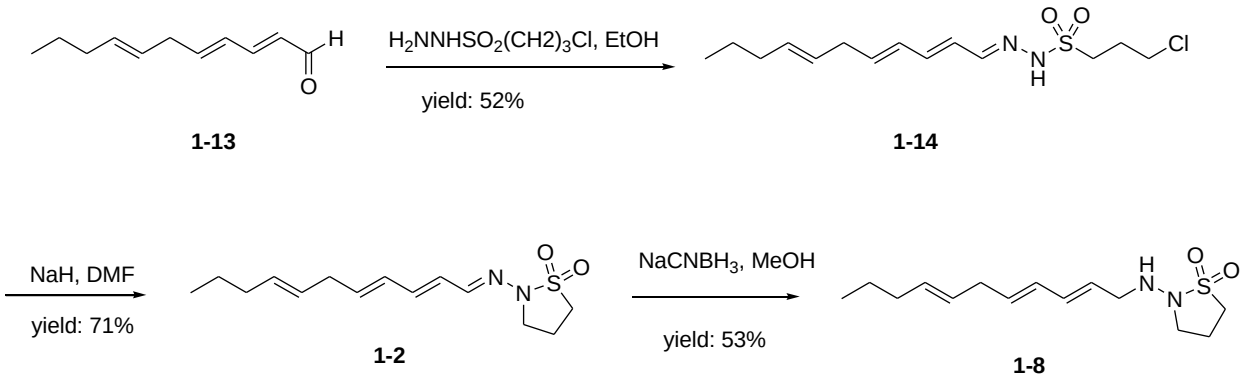

Scheme 1.3. Syntheses of compounds 1-2 and 1-8.

Synthesis of compounds **1-6**, **1-10** and **1-12** were shown in Scheme 1.4. The intermediate aldehyde **1-13** underwent reductive amination with hydroxylamine and the formed imine was further reduced by $NaCNBH_3$ to give compound **1-10**. The hydroxyl group in compound **1-10** was displaced by isocyanate followed by cyclization under basic conditions to give compound **1-12**. Hydroxyl amine **1-10** was treated with *p*-diazonium benzoic acid to give compound **1-6**.

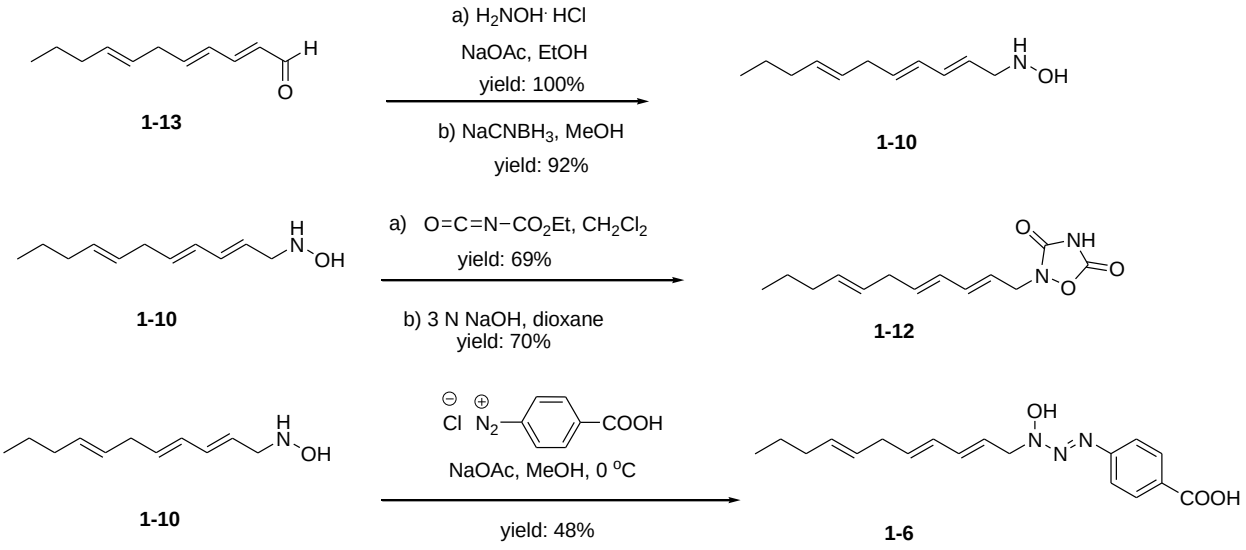

Scheme 1.4. Syntheses of compounds 1-6, 1-10 and 1-12.

Similar to the synthesis of compound **1-6**, compound **1-7** was obtained from a different aldehyde (compound **1-13-4)** as shown in Scheme 1.5.

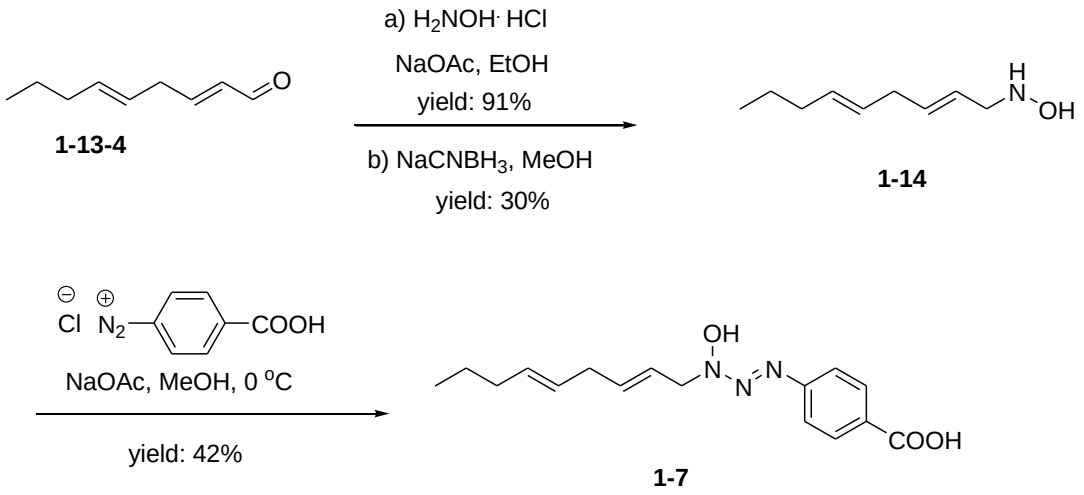

Scheme 1.5. Synthesis of compound 1-7.

1.4 Bio-evaluaion

Bio-evaluations were done by our collaborators. The *in vitro* and *in situ* ACSL inhibition tests were carried out by the Weis group in the Biomedical Sciences Department, Texas Tech University. Inhibition of leukocyte recruitment was conducted by Hung Pham, Qian Chen and Lindon H. Young in the Department of Pathology, Philadelphia College of Osteopathic Medicine. (Description of bio-methods was adapted with permission from supporting information of Prior et. al[25] *Bioorganic & Medicinal Chemistry Letters* **2014**, *24*, 1057-1061. Copyright © 2014 Elsevier Ltd. License #4077240598278)

All of the synthesized triacsin C analogs (compounds**1-1** to **1-12**) were screened for ACSL inhibition *in vitro*. Selected compounds (**1-1**, **1-2**, **1-3**, **1-4**, **1-7** and **1-9**) were tested further for ACSL inhibition *in situ*. Finally, compounds **1-1** and **1-9** were tested *in vivo* for inhibition of leukocyte recruitment.

1.4.1 Methods

1.4.1.1 The *in vitro* ACSL inhibition

The activities of compounds **1-1** through **1-12** to inhibit ACSL were measured in an *in vitro* assay. Immortalized mouse brain endothelial cells (bEND3 cells) were grown to confluence in

25cm^2 tissue culture flasks. Confluent cultures were rinsed three times with ice-cold calcium and magnesium free phosphate buffered saline (CMFPBS), then dissolved in 0.5 mL solubilization buffer. The solubilized cells were assayed immediately for FACS activity as described.[26] Briefly, 50 µL of solubilized cells were added to 100 µL of ACSL assay cocktail containing the appropriate concentration of triacsin C or analog. The reaction was allowed to proceed for 2 minutes and terminated by the addition of 1.5 mL stop solution (isopropanol:*n*-heptane; 2M H_2SO_4, 40:10:1). Unreacted substrate was removed by adding 1.5 mL *n*-heptane and 1 mL DI H_2O followed by vigorous vortexing. The organic layer was discarded and the aqueous layer was re-extracted twice with 2 mL *n*-heptane containing 4 mg/mL palmitic acid. The radioactivity in 1 mL of the final aqueous layer was determined by liquid scintillation spectrometry.

ACSL activity was normalized to the control (no drug) activity, and IC_{50} values were calculated using the constrained three-parameter log (inhibitor) *vs.* response function of the Prism 6.0 statistical analysis package.

A general *in vitro* ACSL inhibition test procedure was summarized in Figure 1.6.

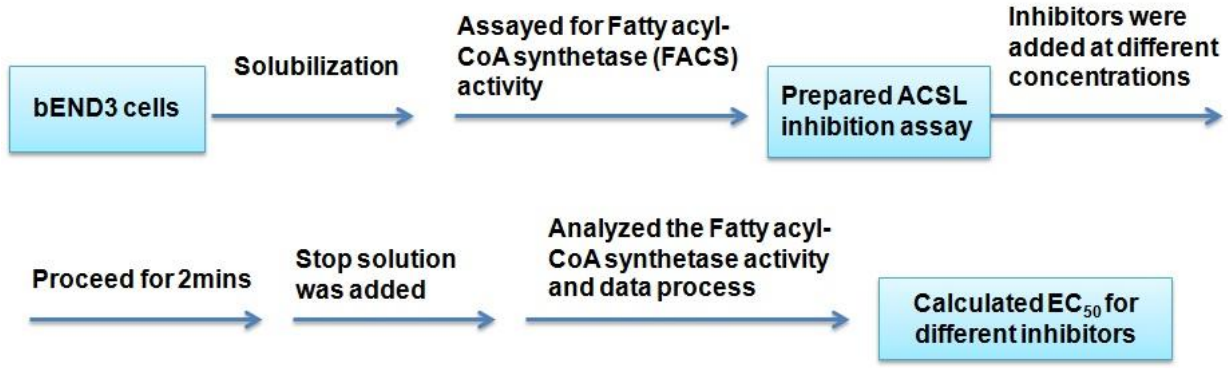

Figure 1.6. General procedure for *in vitro* ACSL inhibition test (conducted in Dr. Weis group).

1.4.1.2 The *in situ* ACSL inhibition

Compounds **1-1**, **1-2**, **1-3**, **1-4**, **1-7** and **1-9** were tested *in situ* for the ability to inhibit [^{14}C]-palmitic acid incorporation into extractable lipids. The bEND3 cells were grown to confluence in 6-well cluster plates. Confluent cultures were treated with Dulbecco's Minimal Essential Media (DMEM), supplemented as described, and containing [^{14}C]-palmitic acid (50 mC/mmol, a final

palmitate concentration of about 20 μM) plus the appropriate test compound at the concentrations indicated[26]. The medium contained about 7.4 mg/mL protein, from the fetal calf serum. After 2 hours, the plates were placed in an ice bath, and the media aspirated. The cells were rinsed 3 times with ice-cold CMFPBS, then scraped into 0.5 mL ice-cold CMFPBS and transferred to a glass screw-top tube. Each well was rinsed with an additional 0.5 mL ice-cold CMFPBS, followed by 0.8 mL ice-cold imidazole buffer. The rinses were pooled with the cells and lipids were extracted as described.[27,28] The organic layers were collected in a pre-weighed glass vial, and the total extracted lipid weights were calculated. Radioactivity in both the lipid extract and the aqueous layer were determined by liquid scintillation spectroscopy.

Results were expressed as moles of [^{14}C]-palmitic acid incorporated per μg lipid. Incorporation in the presence of each inhibitor was compared to that in the control (vehicle) cells. Statistical significance was calculated by one-way analysis of variance, using the Prism 6.0 software package.

A general *in situ* ACSL inhibition test procedure was summarized in Figure 1.7.

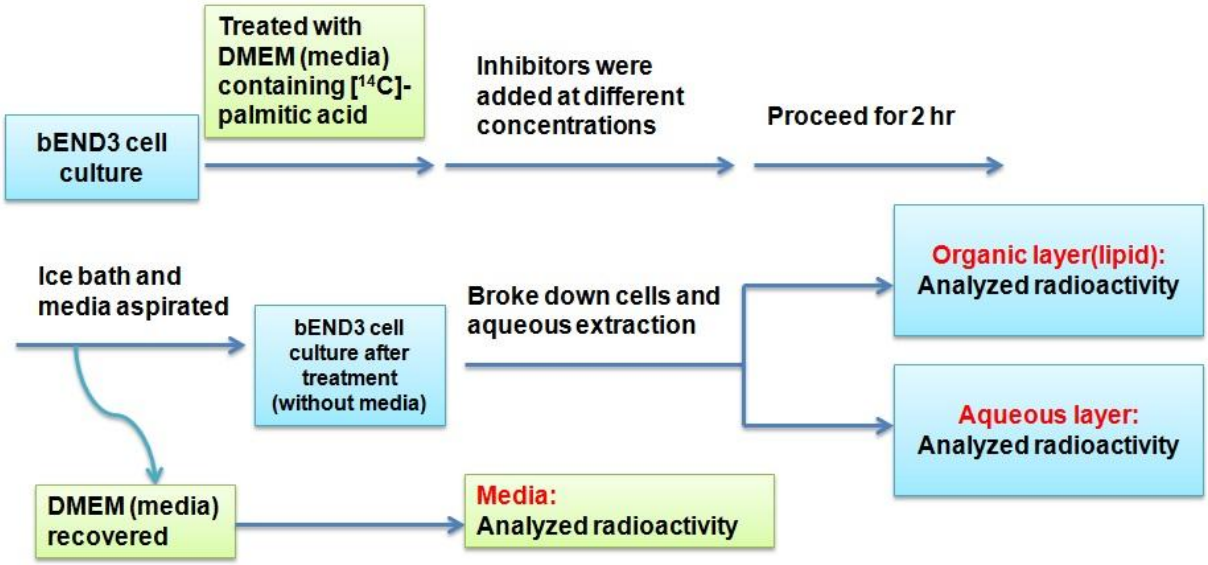

Figure 1.7. General procedure for *in situ* ACSL inhibition test (conducted in Dr. Weis group).

1.4.1.3 Inhibition of leukocyte recruitment

The effect of compounds **1-1** and **1-9** on leukocyte rolling, adhesion and extravasation were evaluated in male Sprague Dawley rats (275 - 325 g; Ace Animals, Boyertown, PA), as described previously.[16] A loop of the iliac mesentery was exteriorized and positioned in a Plexiglas chamber for visualization, then superfused with Krebs-Hensleit buffer (KHB). Leukocyte recruitment was initiated by adding 50 μM L-NAME to the KHB,[29] in the presence or absence of test compound. Leukocyte recruitment in unbranched post-capillary venules (mean diameter 20 ± 0.3 μm) was captured on high-resolution video recordings. The numbers of rolling (moving at a velocity substantially slower than that of red blood cells), adherent (firmly attached to the vascular endothelium for > 30 seconds) and transmigrated (in the tissue adjacent to the post-capillary venules) leukocytes were determined during playback analysis of the recorded images. Statistical significance for each parameter was calculated by analysis of variance for repeated measures, using the Prism 6.0 software package.

The Institutional Animal Care and Use Committee of the Philadelphia College of Osteopathic Medicine approved this study.

1.4.2 Results

1.4.2.1 The *in vitro* ACSL inhibitory activity

All of the synthesized small molecules (compounds **1-1** to **1-12**) were screened for their *in vitro* ACSL inhibitory activity in solubilized brain endothelial bEND3 cells together with triacsin C.

The results were shown in Table 1.2 and Figure 1.8. Except compound **1-2** and compound **1-8**, all of the other ten compounds showed moderate to good ACSL inhibitory ability with median effective concentration (EC_{50}) values ranging from 4.95 to 74.8 μM. Among the ten active analogs, compounds **1-1** (EC_{50} = 5.86 μM) and **1-3** (EC_{50} = 4.95 μM) were found to be lead compounds with micromolar range efficacy. Although they are 10 times less active than triacsin C, which has nanomolar range efficacy, they could act as a good starting point towards the development of more potent inhibitors through further structural optimization.

Compound	EC_{50} (μM)	Compound	EC_{50} (μM)
1-1	5.86 ± 0.54	**1-7**	26.9 ± 3.6
1-2	171 ± 79.0	**1-8**	164 ± 60.8
1-3	4.95 ± 0.74	**1-9**	70.4 ± 14.0
1-4	6.88 ± 0.66	**1-10**	14.8 ± 1.6
1-5	73.1 ± 9.6	**1-11**	9.04 ± 1.45
1-6	74.8 ± 34.8	**1-12**	53.5 ± 33.2
Triacsin C	0.358 ± 0.027		

Table 1.2. ACSL inhibition in solubilized brain endothelial bEND3 cells. The EC_{50} values were calculated by fitting the velocity versus inhibitor concentration to the constrained three-parameter log (inhibitor) versus response fuction of the Prism 6.0 statistical snalysis package. (This table was adapted with permission from Prior et. al[25] *Bioorganic & Medicinal Chemistry Letters* 2014, *24*, 1057-1061. Copyright © 2014 Elsevier Ltd. License #4077240598278)

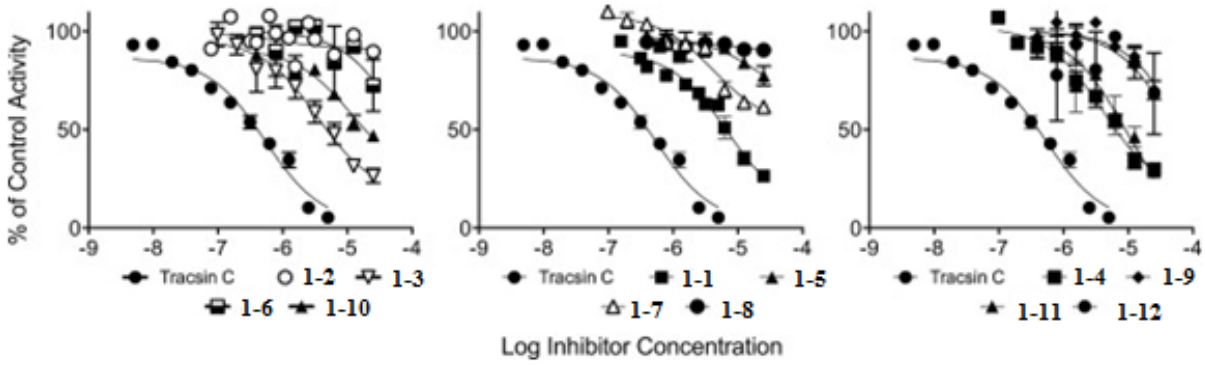

Figure 1.8. Concentration effect curves of the inhibition of ACSL activity in solubilized brain endothelial bEND3 cells for each of the analogs, as compared to triacsin C. (This figure was adapted with permission from Prior et. al[25] *Bioorganic & Medicinal Chemistry Letters* 2014, *24*, 1057-1061. Copyright © 2014 Elsevier Ltd. License #4077240598278)

1.4.2.2 The *in situ* ACSL inhibitory activity

Compounds **1-1**, **1-2**, **1-3**, **1-4**, **1-7** and **1-9** were tested for their *in situ* ACSL inhibition using [^{14}C]-palmitic acid. Data were calculated by analyzing the radioactivities in the recovered media and aqueous layer and organic layer after extraction. The *in situ* ACSL inhibition results were shown in Figure 1.9.

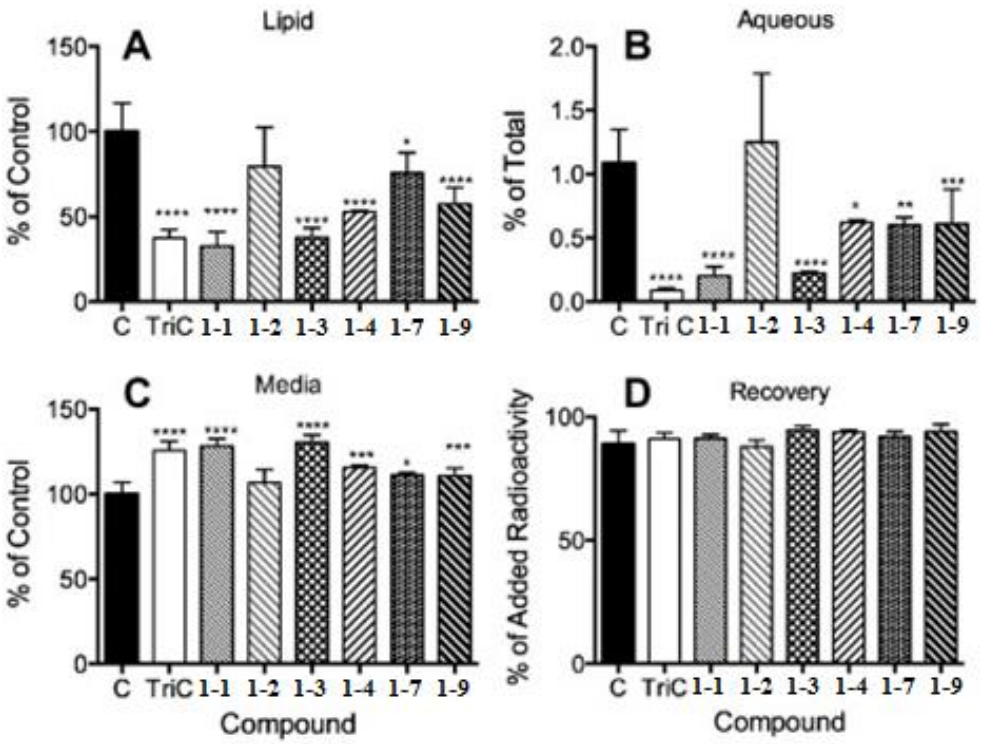

Figure 1.9. The *in situ* inhibition of ACSL by triacsin C and analogs in bEND3 brain cells, as evaluated by the incorporation of [^{14}C]-palmitic acid into extractable lipid (A), aqueous (B), media (C), and recovery (D). Triacsin C was used at 1.5 µM, while all other compounds were evaluated at 15 µM. Differences between the treatment groups and control were evaluated by one-way ANOVA, followed by Dunnett's t test for significance. * = $p < 0.05$; ** = $p < 0.01$; *** = $p < 0.001$; **** = $p < 0.0001$. n= 3-9 independent experiments. (This figure was adapted with permission from Prior et. al[25] *Bioorganic & Medicinal Chemistry Letters* 2014, *24*, 1057-1061. Copyright © 2014 Elsevier Ltd. License #4077240598278)

As shown in Figure 1.9 (A), in the presence of ACSL inhibitors, the radioactivity of lipid layer all apparently decreased except compounds **1-2** and **1-7** in the lipid. The decreased radioactivity is due to the reduced amount of [^{14}C]-palmitate in the lipid. In other words, ACSL function in the cell was inhibited and led to less formation of [^{14}C]-palmitate, which entered the organic layer after extraction. Figure 1.9 (B) showed the efficiency of aqueous extraction. Except compound **1-2**, all other compounds possess less than 0.7% of the total radioactivity in the aqueous layer, which means through extraction, most [^{14}C]-palmitate entered the organic layer. In Figure 1.9 (C), all compounds have over 100% radioactivity than control sample, because more unreacted [^{14}C]-palmictic acid was left behind inside the media due to the inhibition of *in situ* ACSL activity. Figure 1.9 (D) indicated that the total recovery of radioactivity are almost same. This excluded the possibility that the reduction of lipid layer recovered radioactivity was due to

decomposition of [^{14}C]-palmitic acid. The constant total recovery verified that reduced [^{14}C]-palmitate amount is the main reason for the radioactivity loss in lipid, in other words, inhibition of ACSL activity did occur in the cell treated with synthesized small molecules.

1.4.2.3 Leukocyte recruitment inhibition

Compounds **1-1** and **1-9** were further tested for their leukocyte recruitment inhibition and results were shown in Figure 1.10.

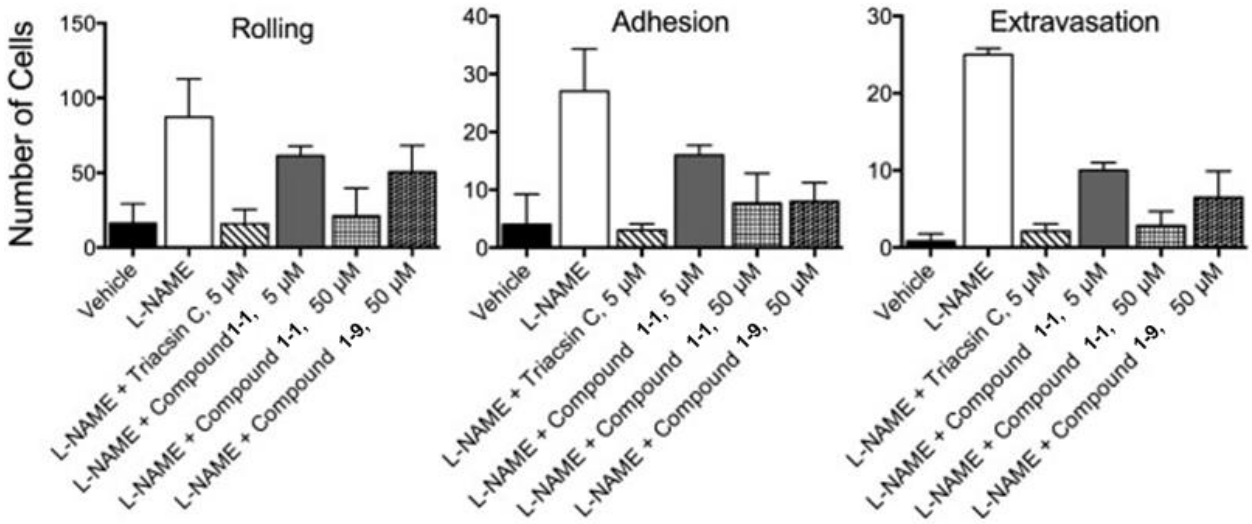

Figure 1.10. The L-NAME induced leukocyte recruitment at 120 minutes in the presence of compounds 1-1 and 1-9. Rolling, adhesion and extravasation were measured in post-capillary venules of the mesentery, a model of ischemia, and in the presence or absence of 5 or 50 µM compound 1-1 or 50 µM compound 1-9. The rolling, adhesion and extravasation rates for 50 µM compound **1-1** and 5 µM triacsin C were not different from each other nor were they different from vehicle alone. When evaluated at 5 µM, compound **1-1** inhibited the recruitment to about half the extent as at 50 µm. Compound **1-9** at 50 µM was about as effective as compound **1-1** at 5 µM. Each bar represents the mean ± SEM of 3 to 7 independent experiments. (This figure was adapted with permission from Prior et. al[25] *Bioorganic & Medicinal Chemistry Letters* 2014, *24*, 1057-1061. Copyright © 2014 Elsevier Ltd. License #4077240598278)

Figure 1.10 suggested that compounds **1-1** and **1-9** could inhibit the L-NAME induced leukocyte rolling, adhesion and extravasation. Compound **1-1** is more potent than **1-9** in leukocyte recruitment inhibition. Although compound **1-1** is still 10 times less effective than triacsin C, but it could act as a good start point. Compared with triacsin C, compound **1-1** is still a competitive

lead compound with much easier synthetic routes. And through further structural optimization, it could lead to the discovery of more efficient inhibitors.

1.4.3 Discussion

1.4.3.1 Structure-activity relationship of the synthesized triacsin C analogs towards *in vitro* ACSL inhibitory ability

Changes in structural moieties which may have an effect on *in vitro* ACSL inhibitory activity:

Entry 1. Head group

- 4-amino benzoic acid: **1-1**, **1-3**, **1-4**

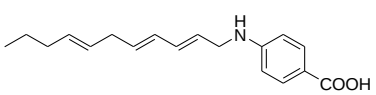

1-1 (EC_{50} = 5.86 uM)

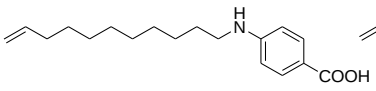

1-3 (EC_{50} = 4.95 uM)

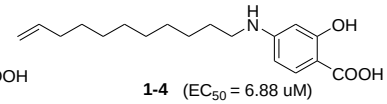

1-4 (EC_{50} = 6.88 uM)

- 4-diazenylbenzoic acid: **1-5**, **1-6**,**1-7**

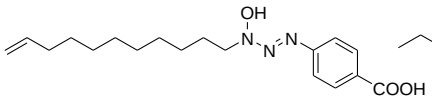

1-5 (EC_{50} = 73.1 uM)

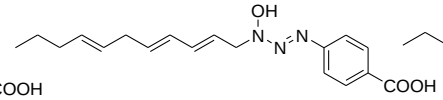

1-6 (EC_{50} = 74.8 uM)

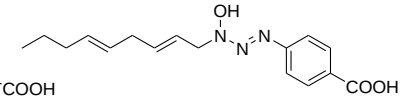

1-7 (EC_{50} = 26.9 uM)

- 1,2,4 oxadiazolidine-3,5-dione : **1-11**, **1-12**

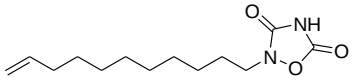

1-11 (EC_{50} = 9.04 uM)

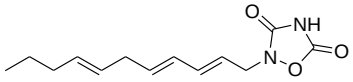

1-12 (EC_{50} = 53.5 uM)

- isothiazolidine dioxides **1-2**, **1-8**

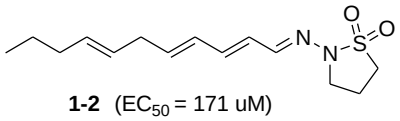

1-2 (EC_{50} = 171 uM)

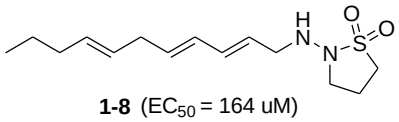

1-8 (EC_{50} = 164 uM)

Entry 2. H-bond donor in head group: **1-1** Vs **1-4**

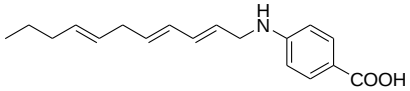

1-1 (EC_{50} = 5.86 uM)

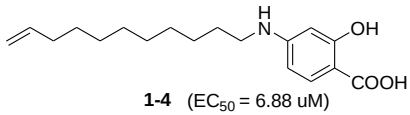

1-4 (EC_{50} = 6.88 uM)

Entry 3. Length of aliphatic chain: **1-6** Vs **1-7**

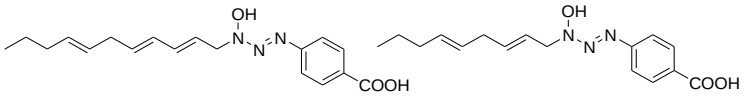

1-6 (EC_{50} = 74.8 uM) **1-7** (EC_{50} = 26.9 uM)

Entry 4. Conjugated diene moiety:

❖ **1-1** Vs **1-3** **1-5** Vs**1-6**

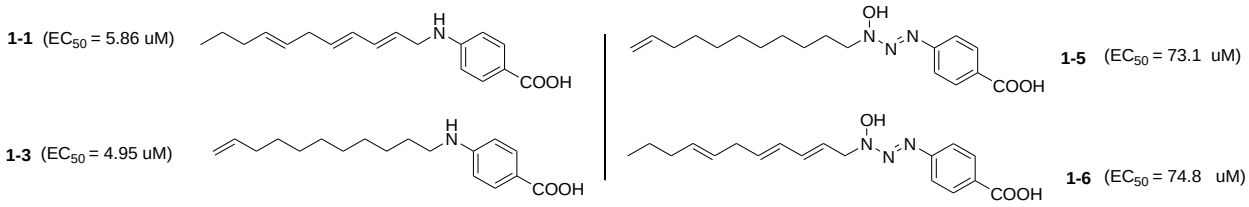

1-1 (EC_{50} = 5.86 uM)

1-3 (EC_{50} = 4.95 uM)

1-5 (EC_{50} = 73.1 uM)

1-6 (EC_{50} = 74.8 uM)

Entry 5. Acidic head group: **1-10**, **1-9** Vs **triacsin C**

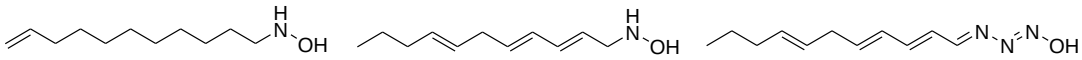

1-9 (EC_{50} = 70.4 uM) **1-10** (EC_{50} = 14.8 uM) **Triacsin C** (EC_{50} = 0.358 uM)

Table 1.3. Structure-activity relationship of triacsin C analogs towards ACSL inhibitory ability (*in vitro*).

The isothiazolidine dioxides structural moiety (Entry 1, compounds **1-2** and **1-8)** turned out not to be a good head group. The *p*-amino benzoic acid was the most active head group (Entry 1, compounds **1-1**, **1-3**, **1-4**), however, adding a N=N bond between the amine and benzoic acid greatly decreased activity (Entry 1, compounds **1-5**, **1-6**, **1-7**). Introducing hydrogen bond donating group in the head group phenyl ring does not increase its activity (Entry 2, compound **1-4**). The conjugated diene moiety is not necessary for effectiveness (Entry 4, compounds **1-1** and **1-3**). Changing head group to more acidic 1,2,4 oxadiazolidine-3,5-dione does not improve efficiency (Entry 1, compounds **1-11** and **1-12**). The lack of the hydrophilic head group will lead to a decrease of activity (Entry 5, compounds **1-9** and **1-10**).

In summary, acidic head group structural moiety is needed when designing triacsin C analogs while conjugated diene structural moiety in the long aliphatic chain does not play so significant roles in potency.

1.4.3.2 Concerns

Triacsin C is believed to inhibit ACSL activity by blocking the substrate binding site.[13] Our analogs are supposed to work in the same way. However, there is no evidence that which kind of interaction between the inhibitors and substrate binding site plays an important role. Further computational docking can be applied to illustrate the binding mode. Triacsin C is a nonspecific inhibitor, structural modification on triacsin C analogs towards improving their sub-type selectivity among different ACSL isomers could be explored in the future. So far only inhibition of leukocyte recruitment is done as the indicator for reducing I/R injury. Later, more experiments can be done to discovery more direct evidence of attenuation of I/R injury such as reduced size of infarction.

1.5 Conclusion

A small library of triacsin C analogs were designed and synthesized. Straight forward synthetic routes were developed and most steps are with moderate to good yield. ACSL inhibition tests showed promising results on the discovery of active triacsin C analogs as ACSL inhibitors. All of the designed triacsin C analogs inhibit ACSL activity except compounds **1-2** and **1-8**. Compounds **1-1** and **1-3** have the greatest activity with EC_{50} values of 5.86 and 4.95 μM, respectively. Structure-activity relationship was discussed based on the ACSL inhibition results. Results of inhibition of leukocyte recruitment indicated that inhibiting ACSL could attenuate I/R injury which is associated with vascular inflammatory.

1.6 Synthetic experimental procedures

1.6.1 General

Chemicals were purchased from Fisher Scientific and VWR international LLC. NMR spectra were taken from a 400 MHz Spectrometer (Varian Inc.) in chloroform-D unless otherwise informed. Mass spectra were obtained from an API 2000-triple quadrupole ESI-MS/MS mass spectrometer (Applied Biosystems). Compounds **1-13** and **1-2** were synthesized following reported procedures[15,18] and characterized by ^{1}H NMR and MS, and the spectra are identical to those reported.

1.6.2 Representative synthesis

1.6.2.1 *(2E,4E,7E)-N-Undeca-2,4,7-trienylhydroxylamine (Compound 1-10).*

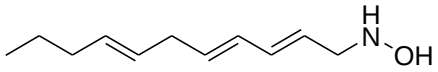

1-10

To a solution of hydroxylamine hydrochloride (0.61 mmol) and sodium acetate (0.61 mmol) in 0.2 mL of water was added a solution of aldehyde **1-13** (0.12 mmol) in 2 mL of EtOH. After stirring at 25^{o}C for 2 h, the reaction solution was diluted with water and extracted twice with CH_2Cl_2. The combined organic layers were washed with brine, dried over MgSO4, filtered and concentrated to yield 22 mg (100% yield) of the oxime intermediate as an oil. To a solution of oxime intermediate (0.22 mmol) and 80 L of 3 N HCl in 2 mL of MeOH, was added $NaCNBH_3$ (0.6 mmol) in two portions, and stirred at 25^{o}C for 3 days. The reaction was diluted with water and extracted three times with CH_2Cl_2. The combined organic layers were washed with brine, dried over MgSO4, filtered and concentrated to give 37 mg (92% yield) of compound **1-10** as a solid. ^{1}H NMR δ ppm 6.23 (dd, J = 14.9, 10.5 Hz, 1H), 6.05 (dd, J = 14.9, 11.2 Hz, 1H), 5.60 - 5.73 (m, 2H), 5.35 - 5.49 (m, 2H), 3.56 (d, J = 6.6 Hz, 2H), 2.77 (t, J = 5.7 Hz, 2H), 1.93 - 2.01 (m, 2H), 1.32 - 1.44 (m, 2H), 0.85 - 0.93 (m, 3H). 13C NMR δ ppm 134.3, 133.6, 131.7, 129.9, 127.5, 126.1, 55.83, 35.5, 34.7, 22.6, 13.7. MS (positive mode), m/z calcd for $C_{11}H_{20}NO$ $(M+H)^{+}$ 182.2, found 182.1.

1.6.2.2 *N-((4-Hydroxycarbonyl)pheynlazo)-N-(2E,4E,7E)-(undeca-2,4,7-trienyl) hydroxylamine (Compound 1-6)*

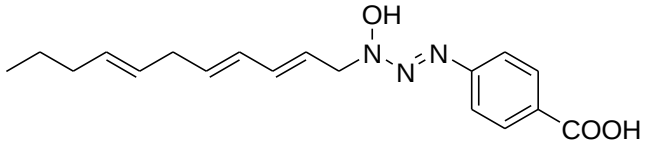

1-6

To a cold (0^{o}C) solution of hydroxylamine **1-10** (83 μmol) in 1 mL of MeOH was added dropwise an aqueous solution of 4-(hydroxycarbonyl)phenyldiazonium chloride (0.083 mmol) and sodium acetate (0.50 mmol) in 1 mL of water concurrently. After stirring at 0^{o}C for 20 min the reaction was diluted with diethyl ether and water, acidified with acetic acid to pH = 4. The

organic layer was washed twice with water, brine, dried over $NaSO_4$, filtered, concentrated, and column chromatographed on silica gel using a mixture of diethyl ether and hexane (1:1) as eluent to yield 13 mg (48% yield) of compound 1-**6** as a solid. ^{1}H NMR δ ppm 10.27 (s, 1H), 8.06 (d, *J* = 8.6 Hz, 2H), 7.17 (d, *J* = 8.6 Hz, 2H), 6.41 (dd, *J* = 15.5, 11.3 Hz, 1H), 6.08 (dd, *J* = 15.5, 10.7 Hz, 1H) 5.77 - 5.87 (m, 2H), 5.33 - 5.49 (m, 2H), 4.74 (d, *J* = 7.0 Hz, 2H), 2.80 (t, *J* = 6.3 Hz, 2H), 1.93 - 2.02 (m, 2H), 1.32 - 1.43 (m, 2H), 0.89 (t, *J* = 7.4 Hz, 3H). ^{13}C NMR δ ppm 171.3, 144.5, 137.7, 136.7, 132.4, 130.4, 129.2, 127.3, 123.3, 120.5, 113.9, 66.0, 35.8, 34.9, 22.8, 13.9. MS (negative mode), m/z calcd for $C_{18}H_{22}N_3O_3$ $(M-H)^-$ 328.2, found 328.3.

1.6.2.3 *2-((2E,4E,7E)-Undeca-2,4,7-trienylamino)-1,1-dioxo-1-isothiazolidine (Compound 1-8)*

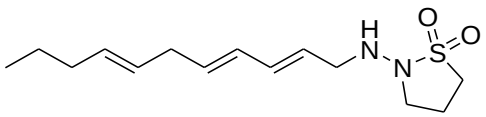

1-8

To a solution of 8 mg (28 μmol) of compound **1-2** in 3 mL of methanol was added 9 mg (0.14 mmol) $NaCNBH_3$ followed by 2 drops of 3 M HCl in methanol. The solution was stirred at 25^{o}C for 45 min., diluted with aqueous $NaHCO_3$ solution, and extracted with CH_2Cl_2 twice. Combined organic layers were washed with brine, dried over $MgSO_4$, fitered, concentrated and column chromatographed on silica gel using a gradient mixture of hexane and diethyl ether as eluent to give 4.2 mg (53% yield) of compound **1-8**. ^{1}H NMR δ ppm 6.22 (dd, *J* = 15.0, 10.0 Hz, 1H), 6.05 (dd, *J* = 15.0, 10.0 Hz, 1H), 5.71 (dt, *J* = 15.0, 7.0 Hz, 1H), 5.62 (dt, *J* = 15.0, 7.0 Hz, 1H), 5.49 – 5.36 (m, 2 H), 4.22 (bs, 1H, NH), 3.82 (d, *J* = 7.0 Hz, 2 H, CH_2N), 3.168 (dd, *J* = 6.5, 6.3 Hz, 2H), 3.08 (q, *J* = 5.0 Hz, 2H), 2.78 (t, *J* = 5.0 Hz, 2H), 2.31 (pent, *J* = 5.6 Hz, 2H), 1.98 (q, *J* = 7.6 Hz, 2H), 1.38 (sextet, *J* = 7.6 Hz, 2H), 0.90 (t, *J* = 7.6 Hz, 3H). ^{13}C NMR δ ppm 134.9, 134.1, 131.8, 129.5, 127.4, 124.7, 49.6, 45.3, 35.6, 34.7, 29.7, 28.5, 22.6, 13.7. MS (positive mode), m/z calcd for $C_{14}H_{24}N_2NaO_2S$ $(M+Na)^+$ 307.1, found 307.2.

1.6.2.4 *2-((2E,4E,7E)-Undeca-2,4,7-trienyl)-(1,2,4)oxadiazolidine-3,5-dione (Compound 1-12)*

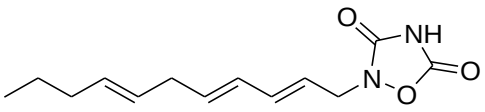

1-12

To a solution of hydroxylamine **1-10** (83 μmol) in 1 mL of CH_2Cl_2 was added ethyl isocyanoformate (83 μmol), and the solution was stirred at 25°C for 3 h. The reaction solution was diluted with water, and extracted with diethyl ether. The organic layer was washed with brine, dried over $MgSO_4$, filtered and concentrated to give 20 mg (69% yield) of the corresponding carbamate intermediate as an oil. To a solution of the above carbamate intermediate (0.057 mmol) in 3 mL of dioxane at 0°C was added dropwise 3 N NaOH (0.14 mmol), and the solution was stirred at 25°C for 18 h. The reaction solution was diluted with water, acidified to pH = 4 using 2 N HCl, and extracted three times with ethyl acetate. The combined organic layers were washed with brine, dried over $MgSO_4$, filtered and concentrated, and placed under high vacuum for 12 h to give 10 mg (70% yield) of compound **1-12** as an oil. ^{1}H NMR δ ppm 6.13 - 6.29 (m, 1H), 5.94 - 6.07 (m, 1H), 5.62 - 5.75 (m, 1H), 5.23 - 5.60 (m, 3H), 4.16 - 4.30 (m, 2H), 2.65 - 2.84 (m, 2H), 1.92 - 2.05 (m, 2H), 1.27 - 1.41 (m, 2H), 0.83 - 0.93 (m, 3H). ^{13}C NMR δ ppm 156.9, 151.8, 137.5, 136.41, 132.4, 129.1, 127.3, 120.6, 51.4, 35.9, 35.0, 22.9, 14.0. MS (negative mode), m/z calcd for $C_{13}H_{17}N_2O_3$ $(M-H)^-$ 249.1, found 249.2.

1.6.2.5 *N-((4-Hydroxycarbonyl)phenylazo)-N-(nona-2E,5E-dienyl) hydroxylamine (Compound 1-7)*

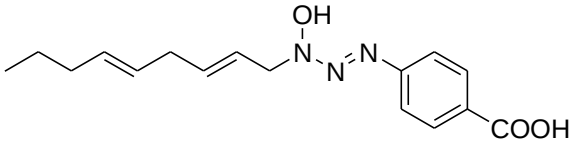

1-7

To a solution of hydroxylamine hydrochloride (3.62 mmol) and sodium acetate (3.62 mmol) in 1.2 mL of water was added a solution of 2*E*,5*E*-nonadienal (compound **1-13-4**, 0.73 mmol) in 10 mL of EtOH and the resulting solution was stirred at 25°C for 2 h. The solution was diluted with water and extracted three times with dichloromethane. The combined organic layers were washed with brine, dried over $MgSO_4$, filtered and concentrated to give 0.10 g (91% yield) of the corresponding oxime intermediate as an oil. To a solution of the above oxime (0.65 mmol) and

0.24 mL of 3 N HCl in 5 mL of MeOH was added $NaCNBH_3$ (1.7 mmol) in portions, and stirred at 25^{o}C for 18 h. The reaction solution was diluted with water, basified to pH = 10 using 3 N NaOH, and extracted three times with CH_2Cl_2. The combined organic layers were washed with brine, dried over $MgSO_4$, filtered, and concentrated to yield 30 mg (30% yield) of hydroxylamine **1-14**. To a cold (0^{o}C) solution of hydroxylamine **1-14** (0.19 mmol) in 1 mL of MeOH was added dropwise an aqueous solution of 4-(hydroxycarbonyl)phenyldiazonium chloride (0.19 mmol) and aqueous sodium acetate (1.2 mmol) concurrently. The solid precipitate was collected by filtration and washed three times with cold water, dried under vacuum to give 25 mg (42% yield) of compound **1-7** as a solid. ^{1}H NMR δ ppm 10.27 (br. s., 1H), 8.06 (d, *J* = 8.6 Hz, 2H), 7.16 (d, *J* = 8.6 Hz, 2H), 5.90 - 5.98 (m, 1H), 5.71 - 5.80 (m, 1H), 5.36 - 5.53 (m, 2H), 4.69 (d, *J* = 6.6 Hz, 2H), 2.81 (t, *J* = 5.9 Hz, 2H), 1.92 - 2.03 (m, 2H), 1.33 - 1.42 (m, 2H), 0.89 (t, *J* = 7.4 Hz, 3H). ^{13}C NMR δ ppm 170.4, 144.3, 137.9, 132.6, 132.1, 126.5, 120.7, 113.8, 113.7, 65.8, 35.2, 34.6, 22.5, 13.7. MS (negative mode), m/z calcd for $C_{16}H_{20}N_3O_3$ $(M-H)^-$ 302.2, found 302.1.

References

(1) Hisanaga, Y.; Ago, H.; Nakagawa, N.; Hamada, K.; Ida, K.; Yamamoto, M.; Hori, T.; Arii, Y.; Sugahara, M.; Kuramitsu, S.; Yokoyama, S.; Miyano, M. Structural Basis of the Substrate-specific Two-step Catalysis of Long Chain Fatty Acyl-CoA Synthetase Dimer. *J Biol Chem* **2004**, *279*, 31717-31726.

(2) Linder, M. E.; Deschenes, R. J. Palmitoylation: policing protein stability and traffic. *Nat Rev Mol Cell Biol* **2007**, *8*, 74-84.

(3) Kalogeris, T.; Baines, C. P.; Krenz, M.; Korthuis, R. J. Cell Biology of Ischemia/Reperfusion Injury. *International review of cell and molecular biology* **2012**, *298*, 229-317.

(4) Braunwald, E.; Kloner, R. A. Myocardial reperfusion: a double-edged sword? *Journal of Clinical Investigation* **1985**, *76*, 1713-1719.

(5) Farb, A.; Kolodgie, F. D.; Jenkins, M.; Virmani, R. Myocardial infarct extension during reperfusion after coronary artery occlusion: pathologic evidence. *Journal of the American College of Cardiology* **1993**, *21*, 1245-1253.

(6) Flaherty, J. T. Myocardial injury mediated by oxygen free radicals. *The American journal of medicine* **1991**, *91*, 79s-85s.

(7) Grech, E. D.; Bellamy, C. M.; Jackson, M. J.; Muirhead, R. A.; Faragher, E. B.; Ramsdale, D. R. Free-radical activity after primary coronary angioplasty in acute myocardial infarction. *American Heart Journal* **1994**, *127*, 1443-1449.

(8) Kazui, M.; Andreoni, K. A.; Williams, G. M.; Perler, B. A.; Bulkley, G. B.; Beattie, C.; Donham, R. T.; Sehnert, S. S.; Burdick, J. F.; Risby, T. H. Visceral lipid

peroxidation occurs at reperfusion after supraceliac aortic cross-clamping. *Journal of Vascular Surgery* **1994**, *19*, 473-477.

(9) Lefer, A. M.; Lefer, D. J. The role of nitric oxide and cell adhesion molecules on the microcirculation in ischaemia-reperfusion. *Cardiovasc Res* **1996**, *32*, 743-751.

(10) Hartman, J. C.; Anderson, D. C.; Wiltse, A. L.; Lane, C. L.; Rosenbloom, C. L.; Manning, A. M.; Humphrey, W. R.; Wall, T. M.; Shebuski, R. J. Protection of ischemic/reperfused canine myocardium by CL18/6, a monoclonal antibody to adhesion molecule ICAM-1. *Cardiovasc Res* **1995**, *30*, 47-54.

(11) Nakano, H.; Kuzume, M.; Namatame, K.; Yamaguchi, M.; Kumada, K. Efficacy of intraportal injection of anti-ICAM-1 monoclonal antibody against liver cell injury following warm ischemia in the rat. *American journal of surgery* **1995**, *170*, 64-66.

(12) Leick, M.; Azcutia, V.; Newton, G.; Luscinskas, F. W. Leukocyte Recruitment in Inflammation: Basic Concepts and New Mechanistic Insights Based on New Models and Microscopic Imaging Technologies. *Cell and tissue research* **2014**, *355*, 647-656.

(13) Vessey, D. A.; Kelley, M.; Warren, R. S. Characterization of triacsin C inhibition of short-, medium-, and long-chain fatty acid: CoA ligases of human liver. *Journal of biochemical and molecular toxicology* **2004**, *18*, 100-106.

(14) Omura, S.; Tomoda, H.; Xu, Q. M.; Takahashi, Y.; Iwai, Y. Triacsins, new inhibitors of acyl-CoA synthetase produced by Streptomyces sp. *J Antibiot (Tokyo)* **1986**, *39*, 1211-1218.

(15) Kim, Y.; George, D.; Prior, A. M.; Prasain, K.; Hao, S.; Le, D. D.; Hua, D. H.; Chang, K.-O. Novel Triacsin C Analogs as Potential Antivirals against Rotavirus Infections. *European journal of medicinal chemistry* **2012**, *50*, 311-318.

(16) Blakeman, N.; Chen, Q.; Tolson, J.; Rueter, B.; Diaz, B.; Casey, B.; Young, L. H.; Weis, M. T. Triacsin C, a fatty acyl coA synthetase inhibitor, improves cardiac performance following global ischemia. *Am J Biomed Sci* **2012**, *4*, 249-261.

(17) Blakeman, N.; Chen, Q.; Young, L.; Weis, M. Evidence that fatty acyl CoA synthetase is a mediator of ischemia/reperfusion injury (I/R) in the rat. *The FASEB Journal* **2011**, *25*, 821.832.

(18) Tanaka, H.; Yoshida, K.; Itoh, Y.; Imanaka, H. Studies on new vasodilators, WS-1228 A and B. II. Structure and synthesis. *J Antibiot (Tokyo)* **1982**, *35*, 157-163.

(19) Lipinski, C. A.; Lombardo, F.; Dominy, B. W.; Feeney, P. J. Experimental and computational approaches to estimate solubility and permeability in drug discovery and development settings. *Advanced Drug Delivery Reviews* **1997**, *23*, 3-25.

(20) Veber, D. F.; Johnson, S. R.; Cheng, H.-Y.; Smith, B. R.; Ward, K. W.; Kopple, K. D. Molecular Properties That Influence the Oral Bioavailability of Drug Candidates. *Journal of Medicinal Chemistry* **2002**, *45*, 2615-2623.

(21) Thornber, C. W. Isosterism and molecular modification in drug design. *Chemical Society Reviews* **1979**, *8*, 563-580.

(22) Lima, L. M.; Barreiro, E. J. Bioisosterism: a useful strategy for molecular modification and drug design. *Current medicinal chemistry* **2005**, *12*, 23-49.

(23) Weis, M. T.; Tolson, J.; Chen, Q.; Young, L. TRIACSIN C, A FATTY ACYL COA SYNTHETASE (FACS) INHIBITOR, IMPROVES CARDIAC PERFORMANCE FOLLOWING GLOBAL ISCHEMIA. *The FASEB Journal* **2012**, *26*, 1136.1118.

(24) http://www.molinspiration.com/services/logp.html.

(25) Prior, A. M.; Zhang, M.; Blakeman, N.; Datta, P.; Pham, H.; Chen, Q.; Young, L. H.; Weis, M. T.; Hua, D. H. Inhibition of long chain fatty acyl-CoA synthetase (ACSL) and ischemia reperfusion injury. *Bioorganic & Medicinal Chemistry Letters* **2014**, *24*, 1057-1061.

(26) Weis, M. T.; Brady, M.; Moore, M.; Crumley, J.; Stallone, J. N. Inhibiting Long-Chain Fatty Acyl CoA Synthetase Does Not Increase Agonist-Induced Release of Arachidonate Metabolites from Human Endothelial Cells. *Journal of Vascular Research* **2005**, *42*, 275-283.

(27) Steenbergen, C.; Jennings, R. B. Relationship between lysophospholipid accumulation and plasma membrane injury during total in vitro ischemia in dog heart. *Journal of molecular and cellular cardiology* **1984**, *16*, 605-621.

(28) Palazzo, A. J.; Malik, K. U.; Weis, M. T. Vasopressin stimulates the mobilization and metabolism of triacylglycerol in perfused rabbit hearts. *The American journal of physiology* **1991**, *260*, H604-612.

(29) Davenpeck, K. L.; Gauthier, T. W.; Lefer, A. M. Inhibition of endothelial-derived nitric oxide promotes P-selectin expression and actions in the rat microcirculation. *Gastroenterology* **1994**, *107*, 1050-1058.

Chapter 2 - Design, synthesis and bio-evaluation of 1,3,4-oxadiazole derivatives as T-type calcium channel inhibitors

2.1 Background and significance

2.1.1 T-type calcium channel

Voltage-gated calcium channels (VGCCs) are transmembrane, multi-subunit proteins that modulate influx of calcium ion (Ca^{2+}) into the cell in response to membrane depolarization. According to different activation potentials, generally VGCCs can be classified as high voltage-activated (L-, N-, P-/Q- and R-types) and low voltage-activated (T-type).[1,2] T-type calcium channels are characterized with transient and tiny Ca^{2+} currents and composed of five subunits (Figure 2.1). As shown in Figure 2.1, α1 is central pore-forming subunit and is the primary subunit while the others are called auxiliary subunits regulating channel properties.[1] Among different auxiliary subunits, β is an intracellular subunit; α2 and δ subunits form a glycoprotein dimer and γ subunit is a transmembrane glycoprotein.[2,3] Based on the differences between pore-forming α1 subunit, T-type calcium channels are classified into three sub-types: Cav3.1 (α1G), Cav3.2 (α1H), and Cav3.3 (α1I).[3-7] The three sub-types are heterogeneously expressed in the brain and organs such as the heart, vascular smooth muscle, non-vascular smooth muscle, skeletal muscle and others.[8-13]

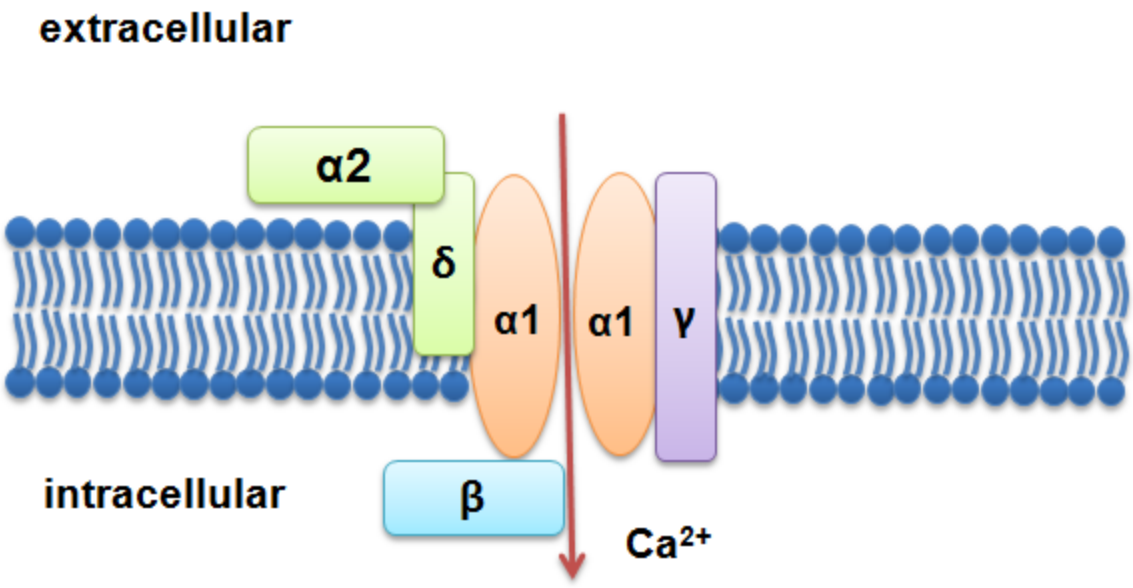

Figure 2.1. T-type calcium channels (cartoon presentation) are multi-subunits protein complexes.

Although T-type calcium currents were first discovered in 1975 by Hagiwara et al.[14], until recently T-type calcium channels have drawn great attention with the discoveries of different genes encoding α1 subunits[3-7]. The opening of calcium channels leads to a Ca^{2+} influx, which increases both membrane depolarization and intracellular Ca^{2+} concentration. The changing in intracellular Ca^{2+} concentration has an effect on some important processes like muscle contraction[13], electrical conduction, neurotransmission and others[3]. T-type calcium channels have been reported to be involved in the mechanisms of cell development, hormone secretion, epilepsy and others.[15]

2.1.2 Epilepsy and T-type calcium currents influx

Seizure is defined as "*disturbances in the electrical activity of the brain*" and epilepsy is defined as "*two or more unprovoked seizures separated by at least 24 hours*".[16] Based on an epilepsy report[17] published by Institute of Medicine (MOI) in 2012, there are 2.2 million people in the United States have epilepsy and around 150,000 new cases of epilepsy are diagnosed each year. Ranking right after migraine, stroke, and Alzheimer's disease, epilepsy has become the 4th most frequently occurring neurological disease in the United States.[18]

Upon the exploration of epilepsy models, changes in the cellular Ca^{2+}concentration have been found. Back to 1977, Heinemann et al.[19] found that during the process of seizures, intracellular calcium concentration increased and extracellular calcium concentration decreased. This discovery led to a hypothesis that an increased calcium currents would result in epilepsy. Later, more research results were reported to support this hypothesis. In 1995, Tsakiridou et al.[20] studied absence epilepsy on rodent models and they found that increased T-type currents were first observed in select thalamic nuclei from genetic absence epileptic rats. However, there was no effect for the amplitude of L-type currents, indicating that epilepsy results from increasing T-type currents. Thus, T-type calcium channels could be a good target for the treatment of epilepsy. Nowadays, although many T-type calcium channel inhibitors have been reported,[21-23] only small amount of the reported inhibitors could have a chance to enter clinical trial. Most of them are failed in the pre-clinical studies. Discovery of more new T-type calcium channel inhibitors are still needed.

2.2 Research objectives

Research objective 1: Design and synthesize small molecules as T-type calcium channel inhibitors.

Research objective 2: Study the structure-activity relationship (SAR) of synthesized small molecules based on their inhibitory ability towards T-type calcium channels. (This biological study was performed in our collaborator, Dr. Ximin Simon Xie's laboratory)

Research Objective 3: Explore the relation between inhibition of T-type calcium channels and seizure. (This biological study was performed in our collaborator, Dr. Ximin Simon Xie's laboratory)

2.3 Molecular design and synthetic routes

2.3.1 Reported T-type calcium channel blockers

Some of the reported T-type calcium channel blockers were summarized in Figure 2.2 and most of them were covered by patents[21]. Mibefradril was a FDA approved anti-hypertension drug and put into market in 1997. It selectively inhibited T-type (IC_{50} = 0.1 μM) over L-type (IC_{50} = 3

μM) calcium channels[24]. However, later severe drug-drug interactions were discovered, and mibefradril was retracted from market in 1998.[25]

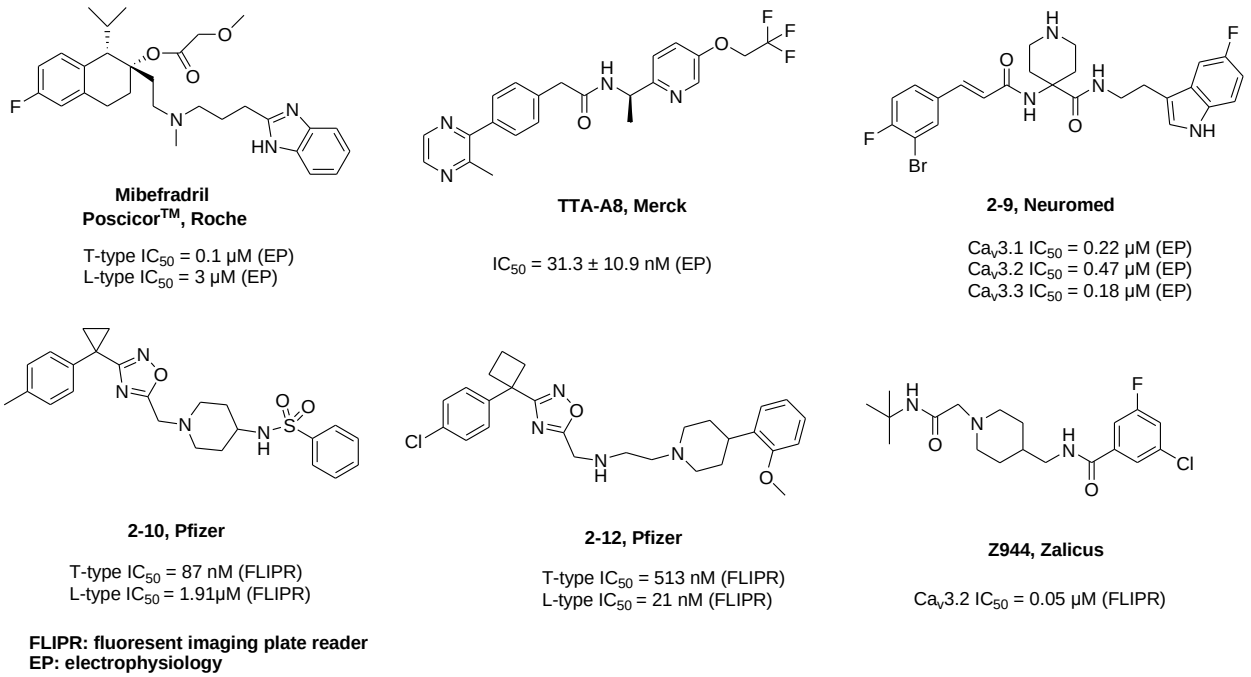

Figure 2.2. Reported T-type calcium channel blockers.[21,24,26-30]

There are some common structural features shared by the reported blockers. All of them have at least one aromatic ring. All of them have at least one basic N atom. Most of them have amide bond in their structures. Most of them have flexible aliphatic linkers. The molecule is not planar. These common features are good guidance in the molecular design.

2.3.2 Oxadiazoles derivatives as T-type Ca^{2+} channel inhibitors

1,3,4-Oxadiazole structural motif has played an important role in the field of drug discovery because that it has wide range of biological activities including anti-inflammatory, anticancer, antibacterial, and others.[31-33] Oxadiazole compounds have been reported to act as L- and T-type calcium channel blockers.[29,30,34] In 2011, Xiang et al[23] conducted a T-type Calcium channel high throughput screen (HTS) among 110,720 compounds in MLSCN/MLPCN (Molecular Libraries Screening /Production Center Network) library. Through several different HTS screens as described in the reference[23], finally, only 1 hit compound CID3373841 (Figure 2.3) was confirmed to selectively inhibit T-type calcium channel towards L- and N- type channels. Further

structural optimization lead to a more potent T-type calcium channel inhibitor CID46943243[23] (Figure 2.3), which suggested that 1,3,4-oxadiazole could be a good pharmacophore for the inhibition of T-type calcium channels.

CID3373841
IC_{50}= 2.5 μM

CID46943243
IC_{50}= 810 nM

Figure 2.3. Chemical structures of compound CID3373841 and compound CID46943243.

2.3.3 Molecular design

A series of small molecules containing 1,3,4-oxadiazole core was designed as shown in Figure 2.4. The 1,3,4-oxadizole core was kept in all proposed small molecules considering its efficacy-necessary. Branches on both sides were replaced with various functional groups to achieve better bioactivities (Figure 2.4). Modifications in part A were focused on the substitution of different aromatic rings to adjust the molecular lipophilicity. Diverse functional groups were introduced in part B to explore the structural features which may have an effect on potency, such as rigidity, flexibility, planarity, aromaticity, steric hindrance and others.

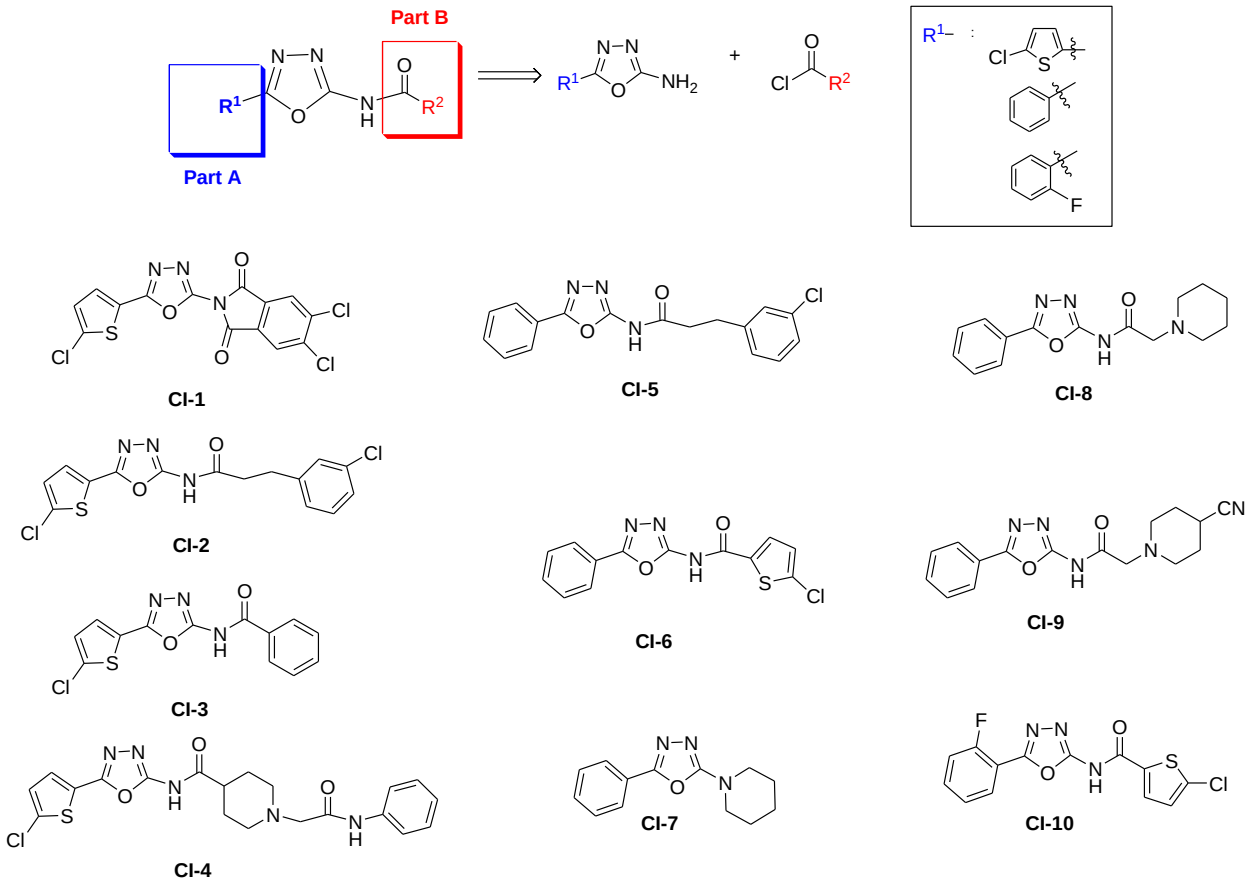

Figure 2.4. Designed substituted 1,3,4-oxadiazole compounds as T-type calcium channel inhibitors.

Predicted Log P values were calculated using interactive log P calculator (© Molinspiration Cheminformatics 2017)[35], which is available online. The calculated results were shown in Table 2.1. Except compound **CI-6** with log P value slightly over 5, all other designed 1,3,4-oxadiazole derivatives have predicted log P values between 2 to 5, which follow the Lipinski rules.

Compound	Chemical Structure	Molecular Weight	log P value
CI-1	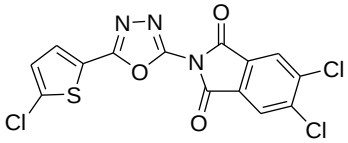	400.62	5.06
CI-2	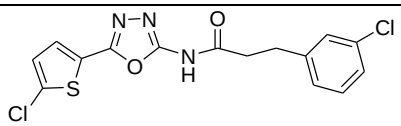	368.24	4.67

CI-3	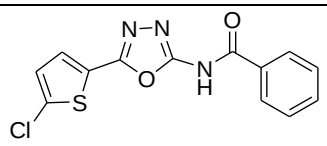	305.74	3.41
CI-4	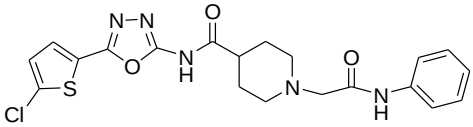	445.92	3.67
CI-5	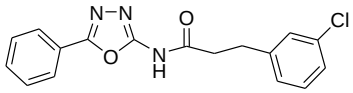	327.76	4.08
CI-6	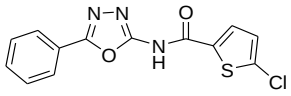	305.74	3.52
CI-7	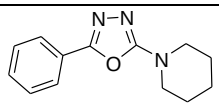	229.28	2.94
CI-8	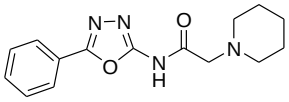	286.33	2.42
CI-9	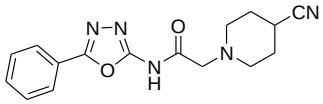	311.34	2.06
CI-10	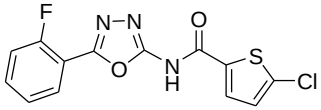	323.73	3.64

Table 2.1. Molecular weights and log P values of designed 1,3,4-oxadiazole derivatives.

2.3.4 Synthetic routes

The synthetic work was collaborated with Ms. Medha J. Gunaratna, graduate student in Hua group and I carried out the syntheses of compounds **CI-1**, **CI-2**, **CI-3**, **CI-4** and **CI-6**. The synthetic routes were shown as follows (Scheme 2.1 - Scheme 2.5). The synthesis of 1,3,4-oxadiazole ring was followed by reported procedure (Scheme 2.1).[36] Commercially available thiosemicarbazide (compound **2-1**) coupled with different acyl chlorides, and the resulting amide intermediates (compounds **2-2** and **2-3**) underwent cyclization reaction to give the 1,3,4-oxadiazole rings (compounds **2-4** and **2-5**).

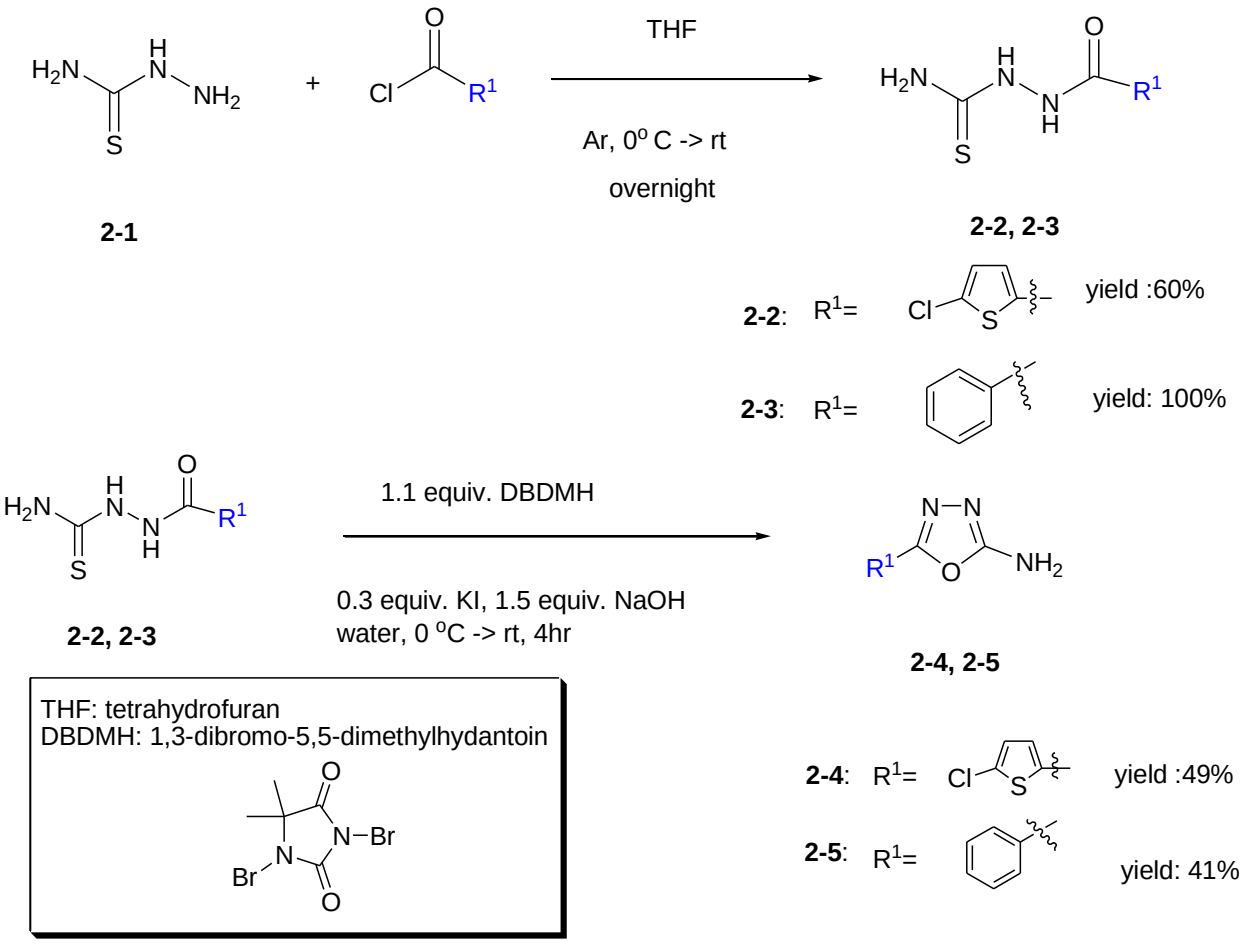

Scheme 2.1. Syntheses of compounds 2-4 and 2-5.

Possible mechanism of cyclization was shown in Scheme 2.2[31,37]. KI was first oxidized by DBDMH to form I_2. The acyl-substituted thiosemicarbazide (compound **2-a**) was activated by the formed I_2 followed by elimination, cyclization and finally produced the designed ring compound **2-e**.

Step 1: DBDMH works as an effective oxidant oxidizing KI to I_2.

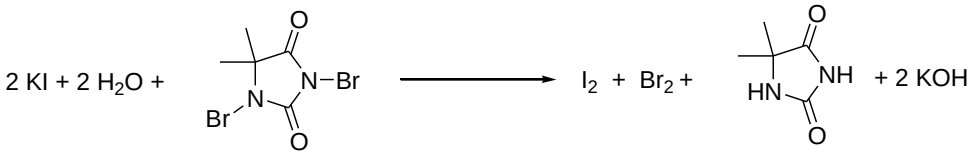

Step 2: Cyclization

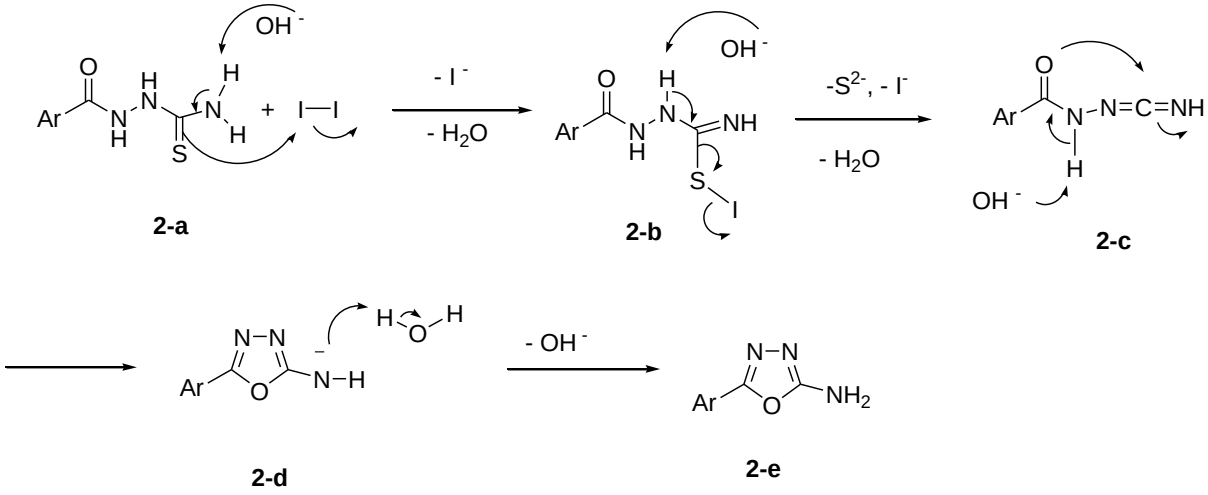

Scheme 2.2. Possible mechanism of formation of 1,3,4-oxadiazole ring.[31,37]

Syntheses of compounds **CI-1**, **CI-2**, **CI-3** and **CI-4** were shown in Scheme 2.3. Generally, amine **2-4** underwent replacement reactions with various acyl chorides under basic conditions to give designed amide compounds (**CI-1**, **CI-2** and **CI-3**). One problem is that the reaction pathway was not efficient considering the low to moderate reaction yields. After finding the hit compounds, further reaction condition optimization is needed to improve the yield. One possible reason for the low reaction yield was poor solubility of amide **2-4**. Compound **2-4** was not completely dissolved in dichloromethane. Changing solvents to *N*,*N*-dimethyl formamide (DMF) could be a way to improve the reaction yield. Slightly different from the syntheses of **CI-1**, **CI-2** and **CI-4**, compound **CI-4** was synthesized through coupling reaction between amine **2-4** and carboxylic acid **2-6**. Carboxylic acid is less electrophilic than acyl chloride, so coupling reagent EDC was used to activate the carboxylic acid group.

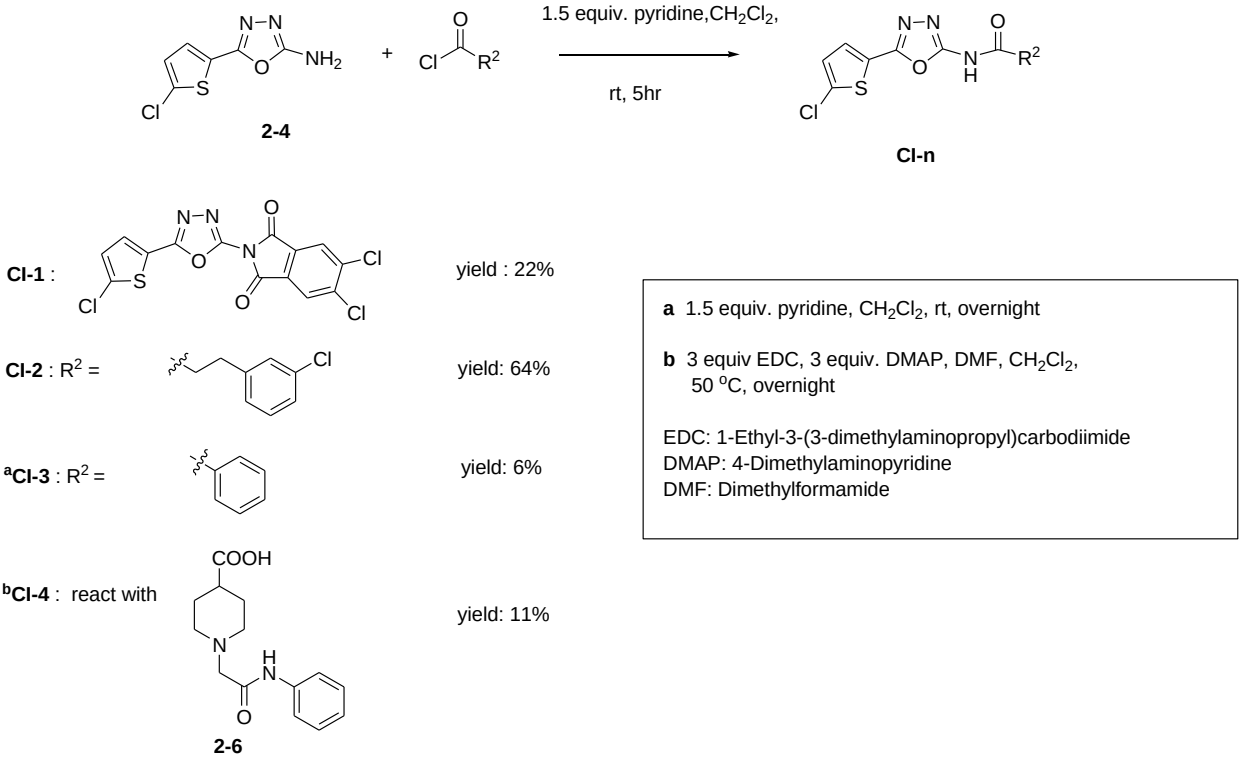

Scheme 2.3. Syntheses of compounds CI-1, CI-2, CI-3 and CI-4.

Synthesis of compound **2-6** was shown in Scheme 2.4. The acyl chloride **2-6-2** underwent replacement reaction with 4-cyanopiperidine (compound **2-6-1**) under basic conditions. The resulting cyanide **2-6-3** was further hydrolyzed using 3 N NaOH aqueous solution in methanol to produce corresponding carboxylic acid **2-6**.

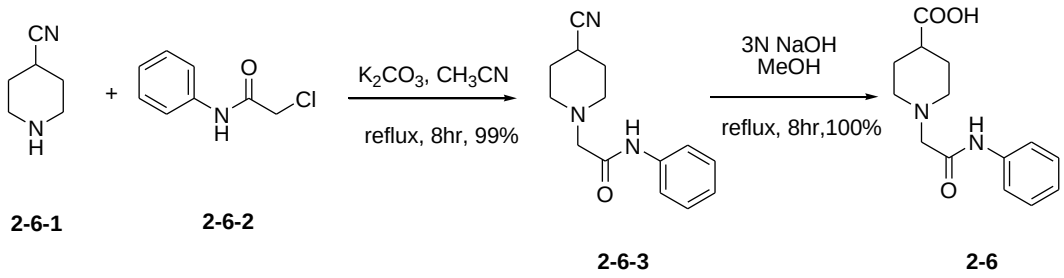

Scheme 2.4. Synthesis of compound 2-6.

Synthesis of compound **CI-6** was shown in Scheme 2.5. 5-Chlorothiophene-2-carboxylic acid (compound **2-7)** reacted with oxalyl chloride to give acyl chloride **2-8**, which further underwent replacement reaction with amine **2-5** under basic conditions to produce compound **CI-6**.

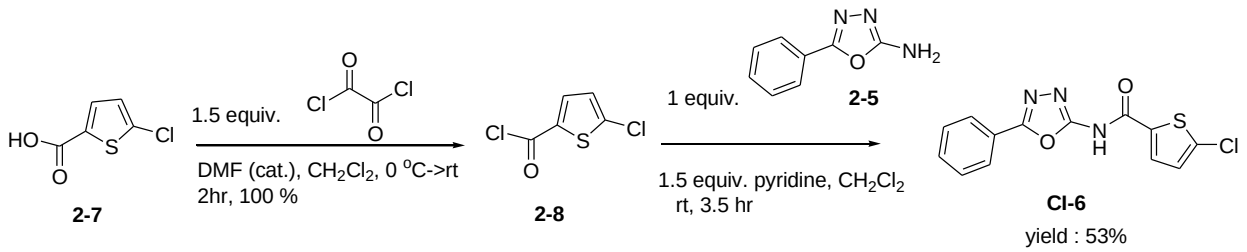

Scheme 2.5. Synthesis of compound CI-6.

2.4 Bio-evaluation

Bio-evaluation was performed by our collaborators Dr. Bende Zou, Dr. Christopher A. Lieu and Dr. Conrado Pascual in Dr. Xinmin (Simon) Xie's laboratory at AfaSci Research Laboratory in Redwood City, California.

2.4.1 Methods

2.4.1.1 Patch clamp recordings

Patch clamp recordings experiments were performed following reported procedure[38] (Description of the patch clam recording method was reprinted with permission from Jianyu Lu et al.[38] *Bioorganic & Medicinal Chemistry* **2015**, *23*, 5985-5998. Copyright © 2015 Elsevier Ltd. License #4073710444987) and the mouse dorsal root ganglion (DRG) was prepared following reported procedure[38].

Whole-cell voltage clamp recordings were performed on large size (30-50 μM in diameter) mouse dorsal root ganglion (DRG) neurons within 2 days after acutely dissociation. All experiments were performed at room temperature (around 21^{o}C). Whole-cell currents were recorded using a MultiClamp 700B amplifier and analyzed offline with pClAMP10.4 software (Axon CNS, Molecular Devices, formerly Axon Instruments). To record calcium currents, the external solution was composed of (in mM) 115 choline-Cl, 30 TEA-Cl, 2 $CaCl_2$, 10 glucose and 10 HEPES (pH 7.30-7.4 adjusted with TEA-OH and osmolality verified as 295 mOsm/kg). The internal solution was composed of (in mM) 125 CsCl, 10 HEPES (acid), 10 EGTA, 2 $CaCl_2$, 1 $MgCl_2$, 4 MgATP and 0.3 MgGTP (pH 7.3-7.4 adjusted with CsOH, and the osmolality verified as 295 mOsm/kg). Since sodium component was removed in the external solution, TTX was not

needed. To record sodium currents, the external solution was remained as modified Kreb's solution specified above. The internal solution was composed of (in mM) 120 CsF, 10 HEPES, 11 EGTA, 1 $CaCl_2$, 1 $MgCl_2$, 10 TEA-Cl, 4 MgATP and 0.3 MgGTP (pH 7.3-7.4 adjusted with CsOH). In this recording condition, no obvious calcium components were observed in most cells. Occasionally, some L-type calcium components were observed but completely decayed quickly, perhaps due to high concentration of sodium component in the external solution. To record potassium currents, the external solution was remained as a modified Kreb's solution specified above. The internal solution was composed of (in mM) 65 KCl, 80 KF, 5 KOH, 10 EGTA, 2 MgATP (pH 7.350-7.4 adjusted with KOH). Recording electrodes were pulled by P-87 puller (Sutter Instrument Co.). The tip of resistance was 3–4 MΩ in bath and the series resistance was less than 10 MΩ after whole cell configuration. All compounds were purchased from Sigma unless specifically remarked. Drugs were bath applied to 1.5 mL external solution in the recording chamber and the final concentration was calculated as an even diffusion system.

2.4.1.2 Seizure models

Seizure models were induced by pentylenetetrazole [40 mg/kg, intraperitoneal (i.p.) route] or maximal electronic shocks in mice following reported *in vivo* pharmacology assays[39]. Oxadiazole molecules were administered at 30 mg/kg concentration (i.p.).

***in vivo* Pharmacology Assays**(The description of methods was adapted with permission from Kristian Kaufmannet al[39], *ACS Chemical Neuroscience* **2013**, *4*, 1278-1286. Copyright © 2013 American Chemical Society.)

For the pentylenetetrazole (PTZ)-induced seizure model, male mice (C57/BL6, 8-10 months old, approximately 30 g) were injected intraperitoneally with either compounds **CI-2** and **CI-6** (30 mg/kg), sodium valproate (150 mg/kg), or vehicle (2% DMSO in 0.5% aqueous hydroxypropyl cellulose). After 30 min, PTZ was administered intraperitoneally (40 mg/kg). Immediately following administration of PTZ, the amount of time elapsed until the onset of convulsions, and death was recorded. If a mouse did not die after 20 min post-PTZ, the mouse was euthanized by isoflurane inhalation. The average convulsion latencies (in minutes) and the fatality rates of the

CI-2 and **CI-6** group, the sodium valproate group, and the vehicle group were compared (n = 8 mice/group).

For the maximal electroshock seizure (MES) model, male, C57/BL6 mice (8-10 months old, approximately 30 g), were injected intraperitoneally with either compounds **CI-2** and **CI-6** (30 mg/kg), sodium valproate (150 mg/kg) or vehicle. MES stimulation was applied, 30 min after injection, through trans auricular (ear-clip) electrodes from an electroshock apparatus, HSE Shock Stimulator Type 221, (Harvard Apparatus, Holliston, MA) using the following parameters: 100 mA fixed current, a 50-60 Hz pulse frequency, a 0.6 ms pulse width, and a 0.3 s stimulus duration. Animals were restrained by hand when applying the electrodes and released at the moment of stimulation to permit observation of the seizure throughout its entire course. Upon completion of the electrical stimulus, the time to onset of seizures was recorded. A 10 min cutoff was applied to all mice after which time the mice were euthanized by isoflurane inhalation. In this modified MES test, the electrical stimulus that was applied was sufficient to induce seizures and death from maximal seizure in 100% of the mice. For the MES study, the test groups contained 10 animals, 8 animals, and 7 animals for the vehicle, sodium valproate, and **CI-2** and **CI-6** treatments, respectively.

In all cases, experiments were conducted in a blind manner with respect to the experimenters. Data were evaluated in Excel using one-tailed, unpaired Student's t test, assuming populations with unequal variance.

2.4.2 Results and discussion

2.4.2.1 Inhibition of T-type calcium channel and seizure

All of the synthesized small molecules (**CI-1** to **CI-10**) were tested for their T-type calcium current inhibition. Five of the compounds (**CI-1**, **CI-2**, **CI-3**, **CI-6** and **CI-7**) were tested for their inhibition selectivity towards sodium and potassium currents. Two of them (compound **CI-2** and **CI-6**) were further tested towards their inhibition of seizure induced death in mice models. The bio-evaluation results were summarized in Table 2.2. Except compounds **CI-5**, **CI-8** and **CI-9**, all other designed molecules showed inhibition towards T-type calcium currents.

In the seizure inhibition study of mice models, fatality rate is calculated as the percentage of mice within each treatment group that dies within the 20 min observation period. Fatality rate was used to characterize a **CI** compound's ability to prevent death resulting from PTZ-induced seizures. Percentage of inhibition of seizure induced death was used to show the final results in Table 2.2 and it was calculated as 100%-fatality rate.

Code name	**Chemical structure**	**Inhibition**			
		T-Ca % 1 μM	**Na % 1 μM**	**K % 1 μM**	**Inhibition of seizure induced death (%)**
CI-1	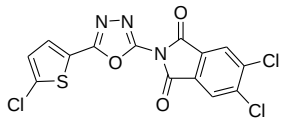	9.8 (1, 3.3 μM)	0 (1, 3.3 μM)	-17.8 (3.3 μM)	0
CI-2	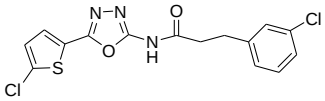	20.4	82.2 (3.3 μM)	-15.6 (3.3 μM)	29.6
CI-3	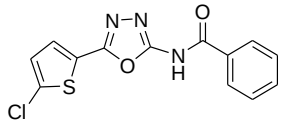	24.4	-71.8	-28.6	NT
CI-4	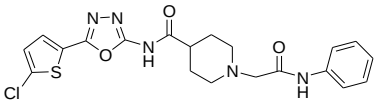	79.5	NT	NT	NT
CI-5	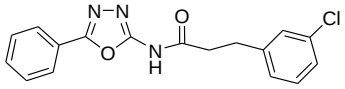	5	NT	NT	NT
CI-6	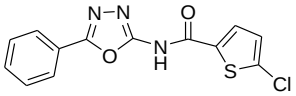	50 IC_{50}=0.93 μM	16.5 ±8.9% (n=7)	24.1	72.1
CI-7	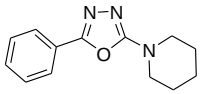	64.6 ± 14.1% (n=2)	25.7 ±6.3% (n=5)	21.9 ± 8.6% (n=4)	NT
CI-8	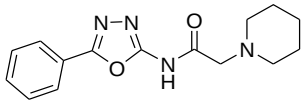	inactive	NT	NT	NT
CI-9	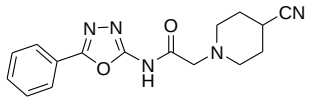	inactive	NT	NT	NT

CI-10	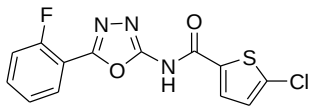	60.9	NT	NT	NT

Table 2.2. *in vitro* and *in vivo* Bioactivities of synthesized 1,3,4-oxadiazole derivatives. (NT: not test)

Among the active T-type calcium channel inhibitors, two compounds (**CI-6** and **CI-7**) showed some extent selectivity in the inhibition of T-type calcium currents towards sodium and potassium currents. As summarized in Table 2.3, both **CI-6** and **CI-7** showed good inhibition (> 50%) in T-type Ca^{2+} currents and lower inhibition (~20 %) of voltage-gated Na^{+} or K^{+} currents

Code name	**Chemical structure**	**Inhibition**		
		T-Ca **% 1 µM**	**Na** **% 1 µM**	**K** **% 1 µM**
CI-6	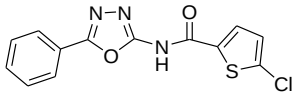	50 IC_{50}=0.93 µM	16.5 ±8.9 (n=7)	24.1
CI-7	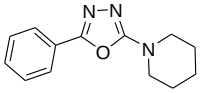	64.6 ± 14.1% (n=2)	25.7 ±6.3% (n=5)	21.9 ± 8.6% (n=4)

Table 2.3. Compounds CI-6 and CI-7 showed selective T-type calcium channel inhibition.

Studies on seizure induced death in mice models were performed on **CI-2** and **CI-6** and the results were summarized in Table 2.4. **CI-2** had low inhibition (20% inhibition) towards T-type calcium channel and suppressed 29.6% seizure induced death. **CI-6** was a better T-type calcium channel inhibitor (50% inhibition) and led to a prominent enhancement (from 29.6% to 72.1%) in the inhibition of seizure induced death. Results of seizure model studies indicated that inhibition of T-type calcium channels would lead to inhibition of seizure. Thus, T-type calcium channels could be a potential biological target for the treatment of epilepsy.

Code name	Chemical structure	Inhibition			
		T-Ca % 1 µM	Na % 1 µM	K % 1 µM	Inhibition of seizure induced death(%)
CI-2	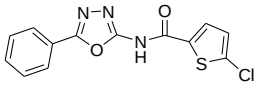	20.4	82.2 (3.3 µm)	-15.6 (3.3 µm)	29.6
CI-6	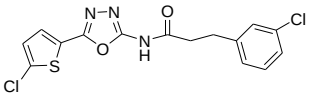	50 IC_{50}=0.93 µM	16.5 ±8.9 (n=7)	24.1	72.1

Table 2.4. Inhibition results of seizure induced death in mice models for compounds CI-2 and CI-6

2.4.2.2 Structure-activity relationship towards inhibition of T-type calcium channel

As summarized in Table 2.5, the oxadiazole pharmacophore does not tolerate aliphatic rings in part B (compounds **CI-5**, **CI-8** and **CI-9**), aromaticity (compounds **CI-6** and **CI-10**) or rigidity (compound **CI-7**) is needed. Enhancement of T-type calcium channel inhibition can be achieved through further structural modification of in part A (compound **CI-6** versus **CI-10**).

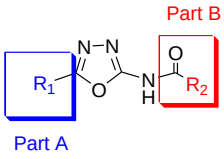

Code name	Chemical Structral	Inhibition T-Ca % 1 µM	Code name	Chemical Structral	Inhibition T-Ca % 1 µM
CI-5	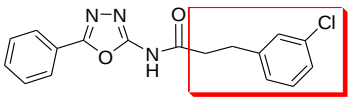	5	**CI-8**	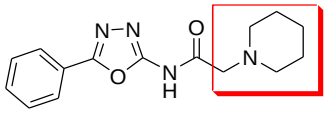	inactive
CI-6	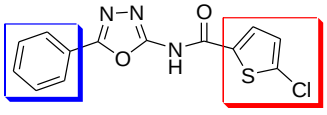	50	**CI-9**	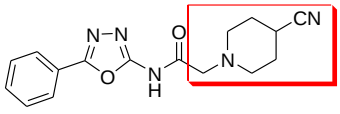	inactive

CI-7	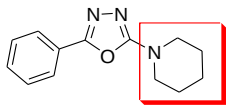	64.6	**CI-10**	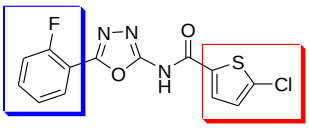	60.9

Table 2.5. Structure-activity relationship (SAR) summary towards inhibition of T-type calcium channel.

2.4.2.3 Lead compound CI-6 versus reported T-type calcium channel inhibitor Z944

Z944 (Figure 2.5) is a T-type calcium channel inhibitor reported by Zalicus Inc. in the year of 2012[40]. It is a new drug discovered for the treatment of pain and now in initial phase two of clinical trial. Inhibitions of different channels (Ca^{2+}, Na^{+}, K^{+}) by **Z944** using patch clamp recordings were performed. The **Z944** test results were compared with our lead compound **CI-6** as shown in Figure2.6. **CI-6** had dose dependently effect on the inhibition of T-type Ca^{2+} currents suggesting its specific inhibition (Figure 2.6.A). Unlike **CI-6** that can selectively inhibit T-type Ca^{2+} over Na^{+} (Figure 2.6.B) and K^{+} currents (Figure 2.6.C), **Z944** also blocked Na^{+} currents in a dose dependently manner (Figure 2.6.D).

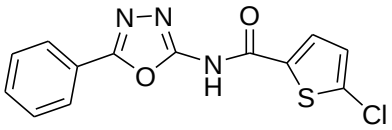

CI-6

T-type IC_{50} = 0.93 μM (EP)

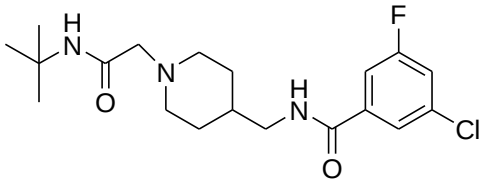

Z944, Zalicus

$Ca_v3.2$ IC_{50} = 0.05 μM (FLIPR)

FLIPR: fluoresent imaging plate reader
EP: electrophysiology

Figure 2.5. Chemical structures of Z944 and compound CI-6.

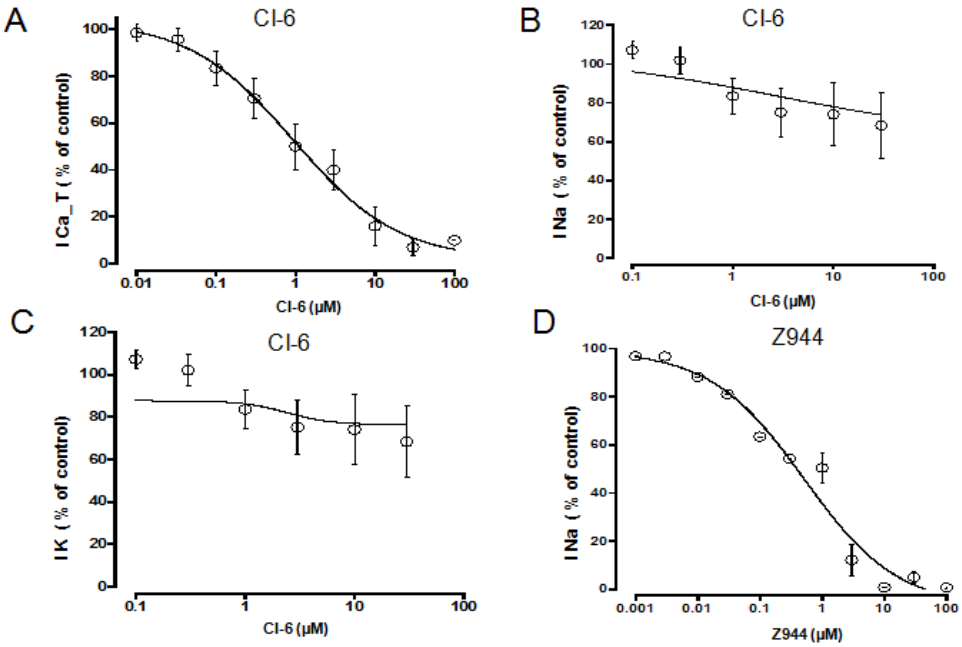

Figure 2.6. CI-6 blocked the native T-type calcium currents recorded on DRG neurons in dose dependently manner (A). CI-6 slightly inhibited sodium (B) and potassium (C) mediated currents recorded on DRG. The effect was not dose dependently, suggesting the unspecific inhibition. (D) Z944 blocked the voltage dependent sodium currents. Each point represents the averaged data of 3-7 cells. (This figure was reprinted from Poster #152.08/M33, which was presented by Simon Xie, et al. at Neuroscience 2015 Annual Meeting in Chicago.[41]**)**

2.4.2.4 Concerns

The bio-evaluations performed so far were just focused on the evaluation of efficacy. With an understanding of structure-activity relationship (SAR), more derivatives could be designed and synthesized in order to find more potent inhibitors in the future. However, attentions should not only be addressed on the improvement of potency. More explorations for their pharmacokinetics properties needed to be done in order to find lead compounds with good drug-like properties. One major drawback of the current designed 1,3,4-oxadiazole derivatives is poor solubility. Future structural optimization should pay more attention to the increase of solubility.

2.5 Conclusion

A series of 1,3,4-oxadiazole derivatives was designed and synthesized as T-type calcium channel blockers. The designed small molecules were screened for their ability and selectivity towards inhibition of T-type calcium channels. Two hit compounds (**CI-6** and **CI-7**) were found to possess good inhibition on T-type Ca^{2+} currents and lower inhibition on voltage-gated Na^{+} or K^{+} currents. Structure-activity relationship (SAR) was discussed based on the results of T-type calcium currents inhibition. Either aromaticity or rigidity is efficacy-necessary in the construction of part B. Studies on seizure models in mice showed that inhibition of T-type calcium channel could lead to inhibition of seizure induced death. Among various 1,3,4-oxadiazole derivatives, compound **CI-6** was found to be the lead compound. **CI-6** was a good T-type calcium channel inhibitor (IC_{50} = 0.93 μM), which could suppress 72% seizure induced death in mice models. Further structural optimization of **CI-6** could be conducted in the future to discover more potent inhibitors with better drug-like properties.

2.6 Synthetic experimental procedures

2.6.1 General

Chemicals were purchased from Fisher Scientific, VWR international LLC and Chem-Impex International, Inc.. NMR spectra were taken from a 400 MHz Spectrometer (Varian Inc.) in chloroform-D unless otherwise informed. Mass spectra were obtained from an API 2000-triple quadrupole ESI-MS/MS mass spectrometer (Applied Biosystems).

2.6.2 Representative synthesis

2.6.2.1 *N-(Carbamothioylamino)-5-chlorothiophene-2-carboxamide (Compound 2-2)*

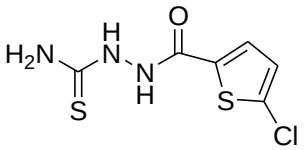

2-2

To a solution of 1 g (6.1 mmol, 1 equiv.) of 5-chlorothiophene-2-carboxylic acid (commercially available from Chem-Impex International, Inc.) in 13 mL of distilled ethyl acetate at 0^{o}C, 940

mg (7.4 mmol, 1.2 equiv.) of oxalyl chloride was added followed by the addition of 2 drops of distilled *N*,*N*-dimethyl formamide (DMF). The resulting reaction solution was kept stirring under argon at 0^{o}C for 2 h and concentrated to dryness to yield 5-chlorothiophene-2-carbonyl chloride. The crude acyl chloride was directly used in the next step without further purification, assuming the yield of 5-chlorothiophene-2-carbonyl chloride was 100%.

A suspension of 1.22 g (13 mmol, 2.2 equiv.) of thiosemicarbazide (compound **2-1,** commercially available from Chem-Impex International, Inc.) in 10 mL of distilled THF was cooled to 0^{0}C under argon. To it, a solution of 1.105g (6.1mmol, 1 equiv.) of 5-chlorothiophene-2-carbonyl chloride in 10 mL of distilled THF was added slowly under argon at 0^{0}C. Allowed the resulting reaction mixture to slowly warm to room temperature and kept it stirring overnight. To the reaction mixture, 100 mL of distilled water was added. The precipitated white solid crude product was collected by filtration, washed with distilled water, and dried under vacuum to yield 870 mg (60% yield) of compound **2-2** as a white solid. ^{1}H NMR (DMSO-d_6) δ ppm 7.22 (d, J=4.30 Hz, 1 H) 7.61 - 7.76 (m, 2 H) 7.92 (br. s., 1 H) 9.37 (br. s., 1 H) 10.50 (s, 1 H). MS (positive mode), m/z calcd for $C_6H_6ClN_3OS_2Na$ $(M+Na)^+$ 258.0, found 258.3.

2.6.2.2 ***1-Benzoyl-3-thiosemicarbazide (Compound 2-3)***

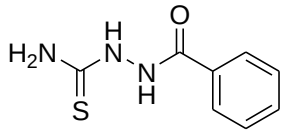

2-3

A suspension of 4 g (43.8mmol, 2.2 equiv.) of thiosemicarbazide (compound **2-1,** commercially available from Chem-Impex International, Inc.) in 100 mL of distilled THF was cooled to 0^{0}C under argon. To it, a solution of 2.8 g (19.91mmol, 1equiv.) of benzoyl chloride (commercially available from Fisher Scientific) in 20 mL of distilled THF was added slowly under argon at 0^{0}C. Allowed the resulting reaction mixture to slowly warm to room temperature and kept it stirring under argon overnight. Reaction solution was concentrated to get rid of most THF. To the reaction residue, 100 mL of distilled water and 10 mL of saturated $NaHCO_3$ solution were added. The precipitated white solid crude product was collected by filtration, washed with hexane and dried under vacuum to yield 3.8 g (100% yield) of compound **2-3** as a white solid. ^{1}H NMR (DMSO-d_6) δ ppm 1.91 (m, J=7.00 Hz, 1 H) 7.47 (t, J=7.13 Hz, 2 H) 7.51 - 7.59 (m, 1 H) 7.62

(br. s., 1 H) 7.79 - 7.93 (m, 3 H) 9.36 (br. s., 1 H). MS (positive mode), m/z calcd for $C_8H_9N_3OSNa$ $(M+Na)^+$ 218.05, found 218.1.

2.6.2.3 ***5-(5-Chlorothiophen-2-yl)-1,3,4-oxadiazol-2-amine (Compound 2-4)***

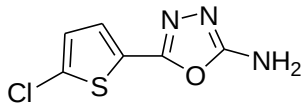

2-4

A solution of 612 mg (3.69 mmol, 0.3 equiv.) of KI in 7 mL of distilled water was cooled to 0^0C. To it, 2.9 g of compound **2-2** (12.3 mmol, 1 equiv.) was added followed by 20 mL of distilled water and 4.6 mL of 4N NaOH aqueous solution (18.45mmol, 1.5 equiv.). To the resulting solution, 3.87 g of 1,3-dibromo-5,5- dimethylhydantoin (13.53 mmol, 1.1 equiv, commercially available from Chem-Impex International, Inc.) was added. The resulting mixture was kept stirring under argon at room temperature for 7 h. To the reaction mixture, 3.6 mL of saturated $NaHSO_3$ aqueous solution was added. Aqueous layer was extracted four times with ethyl acetate (150 mL each time). Combined organic layers were washed with brine, dried over Na_2SO_4, filtered, and concentrated. Crude product was crystallized from ethyl acetated (80 mL) to yield 1.2 g (49% yield) of compound **2-4** as yellow crystals. ^{1}H NMR (DMSO-d_6) δ ppm 7.24 (d, J=4.30 Hz, 1 H) 7.33 - 7.38 (m, 3 H). ^{13}C NMR (DMSO-d_6) δ ppm 163.5, 152.6, 130.7, 128.2, 126.9, 124.6. MS (positive mode), m/z calcd for $C_6H_5ClN_3OS$ $(M+H)^+$ 202.0, found 202.0.

2.6.2.4 ***5-Phenyl-1,3,4-oxadiazol-2-amine (Compound 2-5)***

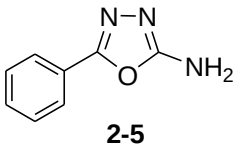

2-5

Procedure was similar to the synthesis of compound **2-4** (see section 2.6.2.3). Started from 3.8 g (19.48 mmol, 1equiv.) of compound **2-3**, 1.3 g (41% yield) of compound **2-5** was obtained as yellow crystals after crystallization. ^{1}H NMR (DMSO-d_6) δ ppm 7.28 (br. s., 2 H) 7.40 - 7.62 (m, 3 H) 7.68 - 7.94 (m, 2 H). MS (positive mode), m/z calcd for $C_8H_8N_3O$ $(M+H)^+$ 162.06, found 162.3.

2.6.2.5 ***5,6-Dichloro-2-(5-(5-chlorothiophen-2-yl)-1,3,4-oxadiazol-2-yl)isoindoline-1,3-dione (Compound CI-1)***

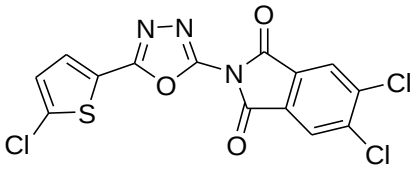

CI-1

To a solution of 94 mg (0.35 mmol, 1 equiv.) of 4,5-dichlorophthalic acid in 4 mL of distilled dichloromethane at 0^{o}C, 107 mg (0.84 mmol, 2.4 equiv.) of oxalyl chloride (commercially available from Fisher Scientific) was added dropwise followed by adding 1 drop of distilled DMF. The resulting reaction solution was kept refluxing under argon for 3.5 h and concentrated to dryness to give 95 mg (100% yield) of 4,5-dichlorobenzene-1,2-dioyl dichloride as a white solid. The formed 4,5-dichlorobenzene-1,2-dioyl dichloride was directly used for next step without purification

To a suspension of 70 mg (0.35 mmol, 1 equiv.) of compound **2-4** in 3 mL of distilled dichloromethane, was added 82 mg (1.04 mmol, 3 equiv.) of anhydrous pyridine and allowed the resulting mixture to cool to 0^{o}C under argon. To it, a solution of 95 mg (0.35 mmol, 1 equiv.) 4,5-dichlorobenzene-1,2-dioyl dichloride in 0.5 mL of distilled dichloromethane was added dropwise at 0^{o}C and kept stirring under argon at room temperature for 5 h. The resulting reaction solution was partitioned between 200 mL of dichloromethane and 30 mL of 10% aqueous $NaHCO_3$ solution. Organic layer was isolated and washed with brine, dried over Na_2SO_4, filtered, concentrated and column chromatographed on silica gel using a gradient mixture of hexane and ethyl acetate as eluent to give 30 mg (22% yield) of compound **CI-1** as a beige solid. ^{1}H NMR (DMSO-d_6) δ ppm 7.40 (d, J=4.00 Hz, 1 H) 7.75 (d, J=4.00 Hz, 1 H) 8.40 - 8.48 (m, 2 H). ^{13}C NMR (DMSO-d_6) δ ppm 161.7, 159.3, 151.2, 138.7, 134.4, 131.1, 131.0, 129.0, 126.5, 122.1. MS (positive mode), m/z calcd for $C_{14}H_4Cl_3N_3O_3SNa$ $(M+Na)^+$ 421.9, found 422.0.

2.6.2.6 ***3-(3-Chlorophenyl)-N-(5-(5-chlorothiophen-2-yl)-1,3,4-oxadiazol-2-yl)propanamide (Compound CI-2)***

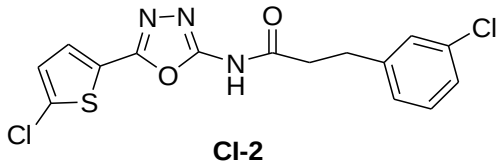

CI-2

To a solution of 46 mg (0.25 mmol, 1 equiv.) of 3-(3-Chlorophenyl)propionic acid (commercially available from Chem-Impex International, Inc.) in 3 mL of distilled ethyl acetate at 0^{o}C, 38 mg (0.30 mmol, 1.2 equiv.) of oxalyl chloride was added followed by adding 1 drop of distilled DMF. The resulting reaction solution was kept stirring under argon at 0^{o}C for 2 h and concentrated to dryness to produce 3-(3-chlorophenyl)propanoyl chloride as a white solid. The crude acyl chloride was directly used for next step without further purification, assuming the yield of 3-(3-chlorophenyl)propanoyl chloride was 100%.

To a suspension of 50 mg (0.25 mmol, 1 equiv.) of compound **2-4** in 3 mL of distilled dichloromethane under argon, was added 30 mg (0.38 mmol, 1.5 equiv.) of anhydrous pyridine. To the resulting reaction mixture, a solution of 50 mg (0.25 mmol, 1 equiv.) of 3-(3-chlorophenyl)propanoyl chloride in 0.3 mL of distilled dichloromethane was added and kept stirring at room temperature under argon for 5 h. The resulting reaction solution was partitioned between 300 mL of ethyl acetate and 40 mL of 10% aqueous $NaHCO_3$ solution. Organic layer was isolated and washed with brine, dried over Na_2SO_4, filtered, concentrated and column chromatographed on silica gel using a gradient mixture of hexane and ethyl acetate as eluent to produce 59 mg (64% yield) of compound **CI-2** as a white solid. ^{1}H NMR (DMSO-d_6) δ ppm 2.78 (t, J = 7.42 Hz, 2 H) 2.91 (t, J = 7.42 Hz, 2 H) 7.16 - 7.41 (m, 5 H) 7.55 (d, J = 3.91 Hz, 1 H). ^{13}C NMR (DMSO-d_6) δ ppm 169.8, 156.9, 155.6, 143.3, 132.9, 132.6, 130.2, 129.1, 128.6, 128.2, 127.1, 126.1, 123.3, 36.8, 29.5. MS (positive mode), m/z calcd for $C_{15}H_{11}Cl_2N_3O_2SNa$ $(M+Na)^+$ 390.0, found 389.9.

2.6.2.7 ***N-(5-(5-Chlorothiophen-2-yl)-1,3,4-oxadiazol-2-yl)benzamide (Compound CI-3)***

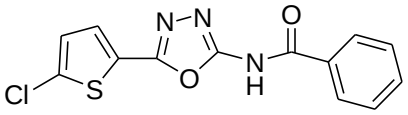

CI-3

To a solution of 70 mg of compound **2-4** (0.347 mmol, 1eq) in 3mL of distilled dichloromethane under argon, 40 μL of anhydrous pyridine (0.347 mmol, 1eq) was added. Allowed the resulting reaction mixture to cool to 0^{0}C. To it, 73 mg of distilled benzoyl chloride (0.520 mmol, 1.5 eq) was slowly added under argon at 0^{0}C. Allowed it to slowly warm to room temperature and kept

stirring for 4 h at room temperature. Reaction solution was diluted with 200 mL of dichloromehane. Organic layer was isolated and washed with saturated $NaHCO_3$ aqueous solution, brine, dried over Na_2SO_4, filtered, and concentrated. Crude product was crystallized from ethanol to produce 5 mg (6% yield) of compound **CI-3**. ^{1}H NMR (DMSO-d_6) δ ppm 7.27 - 7.39 (m, 1 H) 7.47 - 7.59 (m, 2 H) 7.59 - 7.73 (m, 3 H) 7.98 - 8.10 (m, 2 H). MS (positive mode), m/z calcd for $C_{13}H_8CN_3O_2SNa$ $(M+Na)^+$ 328.0, found 328.0.

2.6.2.8 ***2-(4-Cyanopiperidin-1-yl)-N-phenylacetamide (Compound 2-6-3)***

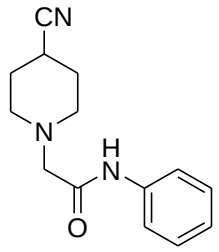

2-6-3

To a mixture of 3 g (17.7 mmol) of 2-chloro-N-phenylacetamide (compound **2-6-2**) and 4.88 g (35.3 mmol) of anhydrous K_2CO_3 in 25 mL of distilled acetonitrile was added 1.95 g (17.7 mmol) of 4-cyanopiperidne (compound **2-6-1**). The resulting reaction mixture was refluxed under argon for 8 h. Organic layer was isolated by filtration, concentrated, and column chromatographed on silica gel using a gradient mixture of dichloromethane and methanol as eluent to give 4.28 g (99% yield) of compound **2-6-3** as a while solid. ^{1}H NMR δ ppm 1.81 - 2.23 (m, 4 H) 2.35 - 2.93 (m, 4 H) 3.10 (s, 2 H) 7.09 (dd, J = 7.80 Hz, 1 H) 7.31 (dd, J = 7.80 Hz, 2 H) 7.48 - 7.63 (m, 2 H). ^{13}C NMR δ ppm 167.9, 137.5, 129.1 (2C), 124.4, 121.3, 119.6 (2C), 62.3 (2C), 51.9, 29.0 (2C), 25.6. MS (positive mode), m/z calcd for $C_{14}H_{18}N_3O$ $(M+H)^+$ 244.0, found 244.5.

2.6.2.9 ***1-((Phenylcarbamoyl)methyl)-N-(5-(5-chlorothiophen-2-yl)-1,3,4-oxadiazol-2-yl)piperidine-4-carboxamide (Compound CI-4)***

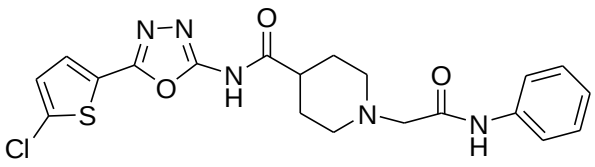

CI-4

To a solution of 138 mg (0.57 mmol, 1 equiv.) of compound **2-6-3** in 5 mL of methanol, 2 mL of 3N NaOH aqueous solution was added and kept refluxing overnight. Concentrated reaction solution to get rid of most methanol. Resulting residue was neutralized with 2 N HCl aqueous solution and lyophilized to dryness under vacuum to yield compound **2-6** together with NaCl as white solids mixture. The crude mixture was directly used for next step without further purification, assuming the yield of carboxylic acid **2-6** was 100%.

A mixture of 150 mg (0.57 mmol, 1 eaquiv.) of compound **2-6**, 114 mg (0.57 mmol, 1 equiv.) of compound **2-4**, 328 mg (1.71 mmol, 3 equiv.) of EDC and 209 mg (1.71 mmol, 3 equiv.) of DMAP in 2 mL of distilled DMF and 2mL of distilled dichloromethane was kept stirring at 50^{o}C overnight under argon. The resulting reaction mixture was diluted with 40 mL of distilled water and adjusted to pH = 3 using 2N HCl aqueous solution. The resulting aqueous layer was extracted with dichloromethane twice. Combined organic layers were washed with brine, dried over Na_2SO_4, filtered, concentrated and column chromatographed on silica gel using a gradient mixture of dichloromethane and methanol as eluent to give 28 mg (11% yield) of compound **CI-4** as a beige solid. ^{1}H-NMR: (400 MHz, DMSO-d_6) δ ppm1.67-1.90 (m, 4H), 2.2 (t, J=11.13 Hz, 2H), 2.87-2.97 (m, 3H), 3.13 (br. s., 2 H), 7.05 (dd, J=7.20 Hz, 1H), 7.26-7.36 (m, 3H), 7.57 (d, J=3.91 Hz, 1H), 7.64 (d, J=8.20 Hz, 2H), 9.69 (br.s., 1H, NH), 11.82 (br.s., 1H, NH). MS (positive mode), m/z calcd for $C_{20}H_{21}ClN_5O_3S$ $(M+H)^+$ 446.1, found 446.3.

2.6.2.10 *5-Chloro-N-(5-phenyl-1,3,4-oxadiazol-2-yl)thiophene-2-carboxamide (Compound CI-6)*

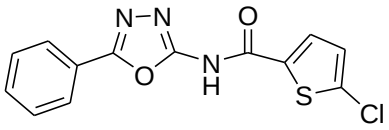

CI-6

The synthesis of 5-chlorothiophene-2-carbonyl chloride was discussed before (see section 2.6.2.1).

To a solution of 300 mg (1.86 mmol, 1 equiv.) of compound **2-5** in 10 mL of distilled dichloromethane, 220 mg (2.79 mmol, 1.5 equiv.) of anhydrous pyridine was added and allowed it to cool to 0^{o}C. To it, a solution of 337 mg (1.86 mmol, 1equiv.) of 5-chlorothiophene-2-

carbonyl chloride in 5 mL of distilled dichloromethane was added dropwise. The resulting reaction mixture was kept stirring under argon at room temperature for 3.5 h. Resulting reaction solution was diluted with 40 mL of 10% $NaHCO_3$ aqueous solution and extracted with dichloromethane three times. Combined organic layers were washed with brine, dried over Na_2SO_4, filtered, concentrated and column chromatographed on silica gel using a gradient mixture of hexane and ethyl acetate as eluent to give 300 mg (53% yield) of compound **CI-6** as a white solid. ^{1}H NMR δ ppm 7.06 (d, J=4.30 Hz, 1 H) 7.49 - 7.67 (m, 3 H) 7.98 (d, J=7.42 Hz, 2 H) 8.12 (d, J=4.30 Hz, 1 H) 8.22 (br. s., 1 H). ^{13}C NMR δ ppm 158.2, 154.3, 151.3, 142.1, 137.3 133.3, 129.9, 129.4, 127.2, 127.1, 122.4. MS (positive mode), m/z calcd for $C_{13}H_8ClN_3O_2SNa$ $(M+Na)^+$ 328.0, found 327.8.

Reference

(1) Catterall, W. A.; Perez-Reyes, E.; Snutch, T. P.; Striessnig, J. International Union of Pharmacology. XLVIII. Nomenclature and structure-function relationships of voltage-gated calcium channels. *Pharmacological reviews* **2005**, *57*, 411-425.

(2) Catterall, W. A. Voltage-gated calcium channels. *Cold Spring Harbor perspectives in biology* **2011**, *3*, a003947.

(3) Iftinca, M. C. Neuronal T-type calcium channels: what's new? Iftinca: T-type channel regulation. *Journal of medicine and life* **2011**, *4*, 126-138.

(4) Cribbs, L. L.; Lee, J. H.; Yang, J.; Satin, J.; Zhang, Y.; Daud, A.; Barclay, J.; Williamson, M. P.; Fox, M.; Rees, M.; Perez-Reyes, E. Cloning and characterization of alpha1H from human heart, a member of the T-type Ca2+ channel gene family. *Circ Res* **1998**, *83*, 103-109.

(5) Monteil, A.; Chemin, J.; Bourinet, E.; Mennessier, G.; Lory, P.; Nargeot, J. Molecular and functional properties of the human alpha(1G) subunit that forms T-type calcium channels. *J Biol Chem* **2000**, *275*, 6090-6100.

(6) Perez-Reyes, E.; Cribbs, L. L.; Daud, A.; Lacerda, A. E.; Barclay, J.; Williamson, M. P.; Fox, M.; Rees, M.; Lee, J. H. Molecular characterization of a neuronal low-voltage-activated T-type calcium channel. *Nature* **1998**, *391*, 896-900.

(7) Lee, J. H.; Daud, A. N.; Cribbs, L. L.; Lacerda, A. E.; Pereverzev, A.; Klockner, U.; Schneider, T.; Perez-Reyes, E. Cloning and expression of a novel member of the low voltage-activated T-type calcium channel family. *J Neurosci* **1999**, *19*, 1912-1921.

(8) McKay, B. E.; McRory, J. E.; Molineux, M. L.; Hamid, J.; Snutch, T. P.; Zamponi, G. W.; Turner, R. W. Ca(V)3 T-type calcium channel isoforms differentially distribute to somatic and dendritic compartments in rat central neurons. *Eur J Neurosci* **2006**, *24*, 2581-2594.

(9) Talley, E. M.; Cribbs, L. L.; Lee, J. H.; Daud, A.; Perez-Reyes, E.; Bayliss, D. A. Differential distribution of three members of a gene family encoding low voltage-activated (T-type) calcium channels. *J Neurosci* **1999**, *19*, 1895-1911.

(10) Vassort, G.; Talavera, K.; Alvarez, J. L. Role of T-type Ca2+ channels in the heart. *Cell Calcium* **2006**, *40*, 205-220.

(11) Cribbs, L. T-type calcium channel expression and function in the diseased heart. *Channels (Austin, Tex.)* **2010**, *4*, 447-452.

(12) Fry, C. H.; Sui, G.; Wu, C. T-type Ca2+ channels in non-vascular smooth muscles. *Cell Calcium* **2006**, *40*, 231-239.

(13) Beam, K. G.; Knudson, C. M. Effect of postnatal development on calcium currents and slow charge movement in mammalian skeletal muscle. *The Journal of general physiology* **1988**, *91*, 799-815.

(14) Hagiwara, S.; Ozawa, S.; Sand, O. Voltage clamp analysis of two inward current mechanisms in the egg cell membrane of a starfish. *The Journal of general physiology* **1975**, *65*, 617-644.

(15) Nilius, B.; Talavera, K.; Verkhratsky, A. T-type calcium channels: The never ending story. *Cell Calcium* **2006**, *40*, 81-88.

(16) http://nationalacademies.org/hmd/~/media/Files/Report%20Files/2012/Epilepsy/epilepsy_slides.pdf.

(17) MOI. *Epilepsy across the spectrum: Promoting health and understanding* for NAP: Washington DC 2012.

(18) http://www.epilepsy.com/learn/epilepsy-statistics.

(19) Heinemann, U.; Lux, H. D.; Gutnick, M. J. Extracellular free calcium and potassium during paroxsmal activity in the cerebral cortex of the cat. *Experimental brain research* **1977**, *27*, 237-243.

(20) Tsakiridou, E.; Bertollini, L.; de Curtis, M.; Avanzini, G.; Pape, H. C. Selective increase in T-type calcium conductance of reticular thalamic neurons in a rat model of absence epilepsy. *J Neurosci* **1995**, *15*, 3110-3117.

(21) Giordanetto, F.; Knerr, L.; Wallberg, A. T-type calcium channels inhibitors: a patent review. *Expert opinion on therapeutic patents* **2011**, *21*, 85-101.

(22) Shipe, W. D.; Barrow, J. C.; Yang, Z.-Q.; Lindsley, C. W.; Yang, F. V.; Schlegel, K.-A. S.; Shu, Y.; Rittle, K. E.; Bock, M. G.; Hartman, G. D.; Tang, C.; Ballard, J. E.; Kuo, Y.; Adarayan, E. D.; Prueksaritanont, T.; Zrada, M. M.; Uebele, V. N.; Nuss, C. E.; Connolly, T. M.; Doran, S. M.; Fox, S. V.; Kraus, R. L.; Marino, M. J.; Graufelds, V. K.; Vargas, H. M.; Bunting, P. B.; Hasbun-Manning, M.; Evans, R. M.; Koblan, K. S.; Renger, J. J. Design, Synthesis, and Evaluation of a Novel 4-Aminomethyl-4-fluoropiperidine as a T-Type Ca2+ Channel Antagonist. *Journal of Medicinal Chemistry* **2008**, *51*, 3692-3695.

(23) Xiang, Z.; Thompson, A. D.; Brogan, J. T.; Schulte, M. L.; Melancon, B. J.; Mi, D.; Lewis, L. M.; Zou, B.; Yang, L.; Morrison, R.; Santomango, T.; Byers, F.; Brewer, K.;

Aldrich, J. S.; Yu, H.; Dawson, E. S.; Li, M.; McManus, O.; Jones, C. K.; Daniels, J. S.; Hopkins, C. R.; Xie, X. S.; Conn, P. J.; Weaver, C. D.; Lindsley, C. W. The Discovery and Characterization of ML218: A Novel, Centrally Active T-Type Calcium Channel Inhibitor with Robust Effects in STN Neurons and in a Rodent Model of Parkinson's Disease. *ACS Chem Neurosci* **2011**, *2*, 730-742.

(24) Abernethy, D. R. Pharmacologic and Pharmacokinetic Profile of Mibefradil, a T- and L-type Calcium Channel Antagonist. *American Journal of Cardiology*, *80*, 4C-11C.

(25) Krayenbuhl, J. C.; Vozeh, S.; Kondo-Oestreicher, M.; Dayer, P. Drug-drug interactions of new active substances: mibefradil example. *European journal of clinical pharmacology* **1999**, *55*, 559-565.

(26) Yang, Z.-Q.; Schlegel, K.-A. S.; Shu, Y.; Reger, T. S.; Cube, R.; Mattern, C.; Coleman, P. J.; Small, J.; Hartman, G. D.; Ballard, J.; Tang, C.; Kuo, Y.; Prueksaritanont, T.; Nuss, C. E.; Doran, S.; Fox, S. V.; Garson, S. L.; Li, Y.; Kraus, R. L.; Uebele, V. N.; Taylor, A. B.; Zeng, W.; Fang, W.; Chavez-Eng, C.; Troyer, M. D.; Luk, J. A.; Laethem, T.; Cook, W. O.; Renger, J. J.; Barrow, J. C. Short-Acting T-Type Calcium Channel Antagonists Significantly Modify Sleep Architecture in Rodents. *ACS Medicinal Chemistry Letters* **2010**, *1*, 504-509.

(27) Galemmo, R.; Hum, G. Di-t-butylphenyl piperazines as calcium channel blockers WO2009132454

(28) Pajouhesh, H.; Kaul, R.; Ding, Y.; Zhu, Y.; Zhang, L.; Chakka, N.; Grimwood, M.; Tan, J.; Zhou, Y. N-piperidinyl acetamide derivatives as calcium channel blockers WO2009146540

(29) Bornemeier, D. A.; Cai, C.; Fors, K. S.; Hagen, T. J.; Holsworth, D. D.; Jalaie, M.; Leonard, D. M.; Moody, T. S.; Take, Y. Oxadiazole compounds as calcium channel antagonists WO2008050200

(30) Cuiman, C.; Duran, J. E.; Fors, K. S.; Hagen, T. J.; Holsworth, D. D.; Jalaie, M.; Leonard, D. M.; Poel, T. J.; Quin, I. J.; Take, Y. Substituted oxadiazole analogs as calcium channel antagonists WO2008117148

(31) de Oliveira, C. S.; Lira, B. F.; Barbosa-Filho, J. M.; Lorenzo, J. G.; de Athayde-Filho, P. F. Synthetic approaches and pharmacological activity of 1,3,4-oxadiazoles: a review of the literature from 2000-2012. *Molecules (Basel, Switzerland)* **2012**, *17*, 10192-10231.

(32) Vaidya, A.; Jain, S.; Jain, P.; Jain, P.; Tiwari, N.; Jain, R.; Jain, R.; Jain, A. K.; Agrawal, R. K. Synthesis and Biological Activities of Oxadiazole Derivatives: A Review. *Mini Rev Med Chem* **2016**, *16*, 825-845.

(33) Chawla, G.; Naaz, B.; Siddiqui, A. A. Exploring 1,3,4-Oxadiazole Scaffold For Anti-inflammatory And Analgesic Activities: A Review Of Literature From 2005-2016. *Mini Rev Med Chem* **2017**.

(34) Bankar, G. R.; Nampurath, G. K.; Nayak, P. G.; Bhattacharya, S. A possible correlation between the correction of endothelial dysfunction and normalization of high blood pressure levels by 1,3,4-oxadiazole derivative, an L-type Ca2+ channel blocker in deoxycorticosterone acetate and N(G)-nitro-l-arginine hypertensive rats. *Chemico-biological interactions* **2010**, *183*, 327-331.

(35) http://www.molinspiration.com/services/logp.html.

(36) Matsuno, K.; Masuda, Y.; Uehara, Y.; Sato, H.; Muroya, A.; Takahashi, O.; Yokotagawa, T.; Furuya, T.; Okawara, T.; Otsuka, M.; Ogo, N.; Ashizawa, T.; Oshita, C.; Tai,

S.; Ishii, H.; Akiyama, Y.; Asai, A. Identification of a New Series of STAT3 Inhibitors by Virtual Screening. *ACS Medicinal Chemistry Letters* **2010**, *1*, 371-375.

(37) Guda, D. R.; Cho, H. M.; Lee, M. E. Mild and convenient one-pot synthesis of 2-amino-1,3,4-oxadiazoles promoted by trimethylsilyl isothiocyanate (TMSNCS). *RSC Advances* **2013**, *3*, 7684-7687.

(38) Lu, J.; Aguilar, A.; Zou, B.; Bao, W.; Koldas, S.; Shi, A.; Desper, J.; Wangemann, P.; Xie, X. S.; Hua, D. H. Chemical synthesis of tetracyclic terpenes and evaluation of antagonistic activity on endothelin-A receptors and voltage-gated calcium channels. *Bioorganic & Medicinal Chemistry* **2015**, *23*, 5985-5998.

(39) Kaufmann, K.; Romaine, I.; Days, E.; Pascual, C.; Malik, A.; Yang, L.; Zou, B.; Du, Y.; Sliwoski, G.; Morrison, R. D.; Denton, J.; Niswender, C. M.; Daniels, J. S.; Sulikowski, G. A.; Xie, X.; Lindsley, C. W.; Weaver, C. D. ML297 (VU0456810), the First Potent and Selective Activator of the GIRK Potassium Channel, Displays Antiepileptic Properties in Mice. *ACS Chemical Neuroscience* **2013**, *4*, 1278-1286.

(40) Tringham, E.; Powell, K. L.; Cain, S. M.; Kuplast, K.; Mezeyova, J.; Weerapura, M.; Eduljee, C.; Jiang, X.; Smith, P.; Morrison, J.-L.; Jones, N. C.; Braine, E.; Rind, G.; Fee-Maki, M.; Parker, D.; Pajouhesh, H.; Parmar, M.; O'Brien, T. J.; Snutch, T. P. T-Type Calcium Channel Blockers That Attenuate Thalamic Burst Firing and Suppress Absence Seizures. *Science Translational Medicine* **2012**, *4*, 121ra119.

(41) Bende Zou, C. A. L., Conrado Pascual, Man Zhang, Sahani M. Weerasekara, Alex Meier, Duy H. Hua, Xinmin (Simon) Xie: Poster #152.08/M33: A novel tricyclic pyrone compound TP70 decreases hyperglycemia in diabetic NOD/ShiLtJ mice and high fat diet-induced diabetes in wildtype mice. In *Neuroscience Annul Meeting* Chicago, 2015.

Chapter 3 - Synthesis and bioevaluation of tricyclic pyrone derivatives for the treatment of Alzheimer's disease (AD)

3.1 Background and significance

3.1.1 Alzheimer's disease (AD)

Alzheimer's disease(AD) is defined as "*a progressive, degenerative disorder that attacks the brain's nerve cells, or neurons, resulting in loss of memory, thinking and language skills, and behavioral changes*"[1] and it is now the sixth leading cause of death in the United States.[2] Current drugs can only alleviate symptoms but not prevent progression of the disease, until now AD is still not curable.[3,4] Nowadays there are only five FDA approved drugs in the market for the treatment of Alzheimer's Disease as shown in Table 3.1.[2] Discovery of new anti-AD drugs and exploration on the mechanism of disease development are needed.

Drug Name	Chemical Structure	Brand Name	Approved for	FDA approved	Action Mechanism[5]
Donepezil	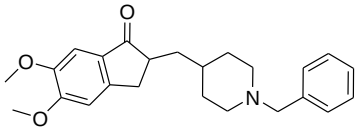	Aricept	All stages	1996	reversible acetyl cholinesterase inhibitor
Galantamine	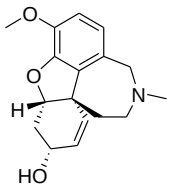	Razadyne	Mild to moderate	2001	cholinesterase inhibitor
Memantine	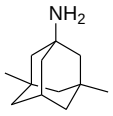	Namenda	Moderate to severe	2003	NMDA receptor antagonist
Rivastigmine	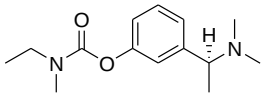	Exelon	All stages	2000	cholinesterase inhibitor
Donepezil and memantine	see above	Namzaric	Moderate to severe	2014	

Table 3.1. FDA approved drugs for the treatment of Alzheimer's disease. (The table was adapted from alz.org website[2])

3.1.2 Previous studies on tricyclic pyrone compounds as anti-Alzheimer's disease drugs

Although the cause of AD is still not clear. It is widely accepted that aggregates of amyloid-β (Aβ) peptides play an important role in the development of AD through initiating a cascade of molecular changes.[6] The Aβ peptides aggregate to form oligomers, which are toxic to neurons and precipitate to form fibrils which are found in AD brains and finally lead to neuronal cell death[7]. Attentions have been drawn to develop molecules which can prevent, or reduce the aggregation of Aβ peptides for the treatment of AD. Previous studies conducted by the Hua group[7-14] have discovered a new class of tricyclic pyrone compounds, which have good oral bioavailability and low toxicity, can reduce Aβ aggregation in the brain. The tricyclic pyrone scaffold was derived from natural product (+)-pyripyropene A (Figure 3.1), a well-known cholesterol acyltransferase (ACAT) inhibitor[15]. ACAT is a cholesterol-regulating enzyme, which was found to be related with increasing Aβ levels in the brain and its inhibition has been reported as a potential anti-AD therapeutic strategy.[16] Exploration on more neuronal protective tricylic pyrone compounds are still needed for the treatment and mechanism study of AD.

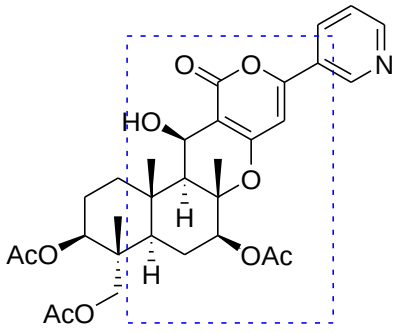

(+)-pyripyropene A

Figure 3.1. Chemical structure of (+)-pyripyropene A.

3.2 Research objectives

Research objective 1: Synthesis of neuronal protective tricyclic pyrone molecules for the study of amelioration of Alzheimer's disease.

Research objective 2: Study of pharmacokinetics properties of discovered active tricyclic pyrone derivatives.

3.3 Syntheses of tricyclic pyrone compounds

CP2 (code name; chemical structure see Figure 3.2) was a reported lead anti-Alzheimer's compound from Hua group and has been studied extensively for its bio-activities and mechanisms of action.[7,9-11,14] In order to discover competitive lead compounds, a series of tricyclic pyrone compounds as shown in Figure 3.2 was screened for their neuronal protective properties. I was involved in the syntheses of compounds **TP70**, **TP82** and **CP2.** Dr. Laxman Pokhrel in Hua group has previously synthesized a small library of tricyclic pyrone compounds including **TP70** and **TP82** as shown in Figure 3.2.[11] However, since large amounts of **TP70** and **CP2** were needed for pharmacokinetics study, I therefore synthesized these two compounds in large quantities and high purities.

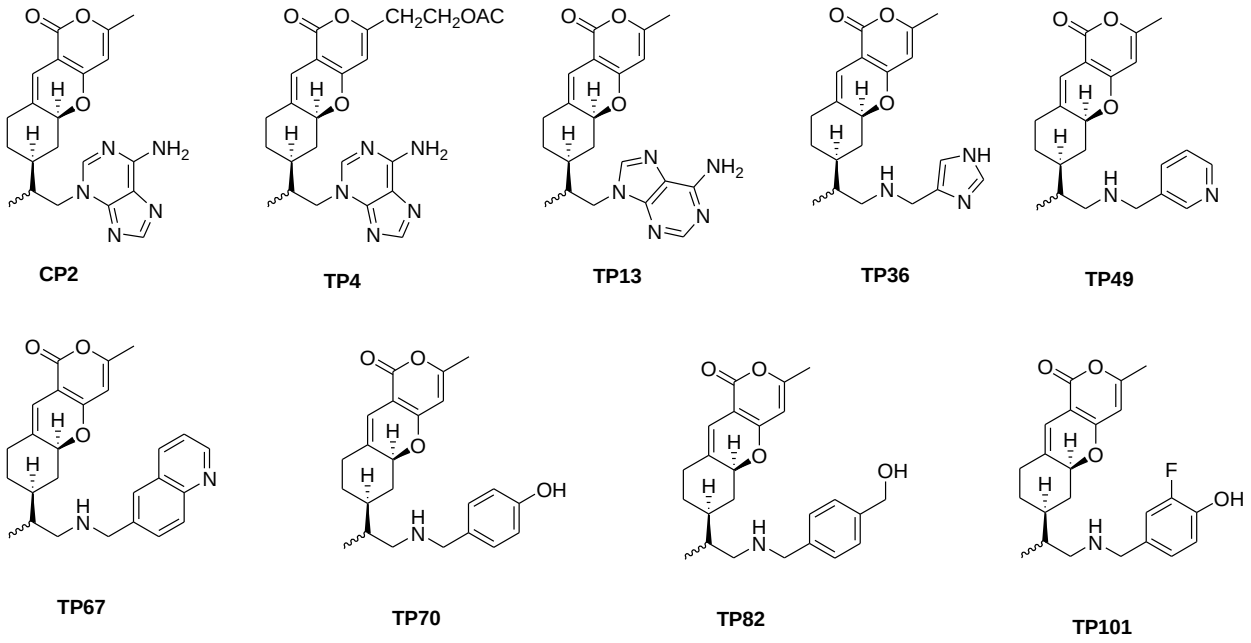

Figure 3.2. Chemical structures of tricyclic pyrone compounds.[11]

3.3.1 Synthetic routes

Syntheses of compounds **TP70**, **TP82** and **CP2** were followed by reported procedures (Laxman Pokhrel et al[11]. 2012; Duy H. Hua et al[8]. 2003). All synthesized molecules were characterized by ^{1}H NMR and MS, the spectra are identical to those reported. Construction of the basic tricyclic pyrone skeleton was shown in Scheme 3.1. $_{L}$-proline acted as a catalyst to activate aldehyde group in (*S*)-(-)-perillaldehyde (compound **3-2**) by forming iminium intermediate, which subsequently condensed and cyclized with 6-methyl-4-hydroxy-2-pyrone (compound **3-1**) to give tricyclic pyrone intermediate **3-3**. Possible explanation of the stereoselectivity in the synthesis of compound **3-3** was shown in Scheme 3.2. Bulky isopropenyl group blocks down face in the proposed intermediate **3-3-7**, so the electron lone pair in carbonyl oxygen prefers to attack from the up face leading to the stereoselectivity.

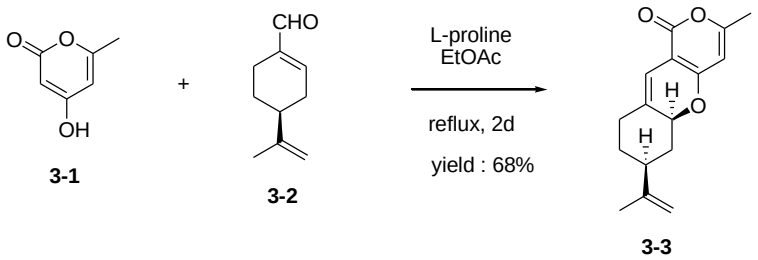

Scheme 3.1. Synthesis of isopropenyl-substituted tricyclic pyrone intermediate (compound 3-3).

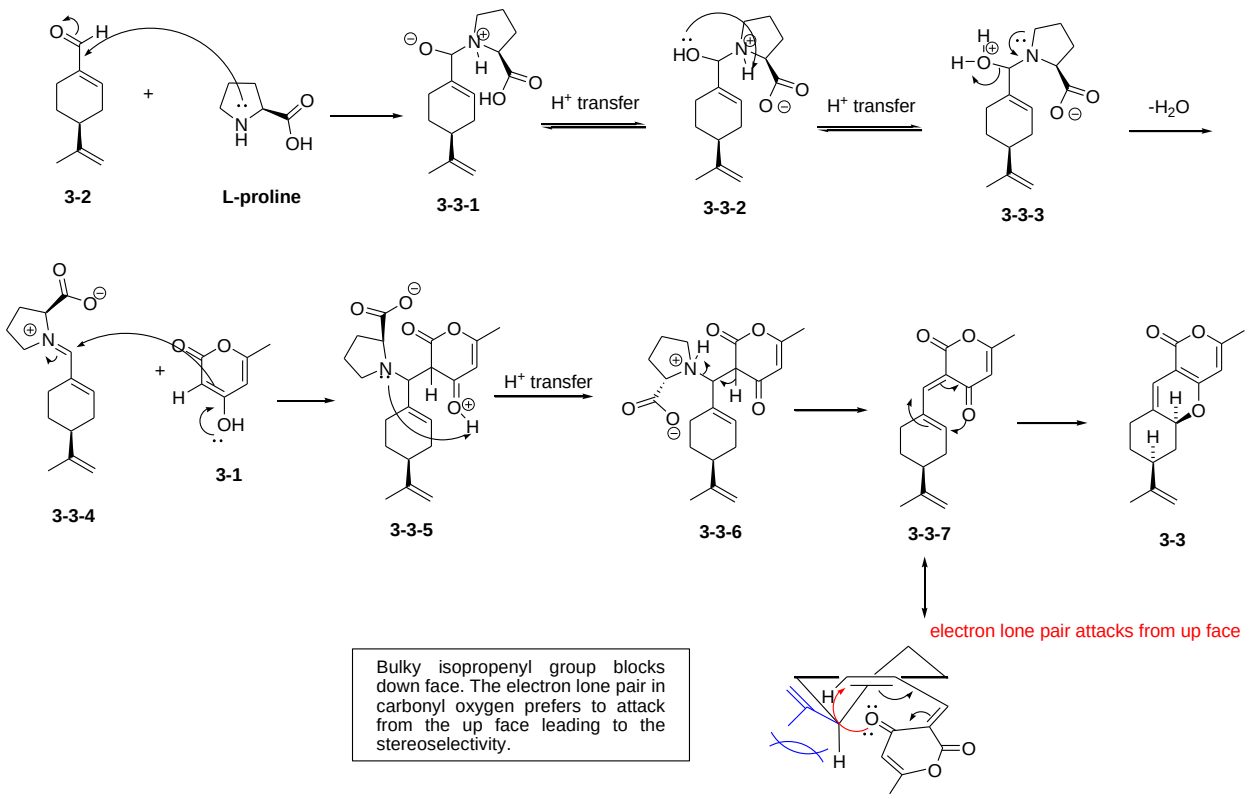

Scheme 3.2. Possible explanation of the stereoselectivity in the synthesis of compound 3-3.

Syntheses of compounds **TP70** and **TP82** were shown in Scheme 3.3. The tricyclic pyrone alkene **3-3** went through hydroboration with borane followed by amination with hydroxylamine-*o*-sulfonic acid to give amine **3-4**, which underwent reductive amination reactions with different aromatic aldehydes (**3-5** or **3-6**) and sodium cyanoborohydride in ethanol to yield **TP70** and **TP82**, respectively.

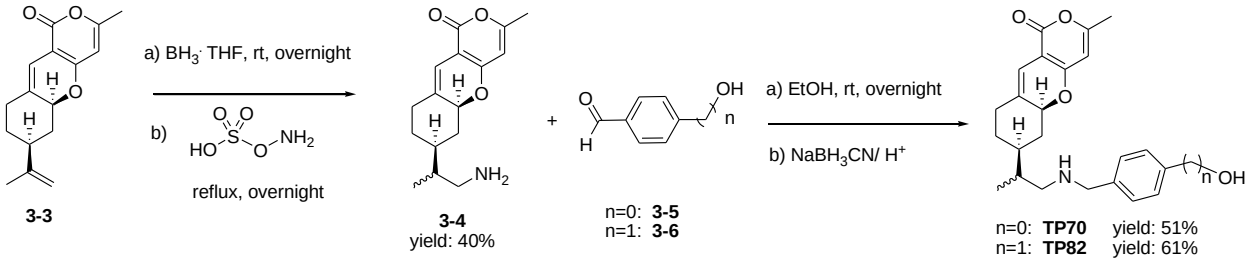

Scheme 3.3. Syntheses of compounds TP70 and TP82.

Synthesis of **CP2** was shown in Scheme 3.4. The tricyclic pyrone alkene **3-3** underwent hydroboration–oxidation reaction to produce alcohol **3-7**, which was first converted into the

mesylate by the treatment with methanesulfonyl chloride and then displacement with adenine in *N*,*N*-dimethylacetatmide (DMA) under reflux reaction conditions to give compound **CP2**.

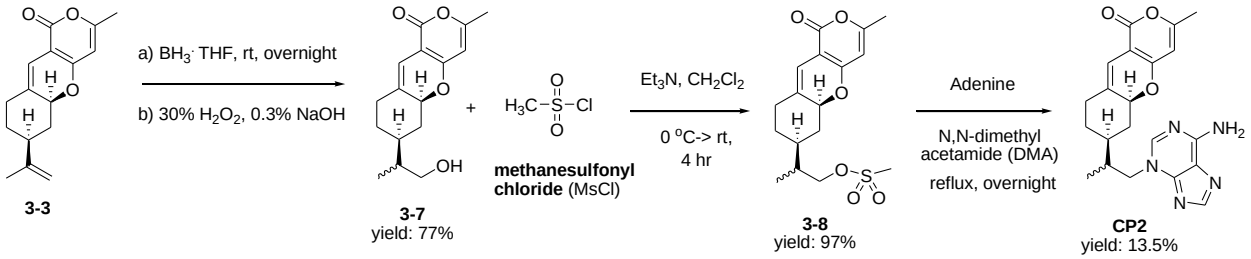

Scheme 3.4. Synthesis of compound CP2.

3.3.2 Purification of CP2

In order to achieve high purity**, CP2** was column chromatographed on silica gel twice followed by crystallization and recrystallization. The purity of **CP2** was determined by HPLC conducted by Dr. Gaochao Huang in Dr. Ping Li's laboratory at the Department of Chemistry, Kansas State University. According to HPLC analysis, the purity of synthesized **CP2** is as high as 97.25%.

3.3.2.1 Column chromatography

- **First time column chromatography**
  - Silica gel was mixed with solvents containing ethyl acetate: dichloromethane: methanol = 4:6:1 + 0.5% $NH_3 \cdot H_2O$ (volume ratio) before packing column.
  - Packed a short and fat column.
  - A gradient mixture of ethyl acetate, dichloromethane and methanol was used as eluent:
    1) 100% ethyl acetate
    2) ethyl acetate: dichloromethane: methanol = 4:6:1 (volume ratio)
    3) ethyl acetate: dichloromethane: methanol = 2:3:1 (volume ratio, **CP2** eluted out)
    4) dichloromethane: methanol = 5:1 (volume ratio)
  - High air pressure was applied when running the column and first column was supposed to be run in a fast way with the purpose to get rid of the most nonpolar and most polar impurities. For example, started from 11 g crude product, 3.6 g product

CP2 together with impurities having similar polarities were obtained after first time column chromatography.

- **Second time column chromatography**
  - Silica gel was mixed with solvents containing ethyl acetate: dichloromethane: methanol = 4:6:1 + 0.5% $NH_3 \cdot H_2O$ (volume ratio) before packing column.
  - Packed a long column.
  - A gradient mixture of ethyl acetate, dichloromethane and methanol was used as eluent:
    1) 100% ethyl acetate
    2) ethyl acetate: dichloromethane: methanol = 4:6:1 (volume ratio)
    3) ethyl acetate: dichloromethane: methanol = 2:3:1 (volume ratio, **CP2** eluted out)
  - Moderate air pressure was applied when running this column and the 2nd column was supposed to be run in a slower way with the purpose to get rid of most impurities having similar polarities to **CP2**. For example, started from 2.2 g impure **CP2** collected from first time column chromatography, 1.6 g **CP2** together with small amount of less polar impurities were obtained after second time column chromatography.

3.3.2.2 Crystallization and recrystallization

- **Crystallization**
  - In a beaker, 1.6 g **CP2** obtained after second time column chromatography was dissolved in 40 mL dichloromethane after gentle heat.
  - To it, 20 mL diethyl ether was added and yellow solid was crystallized out. The resulting mixture was heated at 35^{o}C for a while followed by sonication. Still small amount of yellow solid was not completely dissolved.
  - Allowed the resulting mixture to cool to room temperature, kept in an ice bath and kept in fridge (4^{o}C) overnight. 1.1 g **CP2** was obtained as yellow crystals by filtration and dried under vacuum.
- **Recrystallization**
  - In a beaker, 320 mg **CP2** crystals obtained from first crystallization was dissolved in 10 mL dichloromethane after gentle heat.

- To it, 30 mL diethyl ether was added and yellow solid was crystallized out. The resulting mixture was heated at 35^{o}C for a while followed by sonication. Still small amount of yellow solid was not completely dissolved.
- Allowed the resulting mixture to cool to room temperature, kept in an ice bath and kept in fridge (4^{o}C) overnight. 240 mg pure **CP2** was obtained as yellow crystals by filtration and dried under vacuum.

❖ **NOTE:** Mother liquids from crystallization and recrystallization should be collected and saved for future purification. Do not discard the mother liquid.

3.3.2.3 Purity determination by HPLC analysis

HPLC analysis was conducted by Dr. Gaochao Huang in Dr. Ping Li's laboratory at the Department of Chemistry, Kansas State University.

➢ **HPLC sample preparation:**
- **CP2** sample: 1 mg pure **CP2** (obtained from recrystallization) was dissolved in 1 mL methanol.
- Blank sample: 100% methanol

➢ **HPLC instrument information:**
- Waters 2998 Photodiode Array Detector and Waters 1525 Binary HPLC Pump.

➢ **HPLC Column information:**
- Part Number: 00G-4252-E0
- Description: Luna® 5 µm C18(2) 100 Å, LC
- Column 250 x 4.6 mm, Ea
- S/No. 676866-5
- B/No. 529-112
- Stationary Phase:C18 with TMS endcapping
- Solid Support: Fully Porous Silica
- Format: Column
- Separation Mode: Reversed Phase

➢ **HPLC methods:**
- Eluents: A= water, B= methanol. A gradient mixture of water (solvent A) and methanol (solvent B) was used as eluent as shown in Table 3.2.

- Both the blank (100% methanol) and **CP2** samples (concentration: 1mg **CP2** in 1 mL methanol) were analyzed using the same method (Table 3.2).
- **CP2** has the maximum UV absorption at wavelength 269.1 nm as shown in Figure 3.3.

	Time	Flow	%A	%B	%C	Curve
1	0.01	1.00	70.0	30.0	0.0	6
2	30.00	1.00	10.0	90.0	0.0	6
3	33.00	1.00	10.0	90.0	0.0	6
4	39.00	1.00	70.0	30.0	0.0	6
5	42.00	1.00	70.0	30.0	0.0	6

Table 3.2. A gradient mixture of water (solvent A) and methanol (solvent B) was used as HPLC eluent (conducted by Dr. Gaochao Huang in Dr. Li's laboratory).

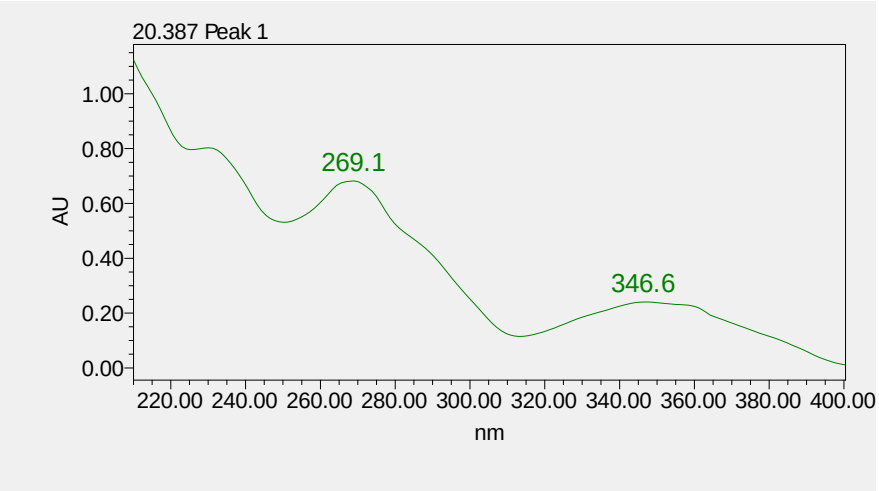

Figure 3.3. UV absorption spectrum of CP2 (conducted by Dr. Gaochao Huang in Dr. Li's laboratory).

➢ **HPLC analysis results:**

- Purity of synthesized **CP2** after recrystallization is 97.25% as shown in Table 3.3.
- HPLC graph (Figure 3.4) for **CP2** was drawn according to the data at wavelength 269.1nm, where CP2 has the maximum UV absorption (see Figure 3.3).

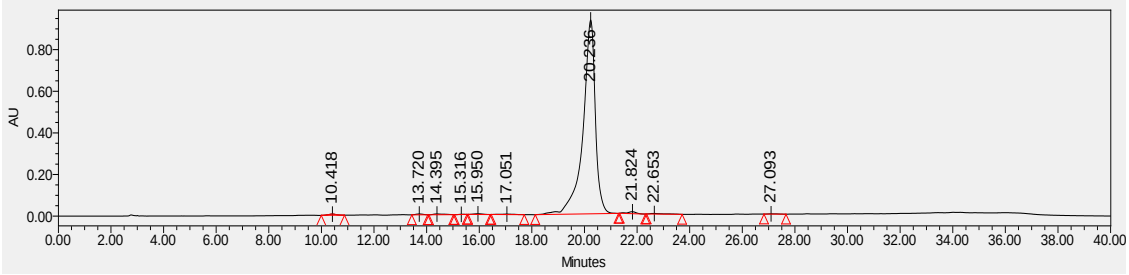

Figure 3.4. Purity of obtained CP2 after recrystallization was determined by HPLC (conducted by Dr. Gaochao Huang in Dr. Li's laboratory).

	Retention Time	Area	% Area	Height	Peak Codes
1	10.418	121947	0.39	5853	I08
2	13.720	75188	0.24	3965	
3	14.395	117769	0.38	3931	
4	15.316	20382	0.07	1449	I08
5	15.950	81129	0.26	3398	
6	17.051	84195	0.27	2344	
7	20.236	30425249	97.25	931718	
8	21.824	204762	0.65	9349	I08
9	22.653	118849	0.38	2738	
10	27.093	35244	0.11	1394	

Table 3.3. Analysis for CP2 HPLC data (conducted by Dr. Gaochao Huang in Dr. Li's laboratory).

3.4 Bioevaluation and discussion

Bioevaluation was performed by Dr. Izumi Maezawa in Professor Lee-Way Jin's laboratory at the Department of Pathology and Laboratory Medicine, University of California Davis Medical Center. Quantification of lead compound **TP70** in plasma and various tissues using HPLC analysis was carried out by Dr. Sahani Weerasekara in Hua group.

Neuronal protective studies in cell-based assay were performed among nine tricyclic pyrone compounds (chemical structures, see Figure 3.2). Except compounds **TP49** and **TP67**, all other compounds showed neuronal protective activities. **TP70** was found to be another lead compound (with similar efficacy to the well-studied **CP2**) and its pharmacokinetics properties were further explored.

3.4.1 Methods

3.4.1.1 Studies on *in vitro* neuronal protective properties

Following reported procedure[9,10,17], nine tricyclic pyrone compounds (see Figure 3.2) were screened for their *in vitro* neural protectivities against cell death using MC65 cell line and the results were shown in Table 3.4 and Figure 3.6. According to previous studies done in the Jin group[9,10], MC65 cell line was used in measuring the neuronal protective efficacy of the tricyclic pyrone derivatives and it is a line of human neuroblastoma that was engineered to conditionally expresses C99. C99 is a 99-residue fragment derived from amyloid processor protein (APP) and can be subsequently cleaved to produce Aβ peptides. The resulting MC65 cell toxicity was induced by oligomeric Aβ peptides, and was determined using a MTT assay.

A general procedure for mesuring *in vitro* neuronal protective properties was summarized in Figure 3.5.

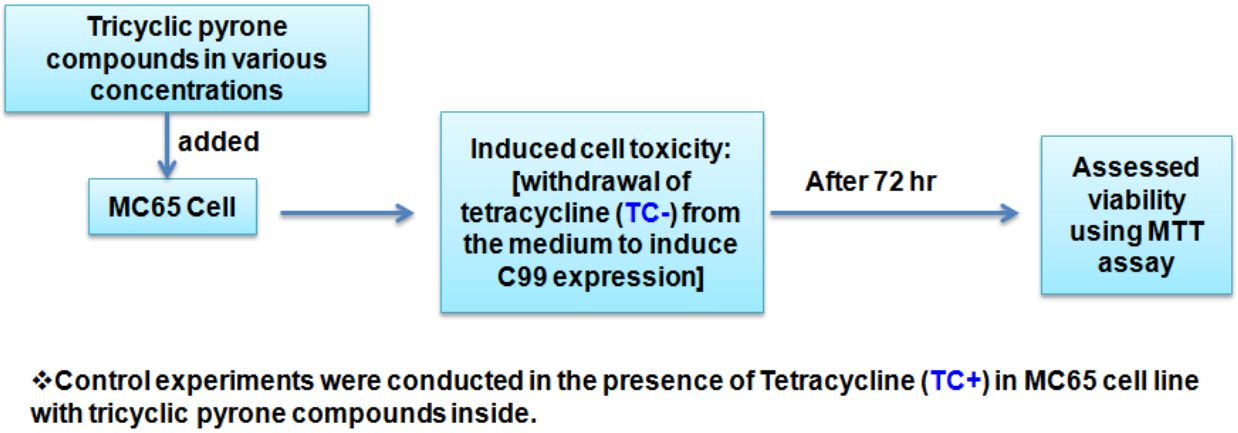

Figure 3.5. General procedure for measuring *in vitro* neuronal protective properties (conducted in Dr. Jin group).

3.4.1.2 Studies on pharmacokinetics properties

Quantification of lead compound **TP70** in plasma and various tissues using HPLC analysis was carried out by Dr. Sahani Weerasekara in Hua group following reported methods.[17]

3.4.2 Results and discussion

3.4.2.1 Studies on *in vitro* neuronal protective properties

Entry	Code Name	ED_{50} (μM)	TD_{50}(μM)	TI
1	**CP2**	0.12	39	325
2	**TP4**	0.26	77	296
3	**TP13**	1.2	>25	>21
4	**TP36**	0.175	51	291
5	**TP49**	inactive (>5)	N/A	N/A
6	**TP67**	inactive (>5)	N/A	N/A
7	**TP70**	0.08	51	291
8	**TP82**	0.09	77	855
9	**TP101**	0.07	50	714

Table 3.4. Results for *in vitro* neuronal protective efficacy of screened tricyclic pyrone compounds. ED_{50}: effective dose for 50% cell survival. TD_{50}: toxic effect for 50% cell death. TI: therapeutic ratio = TD_{50}/ ED_{50}

According to Table 3.4, except compounds **TP49** and **TP67** (Entry 5 and 6) which are not active with high ED_{50} values (>5 μM), all other compounds are active with high TI (therapeutic ratio = TD_{50}/ ED_{50}) values, referring to low toxicities and high efficiencies. Except **TP13** (ED_{50} = 1.2 μM), six of the seven active compounds (**CP2**, **TP4**, **TP13**, **TP36**, **TP70**, **TP82**, and **TP101**) showed low nanomolar range ED_{50} values ranging from 0.07 to 0.26 μM.

Figure 3.6.A indicated that both compounds **TP67** and **TP70** showed dose-dependent response curves. Considering that **TP67** was an inactive compound (with EC_{50} > 5 μM**),** it is **TP70** that reduced the levels of intracellular C99 and oligomeric Aβ peptides (AβO), including low-n-oligomers such as Aβ dimer and high-n-oligomers such as homo- or hetero-oligomeric complexes of Aβ (Aβ-OC) as shown in Figure 3.6.B.

Previous researches done in the Jin group found that α-tocopherol, as an anti-oxidant, inhibited MC65 cells death[18]. CM-H2DCFDA was used to stain cellular reactive oxidative species (ROS) following reported procedure[7]. According to Figure 3.6.C, **TP70** was found to have comparable anti-oxidant activity to α-tocopherol in reducing cell death by blocking ROS production of MC65 cells. No such anti-oxidant effects were found in compounds **CP2** and **TP67** as shown in Figure 3.6.C.

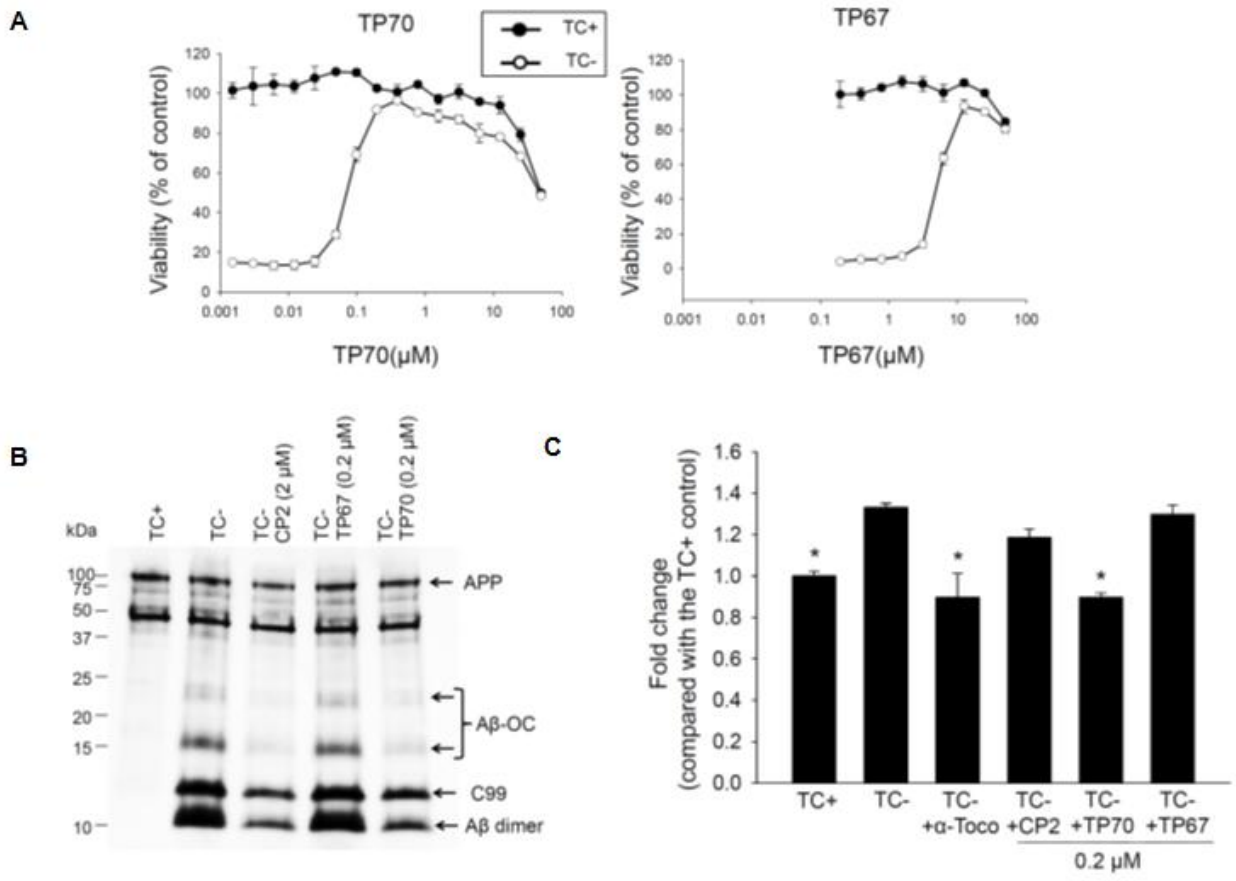

Figure 3.6. The neuroprotective effects of TP70. (*A*) MC65 cells were induced to express oligomeric Aβ peptides (AβO) by withdrawal of tetracycline (TC-) from the medium in the

presence of indicated concentrations of **TP70** or **TP67**. Cultures in the presence of TC (TC+) as well as the drug were used as controls to determine the toxicity of the drug independent of Aβ. At 72 h, viability was assessed by MTT assay. Data are expressed as mean percentage viability (*n*=3) with parallel TC+ cultures without drug set at 100% viability. Error bars represent standard error. The ED_{50}, TD_{50}, and TI values of **TP70** were calculated and listed in Table 3.4. (*B*) MC65 cultures at 24 h after TC withdrawal were homogenized and 5 μg cellular proteins were subjected to Tris/tricine SDS-PAGE and western blot analysis with antibody 6E10 for Aβ1-17. The band pattern was comparable to published data[10,19]; accordingly each band was identified. Both **CP2** and **TP70**, but not **TP67**, reduced the levels of Aβ-OC, C99, and Aβ dimer without altering the level of amyloid processor protein (APP). (*C*) Fluorescence intensity of each culture conditions were expressed as fold change compared to the TC+ (no Aβ expression) condition. *n*=7-8, **p*<0.05 compared to the TC- condition (with Aβ expression). **TP70** and α-tocopherol but not **CP2** or **TP67** reduced ROS levels related to intracellular Aβ expression. (This figure was reprinted from Maezawa et al.[17] *Journal of Alzheimer's Disease*, 2017, accepted in March)

3.4.2.2 Studies on pharmacokinetics properties

Figure 3.7 showed pharmacokinetics (PK) properties of **TP70**.

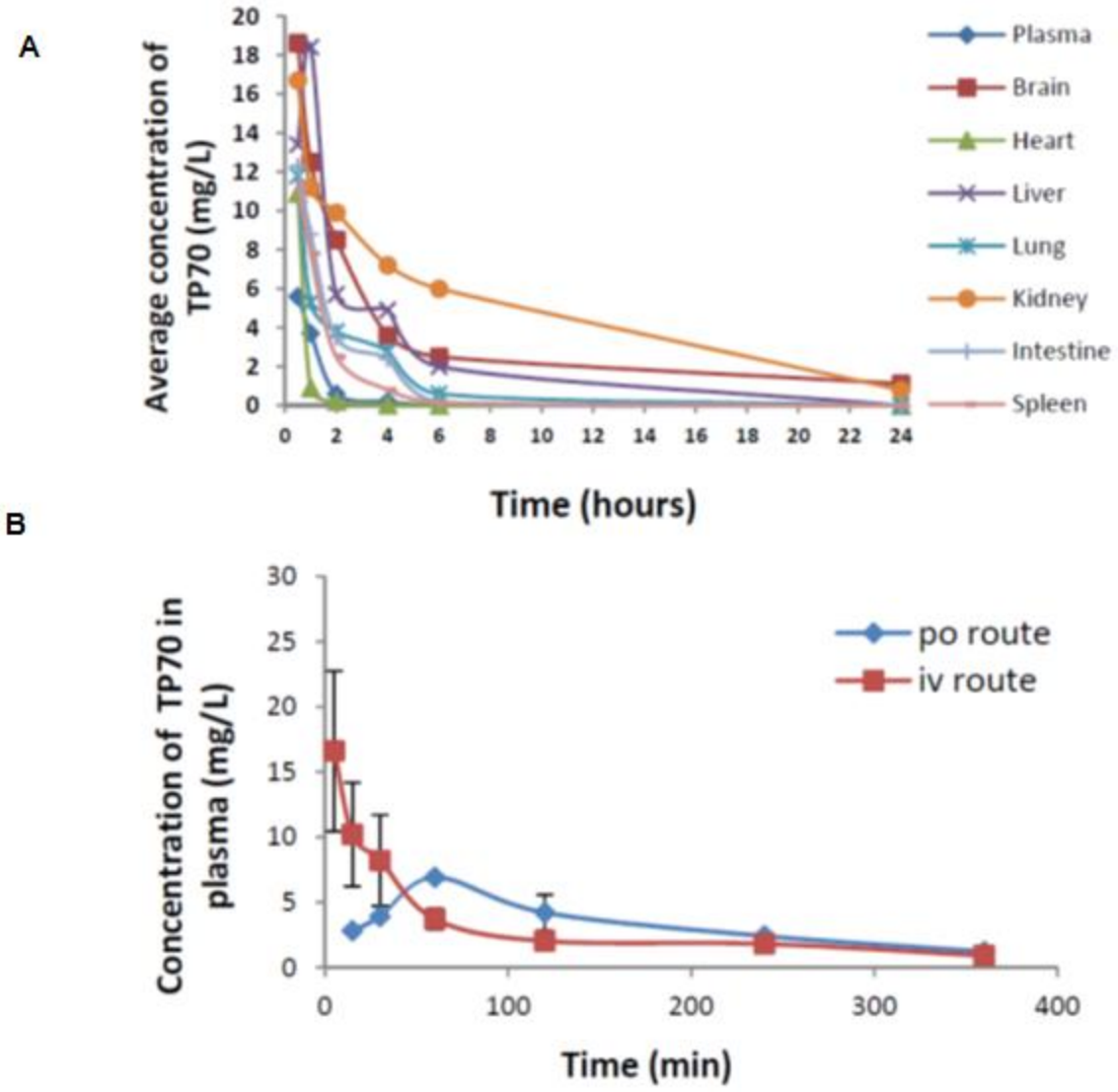

Figure 3.7. Some pharmacokinetics (PK) properties of TP70. (A) Distribution of **TP70** in various tissues and plasma after i.p. administration in 3-month-old male WT C57BL/6 mice (25 mg/Kg body weight) from 0 - 24 h. Shown are the means from three mice per time point. (B) The concentrations of **TP70** in plasma following i.v. and p.o. administration. (This figure was reprinted from Maezawa et al.[17] Journal of Alzheimer's Disease, 2017, accepted in March)

Figure 3.7.A showed the distribution of **TP70** in seven key organs (including brain, heart, liver, lung, kidney, intestine and spleen) together with plasma after i.p. administration from 0.5 - 24 h. Ranking after kidney, brain had the second highest **TP70** concentration, suggesting that **TP70** overcame blood-brain barrier (BBB) and entered central nervous system (CNS) readily. According to Figure 3.7.B, the $t_{1/2}$ (half time) values of **TP70** administered by p.o. and i.v. routes were 160 min and 30 min, respectively and the areas under the curve (AUCs) were 678

(mg•min/L) and 989 (mg•min/L), respectively. Oral bioavailability (F) of **TP70** was calculated as 678 divided by 989, yielding F = 0.68 and indicating high oral bioavailability. Based on the pharmacokinetics (PK) data shown in Figure 3.7, **TP70** possesses high oral bioavailability, good CNS permeability and suitable oral administered half time.

3.5 Conclusion

Nine synthesized tricyclic pyrone compounds were screened for their neuronal protective activities against cell death in MC65 cell assay. Six of them (**CP2**, **TP4**, **TP36**, **TP70**, **TP82** and **TP101**) were found to be active with low nanomolar range ED_{50} values ranging from 0.07 to 0.26 μM. Among the active compounds, **TP70** was found to have dose-dependent response on its neuronal protective property. In addition, similar to α-tocopherol, **TP70** showed anti-oxidation ability, while no such effect was found in **CP2**. Pharmacokinetics studies of **TP70** suggested that it can readily penetrate into the brain and have good oral bioavailability. Based on its good pharmacokinetics properties and low toxicity, **TP70** could be a drug candidate for the treatment of AD.

Reference

(1) http://www.alzfdn.org/AboutAlzheimers/warningsigns.html.

(2) http://www.alz.org/research/science/alzheimers_disease_treatments.asp.

(3) Selkoe, D. J. Alzheimer's disease: genes, proteins, and therapy. *Physiol Rev* **2001**, *81*, 741-766.

(4) Raina, P.; Santaguida, P.; Ismaila, A.; et al. Effectiveness of cholinesterase inhibitors and memantine for treating dementia: Evidence review for a clinical practice guideline. *Annals of Internal Medicine* **2008**, *148*, 379-397.

(5) https://www.drugbank.ca/drugs.

(6) Hardy, J.; Selkoe, D. J. The amyloid hypothesis of Alzheimer's disease: progress and problems on the road to therapeutics. *Science* **2002**, *297*, 353-356.

(7) Hong, H.-S.; Rana, S.; Barrigan, L.; Shi, A.; Zhang, Y.; Zhou, F.; Jin, L.-W.; Hua, D. H. Inhibition of Alzheimer's amyloid toxicity with a tricyclic pyrone molecule in vitro and in vivo. *Journal of Neurochemistry* **2009**, *108*, 1097-1108.

(8) Hua, D. H.; Huang, X.; Tamura, M.; Chen, Y.; Woltkamp, M.; Jin, L.-W.; Perchellet, E. M.; Perchellet, J.-P.; Chiang, P. K.; Namatame, I.; Tomoda, H. Syntheses and bioactivities of tricyclic pyrones. *Tetrahedron* **2003**, *59*, 4795-4803.

(9) Jin, L. W.; Hua, D. H.; Shie, F. S.; Maezawa, I.; Sopher, B.; Martin, G. M. Novel tricyclic pyrone compounds prevent intracellular APP C99-induced cell death. *J Mol Neurosci* **2002**, *19*, 57-61.

(10) Maezawa, I.; Hong, H.-S.; Wu, H.-C.; Battina, S. K.; Rana, S.; Iwamoto, T.; Radke, G. A.; Pettersson, E.; Martin, G. M.; Hua, D. H.; Jin, L.-W. A novel tricyclic pyrone

compound ameliorates cell death associated with intracellular amyloid-β oligomeric complexes. *Journal of Neurochemistry* **2006**, *98*, 57-67.

(11) Pokhrel, L.; Maezawa, I.; Nguyen, T. D. T.; Chang, K.-O.; Jin, L.-W.; Hua, D. H. Inhibition of Acyl-CoA: Cholesterol Acyltransferase (ACAT), Overexpression of Cholesterol Transporter Gene, and Protection of Amyloid β (Aβ) Oligomers-Induced Neuronal Cell Death by Tricyclic Pyrone Molecules. *Journal of Medicinal Chemistry* **2012**, *55*, 8969-8973.

(12) Rana, S.; Hong, H.-S.; Barrigan, L.; Jin, L.-W.; Hua, D. H. Syntheses of tricyclic pyrones and pyridinones and protection of Aβ-peptide induced MC65 neuronal cell death. *Bioorganic & Medicinal Chemistry Letters* **2009**, *19*, 670-674.

(13) Trushina, E.; Rana, S.; McMurray, C. T.; Hua, D. H. Tricyclic pyrone compounds prevent aggregation and reverse cellular phenotypes caused by expression of mutant huntingtin protein in striatal neurons. *BMC Neuroscience* **2009**, *10*, 73.

(14) Zhang, L.; Zhang, S.; Maezawa, I.; Trushin, S.; Minhas, P.; Pinto, M.; Jin, L.-W.; Prasain, K.; Nguyen, T. D. T.; Yamazaki, Y.; Kanekiyo, T.; Bu, G.; Gateno, B.; Chang, K.-O.; Nath, K. A.; Nemutlu, E.; Dzeja, P.; Pang, Y.-P.; Hua, D. H.; Trushina, E. Modulation of Mitochondrial Complex I Activity Averts Cognitive Decline in Multiple Animal Models of Familial Alzheimer's Disease. *EBioMedicine* **2015**, *2*, 294-305.

(15) Obata, R.; Sunazuka, T.; Tomoda, H.; Harigaya, Y.; Ōmura, S. Chemical modification and structure-activity relationships of pyripyropenes; potent, bioavailable inhibitor of acyl-CoA: Cholesterol O-acyltransferase (ACAT). *Bioorganic & Medicinal Chemistry Letters* **1995**, *5*, 2683-2688.

(16) Huttunen, H. J.; Kovacs, D. M. ACAT as a Drug Target for Alzheimer's Disease. *Neuro-Degenerative Diseases* **2008**, *5*, 212-214.

(17) Maezawa, I.; Zou, B.; Weerasekara, S.; Zhang, M.; Xie, X. S.; Hua, D. H.; Jin, L.-W. The Anti-Alzheimer's Amyloid and Neuroprotective Properites of A Novel Tricyclic Pryone Molecule. *Journal of Alzheimer's Disease* **2017**, accepted in March.

(18) Woltjer, R. L.; Maezawa, I.; Ou, J. J.; Montine, K. S.; Montine, T. J. Advanced glycation endproduct precursor alters intracellular amyloid- β/AβPP carboxy-terminal fragment aggregation and cytotoxicity. *Journal of Alzheimer's Disease* **2003**, *5*, 467-476.

(19) Woltjer, R. L.; Nghiem, W.; Maezawa, I.; Milatovic, D.; Vaisar, T.; Montine, K. S.; Montine, T. J. Role of glutathione in intracellular amyloid-α precursor protein/carboxy-terminal fragment aggregation and associated cytotoxicity. *Journal of Neurochemistry* **2005**, *93*, 1047-1056.

Chapter 4 - Chiral-substituted polyvinylpyrrolidones (CSPVP) supported Cu/Au nanoclusters and catalytic cyclization of 5-substituted nona-1,8-dien-5-ols

4.1 Background and significance

In the previous studies reported by the Hua group[1], a new class of chiral-substituted polyvinylpyrrolidones (CSPVP) supported bimetallic nanoclusters were found to be efficient catalysts in asymmetric oxidation reactions with broad substrates scopes and high enantioselectivities. Based on our previous research[1], hydroxyl group has been found to be a directing group which can lead the asymmetric oxidation. The symmetric 5-substituted nona-1,8-dien-5-ols were designed as substrates by desymmetrization to study the hydroxyl group-directed asymmetric oxidation for the reactive allylic C-H. However, no allylic C-H oxidation product was found. Instead, a cyclized lactone product with a stereogenic tetrasubstituted carbon center was obtained in the CSPVP supported Cu/Au nanoclusters-hydrogen peroxide oxidation reaction (Figure 4.1). This developed a simple and new method to construct stereogenic tetrasubstituted carbon centers, which widely existed in natural products[2-4]. More explorations on the CSPVP supported Cu/Au nanoclusters catalyzed cyclization reactions are needed to optimize reaction conditions.

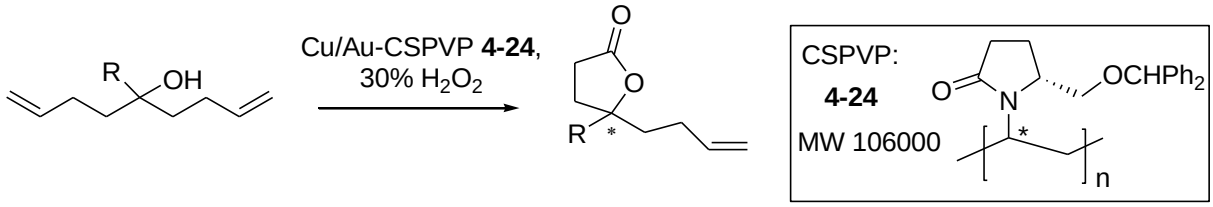

Figure 4.1. CSPVP supported Cu/Au catalyzed cyclization of 5-substituted nona-1,8-dien-5-ols.

4.2 Research objectives

Research objective 1: Study whether the size of the R group on the C-5 stereogenic center of chiral-substituted PVPs (CSPVP) would affect the enantioselectivity of the catalytic oxidation reactions including the ring closing reactions of substituted nona-1,8-diene-5-ols.

Research objective 2: Develop a method to create tetrasubstituted carbon stereogenic center through catalytic cyclization of 5-substituted nona-1,8-dien-5-ols.

4.3. Syntheses and characterizations of chiral-substituted polyvinylpyrrolidones (CSPVP) for stabilization of Cu/Au nanoclusters in catalytic asymmetric oxidation reactions

4.3.1 Syntheses of different C-5 chiral-substituted PVP precursors.

Various C-5 chiral-substituted PVP precursors were synthesized as shown in Figure 4.2. I was involved in the syntheses of compounds **4-1** to **4-5**, and compound **4-6** was synthesized by Mr. Bo Hao, a graduate student in Hua group. Later, it was found that PVP made from precursor **4-6** was the best polymer stabilizer for Pd/Au or Cu/Au nanoclusters with highest enantioselectivities in different kinds of oxidation reactions (Bo Hao et al., 2016[1]). It was found that the size of C-5 substituted functional groups in the pyrrolidone ring has an effect on the enantioselectivity. Generally, the bulkier the size the higher the enantioselectivity produces.[1] However, too bulky C-5 substitution, for example *t*-Bu in compound **4-3** (see Figure 4.2), will prevent the precursor from vinylation after de-Boc proctection and eventually lead to failure in polymerization. That explained why benzhydryloxymethyl derivative **4-6** was the best C-5 substituted group among various functional groups.

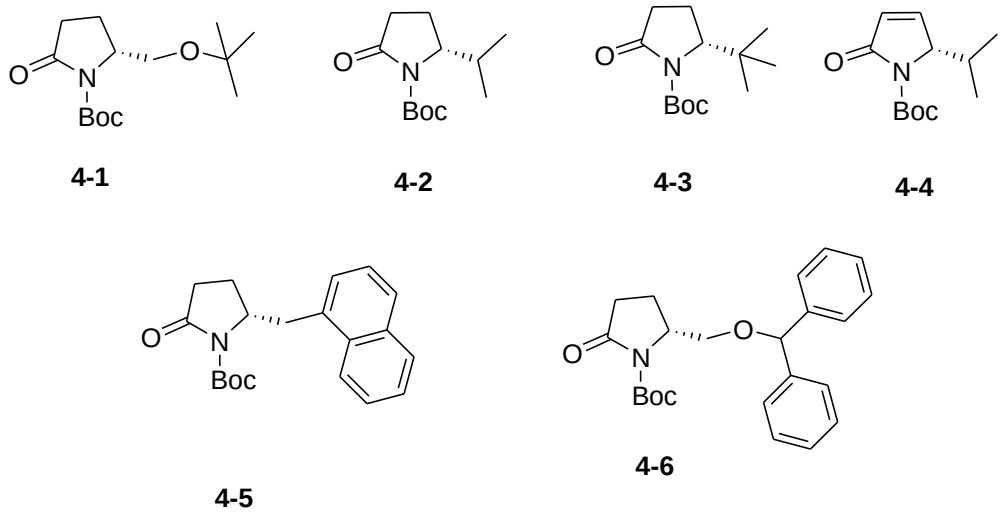

Figure 4.2. Chemical structures of various C-5 chiral-substituted PVP precursors.

Syntheses of compounds **4-1**, **4-2**, **4-3** and **4-5** were shown in Scheme 4.1. Following the reported procedure[5-7], commercial available Boc-protected chiral amino acids were coupled with Meldrum's acid followed by reduction and cyclization to form *N*-Bocpyrrolidone compounds as shown in Scheme 4.1. Possible cyclization mechanism of the formation of pyrrolidone ring was shown in Scheme 4.2. The thermal stability of formed five-member pyrrolidone ring was the driving force of the cyclization reaction.

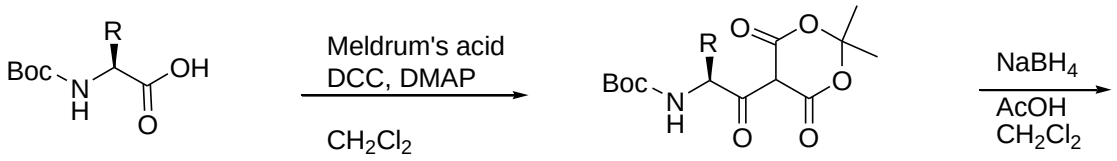

R = CH_2O-t-Bu	**4-7**	R = CH_2O-t-Bu	**4-11**
= isopropyl	**4-8**	= isopropyl	**4-12**
= t-Bu	**4-9**	= t-Bu	**4-13**
= Naphthylmethyl	**4-10**	= Naphthylmethyl	**4-14**

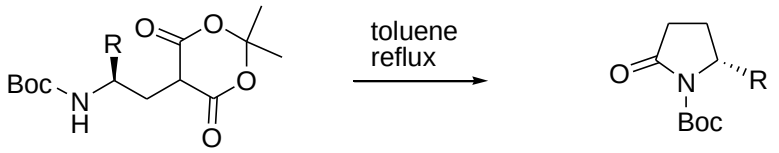

R = CH_2O-t-Bu	**4-15**	R = CH_2O-t-Bu	**4-1** (83% overall yield in three steps)
= isopropyl	**4-16**	= isopropyl	**4-2** (75% overall yield in three steps)
= t-Bu	**4-17**	= t-Bu	**4-3** (85% overall yield in three steps)
= Naphthylmethyl	**4-18**	= Naphthylmethyl	**4-5** (86% overall yield in three steps)

Scheme 4.1. Syntheses of compounds 4-1, 4-2, 4-3 and 4-5.

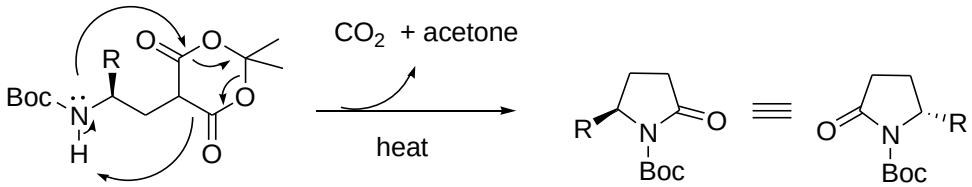

4-a **4-b**

Scheme 4.2. Possible mechanism for the cyclization of pyrrolidone ring.

Synthesis of compound **4-4** was shown in Scheme 4.3. Compound **4-2** was selenylated with benzeneselenyl bromide following the reported procedure[8] to give intermediate **4-19**, which was further oxidized by sodium periodate in 1,4-dioxane/H_2O solution to yield designed alkene **4-4** via selenoxide elimination.

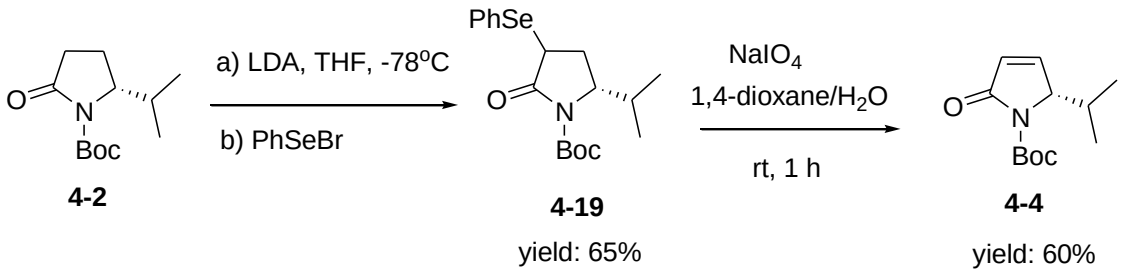

Scheme 4.3. Synthesis of compound 4-4.

4.3.2 Synthesis of chiral-substituted polyvinylpyrrolidones (CSPVP)

(Section 4.3.2 was adapted with permission from Bo Hao et al.[1] *Journal of the American Chemical Society* 2016, *138*, 16839-16848. Copyright © 2016 American Chemical Society.)

The CSPVP (compound **4-24**) used in this project was synthesized by Mr. Bo Hao in Hua group as shown in Scheme 4.4. To prepare uniform micron-size monodisperse particles[9], a dispersion polymerization method[10] was used to prepare polymer **4-24**. The dispersant, poly(5-substituted *N*-vinylpyrrolidinone-co-vinyl acetate) **4-23** was prepared from the copolymerization reactions of respective monomer **4-22** and 1 equiv. of vinyl acetate in the presence of a catalytic amount of azobisisobutyronitrile (AIBN) in refluxing acetone. Polymerization of **4-22** separately with a catalytic amount of AIBN and in the presence of 1% of respective copolymer **4-23** in DMF at 120°C for 7 days gave polymer **4-24.**

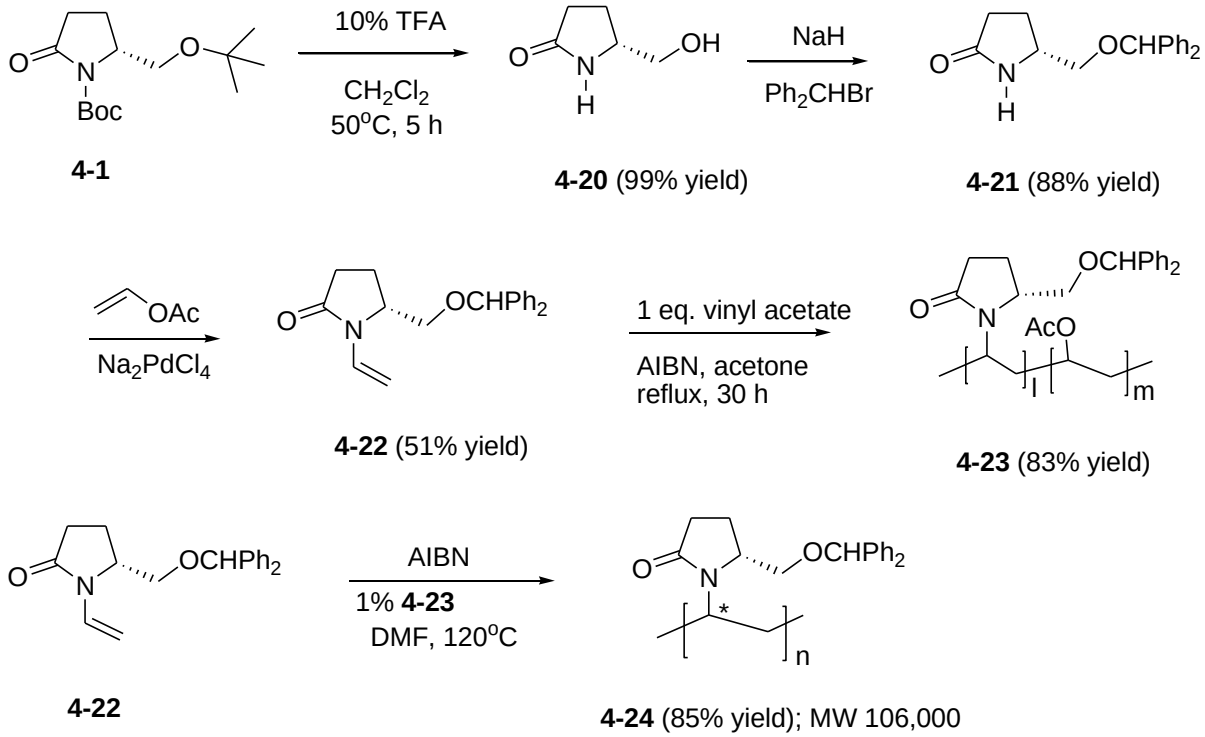

Scheme 4.4. Synthesis of C5-benzhydrol substituted chiral PVP polymer. (The Scheme was adapted with permission from the supporting information of Bo Hao et al.[1] *Journal of the American Chemical Society* 2016, *138*, 16839-16848. Copyright © 2016 American Chemical Society.)

Polymer **4-24** is soluble in water and the molecular weight was determined by gel permeation chromatography. Average molecular weight of CSPVP **4-24** is 106,000. Both *R*- and *S*-stereochemistry are likely presented in the stereogenic center (marked with *) in the polymer alkane backbone, and they are not identifiable. Presumably, this stereogenic center of the polymers can be isotactic, atactic, and syndiotactic,[11] and likely has lesser effect on the asymmetric oxidation reactions.

4.3.3 Syntheses and characterizations of CSPVP supported Cu/Au nanoclusters

(Section 4.3.3 was adapted with permission from Bo Hao et al.[1] *Journal of the American Chemical Society* 2016, *138*, 16839-16848. Copyright © 2016 American Chemical Society.)

Nanoclusters can be prepared by a number of methods including molecular beams, chemical reduction, thermal decomposition, ion implantation, electrochemical synthesis, radiolysis, sonochemical synthesis, and biosynthesis, and are characterized by various analytical

techniques.[12] The Hua group has synthesized various bimetallic nanoclusters including Pd/Au and Cu/Au, using the chemical reduction method[13] in the presence of different chiral polymers such as **4-24**, **4-25** or **4-26** (Figure 4.3). Gold was used due to its high catalytic activity and synergistic electronic effects.[13-19]

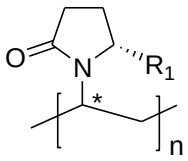

CSPVP

4-24: $R_1 = CH_2OCHPh_2$; MW 106,000
4-25: $R_1 = CH_2O$-t-Bu; MW 68,000
4-26: $R_1 = CH_2Ph$; MW 76,000

Figure 4.3. Chemical structures of chiral-substuted PVP 4-24, 4-25 and 4-26.

For example, a solution of Na_2PdCl_4 (3 equiv.), $HAuCl_4$ (1 equiv.), and CSPVP **4-24** (0.11 equiv.; based on the amount of Au) in water was treated with $NaBH_4$ at 25^{o}C for 30 min to give a light brown to dark grey solution depending on the concentrations. The resulting solution was used in the subsequent catalytic reactions without further manipulation. Similarly, Cu/Au (3:1)-**4-24** was also prepared using CuCl (3 equiv.), $HAuCl_4$ (1 equiv.), and CSPVP **4-24** (0.11 equiv.).

The characterizations of nanoclusters were performed by Mr. Bo Hao in Hua group. Various characterization methods included inductively coupled plasma-mass spectrometry (ICP-MS), transition electron microscopy (TEM), X-ray photoelectron spectroscopy (XPS), AFM, DLS and IR.[1] TEM images revealed average diameters of 3.44 ± 1.63 nm and 3.66 ± 1.95 nm for Pd/Au (3:1)-**4-24** and Cu/Au (3:1)-**4-24**, respectively. In AFM images, 50 - 200 nm in diameters and ~ 6 nm in heights of spherical particles were found, and in DLS, 100 - 140 nm sized nanoparticles were revealed, suggesting the size of nanocluster-**4-24** was ~5 times larger than polymer **4-24**, and the measured sizes of the particles from AFM and DLS were similar.

4.4 CSPVP supported Cu/Au nanoclusters catalyzed cyclization reaction of diene

4.4.1 Syntheses of different 5-substituted nona-1,8-dien-5-ols

Due to limitation of time, I could only complete the syntheses of two 5-substituted nona-1,8-dien-5-ols (compounds **4-S1** and **4-S2**) as shown in Figure 4.4. The synthetic routes were shown in Scheme 4.5. A small library of different 5-substituted nona-1,8-dien-5-ols could be obtained by replacing 5-position with other functional groups (compound **4-SX**, Figure 4.4) following similar synthetic procedures.

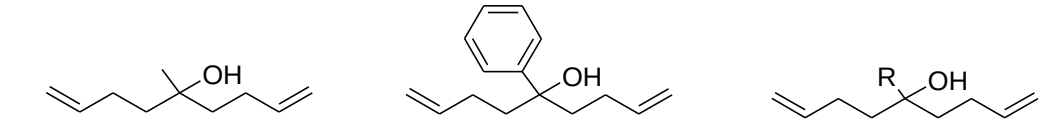

5-methylnona-1,8-dien-5-ol **4-S1**

5-phenylnona-1,8-dien-5-ol **4-S2**

4-SX

Figure 4.4. Chemical structures of synthesized and proposed 5-substituted nona-1,8-dien-5-ols.

Syntheses of diene substrates **4-S1** and **4-S2** were shown in Scheme 4.5. Following the reported procedure[20], 3-butenylmagnesium bromide (**4-26**) underwent nucleophilic addition reaction with either ethyl acetate or isopropyl benzoate to form compounds **4-S1** and **4-S2**, respectively.

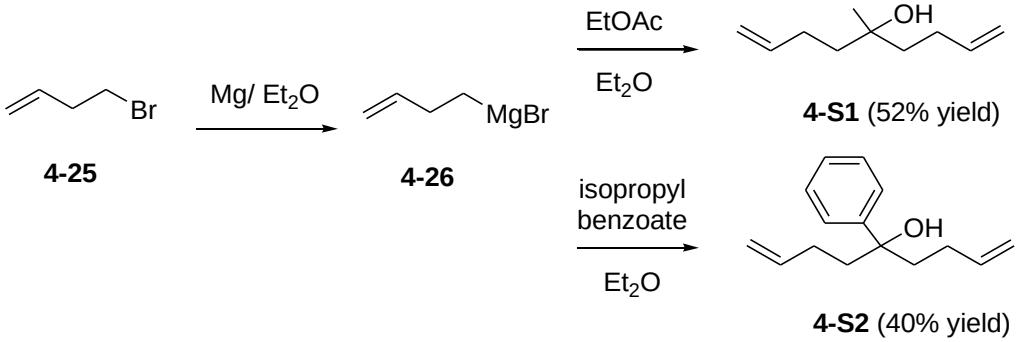

4-25 **4-26**

4-S1 (52% yield)

4-S2 (40% yield)

Scheme 4.5. Syntheses of substrates 4-S1 and 4-S2.

4.4.2 Cyclization experimental procedure

Reaction conditions were summarized in Table 4.1.

Chiral PVP supported Cu/Au nanoclusters was prepared following the reported procedure.[1,13] A solution of 6.5 mg of CuCl and 255 mg of CSPVP **4-24** in 10 mL of DI water was kept stirring for 20 min at room temperature until everything was completely dissolved. Allowed it to cool to 0^oC, 2.19 mL of $HAuCl_4{\cdot}3H_2O$ (c = 10 mmol/L) stock solution was added, followed by 9 mg of $NaBH_4$. Reaction solution turned to be dark grey immediately after adding $NaBH_4$. Resulting reaction solution was kept stirring at 0^oC for another 30 min.

After forming CSPVP-Cu/Au nanoclusters, 10 mL of acetonitrile, 338 mg of compound **4-S1** and 2.2 mL of (w/w) 30% H_2O_2 aqueous solution were added to the solution at 0^oC. Allowed it to warm to room temperature and kept stirring at 50^0C. Reaction was tracked through Thin-layer chromatography (TLC) and ^{1}HNMR. Temperature was increased to 60^0C after 24 h and reaction was stopped after 8 days although small amount of starting material **4-S1** was left behind.

Reaction was diluted with 10 mL of distilled water and extracted with dichloromethane five times. Combined organic layers were washed with brine, dried over $MgSO_4$, filtered concentrated and distilled off solvents. The concentrated residue was column chromatographed on silica gel using a gradient mixture of hexane and diethyl ether as eluent to give 22 mg (6% yield without counting starting material recovery; 7% yield with counting starting material recovery) of lactone product **4-L** as light yellow liquid.

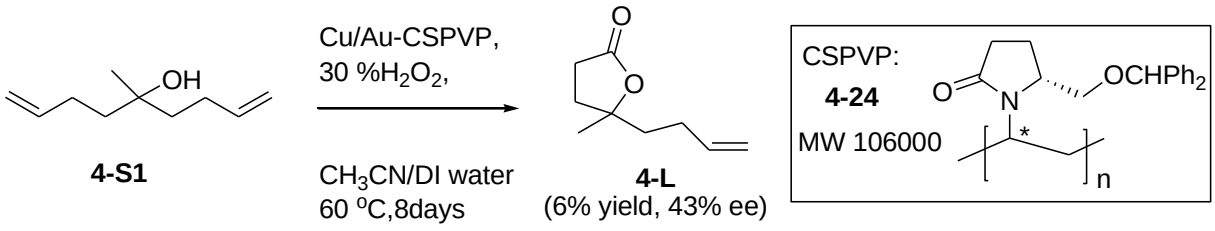

Reagent (Molecular Weight)	**Equivalent**	**mmol**	**Weight**	**Volume**
4-S1 (154)	1 eq.	2.19 mmol	338 mg	
CuCl (99)	0.03 eq.	0.066 mmol	6.5 mg	
$HAuCl_4{\cdot}3H_2O$ (393.8)	0.01 eq.	0.0219 mmol		2.19 mL (c = 10 mM/L)

CSPVP **4-24** (106000)	0.0011 eq.	0.0024 mmol	255 mg	
$NaBH_4$ (38)	0.1 eq.	0.219 mmol	9 mg	
(w/w) 30% H_2O_2 (34.01)	10 eq.	21.9 mmol	2.48 g	2.2 mL (d=1.110 g/mL)
CH_3CN				10 mL
DI water				10 mL

Table 4.1. Reaction conditions of CSPVP-Cu/Au nanoclusters catalyzed cyclization of 5-methylnona-1,8-dien-5-ol (compound 4-S1).

4.5 Discussion

4.5.1 Results, discussion and product characterization.

After 8 days reaction, got 22 mg of lactone product **4-L**, 28 mg of recovered starting material **4-S1**. Most of the reacted starting material **4-S1** went through polymerization to form 150 mg of byproduct polymer, which led to low yield (6% yield) of cyclized lactone. Compound **4-L** was characterized by ^{1}HNMR, ^{13}CNMR, and MS as described in section 4.7.2.11. The regiochemistry of compound **4-L** was analyzed by 2D correlation spectroscopy (COSY) NMR as shown in Figure 4.5. In COSY spectrum, the signals at 2.48 -2.7 ppm (2H) assigned for C3-hydrogens showed correlation with C4-hydrogens at 1.91 - 2.04 ppm (2H); signals at 1.66-1.84 ppm (2H) assigned for C6-hydrogens showed correlation with C7-hygrogens at 2.04 - 2.21 ppm (2H); signals at 5.70 -5.90 ppm (1H) assigned for C8-hydrogen showed correlation with C9-hydrogens at 4.82 - 5.18 ppm (2H); singlet at 1.39 ppm (3H) assigned for the methyl hydrogens had no correlation with other protons. The % ee of compound **4-L** was determined by HPLC using chiral column, Chiralpak AD(-H) column, *n*-hexane : *i*-PrOH = 93:7, flow rate: 0.3 mL/min; t_1 = 53 min and t_2 = 56 min. HPLC analysis was carried out by Mr. Bo Hao in the Hua group and the result was shown in Figure 4.6. Optical purity of obtained compound **4-L** was 44% ee. However, the configurations of two enantiomers couldn't be assigned at this time.

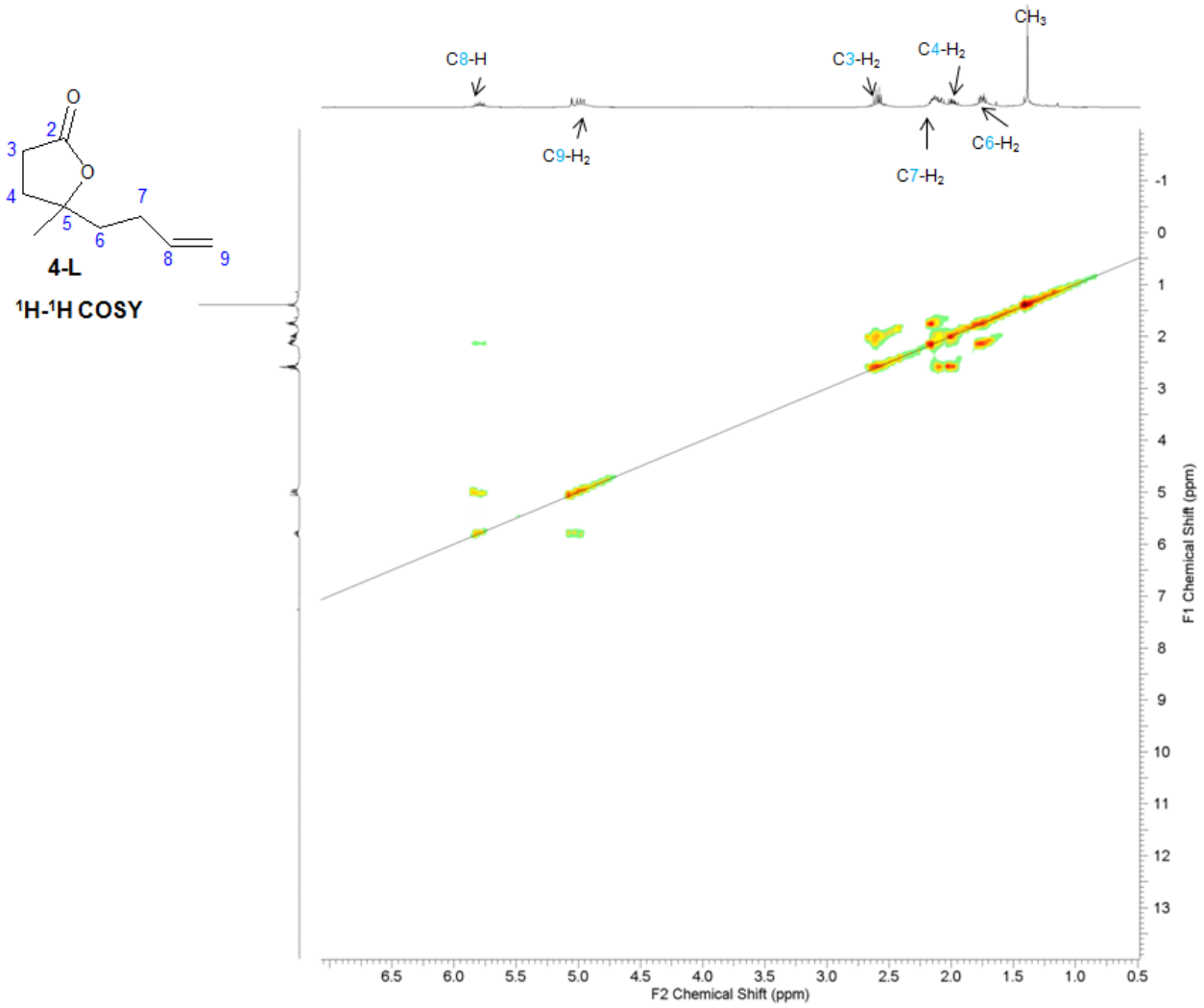

Figure 4.5. ^{1}H-^{1}H COSY spectrum of compound 4-L.

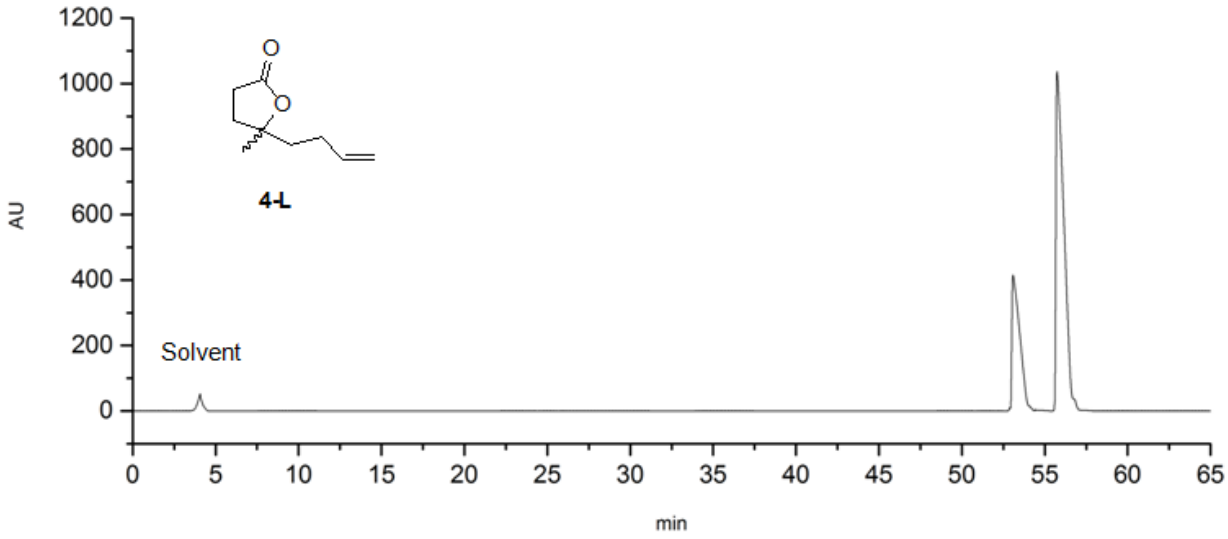

Figure 4.6. Optical purity of obtained compound 4-L was determined by HPLC. (HPLC analysis was carried out by Mr. Bo Hao in the Hua group.)

4.5.2 Concerns

The advantages of this method are catalytic asymmetric cyclization, creating a quaternary carbon stereogenic center in one step and easy synthetic approach to obtain the Cu/Au nanoclusters. The chemical yields and enantioselectivities of the reactions have been improved significantly by Mr. Bo Hao after my initial study (notably, compound **4-S2** provided 95% ee with 75% yield of the cyclized product). The big improvement was achieved by using different chiral-substituted PVP (CSPVP) to stabilize Cu/Au nanoclusters and different substrates such as **4-S2**. Apparently, by introducing bulkier functional group in C3 and C4 positions of CSPVP, better reaction yields and enantioselectivities were obtained.

4.5.3 Future work

The catalytic cyclization of diene substrate **4-S2** is being conducted by Mr. Bo Hao. Much better reaction yields and enantioselectivities have been obtained by using different CSPVP as discussed in section 4.5.2. Reaction temperature was optimized to 50^0C with shorter reaction time (three days). Exploration on a broader substrate scope (Figure 4.4, **4-SX**) could be performed in the future under the optimized reaction conditions. Inspired by the discovery that introducing bulkier functional group in C3 and C4 positions of CSPVP could increase

enantioselectivity and reaction yield, introducing bulkier substitutions in 5-substituted nona-1,8-dien-5-ols could be attempted to further increase reaction yield. We hypothesize that the C-5 methyl group in **4-S1** is too small for the stereoselective desymmetrization reaction. As shown in Figure 4.7, the C(4)-C(5)-O(11) and C(6)-C(5)-O(11) bond-angle values of compounds **4-S1** and **4-S2** were calculated by Chem-3D based on their predicted minimized energy models. The smaller C-C-O bond angle decreased from 109.159^{o} to 107.107^{o} when C5-position was substituted by bigger phenyl group. In other words, the bulkier C-5 substitution pushed -OH group more towards double bond, which could have a higher chance to go through cyclization considering hydroxyl group directing the oxidation[1].

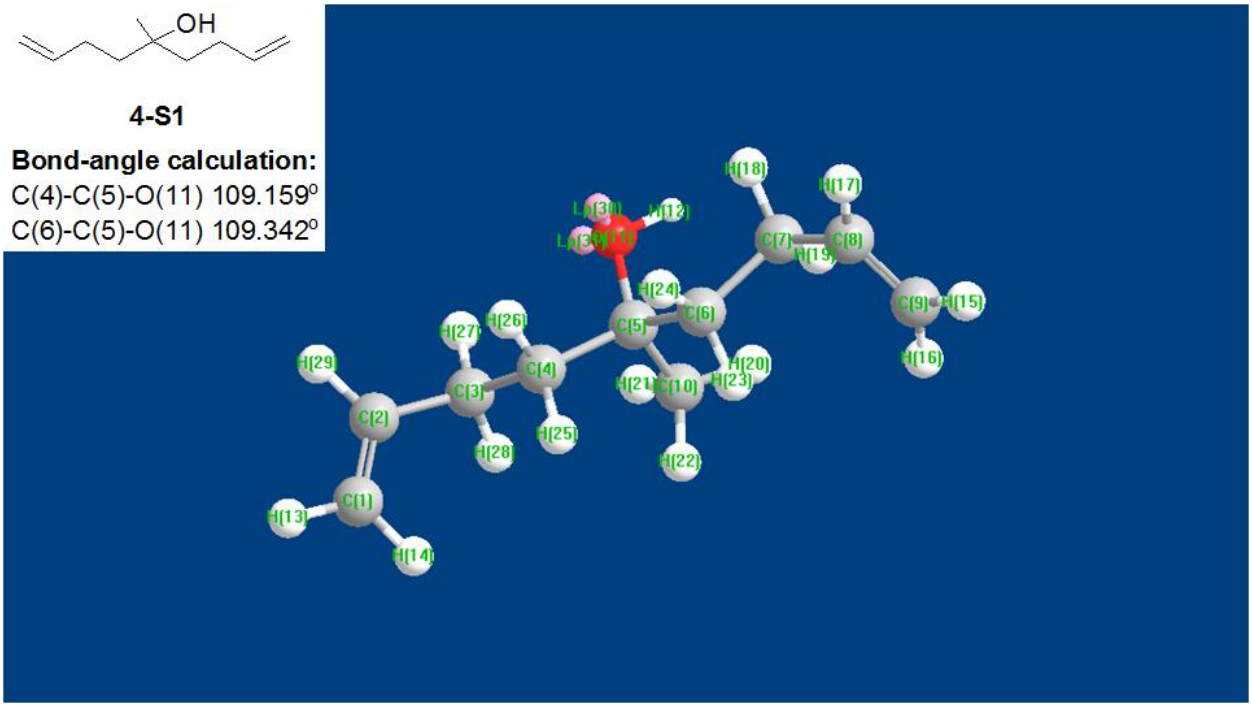

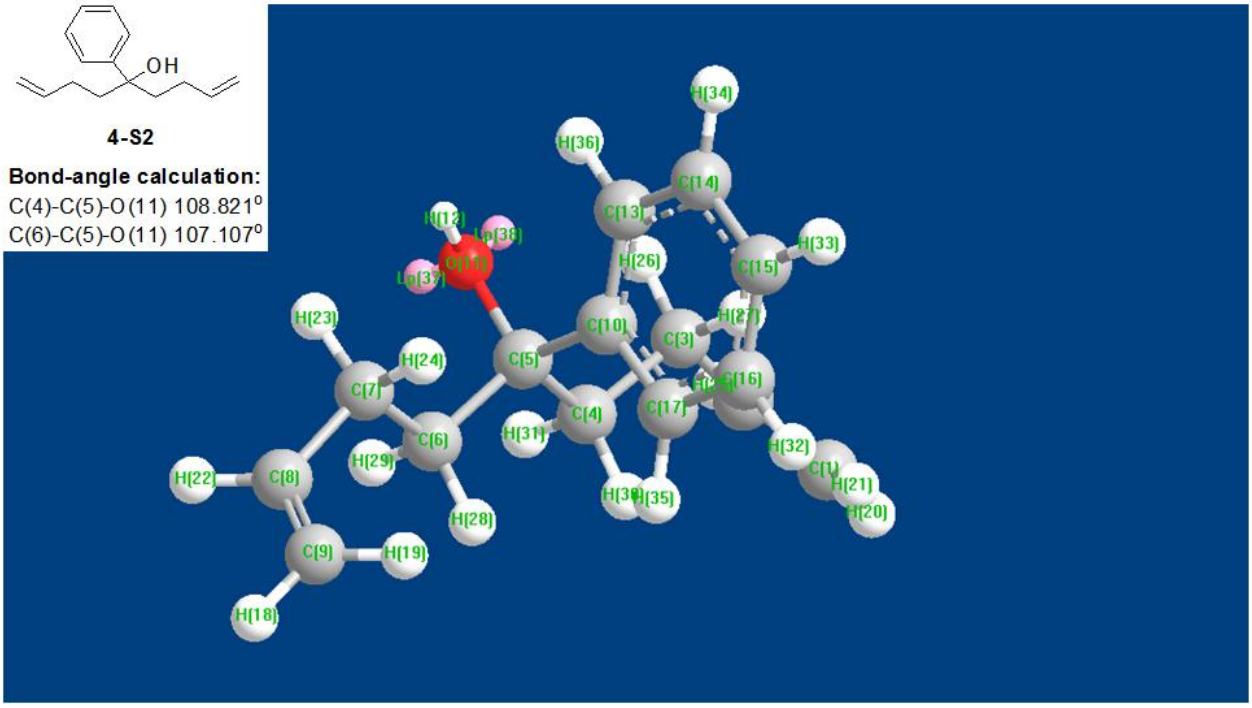

Figure 4.7. Chem-3D calculated C(4)-C(5)-O(11) and C(6)-C(5)-O(11) bond-angle values on minimized energy models of compounds 4-S1 and 4-S2.

4.6 Conclusion

A five-member cyclized lactone possessing a stereogenic tetrasubstituted carbon center was formed in a one-step Cu/Au nanoclusters-hydrogen peroxide oxidation reaction. This developed a novel and simple method to synthesize tetrasubstituted carbon stereogenic center. Significant improvement of reaction yields and enantioselectivities were achieved by introducing bulkier substitution in C3 and C4 positions of CSPVP according to updates from ongoing research.

4.7 Synthetic experimental procedures

4.7.1 General

Chemicals were purchased from Fisher Scientific and VWR international LLC and Chem-Impex International, Inc.. NMR spectra were taken from a 400 MHz Spectrometer (Varian Inc.) in chloroform-D unless otherwise informed. Mass spectra were obtained from an API 2000-triple quadrupole ESI-MS/MS mass spectrometer (Applied Biosystems).

4.7.2 Representative synthesis

(Descriptions of syntheses of compounds **4-11**, **4-15** and **4-1** were reprinted with permission from the supporting information of Bo Hao et al.[1] *Journal of the American Chemical Society* **2016**, *138*, 16839-16848. Copyright © 2016 American Chemical Society.)

4.7.2.1 *(S)-tert-Butyl 3-tert-butoxy-1-(2,2-dimethyl-4,6-dioxo-1,3-dioxan-5-yl)-1-oxopropan-2-ylcarbamate (Compound 4-11)*[5-7]

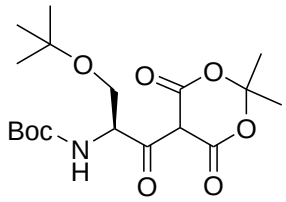

4-11

A solution of 4.0 g (15.3 mmol) of *N*-Boc-*O*-*tert*-butyl-L-serine, 3.3 g (23 mmol) of Meldrum's acid (2,2-dimethyl-1,3-dioxane-4,6-dione), and 2.8 g (22.9 mmol) of 4-(dimethylamino)pyridine (DMAP) in 80 mL of dichloromethane under argon was cooled to 0^{o}C over an ice-water bath. To it, a solution of 3.47 g (16.8 mmol) of *N,N'*-dicyclohexylcarbodiimide (DCC) in 20 mL of dichloromethane was added dropwise. The mixture was stirred for 12 hours under argon and the precipitated (*N,N*'-dicyclohexylurea) was removed by filtration. The filtrate was washed with 50 mL of 5% HCl, and then water, dried (anhydrous Na_2SO_4), and concentrated to dryness leaving 5.83 g of compound **4-11** as a white solid. This compound was used in the following step without further purification. ^{1}H NMR δ ppm 5.67 – 5.63 (m, 1 H), 5.49 – 5.47 (m, 1 H), 3.74 – 3.70 (m, 2 H), 3.62 (s, 1 H, NH), 1.76 (s, 3 H), 1.73 (s, 3 H), 1.46 (s, 9 H), 1.26 (s, 9 H). ^{13}C NMR δ ppm 206.8, 172.7, 152.3, 105.9, 79.0, 75.0, 62.0, 60.6, 59.9, 30.0 (3 C), 28.4 (3 C), 25.6 (2 C). MS (positive mode), m/z calcd for $C_{18}H_{30}NO_8$ $(M+H)^+$ 388.2, found 388.7.

4.7.2.2 *(R)-tert-Butyl 3-tert-butoxy-1-(2,2-dimethyl-4,6-dioxo-1,3-dioxan-5-yl)propan-2-ylcarbamate (Compound 4-15)*

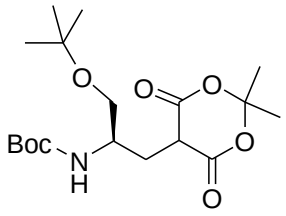

4-15

To a cold (0°C) solution of 5.80 g (15.2 mmol) of compound **4-11** in 150 mL of dichloromethane under argon were added 5.51 g (91.8 mmol) of acetic acid and 1.51 g (39.8 mmol) of $NaBH_4$. The solution was stirred at 0°C for three hours and at 25°C for 12 hours, diluted with 30 mL of water, the dichloromethane layer was separated, and the water layer was extracted with dichloromethane three times. The combined organic layers were washed with water and brine, dried (anhydrous Na_2SO_4), concentrated to give a yellow oil, which was crystallized from diethyl ether to give 5.27 g of compound **4-15** as a white solid. ^{1}H NMR δ ppm 5.08 – 5.09 (m, 1 H), 4.08 – 4.00 (m, 1 H), 3.62 (s, 1 H, NH), 3.45 – 3.41 (m, 2 H), 2.5 – 2.45 (m, 1 H), 2.16 – 2.01 (m, 1 H), 1.80 (s, 3 H), 1.72 (s, 3 H), 1.40 (s, 9 H), 1.05 (s, 9 H); ^{13}C NMR δ ppm 208.0, 174.6, 151.0, 105.7, 79.3, 74.7, 69.8, 49.6, 47.1, 31.9, 28.4, 25.7. MS (positive mode), m/z calcd for $C_{18}H_{32}NO_7$ $(M+H)^+$ 374.2, found 374.0.

4.7.2.3 *(R)-N-(tert-Butoxycarbonyl)-5-(tert-butoxymethyl)-pyrrolidin-2-one (Compound 4-1)*

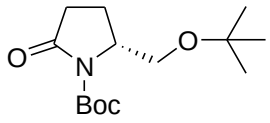

4-1

A solution of 5.26 g (14.10 mmol) of compound **4-13** in 40 mL of toluene under argon was heated to reflux for 6 hours, cooled to 25°C, concentrated under vacuum, and column chromatographed on silica gel using hexane and ethyl acetate (4:1) as eluent to give 3.44 g (83% overall yield in three steps) of compound **3** as a yellow oil. ^{1}H NMR δ ppm 4.09 – 4.07 (m, 1 H), 3.52 (dd, J = 10, 4 Hz, 1 H), 3.31 (dd, J = 10, 1.6 Hz, 1 H), 2.56 (dt, J = 17.6, 9.6 Hz, 1 H), 2.20 (dd, J = 17.6, 9.2 Hz, 1 H), 2.05 – 1.84 (m, 2 H), 1.40 (s, 9 H), 1.02 (s, 9 H). ^{13}C NMR δ ppm 175.3, 150.1, 82.6, 73.2, 62.9, 58.0, 32.5, 28.2, 27.5, 21.7. MS (positive mode), m/z calcd for $C_{14}H_{26}NO_4$ $(M+H)^+$ 272.2, found 272.0.

4.7.2.4 *(R)-tert-Butyl 2-isopropyl-5-oxopyrrolidine-1-carboxylate (Compound 4-2)*

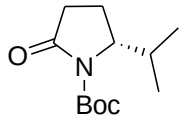

4-2

Following similar procedure described before (see sections 4.7.2.1 to 4.7.2.3), instead of *N*-Boc-*O-tert*-butyl-L-serine, started from 3.9 g (18 mmol, 1eq.) of Boc-L-valine in the beginning and produced 3.08 g (75% overall yield in three steps) of product **4-2** as light yellow oil. ^{1}H NMR δ ppm 0.83 (d, J = 7.03 Hz, 3 H) 0.92 (d, J = 7.03 Hz, 3 H) 1.50 (s, 9 H) 1.74 - 1.86 (m, 1 H) 1.89 - 2.06 (m, 1 H) 2.12 - 2.27 (m, 1 H) 2.32 - 2.57 (m, 2 H) 3.98 - 4.12 (m, 1 H). ^{13}C NMR δ ppm 175.1, 150.4, 82.9, 62.7, 32.5, 30.8, 28.2 (3C), 19.2, 18.2, 16.0. MS (positive mode), m/z calcd for $C_{12}H_{21}NO_3Na$ $(M+Na)^+$ 250.1, found 250.3.

4.7.2.5 *(R)-tert-Butyl 2-tert-butyl-5-oxopyrrolidine-1-carboxylate (Compound 4-3)*

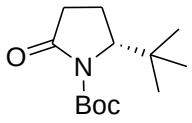

4-3

Following similar procedure described before (see sections 4.7.2.1 to 4.7.2.3), instead of *N*-Boc-*O-tert*-butyl-L-serine, started from 3 g (13 mmol, 1eq.) of Boc-Tle-OH in the beginning and produced 2.7 g (85% overall yield in three steps) of product **4-3** as light yellow oil. ^{1}H NMR δ ppm 0.74 (s, 9 H) 1.34 (s, 9 H) 1.66 - 2.03 (m, 2 H) 2.13 - 2.45 (m, 2 H) 3.93 (d, J = 8.98 Hz, 1 H). 13C NMR δ ppm 175.2, 150.8, 82.7, 65.0, 36.9, 32.6, 27.8 (3C), 26.3 (3C), 20.2. MS (positive mode), m/z calcd for $C_{13}H_{23}NO_3Na$ $(M+Na)^+$ 264.2, found 264.4.

4.7.2.6 *(R)-tert-Butyl 2-((naphthalen-1-yl)methyl)-5-oxopyrrolidine-1-carboxylate (Compound 4-5)*

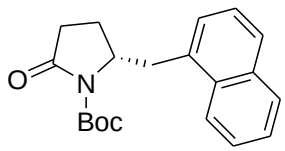

4-5

Following similar procedure described before (see sections 4.7.2.1 to 4.7.2.3), instead of *N*-Boc-*O-tert*-butyl-L-serine, started from 900 mg (2.85 mmol, 1eq) of Boc-L-1-Naphthylalanine in the beginning and produced 792 mg (86% overall yield in three steps) of product **4-5** as light yellow oil. ^{1}H NMR δ ppm 1.57 (s, 9 H) 1.73 - 1.88 (m, 2 H) 2.27 - 2.45 (m, 1 H) 2.48 - 2.69 (m, 1 H) 2.93 (dd, J=13.47, 10.35 Hz, 1 H) 3.80 (dd, J=13.50, 4.10 Hz, 1 H) 4.50 - 4.69 (m, 1 H) 7.15 - 7.64 (m, 4 H) 7.76 (d, J=8.20 Hz, 1 H) 7.85 (d, J=8.20 Hz, 1 H) 8.26 (d, J=8.20 Hz, 1 H).

4.7.2.7 ***(5R)-tert-Butyl 5-isopropyl-2-oxo-3-(phenylselanyl)pyrrolidine-1-carboxylate (Compound 4-19)***[8]

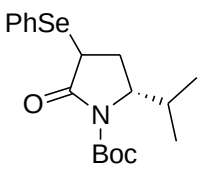

4-19

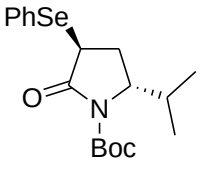

4-19-1

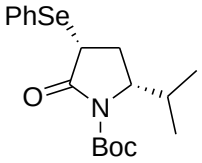

4-19-2

To a solution of 1.18 g (5.19 mmol, 1eq.) of compound **4-2** in16 mL of distilled THF at -78^{o}C, 5.7 mmol (1.1 eq.) of lithium diisopropylamide (LDA) solution was added dropwise and the resulting solution was kept stirring under argon at -78^{o}C for 1h. To it, a solution of 1.28g (5.4 mmol, 1.05 eq.) of phenylselenyl bromide in 13 mL of distilled THF was added dropwise and resulting reaction solution was kept stirring under argon at -78^{o}C for another 15 min. Reaction solution was quenched with saturated NH_4Cl aqueous solution, diluted with distilled water, extracted with dichloromethane three times. Combined organic layers were washed with brine, dried over Na_2SO_4, filtered, concentrated and column chromatographed on silica gel using a gradient mixture of hexane and ethyl acetate as eluent to produce 1.3 g (65% yield) of compound **4-19** as yellow solid. Note: Compound **4-19** is a mixture; the major product was **4-19-1** while small amount **4-19-2** mixed inside. The 65% reaction yield was calculated based on the recovery of mixture **4-19**. ^{1}H NMR δ ppm 0.79 (d, J = 6.64 Hz, 3 H) 0.86 (d, J = 6.64 Hz, 3 H) 1.51 (s, 9 H) 1.96 - 2.11 (m, 1 H) 2.16 - 2.30 (m, 2 H) 3.79 - 3.88 (m, 1 H) 3.90 - 4.04 (m, 1 H) 7.26 - 7.37 (m, 3 H) 7.60 - 7.74 (m, 2 H). **4-19-2**: ^{1}H NMR δ ppm 0.67 (d, J = 7.03 Hz, 3 H) 0.86 (d, J = 7.03 Hz, 3 H) 1.52 (s, 9 H) 1.78 - 1.92 (m, 1 H) 2.30 - 2.53 (m, 2 H) 3.87 - 4.04 (m, 2 H) 7.26 - 7.35 (m, 3 H) 7.64 - 7.71 (m, 2 H).

4.7.2.8 ***(S)-tert-Butyl 2-isopropyl-5-oxo-2H-pyrrole-1(5H)-carboxylate (Compound 4-4)***

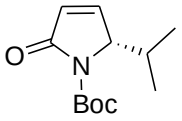

4-4

To a solution of 1.34 g (3.5 mmol, 1 eq.) of compound **4-19,** in 18 mL of 1,4-dioxane and 2 mL of distilled water, 975 mg (4.6 mmol, 1.3 eq.) of sodium periodate was added. The resulting reaction mixture was kept stirring vigorously at room temperature for 1 h. Diluted reaction mixture with 40 mL of 5% ammonium hydroxide solution and extracted with diethyl ether three times. Combined organic layers were washed with water, brine, dried over Na_2SO_4 , filtered, concentrated and column chromatographed on silica gel using a gradient mixture of hexane and ethyl acetate as eluent to give 470 mg (60% yield) of compound **4-4** as colorless oil. ^{1}H NMR δ ppm 0.67 (d, J = 7.03 Hz, 3 H) 1.10 (d, J = 7.03 Hz, 3 H) 1.55 (s, 9 H) 2.48 - 2.71 (m, 1 H) 4.45 - 4.65 (m, 1 H) 5.37 - 7.90 (m, 6 H) 6.14 (dd, J = 6.05, 2.10 Hz, 1 H) 7.12 (dd, J = 6.05, 2.10 Hz, 1 H). ^{13}C NMR δ ppm 169.7, 149.8, 148.0, 128.0, 83.1, 67.5, 29.1, 28.3 (3C), 19.7, 15.1. MS (positive mode), m/z calcd for $C_{12}H_{19}NO_3Na$ $(M+Na)^+$ 248.1, found 248.2.

4.7.2.9 *5-Methylnona-1,8-dien-5-ol (Compound 4-S1)*[20]

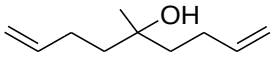

4-S1

To 3-butenylmagnesium bromide (4-26) prepared from 2.66 g (19.7 mmol, 2 eq.) of 4- bromo-1-butene (**4-25**) and 520 mg (21.7 mmol, 2.2 eq.) of magnesium in distilled diethyl ether at 0^{o}C, was added dropwise 867 mg (9.8 mmol, 1 eq.) of distilled ethyl acetate under argon. After 1 h stirring at room temperature under argon, the resulting reaction solution was quenched with saturated NH_4Cl aqueous solution, adjusted to pH around 2 to 3 using 2 N HCl aqueous solution and extracted with diethyl ether. Combined organic layers were washed with brine, dried over $MgSO_4$, filtered and distilled off most solvents. The concentrated residue was column chromatographed on silica gel using a gradient mixture of hexane and diethyl ether as eluent to give 800 mg (52% yield) of compound **4-S1** as colorless liquid. ^{1}H NMR δ ppm 1.18 (s, 3 H) 1.32 (s, 1 H) 1.44 - 1.69 (m, 4 H) 1.94 - 2.23 (m, 4 H) 4.76 - 5.21 (m, 4 H) 5.72 - 5.98 (m, 2 H). ^{13}C NMR δ ppm 139.1 (2C), 114.6 (2C), 72.7, 41.1 (2C), 28.5 (2C), 27.0. MS (positive mode), m/z calcd for $C_{10}H_{18}ONa$ $(M+Na)^+$ 177.1, found 177.1.

4.7.2.10 *5-Phenylnona-1,8-dien-5-ol (Compound 4-S2)*

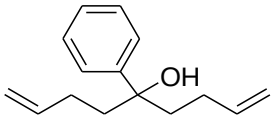

4-S2

To 3-butenylmagnesium bromide (**4-26**) prepared from 1.33 g (9.85 mmol, 2 eq.) of 4- bromo-1-butene (**4-25**) and 260 mg (10.8 mmol, 2.2 eq.) of magnesium in distilled diethyl ether at 0^{o}C, was added dropwise 808 mg (4.92 mmol, 1 eq.) of distilled isopropyl benzoate under argon. After 1 h stirring at room temperature under argon, the resulting reaction solution was quenched with saturated NH_4Cl aqueous solution, adjusted to pH around 2 to 3 using 2 N HCl aqueous solution and extracted with diethyl ether. Combined organic layers were washed with brine, dried over $MgSO_4$, filtered and distilled off most solvents. The concentrated residue was column chromatographed on silica gel using a gradient mixture of hexane and diethyl ether as eluent to give 420 mg (40% yield) of compound **4-S2** as colorless liquid. ^{1}H NMR δ ppm 1.69 - 2.21 (m, 8 H) 4.85 - 5.04 (m, 4 H) 5.62 - 5.90 (m, 2 H) 7.09 - 7.57 (m, 5 H). ^{13}C NMR δ ppm 145.8, 139.0 (2C), 128.4 (2C), 126.7, 125.5 (2C), 114.8 (2C), 77.4, 42.4 (2C), 28.2 (2C). MS (positive mode), m/z calcd for $C_{15}H_{21}O$ $(M+H)^{+}$ 217.1, found 218.1.

4.7.2.11 *5-(But-3-enyl)-dihydro-5-methylfuran-2(3H)-one (Compound 4-L)*

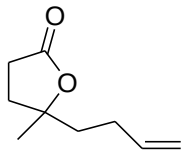

4-L

Reaction was performed as described in section 4.4.2.Started from 338 mg of compound **4-S1** and obtained 22 mg (6% yield) of product **4-L** as light yellow liquid. ^{1}H NMR δ ppm 1.39 (s, 3 H) 1.66 - 1.84 (m, 2 H) 1.91 - 2.21 (m, 4 H) 2.48 - 2.70 (m, 2 H) 4.82 - 5.18 (m, 2 H) 5.70 - 5.90 (m, 1 H). ^{13}C NMR δ ppm 176.8, 137.7, 115.3, 86.6, 40.2, 33.2, 29.3, 28.3, 25.8. MS (positive mode), m/z calcd for $C_9H_{14}O_2Na$ $(M+Na)^{+}$ 177.1, found 177.0.

Reference

(1) Hao, B.; Gunaratna, M. J.; Zhang, M.; Weerasekara, S.; Seiwald, S. N.; Nguyen, V. T.; Meier, A.; Hua, D. H. Chiral-Substituted Poly-N-vinylpyrrolidinones and Bimetallic Nanoclusters in Catalytic Asymmetric Oxidation Reactions. *Journal of the American Chemical Society* **2016**, *138*, 16839-16848.

(2) Peterson, E. A.; Overman, L. E. Contiguous stereogenic quaternary carbons: A daunting challenge in natural products synthesis. *Proc. Natl. Acad. Sci. U. S. A.* **2004**, *101*, 11943-11948.

(3) Büschleb, M.; Dorich, S.; Hanessian, S.; Tao, D.; Schenthal, K. B.; Overman, L. E. Synthetic Strategies toward Natural Products Containing Contiguous Stereogenic Quaternary Carbon Atoms. *Angewandte Chemie International Edition* **2016**, *55*, 4156-4186.

(4) Quasdorf, K. W.; Overman, L. E. Catalytic enantioselective synthesis of quaternary carbon stereocentres. *Nature* **2014**, *516*, 181-191.

(5) Smrcina, M.; Majer, P.; Majerová, E.; Guerassina, T. A.; Eissenstat, M. A. Facile stereoselective synthesis of γ-substituted γ-amino acids from the corresponding α-amino acids. *Tetrahedron* **1997**, *53*, 12867-12874.

(6) Kerr, M. S.; de Alaniz, J. R.; Rovis, T. An Efficient Synthesis of Achiral and Chiral 1,2,4-Triazolium Salts: Bench Stable Precursors for N-Heterocyclic Carbenes. *The Journal of organic chemistry* **2005**, *70*, 5725-5728.

(7) Ward, B. D.; Risler, H.; Weitershaus, K.; Bellemin-Laponnaz, S.; Wadepohl, H.; Gade, L. H. 2-Aminopyrrolines: New Chiral Amidinate Ligands with a Rigid Well-Defined Molecular Structure and Their Coordination to TiIV. *Inorganic Chemistry* **2006**, *45*, 7777-7787.

(8) Le, V. R.; White, A. J. P.; Burrows, J. N.; Barrett, A. G. M. Synthetic studies on the CDEF ring system of lactonamycin. *TETRAHEDRON* **2006**, *62*, 12252-12263.

(9) Kawaguchi, S.; Ito, K.: Dispersion Polymerization. In *Polymer Particles: -/-*; Okubo, M., Ed.; Springer Berlin Heidelberg: Berlin, Heidelberg, 2005; pp 299-328.

(10) Zhai, L.; Shi, T.; Wang, H. Preparation of polyvinylpyrrodione microspheres by dispersion polymerization. *Frontiers of Chemistry in China* **2009**, *4*, 83.

(11) Flebbe, T.; Hentschke, R.; Hädicke, E.; Schade, C. Modeling of polyvinylpyrrolidone and polyvinylimidazole in aqueous solution. *Macromolecular Theory and Simulations* **1998**, *7*, 567-577.

(12) Ferrando, R.; Jellinek, J.; Johnston, R. L. Nanoalloys: from theory to applications of alloy clusters and nanoparticles. *Chemical reviews* **2008**, *108*, 845-910.

(13) Hou, W.; Dehm, N. A.; Scott, R. W. J. Alcohol oxidations in aqueous solutions using Au, Pd, and bimetallic AuPd nanoparticle catalysts. *Journal of Catalysis* **2008**, *253*, 22-27.

(14) Toshima, N.; Yonezawa, T. Bimetallic nanoparticles-novel materials for chemical and physical applications. *New Journal of Chemistry* **1998**, *22*, 1179-1201.

(15) Yao, H.; Kobayashi, R. Chiral monolayer-protected Au–Pd bimetallic nanoclusters: Effect of palladium doping on their chiroptical responses. *Journal of colloid and interface science* **2014**, *419*, 1-8.

(16) Kanaoka, S.; Yagi, N.; Fukuyama, Y.; Aoshima, S.; Tsunoyama, H.; Tsukuda, T.; Sakurai, H. Thermosensitive Gold Nanoclusters Stabilized by Well-Defined Vinyl Ether Star Polymers: Reusable and Durable Catalysts for Aerobic Alcohol Oxidation. *Journal of the American Chemical Society* **2007**, *129*, 12060-12061.

(17) Sophiphun, O.; Wittayakun, J.; Dhital, R. N.; Haesuwannakij, S.; Murugadoss, A.; Sakurai, H. Gold/Palladium Bimetallic Alloy Nanoclusters Stabilized by Chitosan as Highly Efficient and Selective Catalysts for Homocoupling of Arylboronic Acid. *Australian Journal of Chemistry* **2012**, *65*, 1238-1243.

(18) Lu, J.; Toy, P. H. Organic Polymer Supports for Synthesis and for Reagent and Catalyst Immobilization. *Chemical reviews* **2009**, *109*, 815-838.

(19) Deng, D.; Jin, Y.; Cheng, Y.; Qi, T.; Xiao, F. Copper Nanoparticles: Aqueous Phase Synthesis and Conductive Films Fabrication at Low Sintering Temperature. *ACS Applied Materials & Interfaces* **2013**, *5*, 3839-3846.

(20) Brown, H. C.; Negishi, E.; Dickason, W. C. Hydroboration. 70. The polycyclic hydroboration of acyclic and cyclic trienes with borane in tetrahydrofuran and triethylamine-borane. Reexamination of the stereochemistry of isomeric perhydro-9b-boraphenalenes. *The Journal of Organic Chemistry* **1985**, *50*, 520-527.

Appendix A - ^{1}H-NMR and ^{13}C NMR spectra

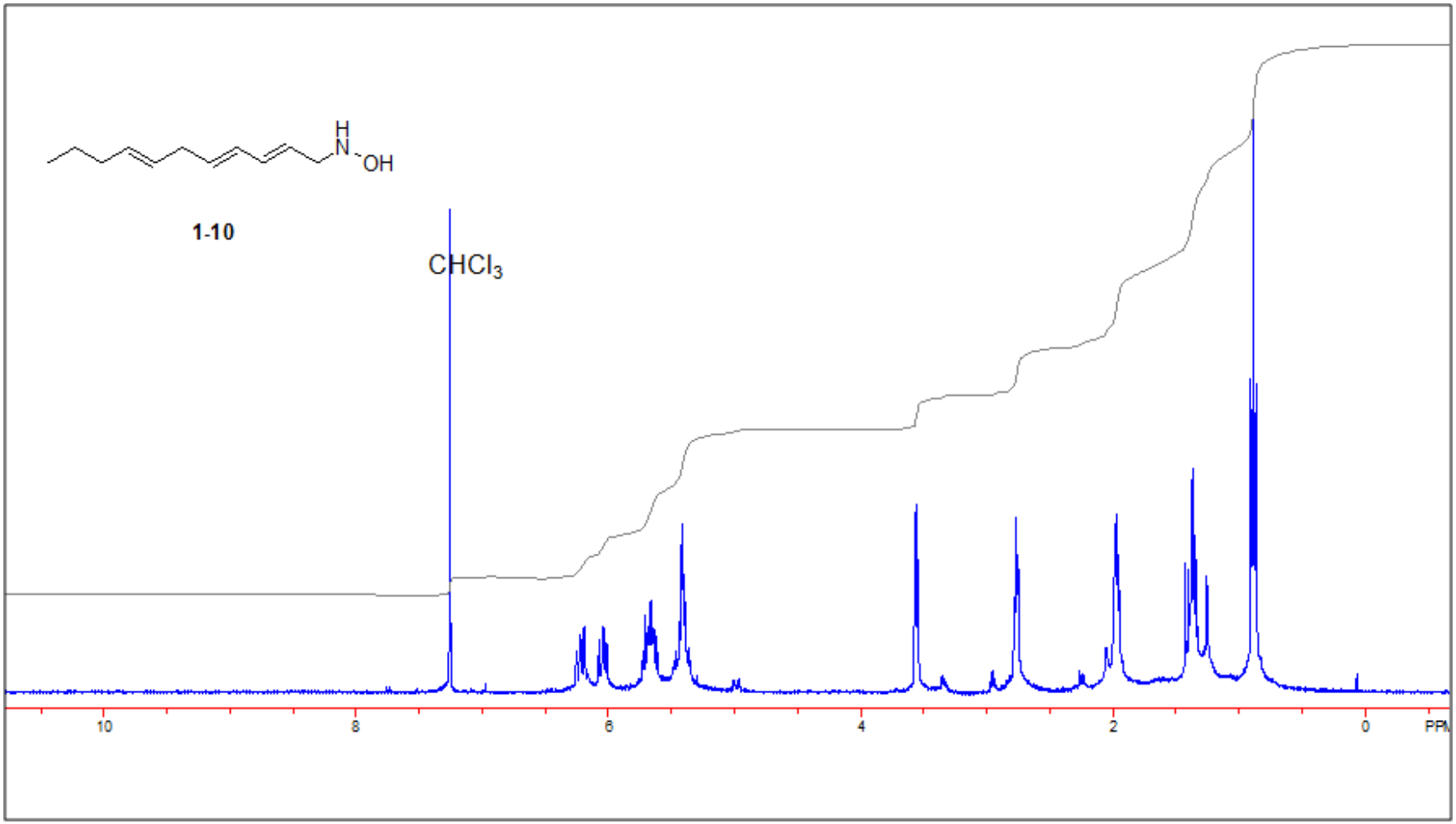
1-10
CHCl3
10
8
6
4
2
0
PPM

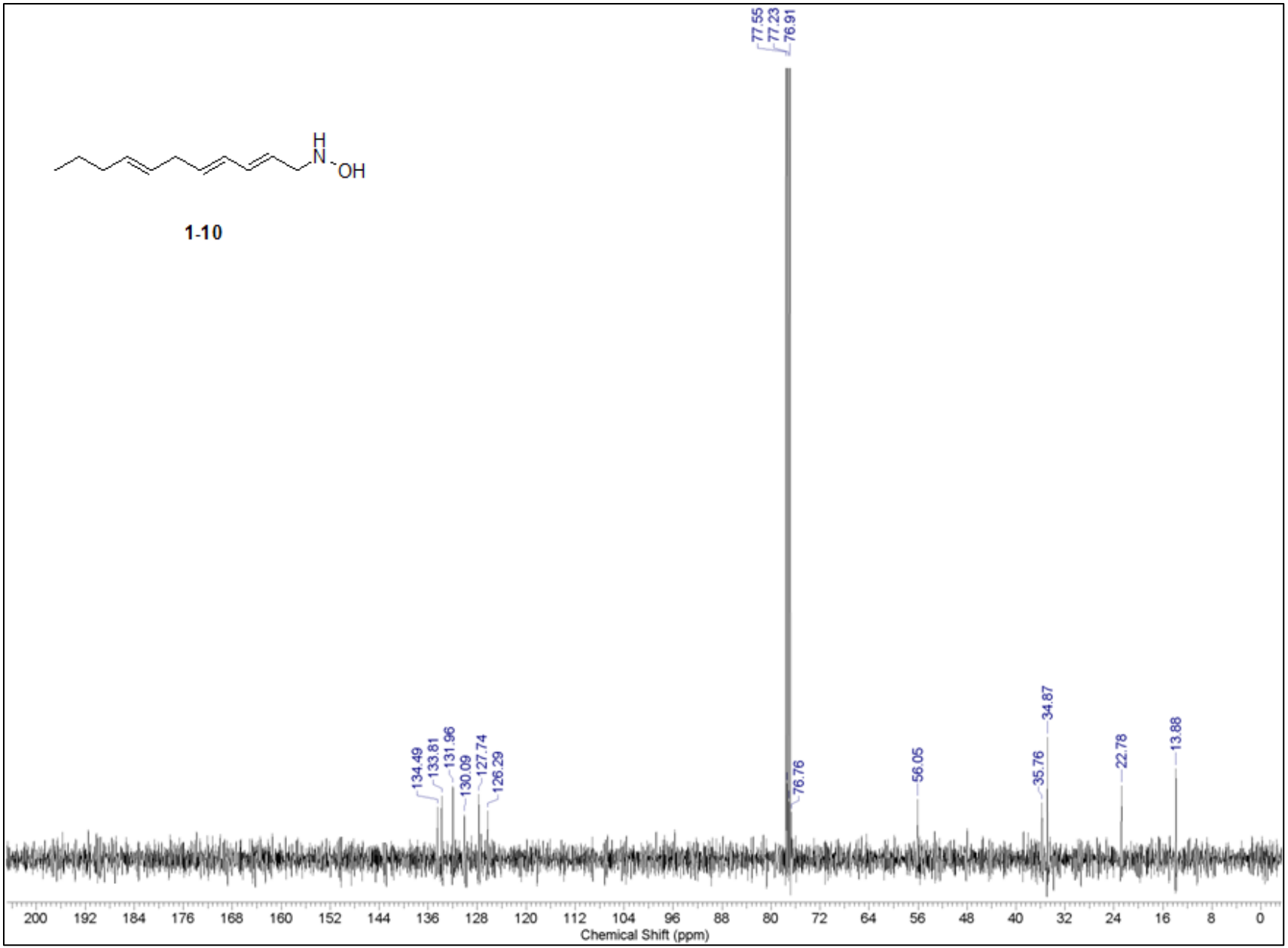
77.55
77.23
76.91
H
N
OH
1-10
134.49
133.81
131.96
130.09
127.74
126.29
76.76
56.05
35.76
34.87
22.78
13.88
200 192 184 176 168 160 152 144 136 128 120 112 104 96 88 80 72 64 56 48 40 32 24 16 8 0
Chemical Shift (ppm)

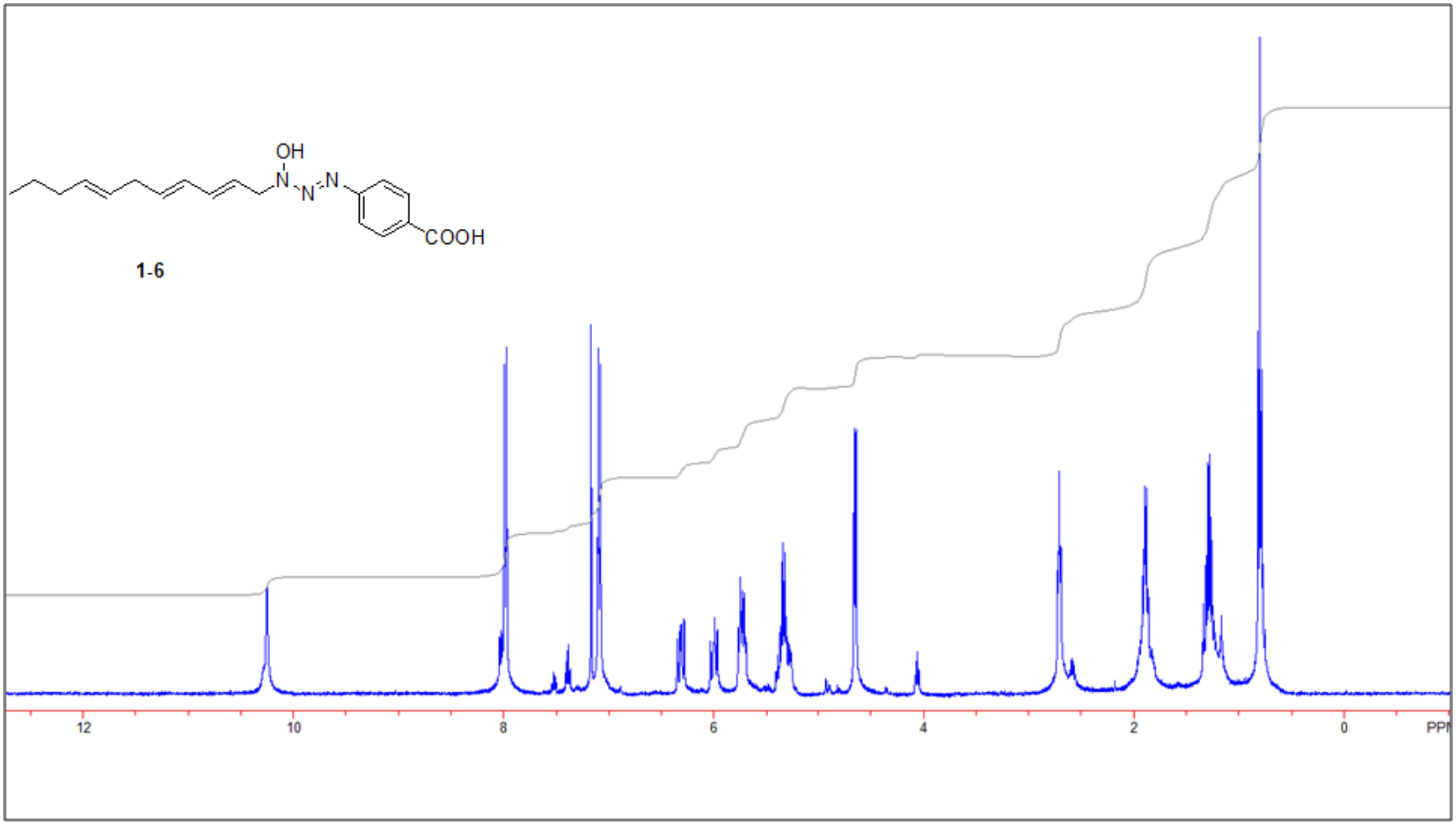
OH
N
N
N
COOH
1-6
12
10
8
6
4
2
0
PPM

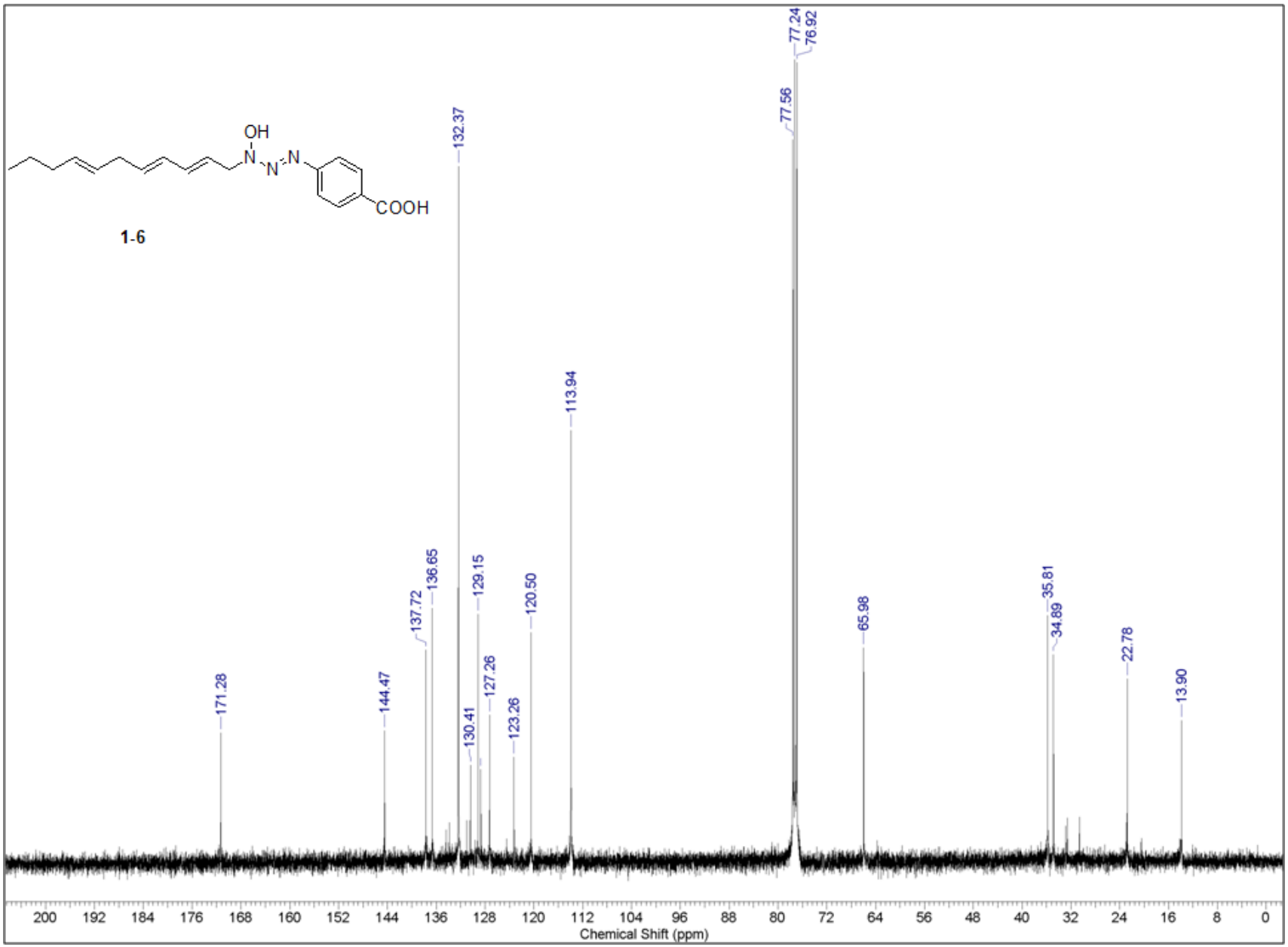
OH
N
N
N
COOH
1-6
171.28
144.47
137.72
136.65
132.37
130.41
129.15
127.26
123.26
120.50
113.94
77.56
77.24
76.92
65.98
35.81
34.89
22.78
13.90
200 192 184 176 168 160 152 144 136 128 120 112 104 96 88 80 72 64 56 48 40 32 24 16 8 0
Chemical Shift (ppm)

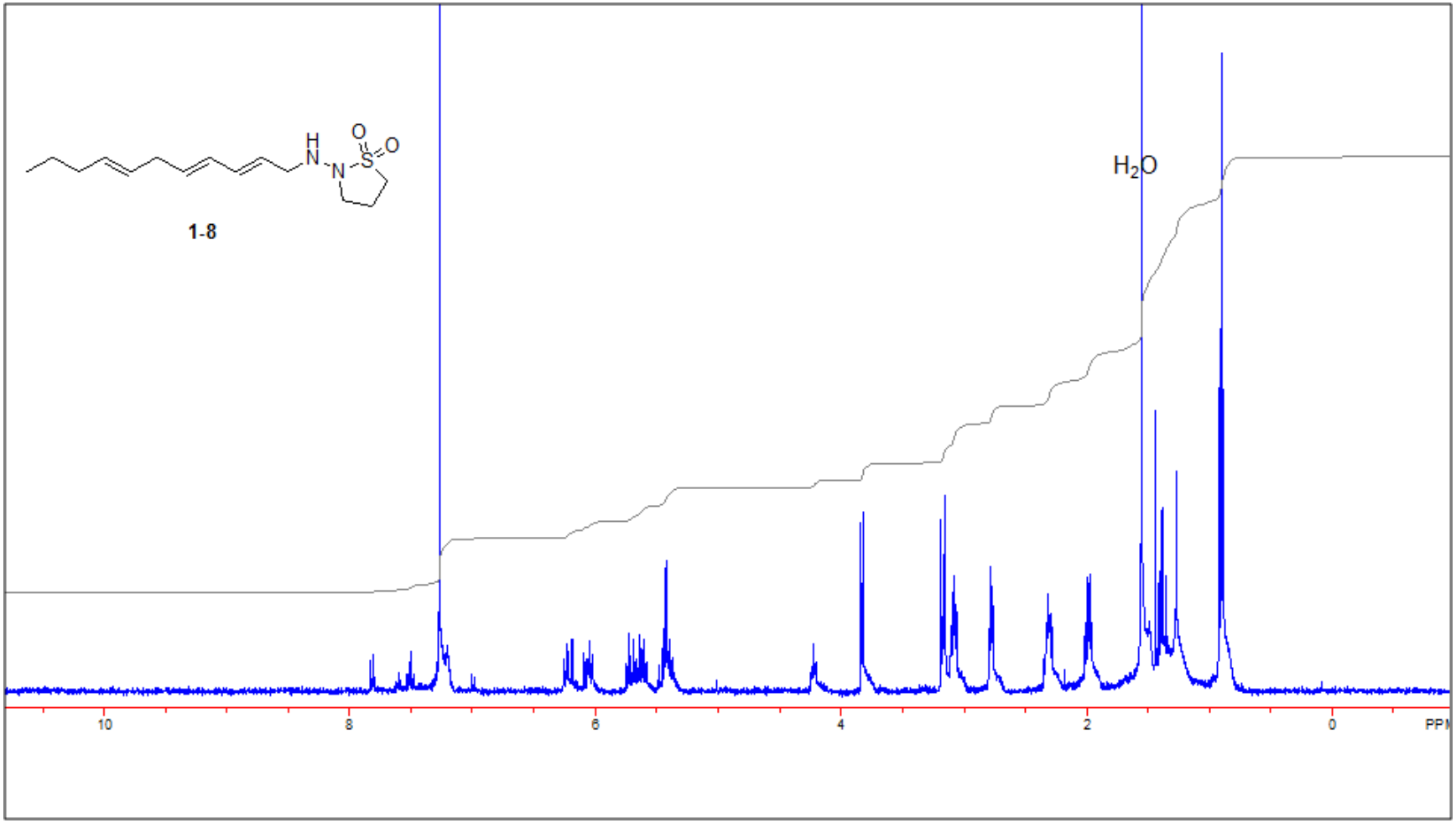
1-8
H
N
N
O
S
O
H2O
10
8
6
4
2
0
PPM

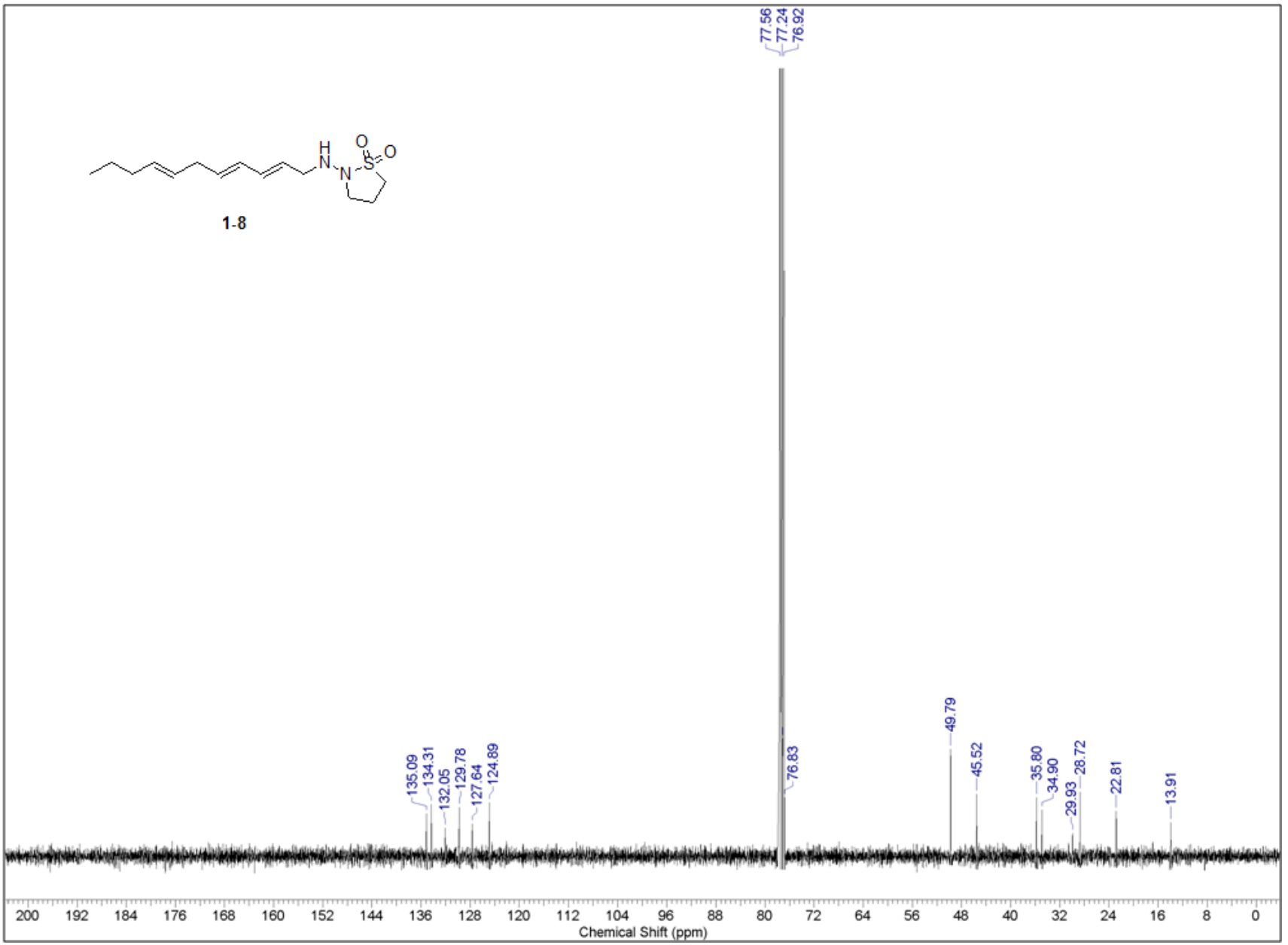
1-8
77.56
77.24
76.92
135.09
134.31
132.05
129.78
127.64
124.89
76.83
49.79
45.52
35.80
34.90
29.93
28.72
22.81
13.91
200 192 184 176 168 160 152 144 136 128 120 112 104 96 88 80 72 64 56 48 40 32 24 16 8 0
Chemical Shift (ppm)

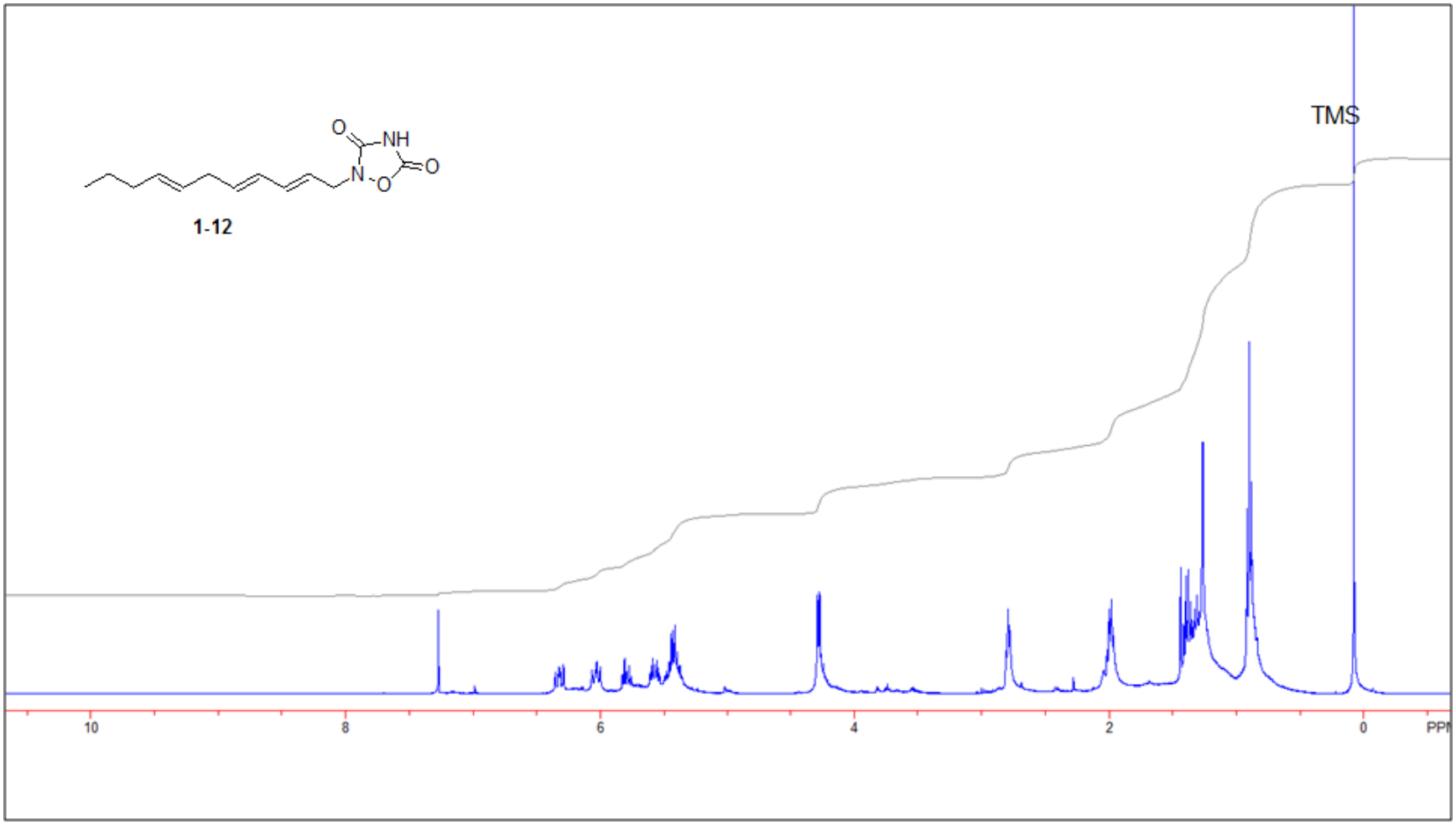
O
NH
N
O
O
1-12
TMS
10
8
6
4
2
0
PPM

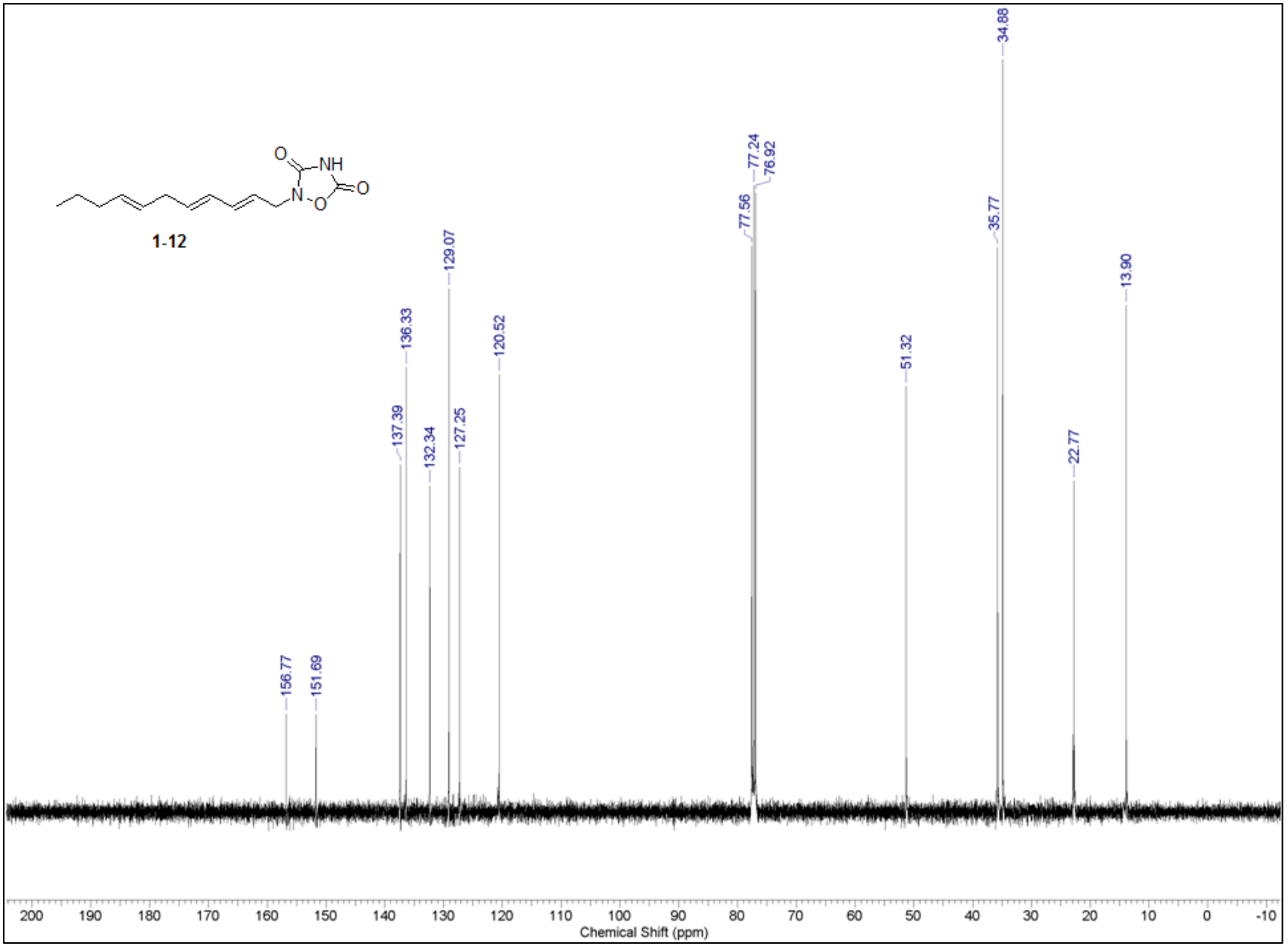
1-12
156.77
151.69
137.39
136.33
132.34
129.07
127.25
120.52
77.56
77.24
76.92
51.32
35.77
34.88
22.77
13.90
200
190
180
170
160
150
140
130
120
110
100
90
80
70
60
50
40
30
20
10
0
-10
Chemical Shift (ppm)

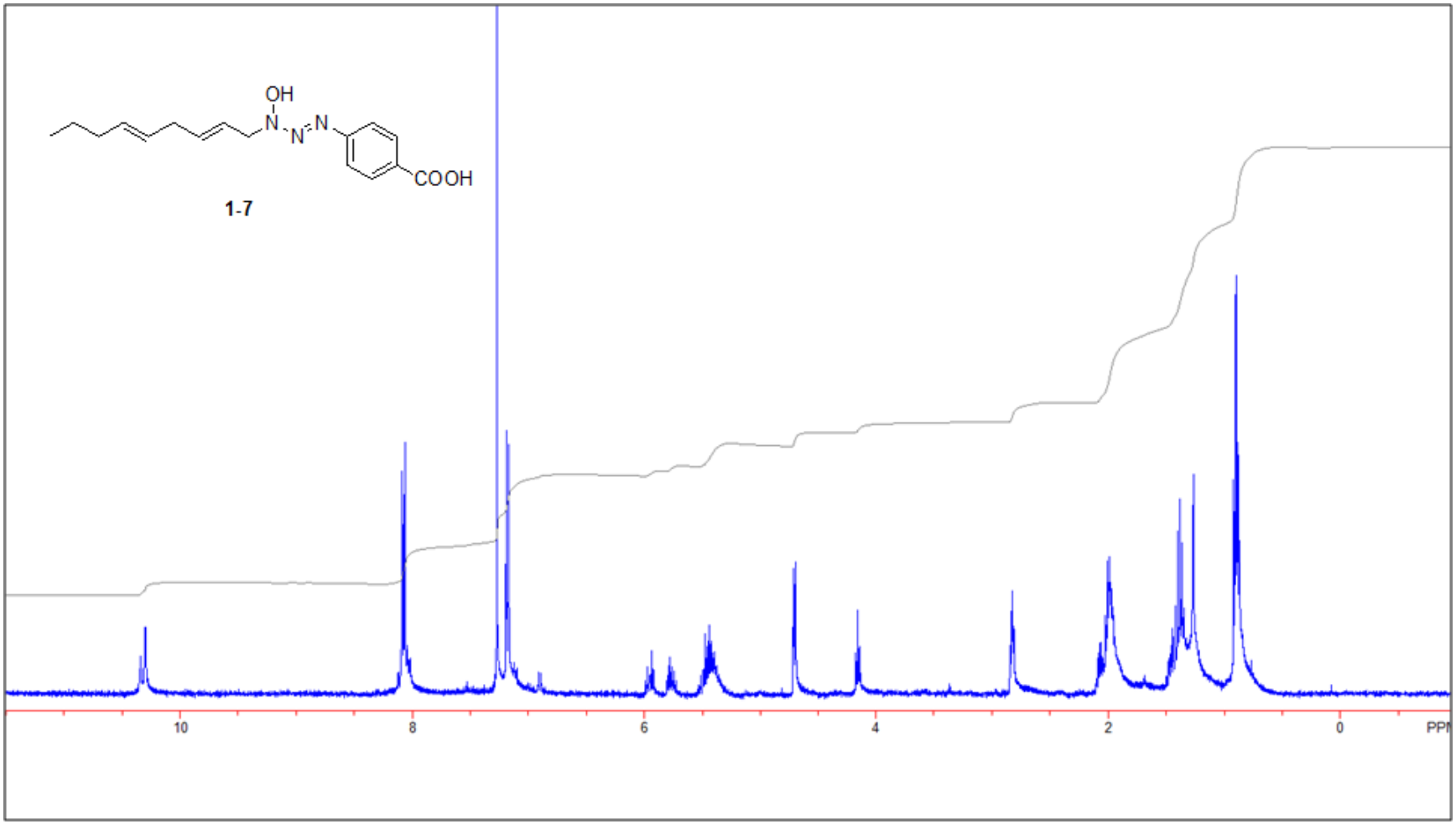
OH
N
N
N
COOH
1-7
10
8
6
4
2
0
PPM

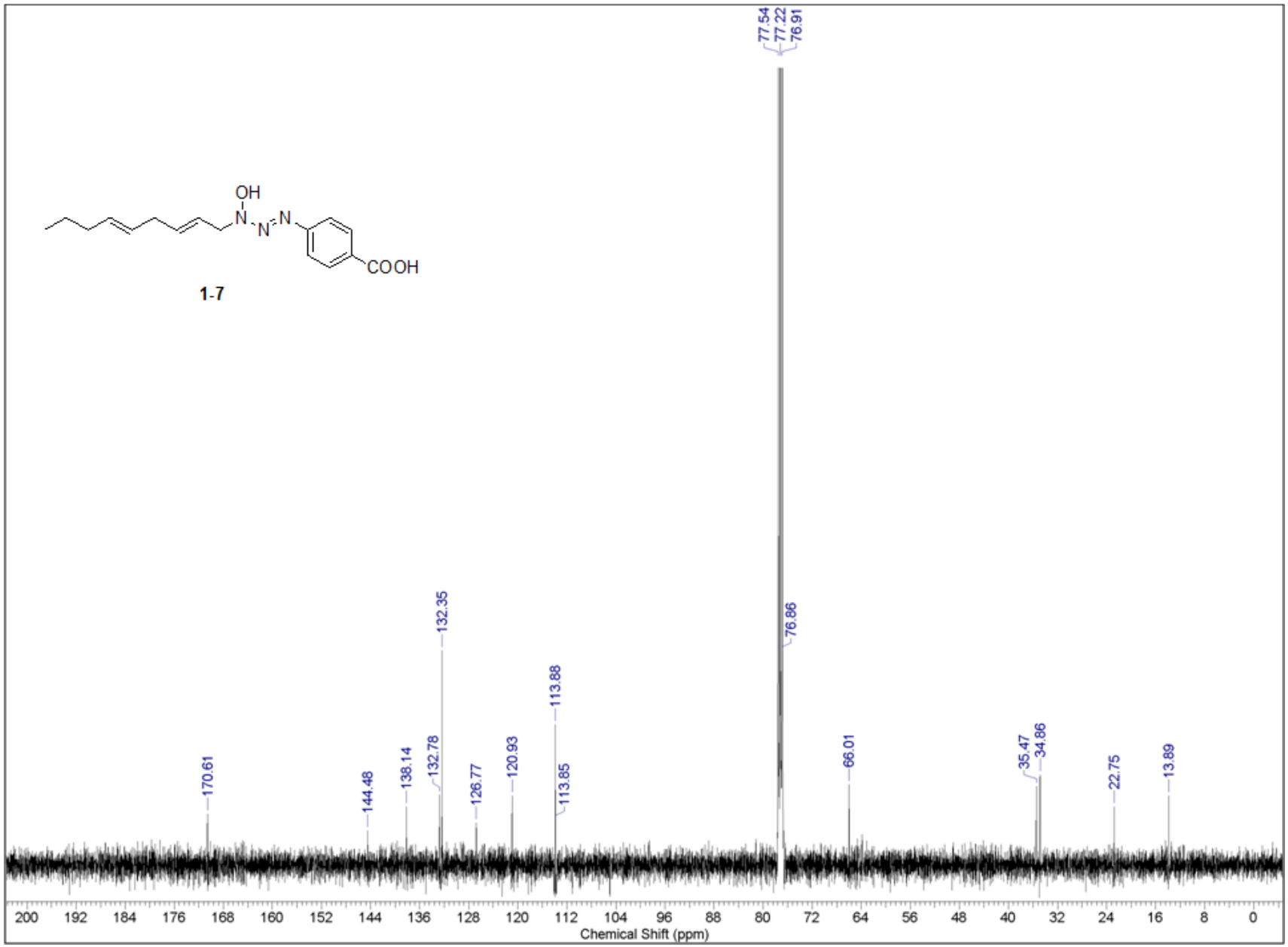
OH
N
N
N
COOH
1-7
77.54
77.22
76.91
76.86
170.61
144.48
138.14
132.78
132.35
126.77
120.93
113.88
113.85
66.01
35.47
34.86
22.75
13.89
200 192 184 176 168 160 152 144 136 128 120 112 104 96 88 80 72 64 56 48 40 32 24 16 8 0
Chemical Shift (ppm)

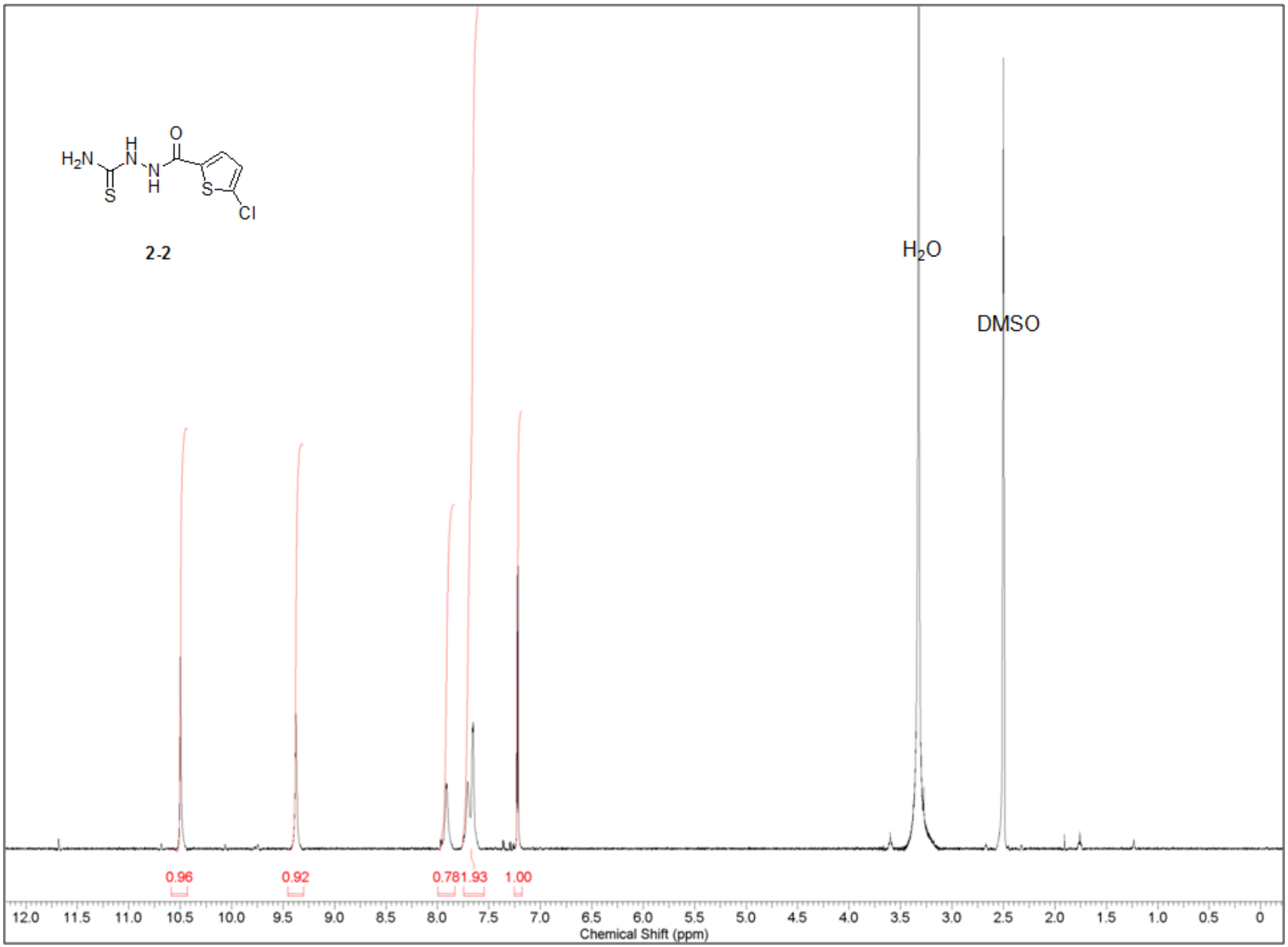
2-2
H2O
DMSO
0.96
0.92
0.78
1.93
1.00
12.0 11.5 11.0 10.5 10.0 9.5 9.0 8.5 8.0 7.5 7.0 6.5 6.0 5.5 5.0 4.5 4.0 3.5 3.0 2.5 2.0 1.5 1.0 0.5 0
Chemical Shift (ppm)

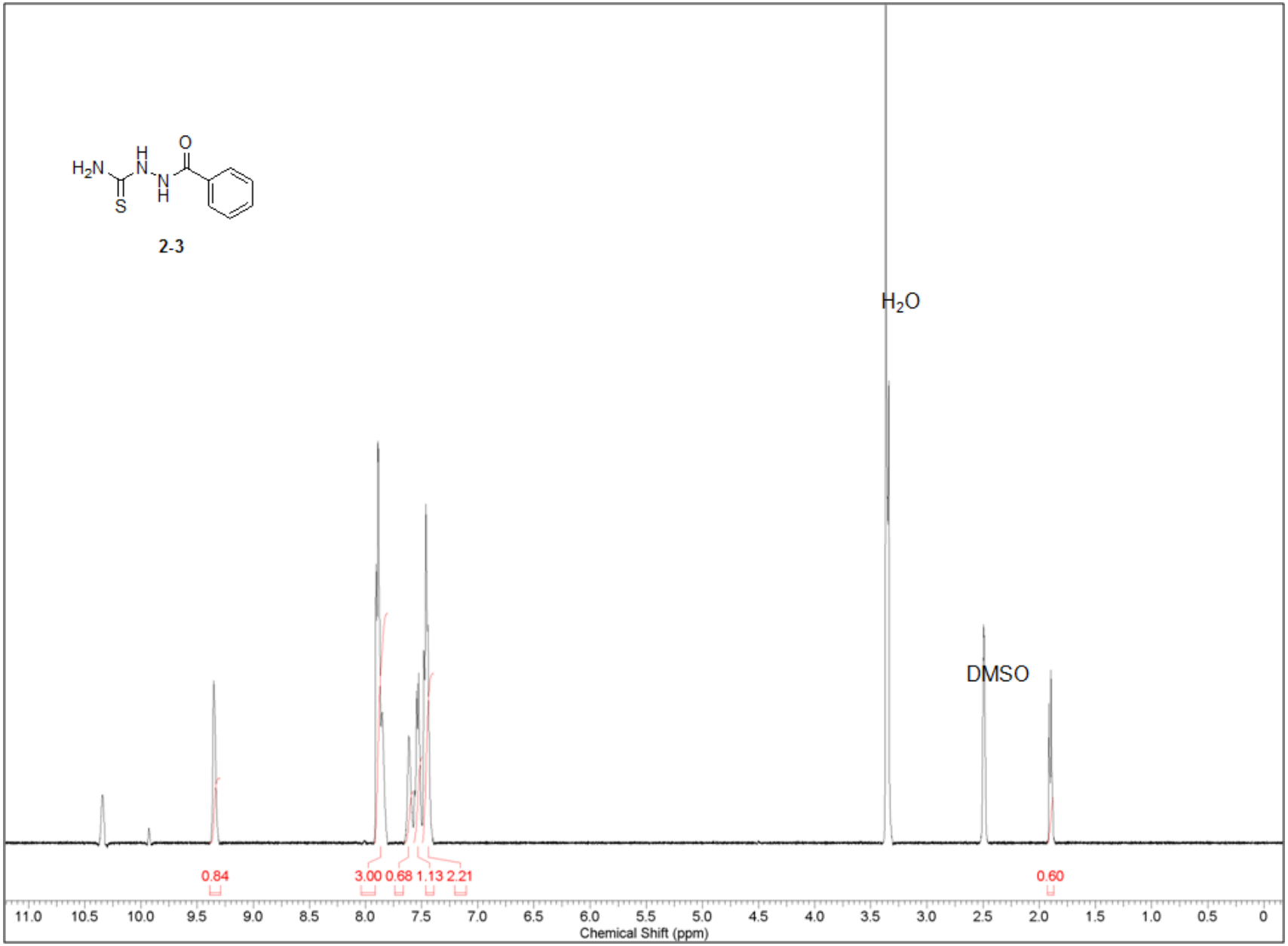
2-3
H2O
DMSO
0.84
3.00
0.68
1.13
2.21
0.60
Chemical Shift (ppm)

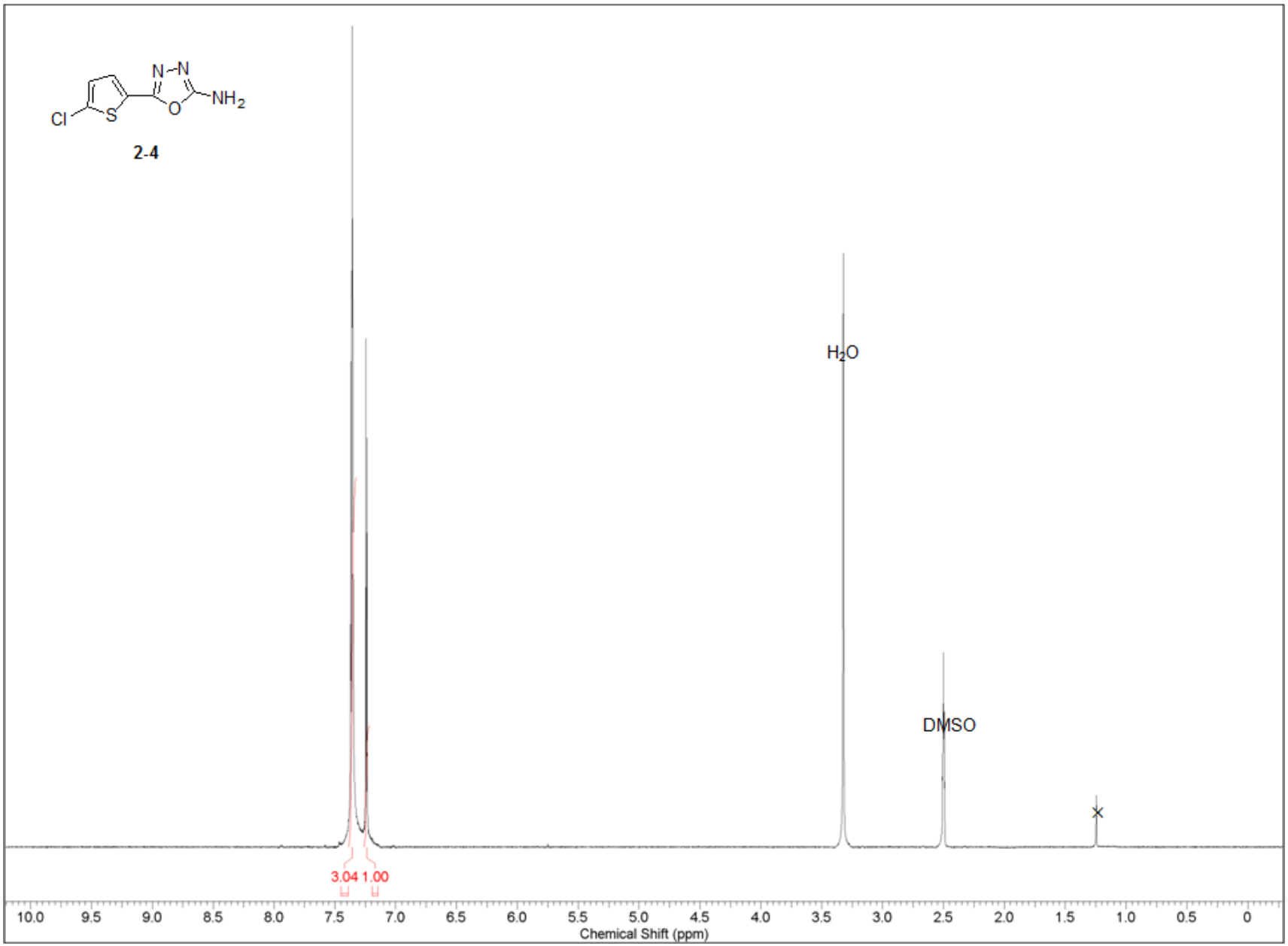
N
N
O
S
Cl
NH2
2-4
H2O
DMSO
3.04
1.00
10.0
9.5
9.0
8.5
8.0
7.5
7.0
6.5
6.0
5.5
5.0
4.5
4.0
3.5
3.0
2.5
2.0
1.5
1.0
0.5
0
Chemical Shift (ppm)

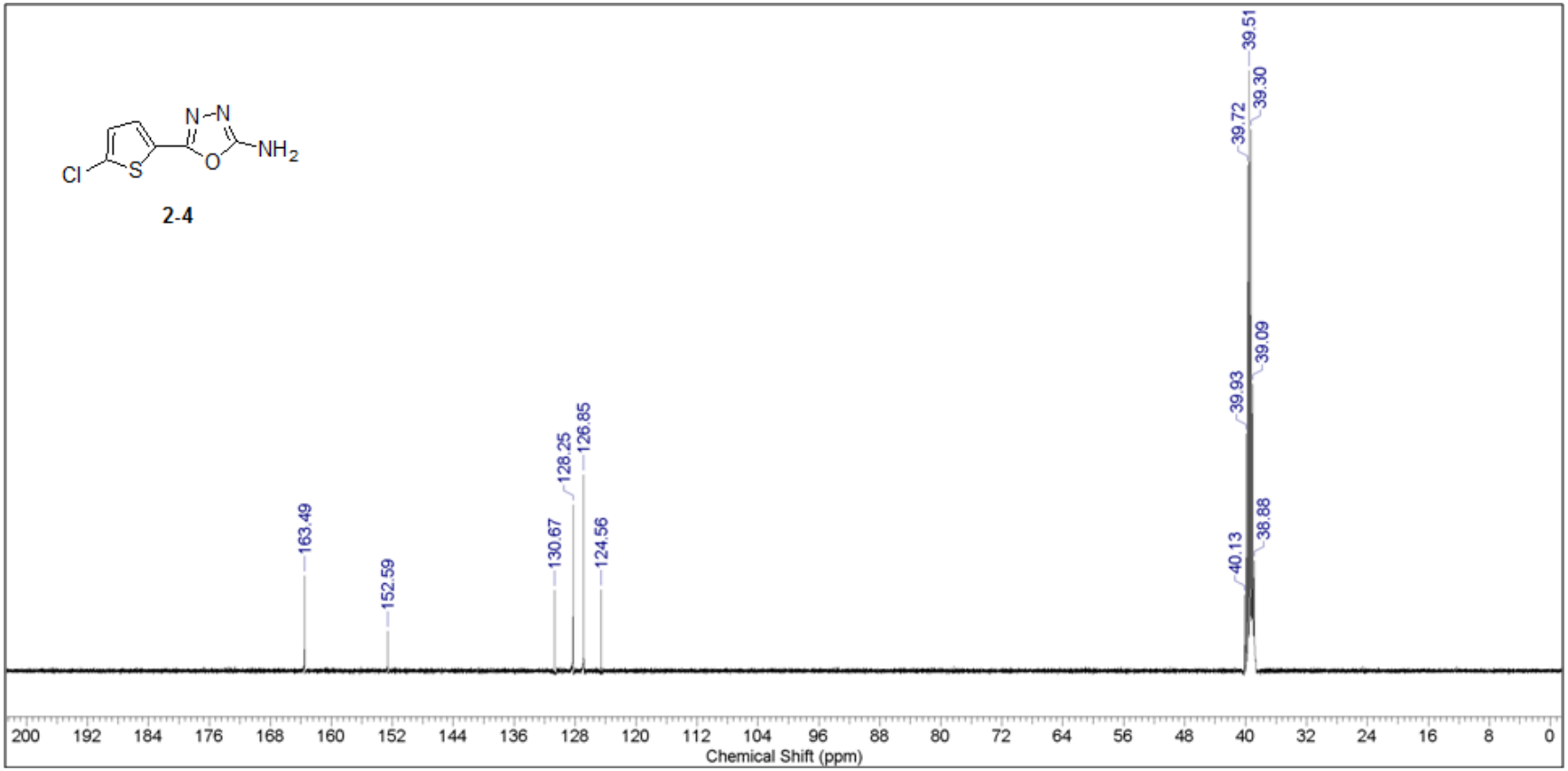
N
N
NH2
Cl
S
O
2-4
163.49
152.59
130.67
128.25
126.85
124.56
40.13
39.93
39.72
39.51
39.30
39.09
38.88
200 192 184 176 168 160 152 144 136 128 120 112 104 96 88 80 72 64 56 48 40 32 24 16 8 0
Chemical Shift (ppm)

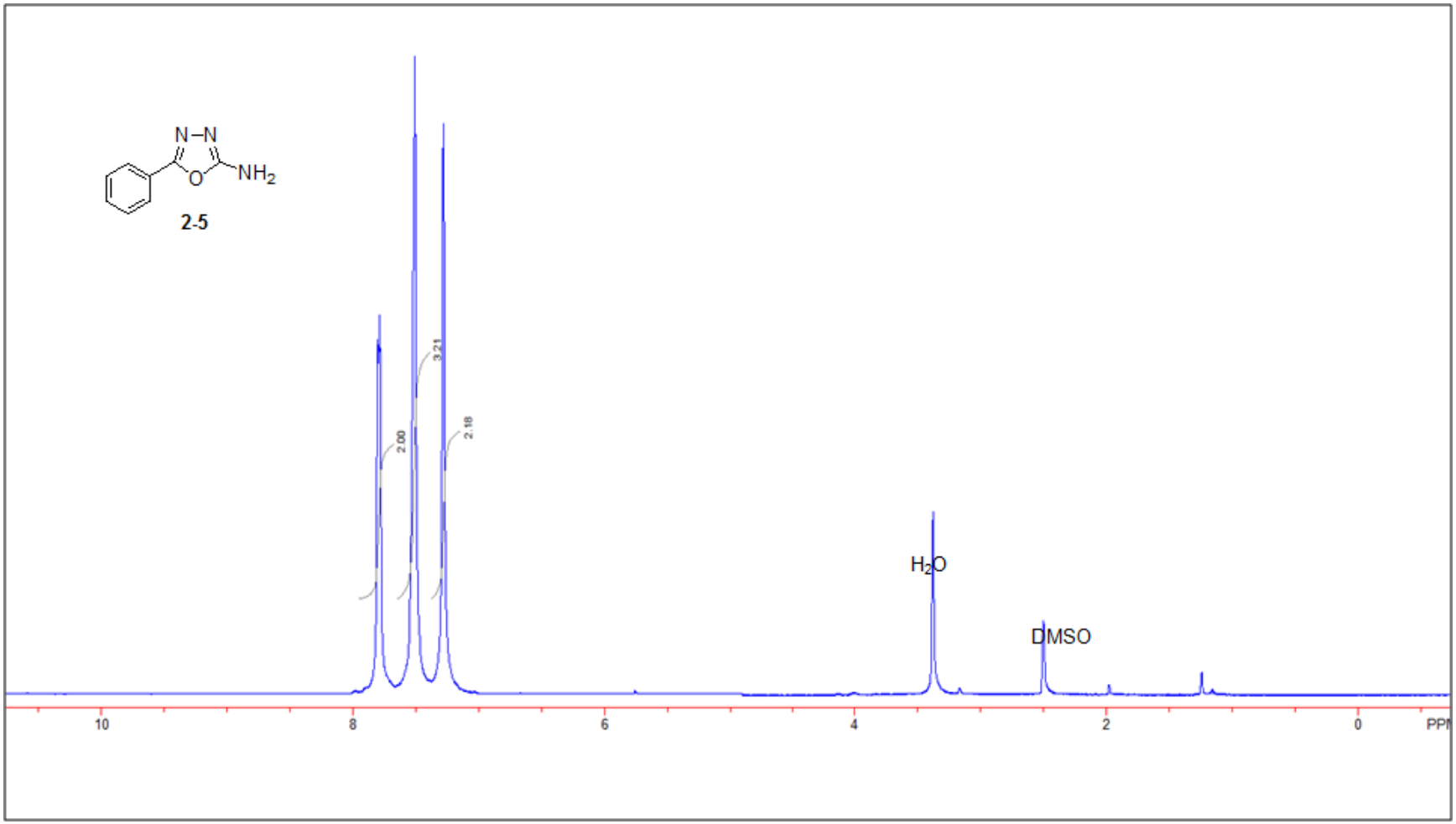
N–N
O
NH2
2-5
2.00
3.21
2.18
H2O
DMSO
10
8
6
4
2
0
PPM

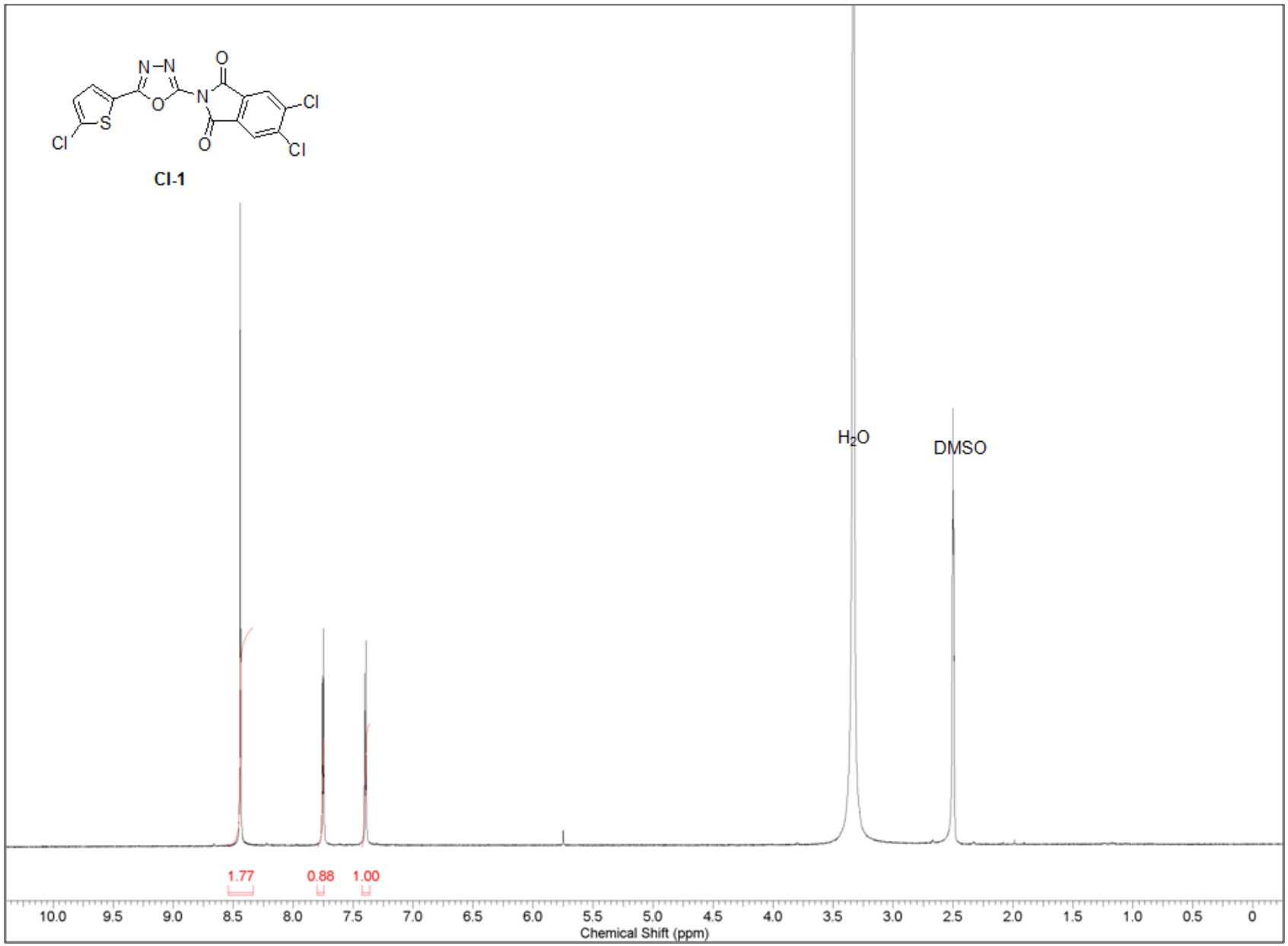
N–N
O
N
O
S
Cl
Cl
Cl
O
CI-1
H2O
DMSO
1.77
0.88
1.00
10.0
9.5
9.0
8.5
8.0
7.5
7.0
6.5
6.0
5.5
5.0
4.5
4.0
3.5
3.0
2.5
2.0
1.5
1.0
0.5
0
Chemical Shift (ppm)

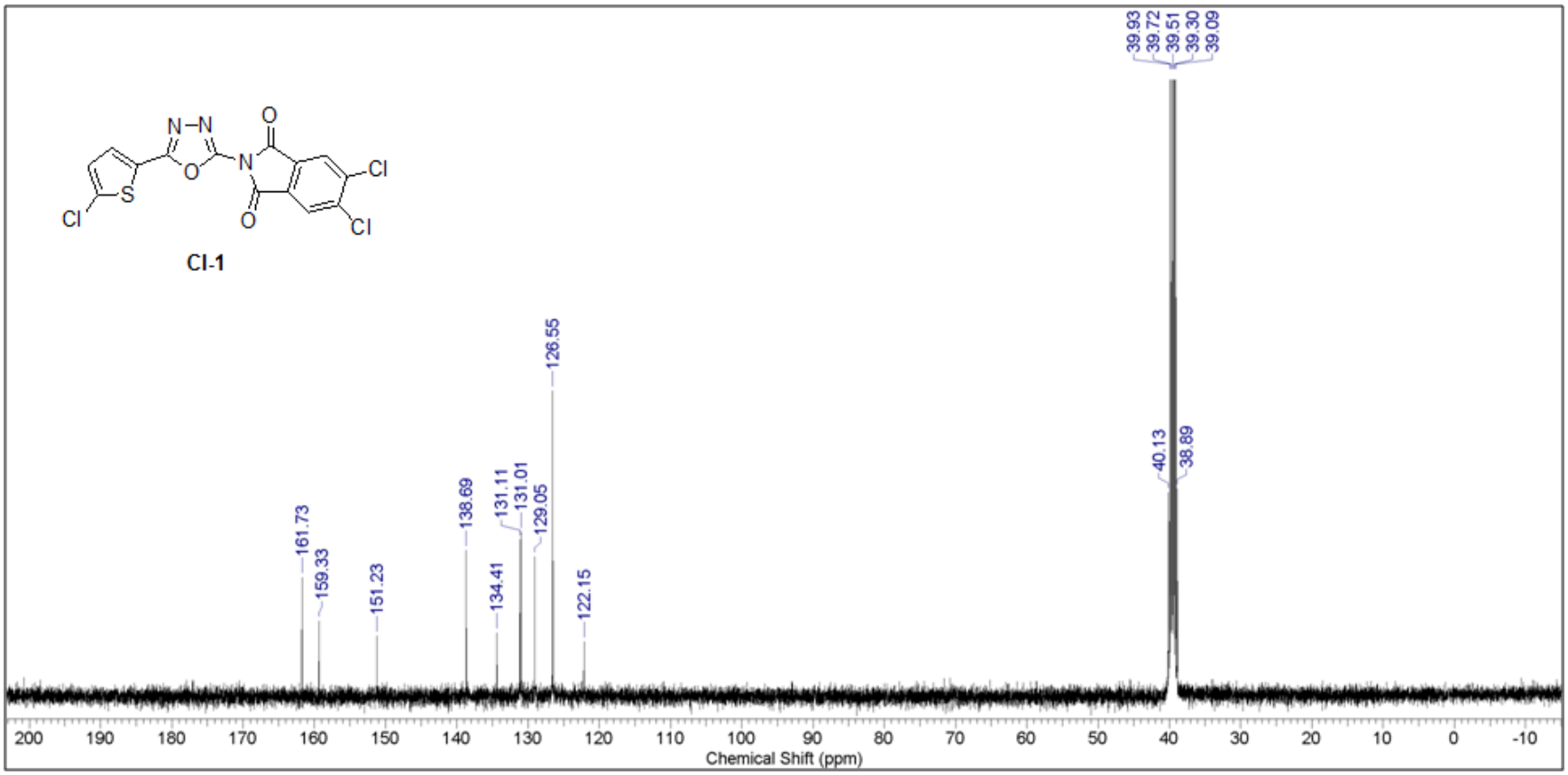
N–N
O
N
O
S
Cl
Cl
Cl
O
CI-1
39.93
39.72
39.51
39.30
39.09
40.13
38.89
126.55
161.73
159.33
151.23
138.69
134.41
131.11
131.01
129.05
122.15
200
190
180
170
160
150
140
130
120
110
100
90
80
70
60
50
40
30
20
10
0
-10
Chemical Shift (ppm)

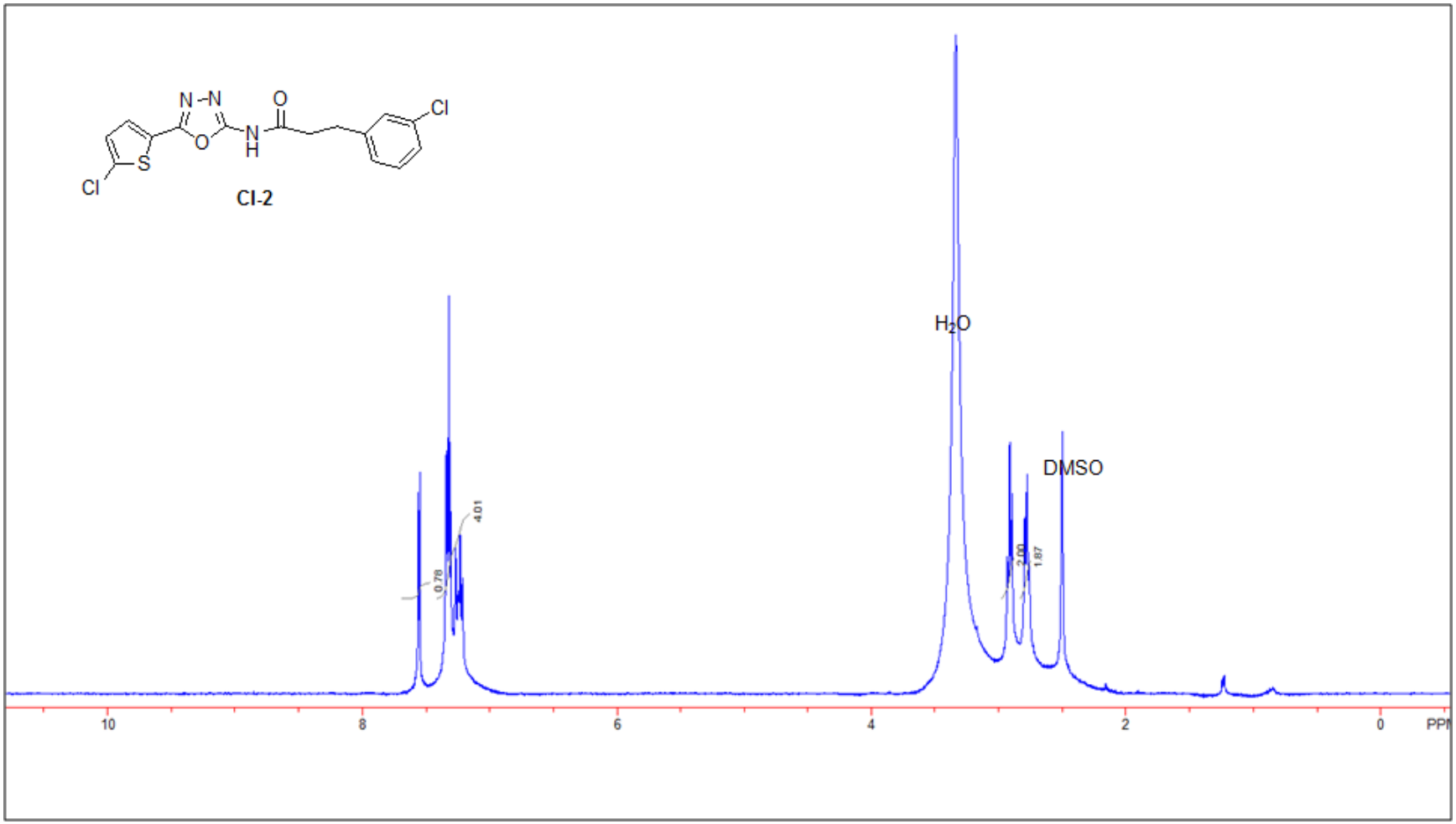
N–N
O
N
H
O
S
Cl
Cl
CI-2
H2O
DMSO
0.78
4.01
2.00
1.87
10
8
6
4
2
0
PPM

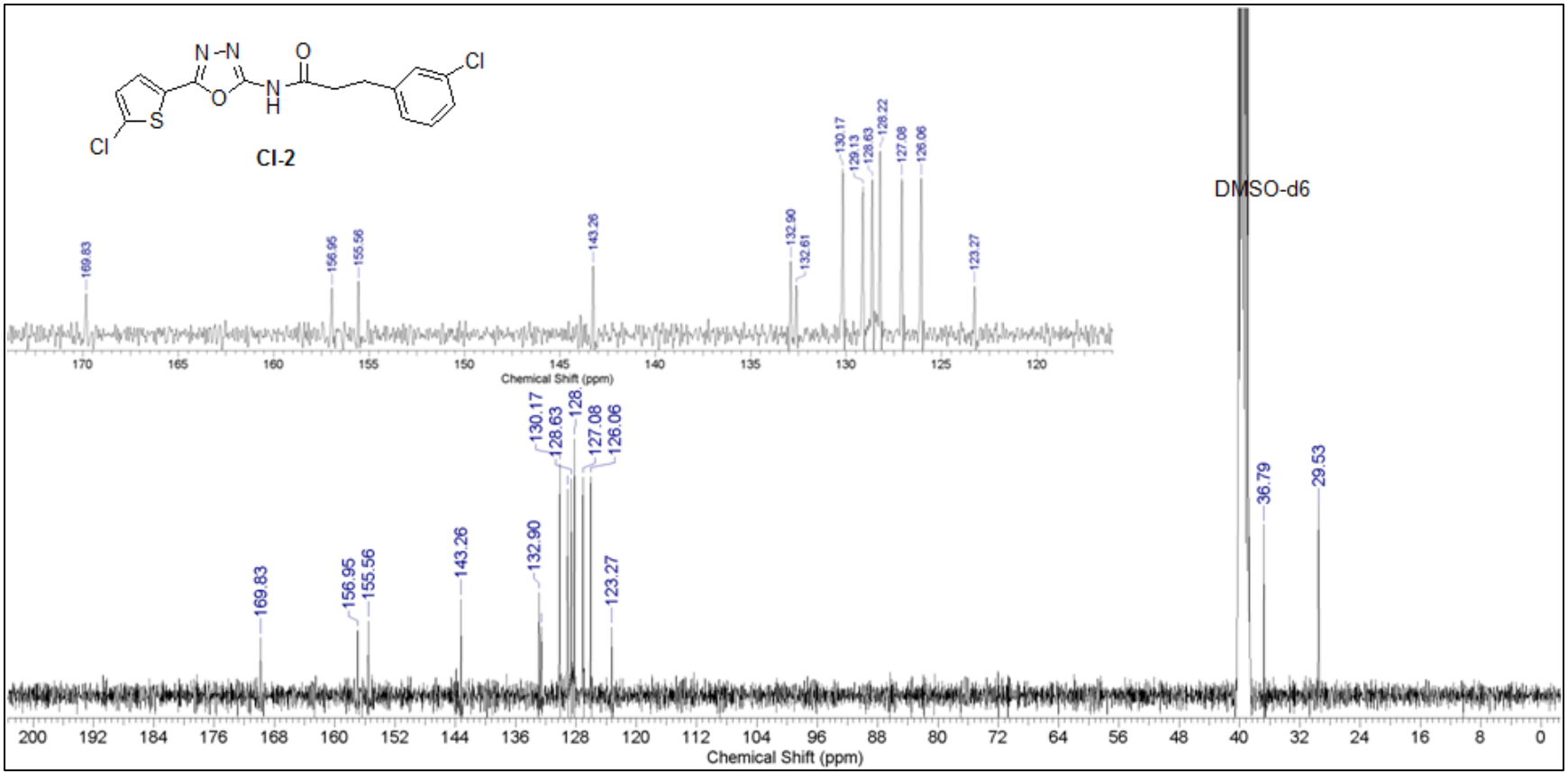
CI-2
DMSO-d6
Chemical Shift (ppm)
Chemical Shift (ppm)

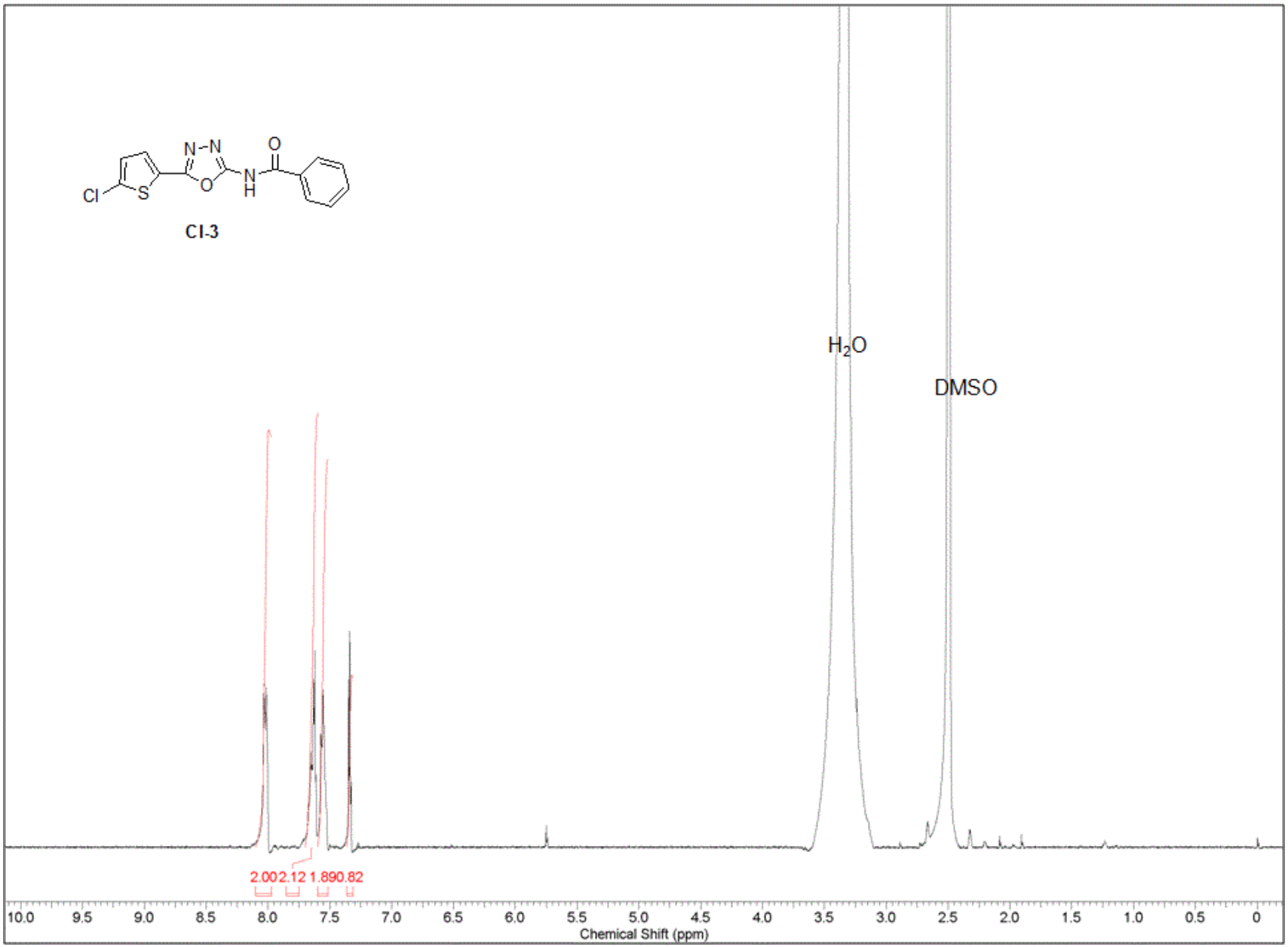
Cl
S
N–N
O
N
H
O
CI-3
H2O
DMSO
2.00
2.12
1.89
0.82
10.0
9.5
9.0
8.5
8.0
7.5
7.0
6.5
6.0
5.5
5.0
4.5
4.0
3.5
3.0
2.5
2.0
1.5
1.0
0.5
0
Chemical Shift (ppm)

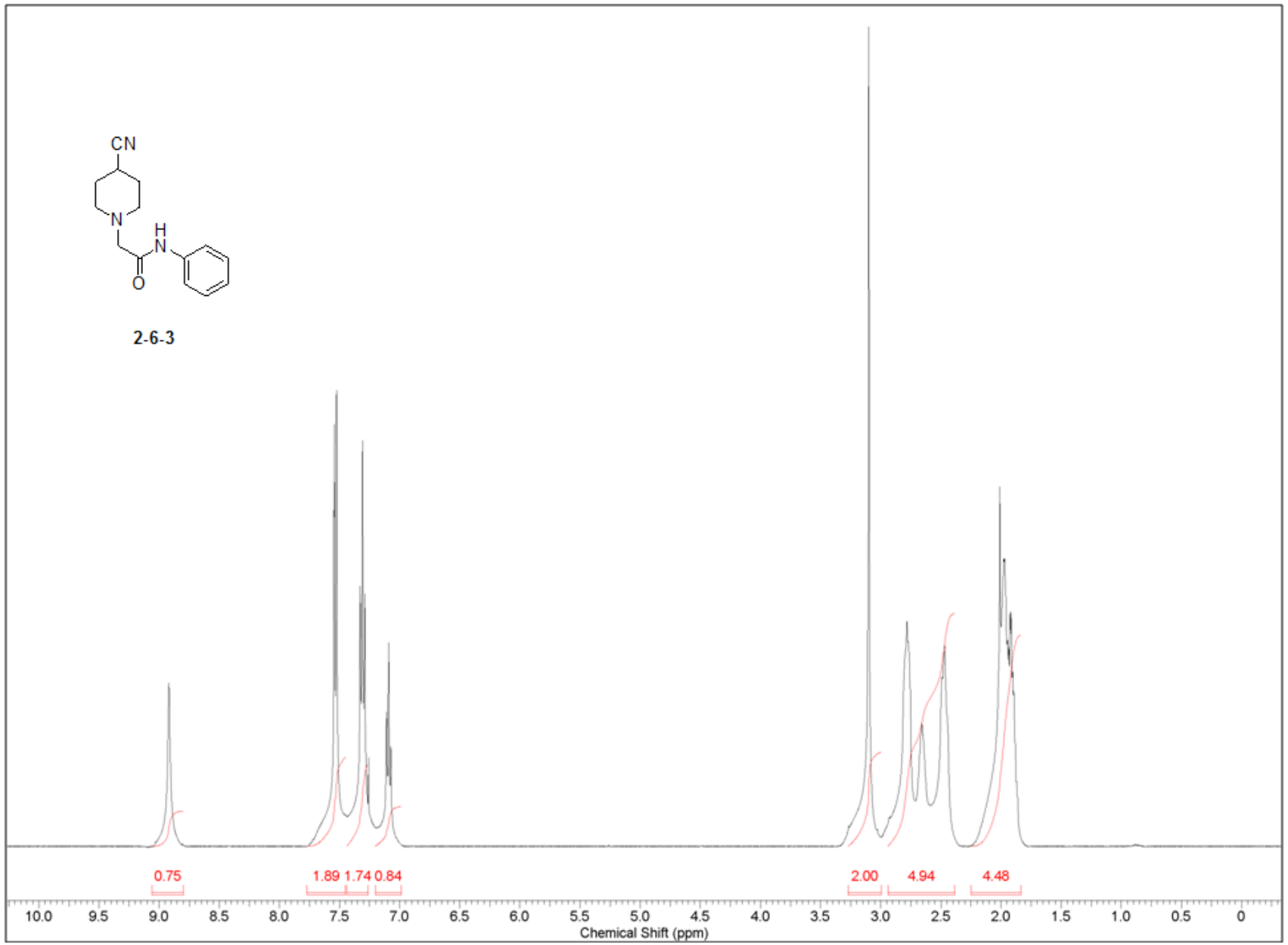
CN
N
H
N
O
2-6-3
0.75
1.89
1.74
0.84
2.00
4.94
4.48
10.0
9.5
9.0
8.5
8.0
7.5
7.0
6.5
6.0
5.5
5.0
4.5
4.0
3.5
3.0
2.5
2.0
1.5
1.0
0.5
0
Chemical Shift (ppm)

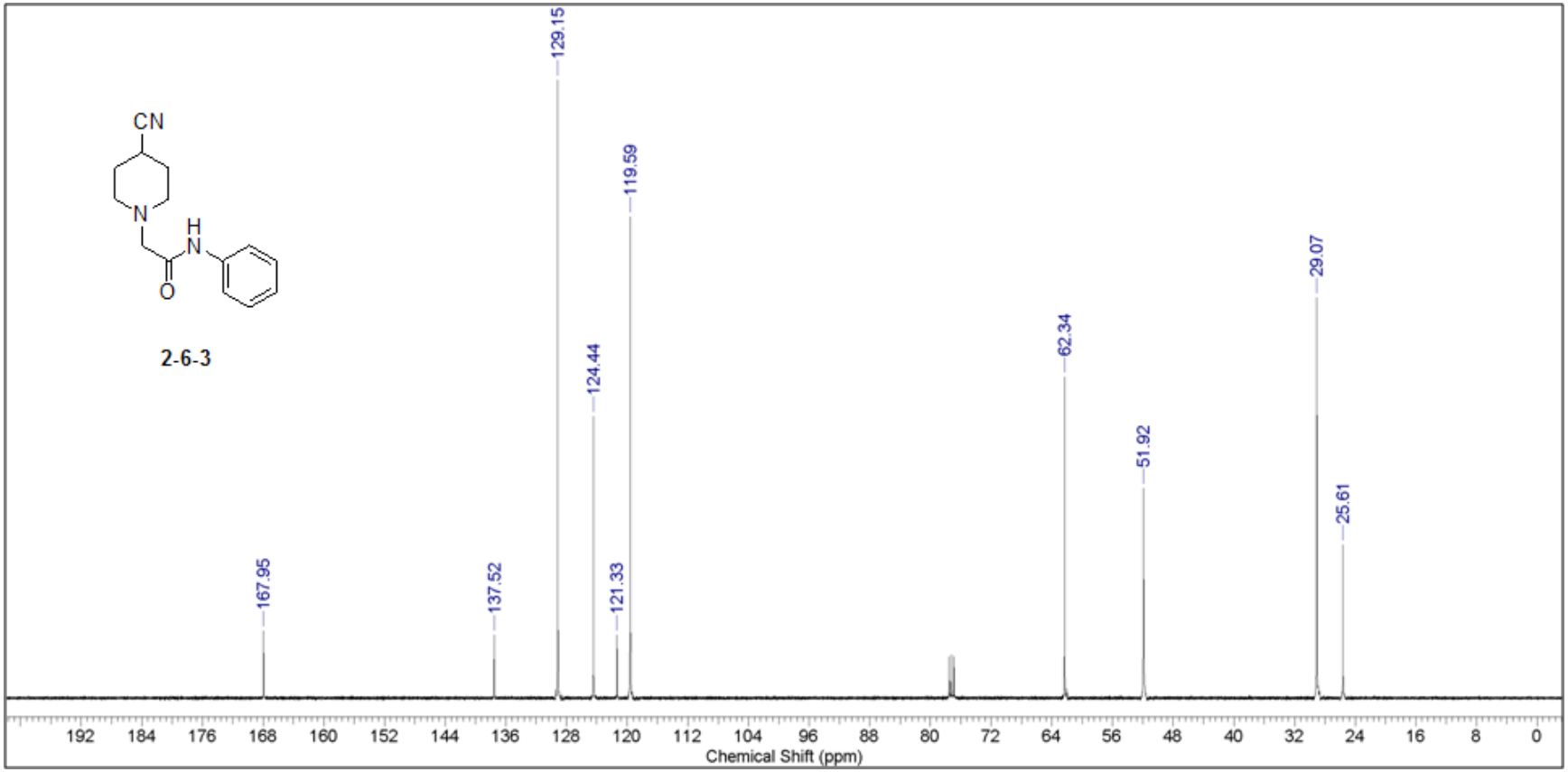
CN
N
H
N
O
2-6-3
129.15
119.59
124.44
62.34
29.07
51.92
25.61
167.95
137.52
121.33
192 184 176 168 160 152 144 136 128 120 112 104 96 88 80 72 64 56 48 40 32 24 16 8 0
Chemical Shift (ppm)

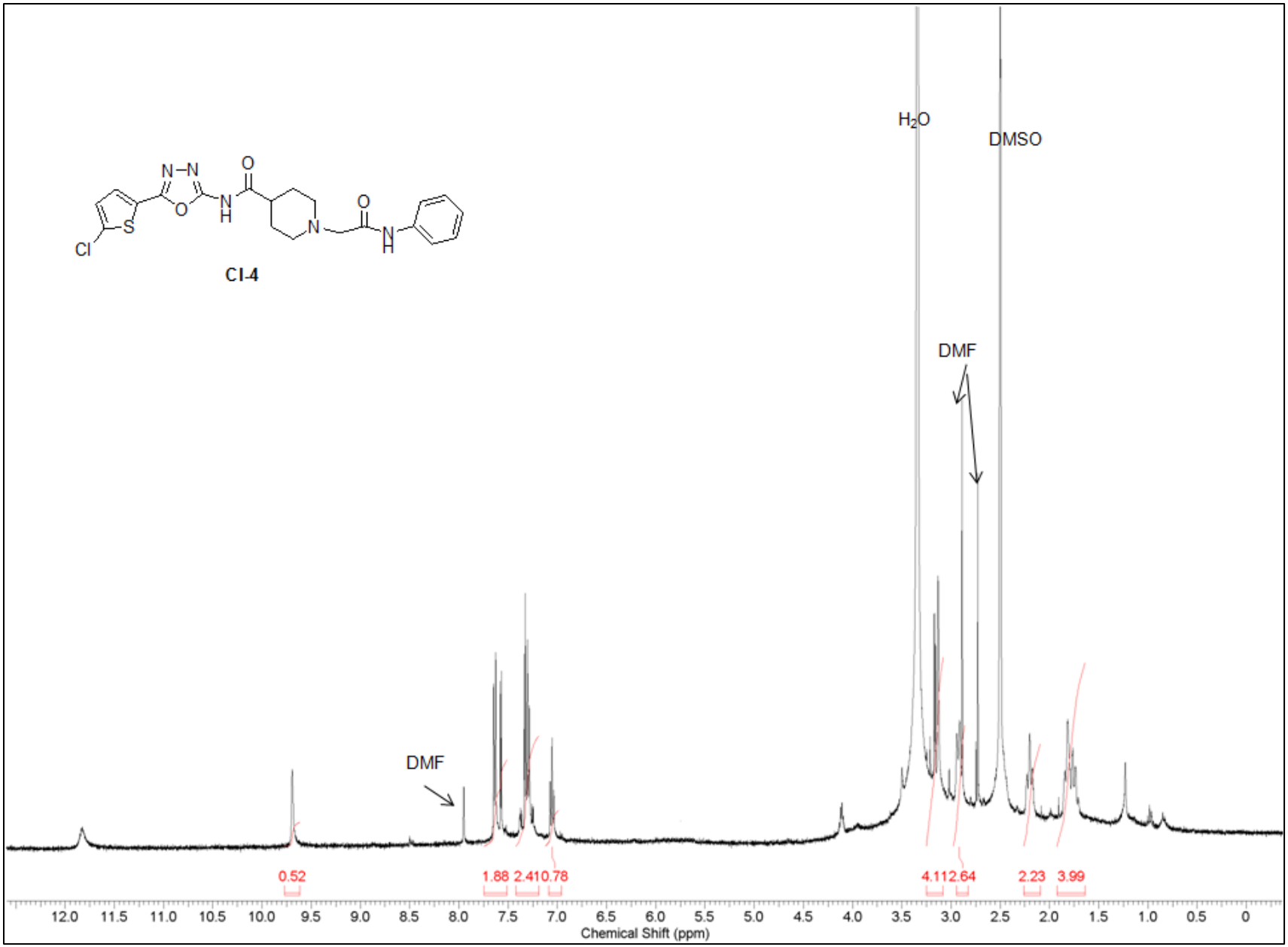
CI-4
H2O
DMSO
DMF
DMF
0.52
1.88
2.41
0.78
4.11
2.64
2.23
3.99
Chemical Shift (ppm)

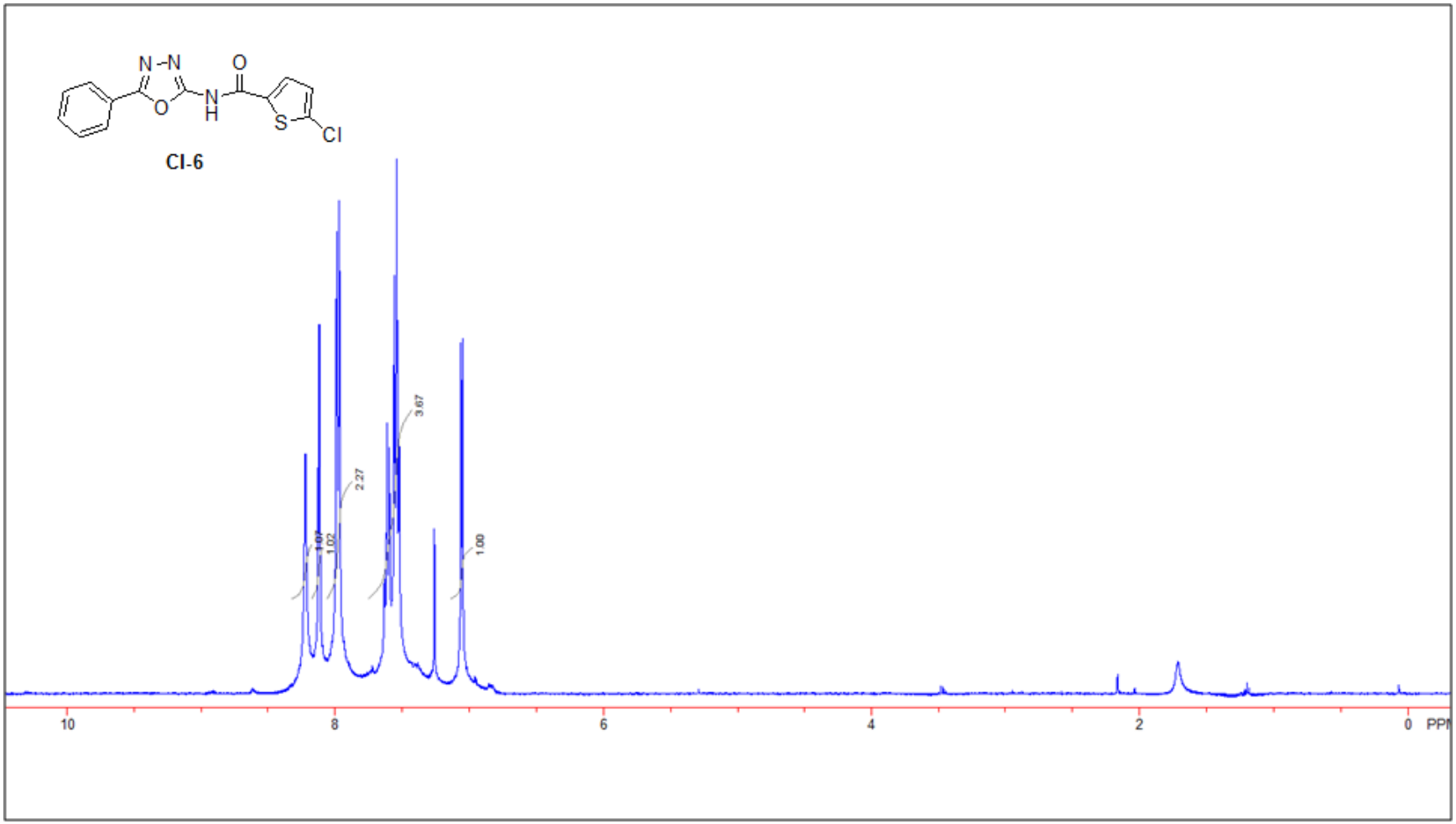
N
N
O
O
N
H
S
Cl
CI-6
3.67
2.27
1.07
1.02
1.00
10
8
6
4
2
0
PPM

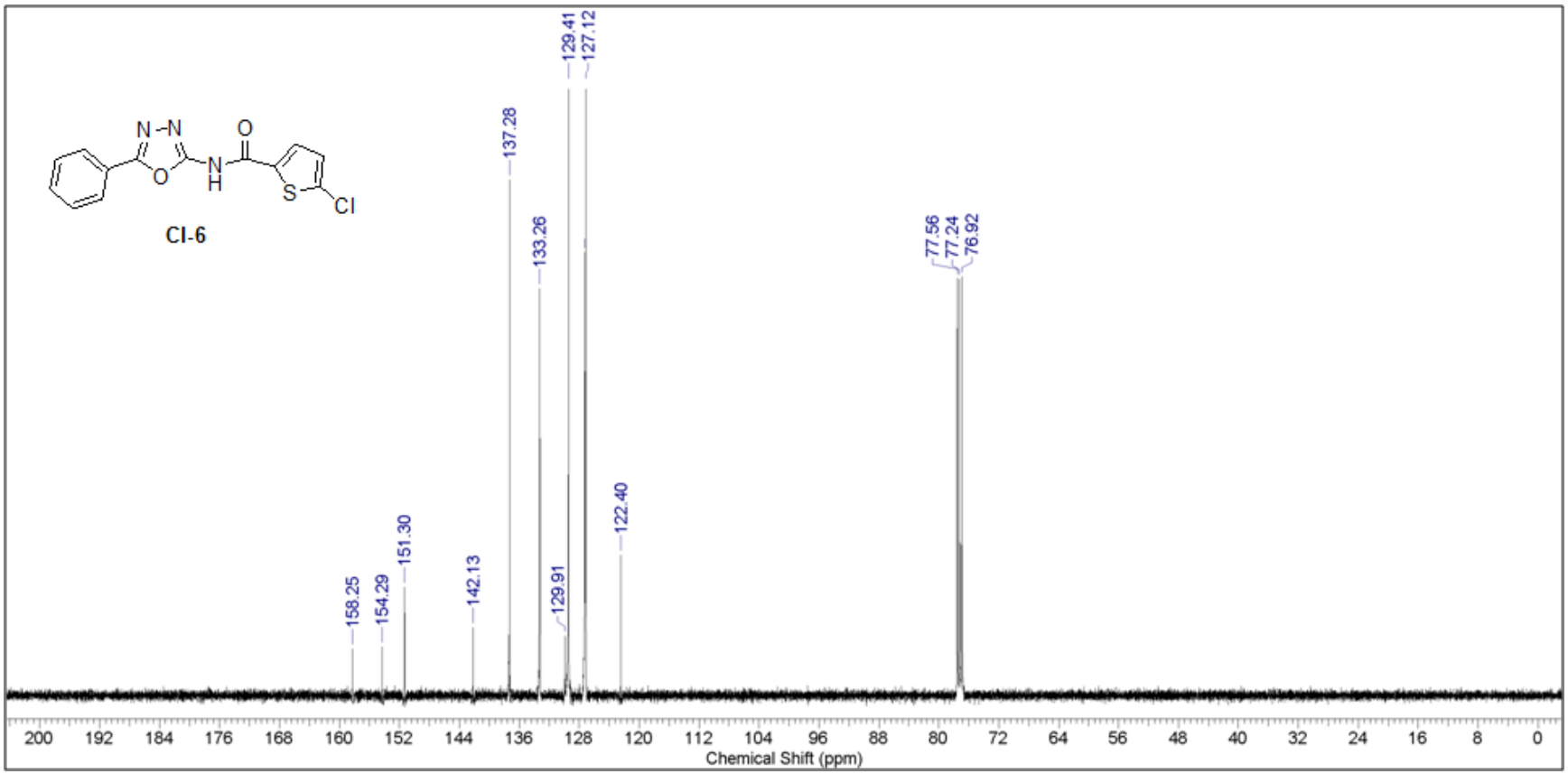
CI-6
158.25
154.29
151.30
142.13
137.28
133.26
129.91
129.41
127.12
122.40
77.56
77.24
76.92
200 192 184 176 168 160 152 144 136 128 120 112 104 96 88 80 72 64 56 48 40 32 24 16 8 0
Chemical Shift (ppm)

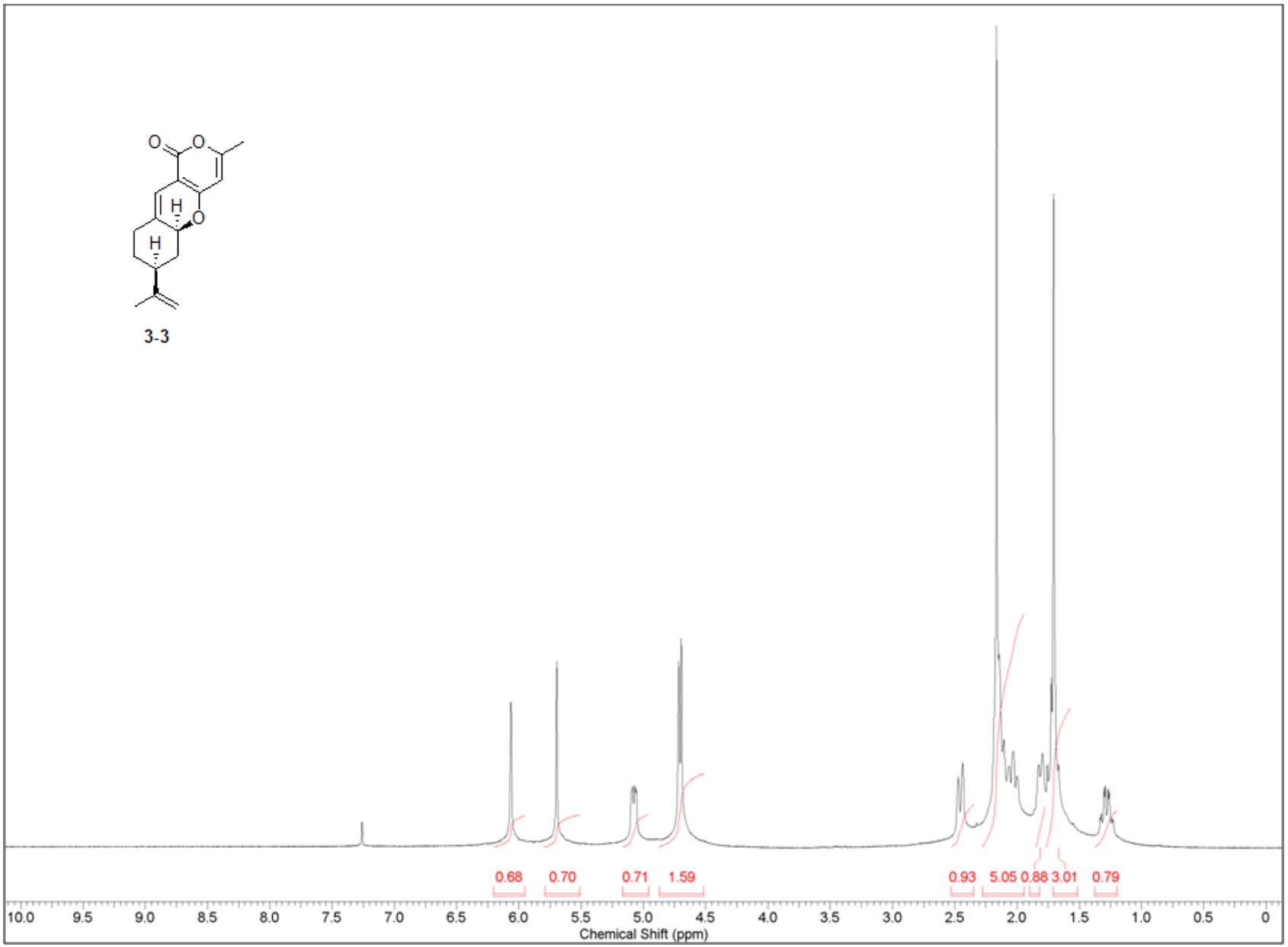
O
O
H
O
H
3-3
0.68
0.70
0.71
1.59
0.93
5.05
0.88
3.01
0.79
10.0
9.5
9.0
8.5
8.0
7.5
7.0
6.5
6.0
5.5
5.0
4.5
4.0
3.5
3.0
2.5
2.0
1.5
1.0
0.5
0
Chemical Shift (ppm)

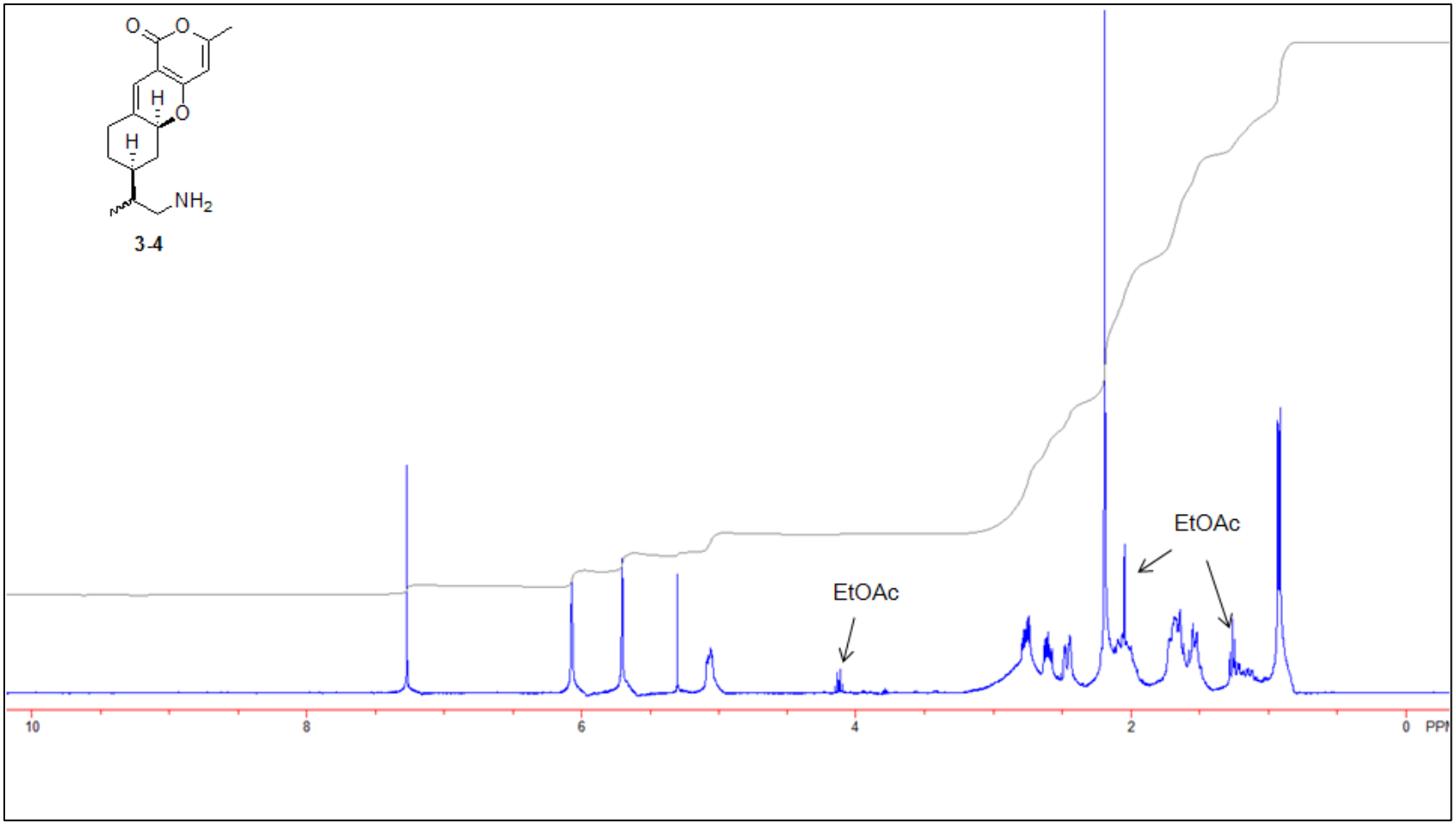
O
O
H
O
H
NH2
3-4
EtOAc
EtOAc
10
8
6
4
2
0
PPM

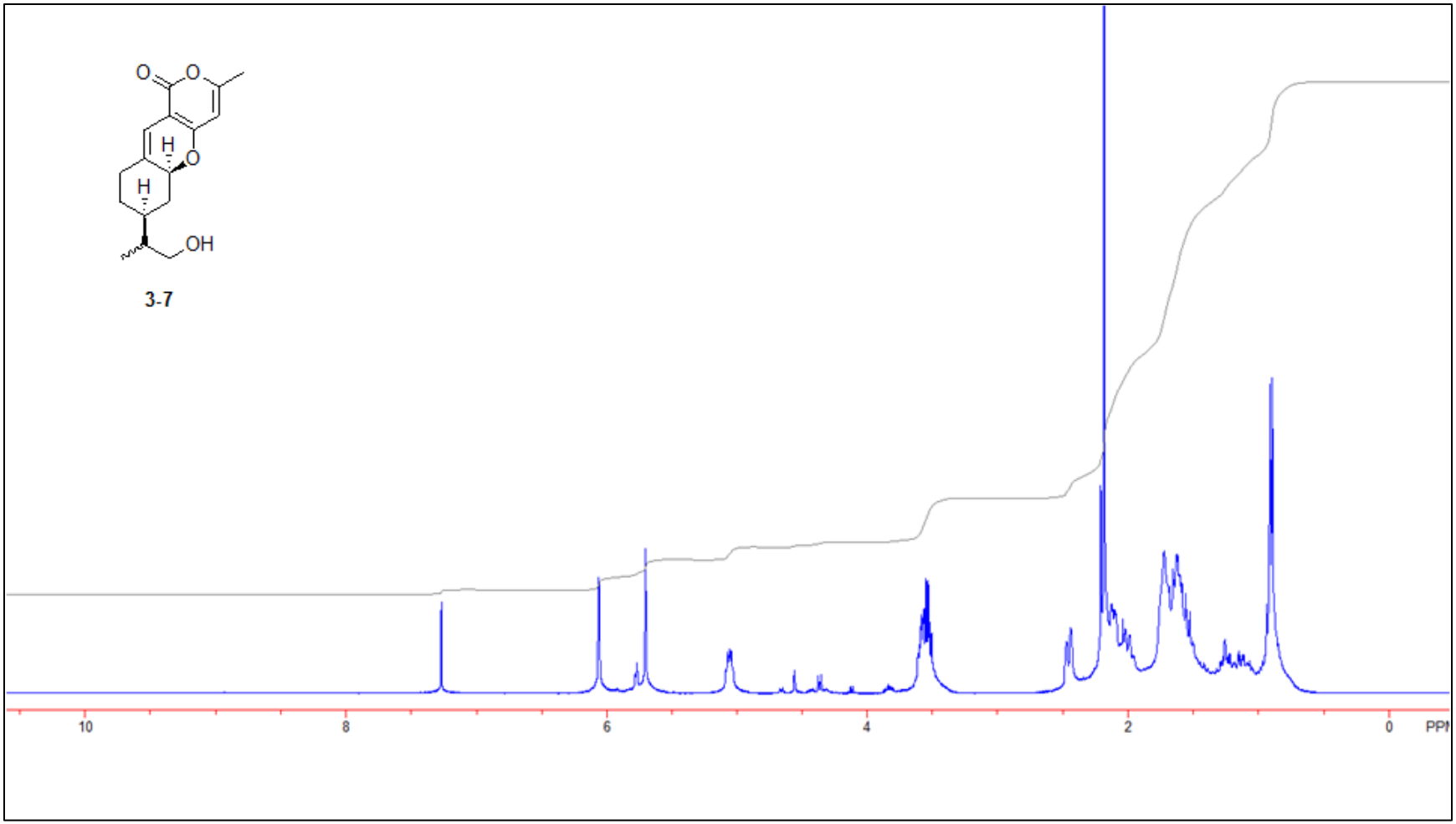

3-7

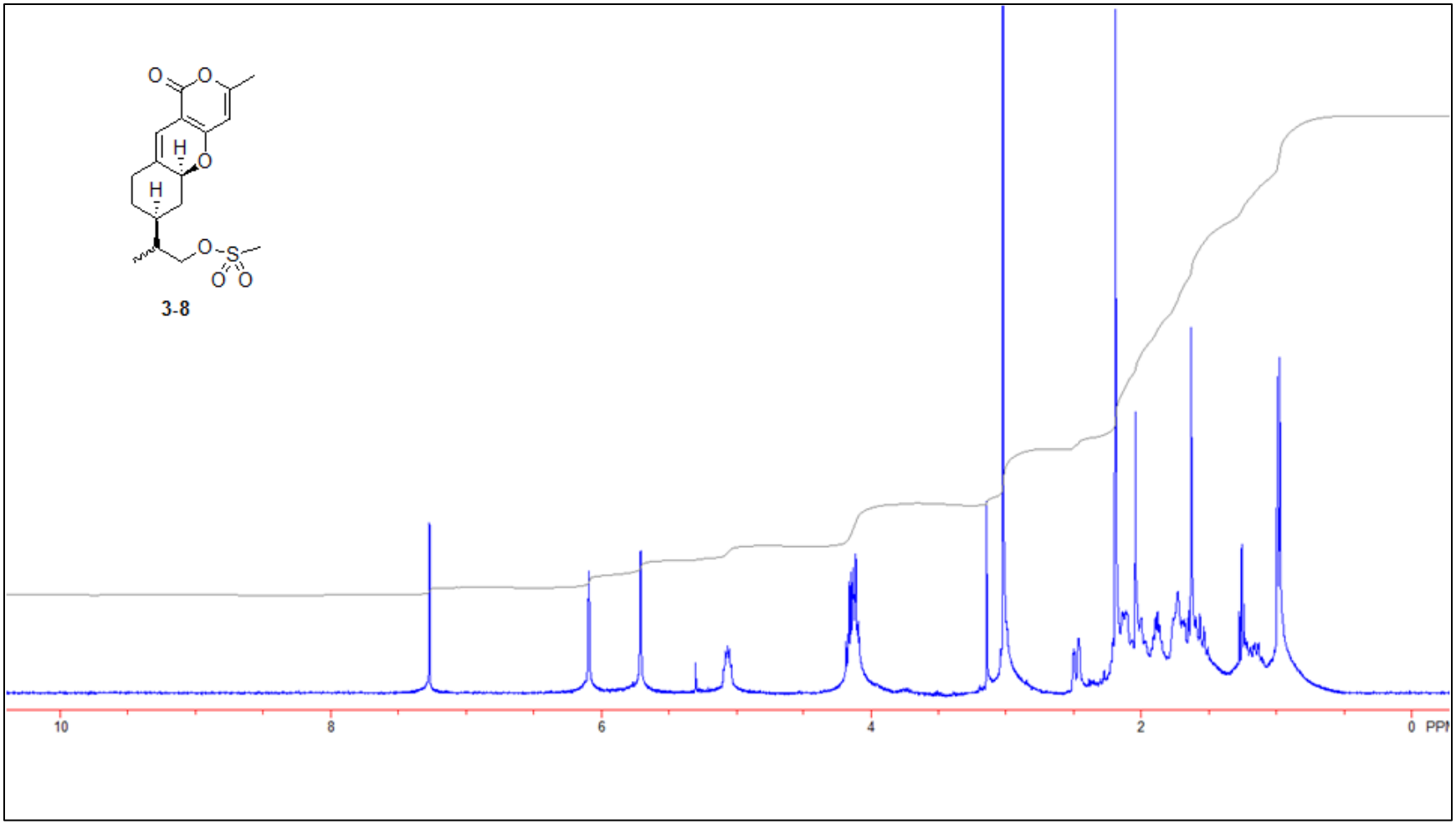
O
O
H
O
H
O
S
O
O
3-8
10
8
6
4
2
0 PPM

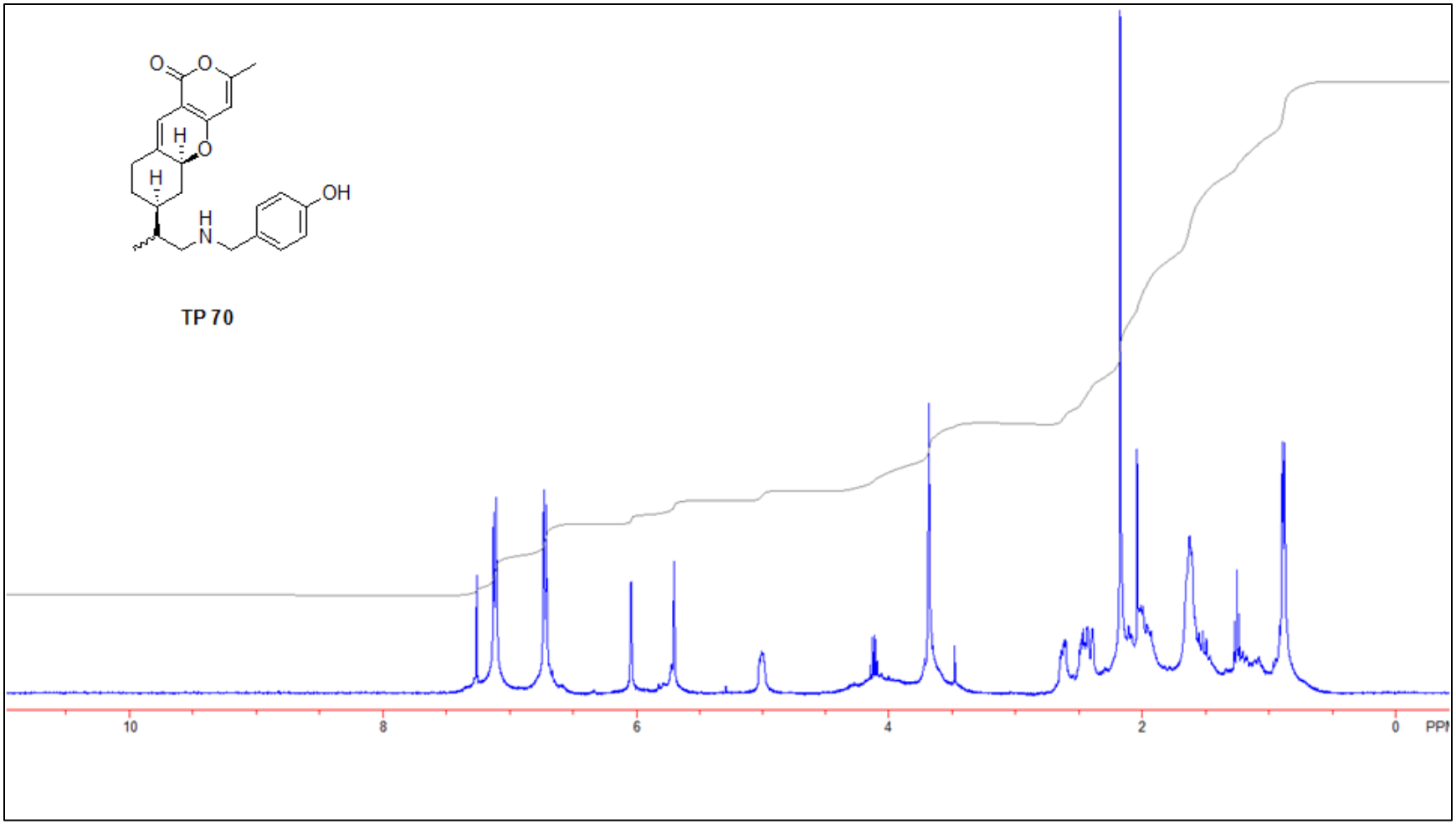
O
O
H
O
H
OH
H
N
TP 70
10
8
6
4
2
0
PPM

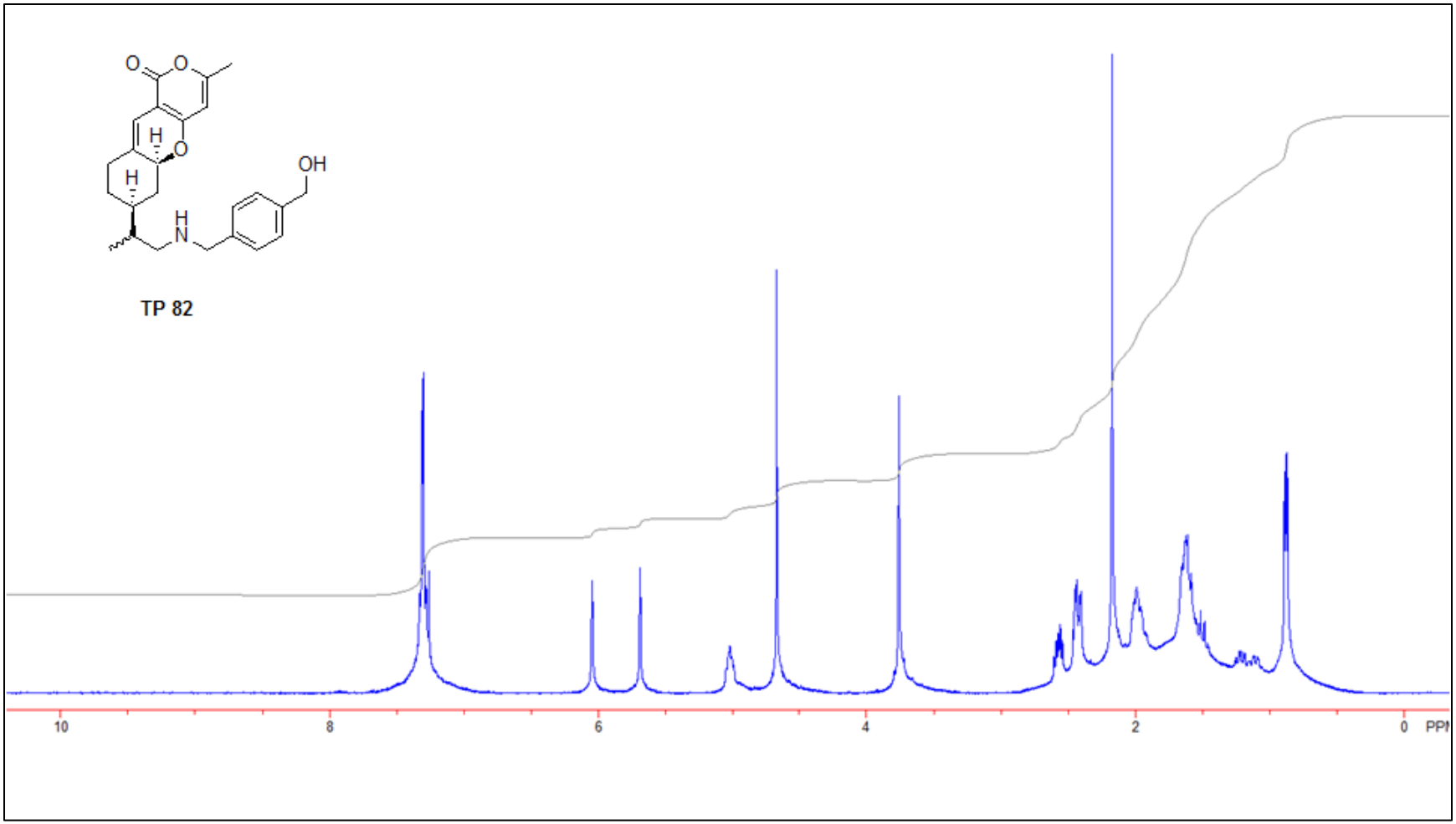
O
O
H
O
H
OH
H
N
TP 82
10
8
6
4
2
0
PPM

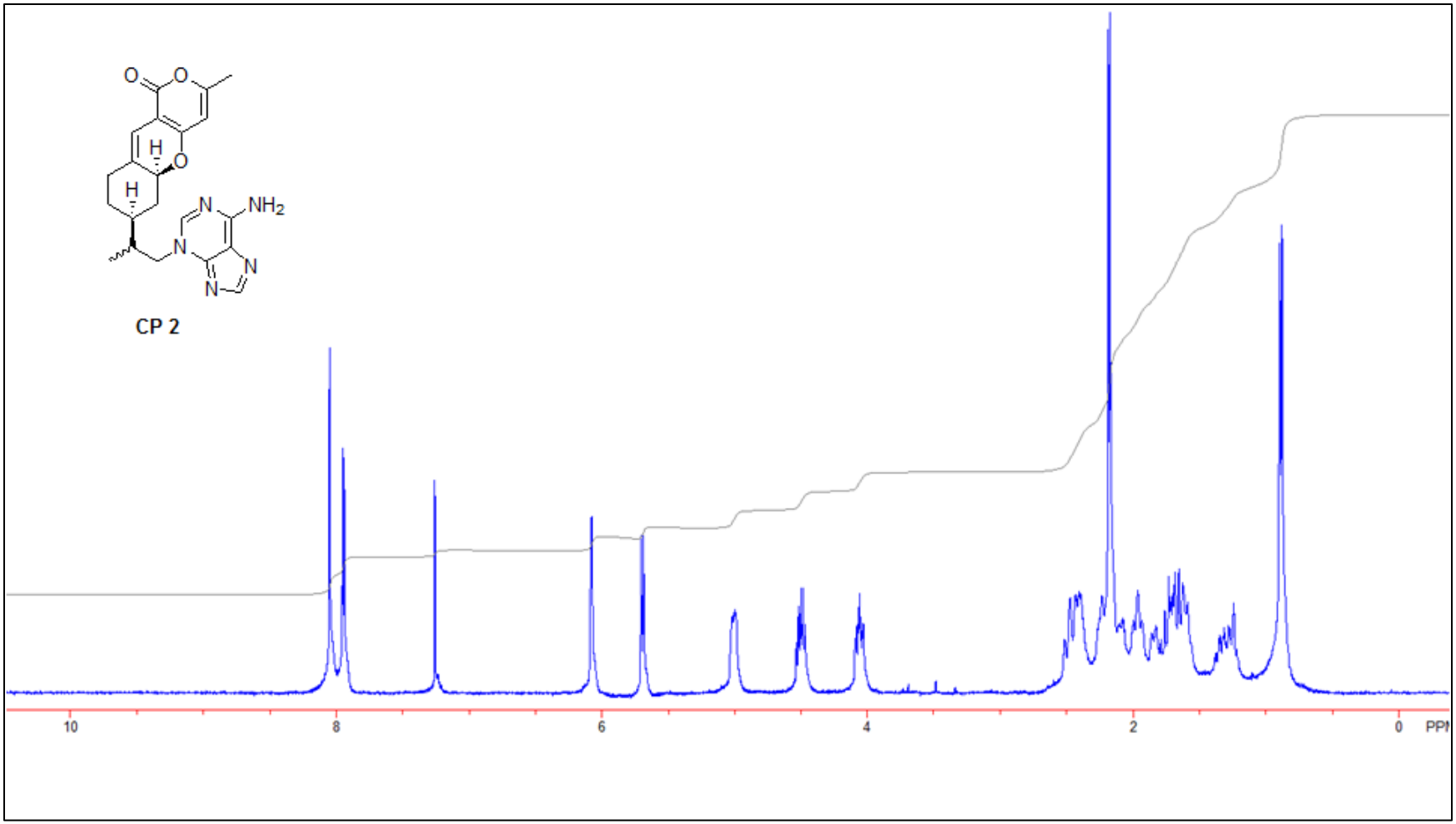
CP 2
10
8
6
4
2
0
PPM

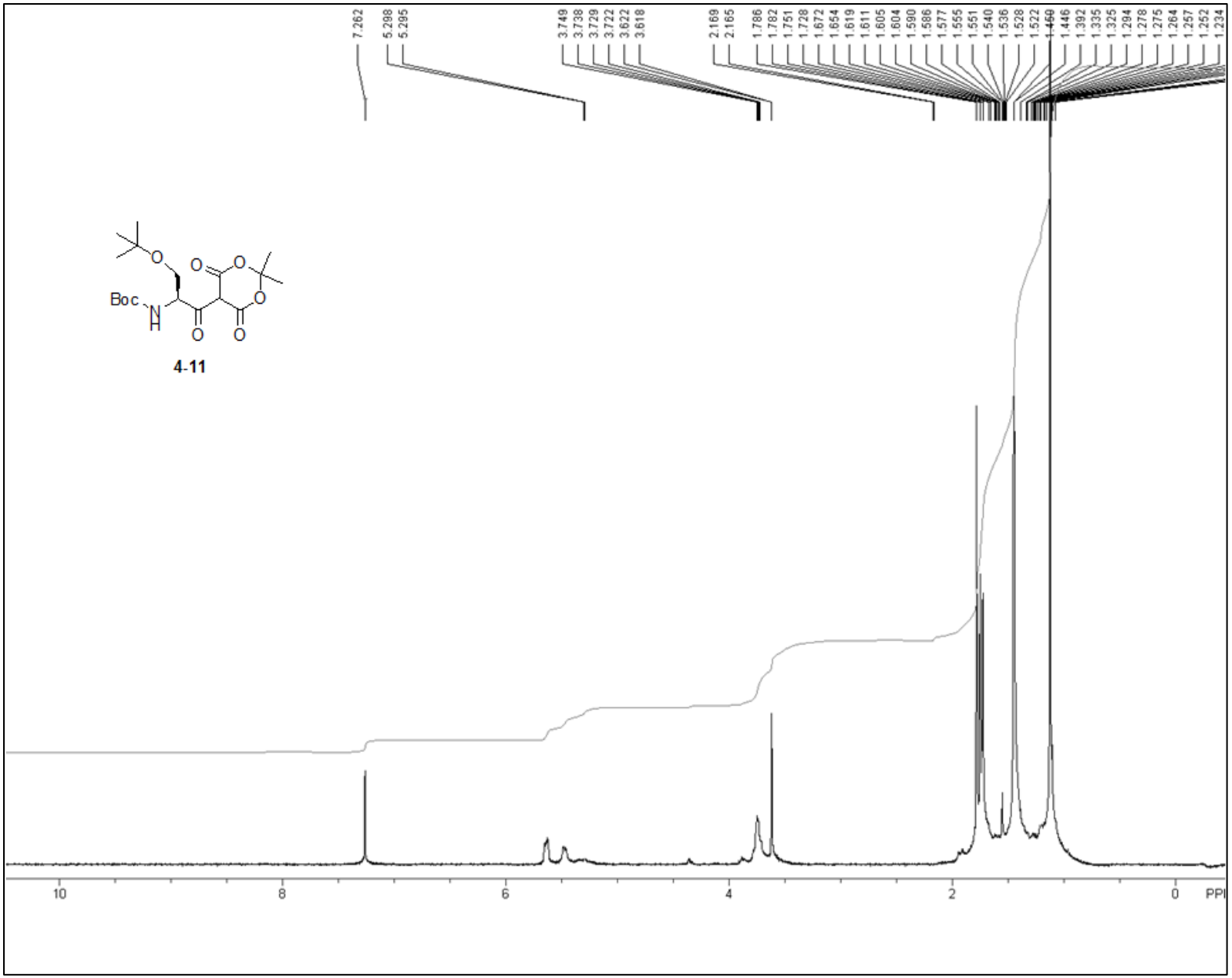
7.262
5.298
5.295
3.749
3.738
3.729
3.722
3.622
3.618
2.169
2.165
1.786
1.782
1.751
1.728
1.672
1.654
1.619
1.611
1.605
1.604
1.590
1.586
1.577
1.555
1.551
1.540
1.536
1.528
1.522
1.460
1.446
1.392
1.335
1.325
1.294
1.278
1.275
1.264
1.257
1.252
1.234
Boc
N
H
O
O
O
O
O
O
O
O
4-11
10
8
6
4
2
0
PPI

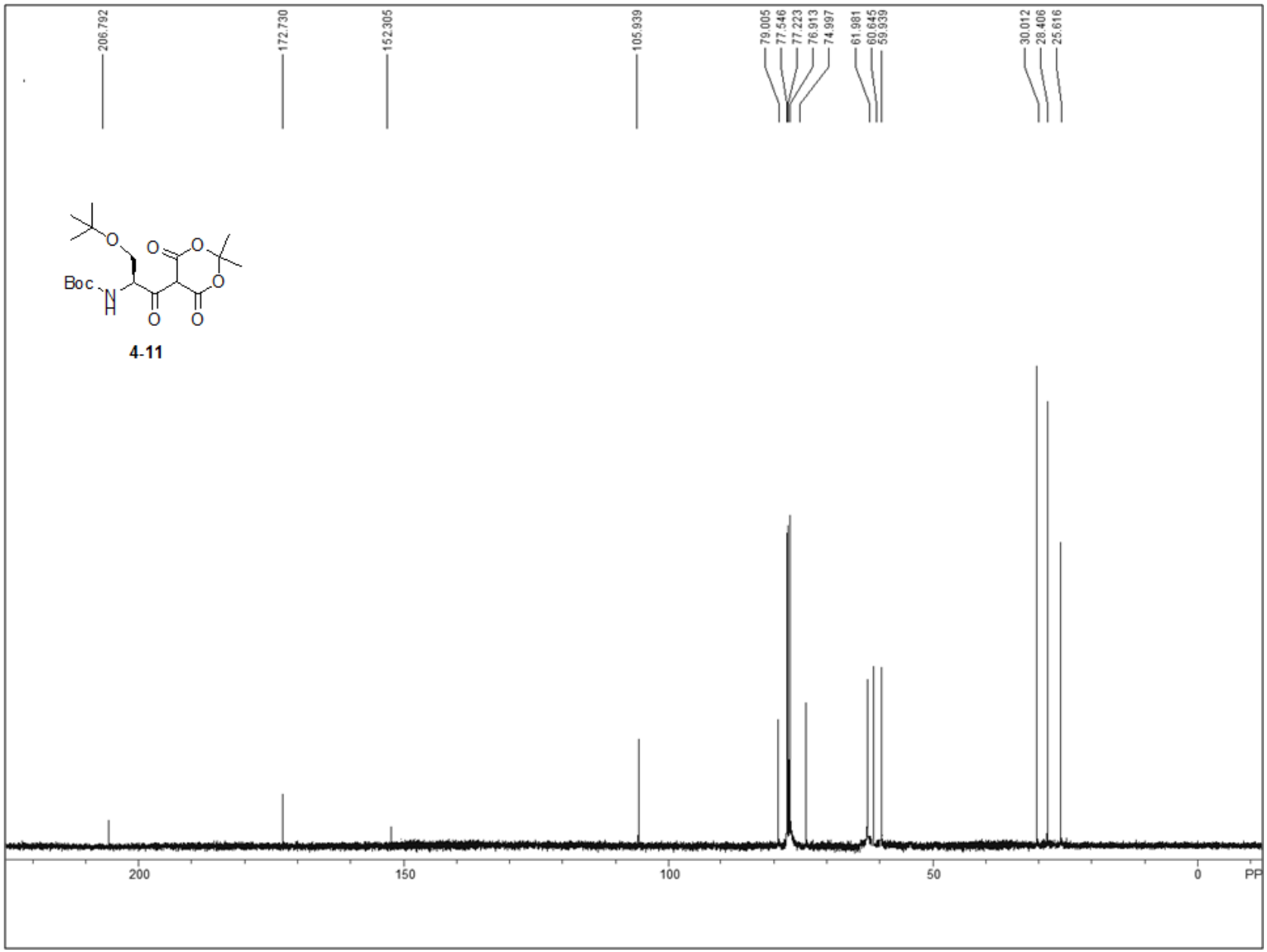
206.792
172.730
152.305
105.939
79.005
77.546
77.223
76.913
74.997
61.981
60.645
59.939
30.012
28.406
25.616
Boc
N
H
O
O
O
O
O
O
O
4-11
200
150
100
50
0
PP

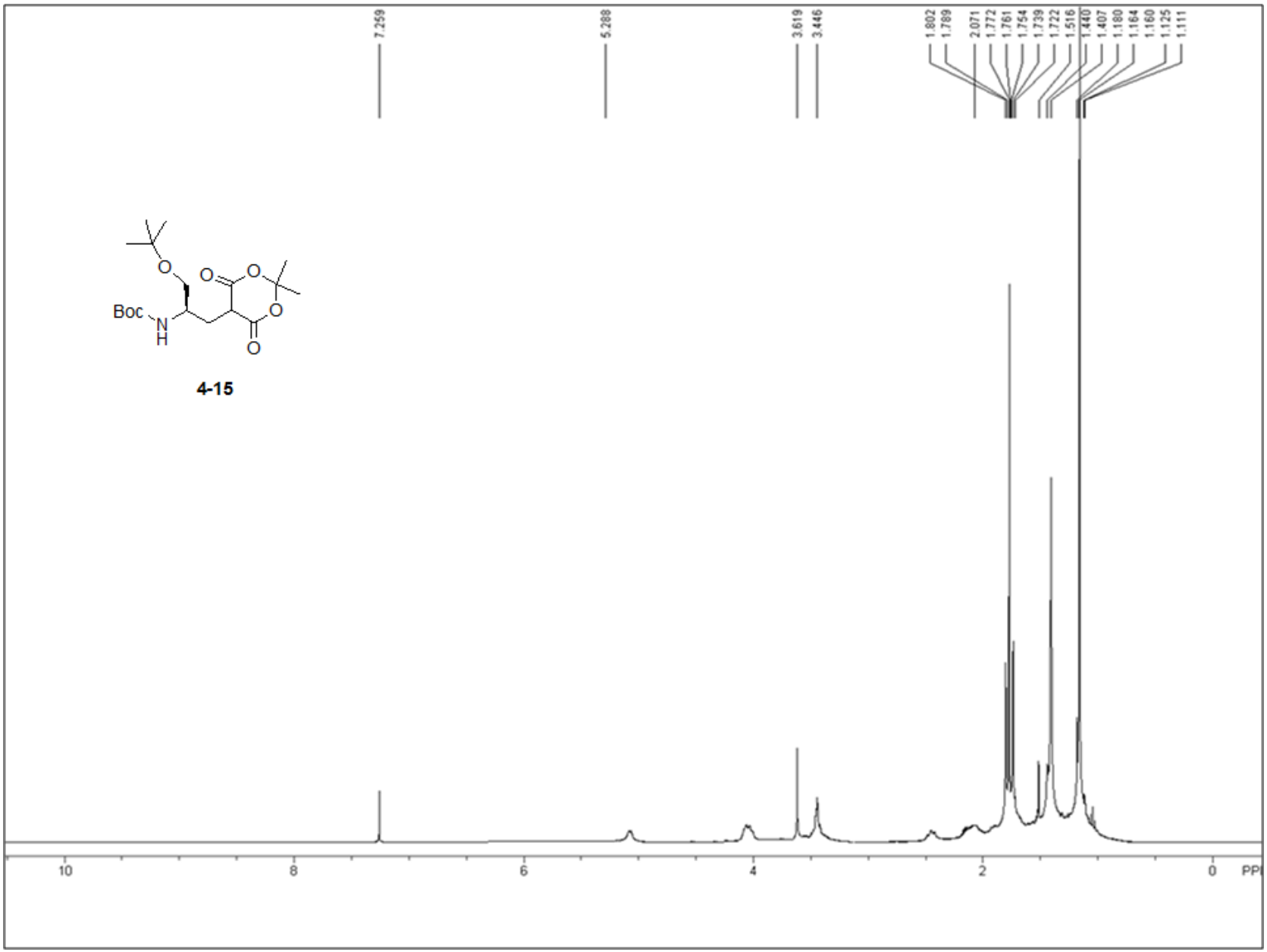
7.259
5.288
3.619
3.446
1.802
1.789
2.071
1.772
1.761
1.754
1.739
1.722
1.516
1.440
1.407
1.180
1.164
1.160
1.125
1.111
Boc
N
H
O
O
O
O
O
O
10
8
6
4
2
0
PP

4-15

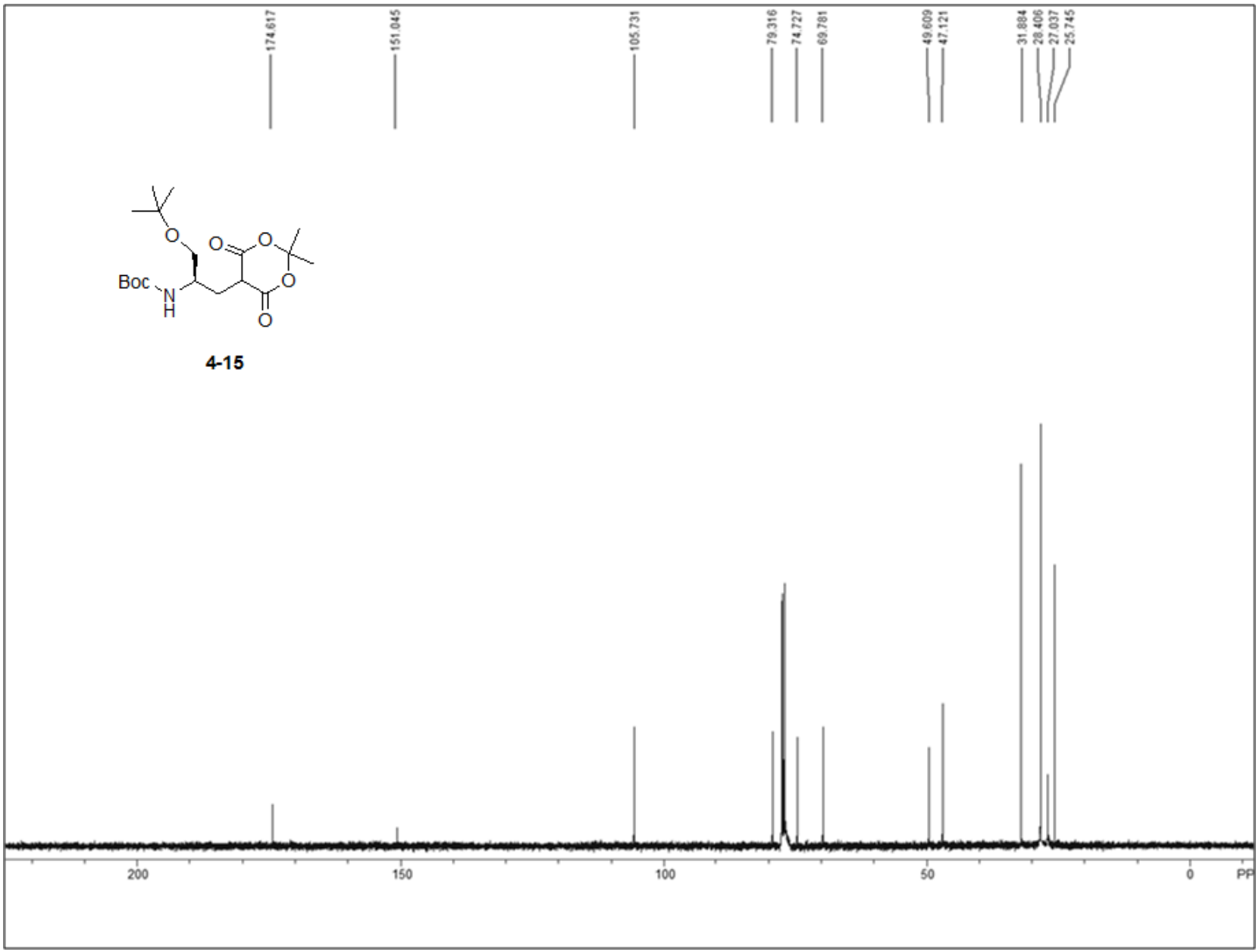
174.617
151.045
105.731
79.316
74.727
69.781
49.609
47.121
31.884
28.406
27.037
25.745
Boc
N
H
O
O
O
O
O
O
200
150
100
50
0
PP

4-15

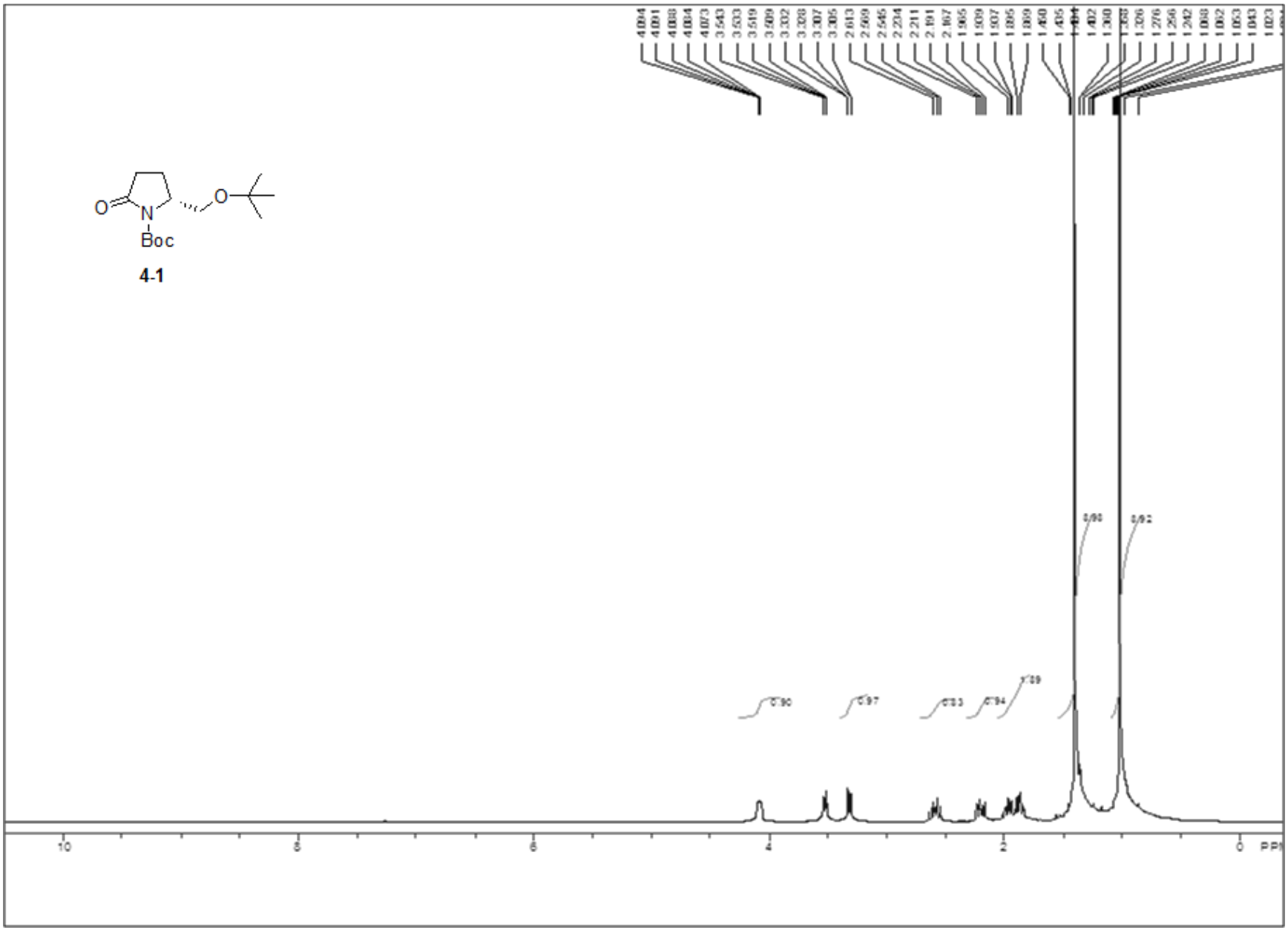
O
N
Boc
O
4-1
10
8
6
4
2
0
PPM

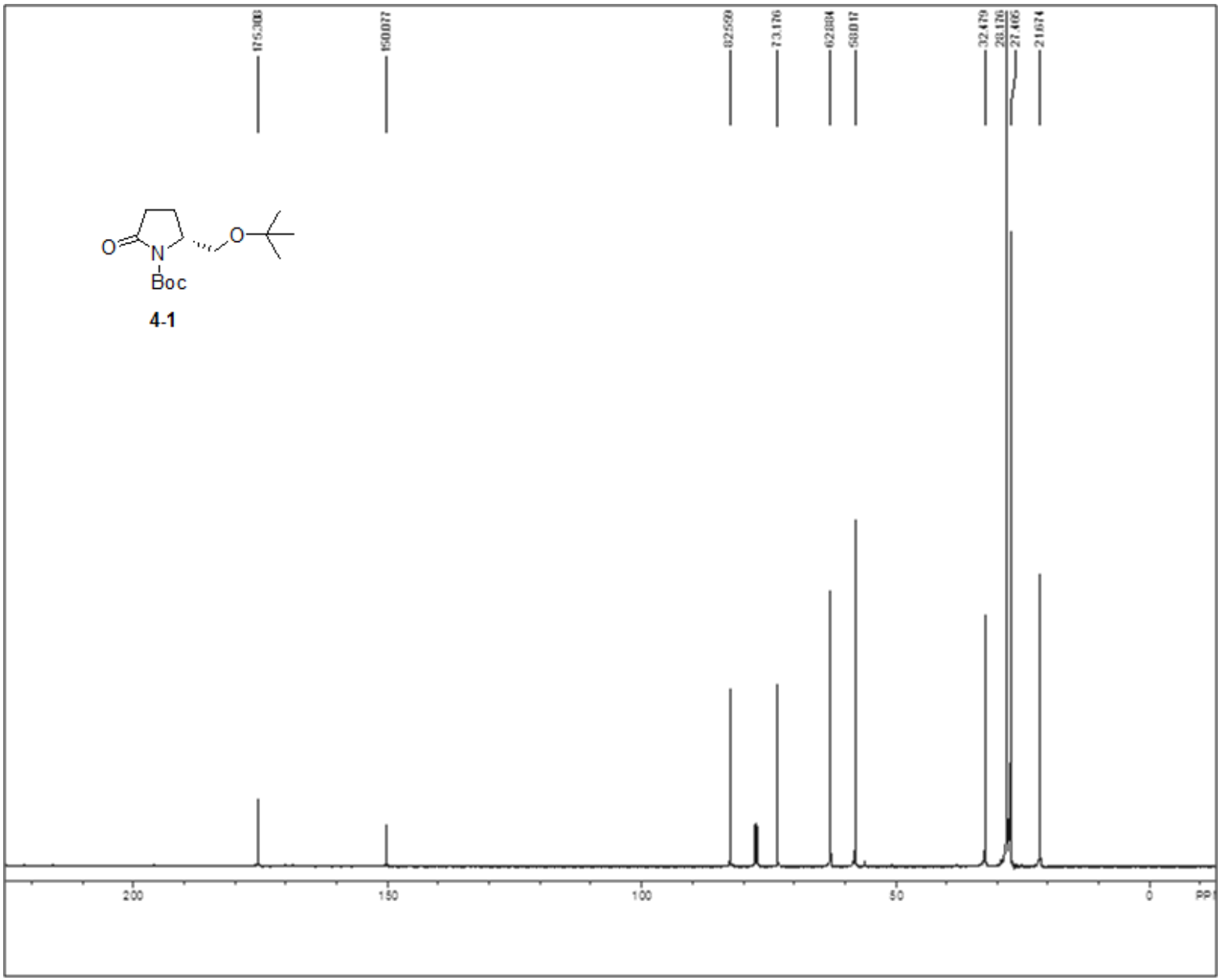
175.303
150.977
82.559
73.176
62.884
59.017
32.479
28.176
27.465
21.674
O
N
Boc
O
4-1
200
150
100
50
0

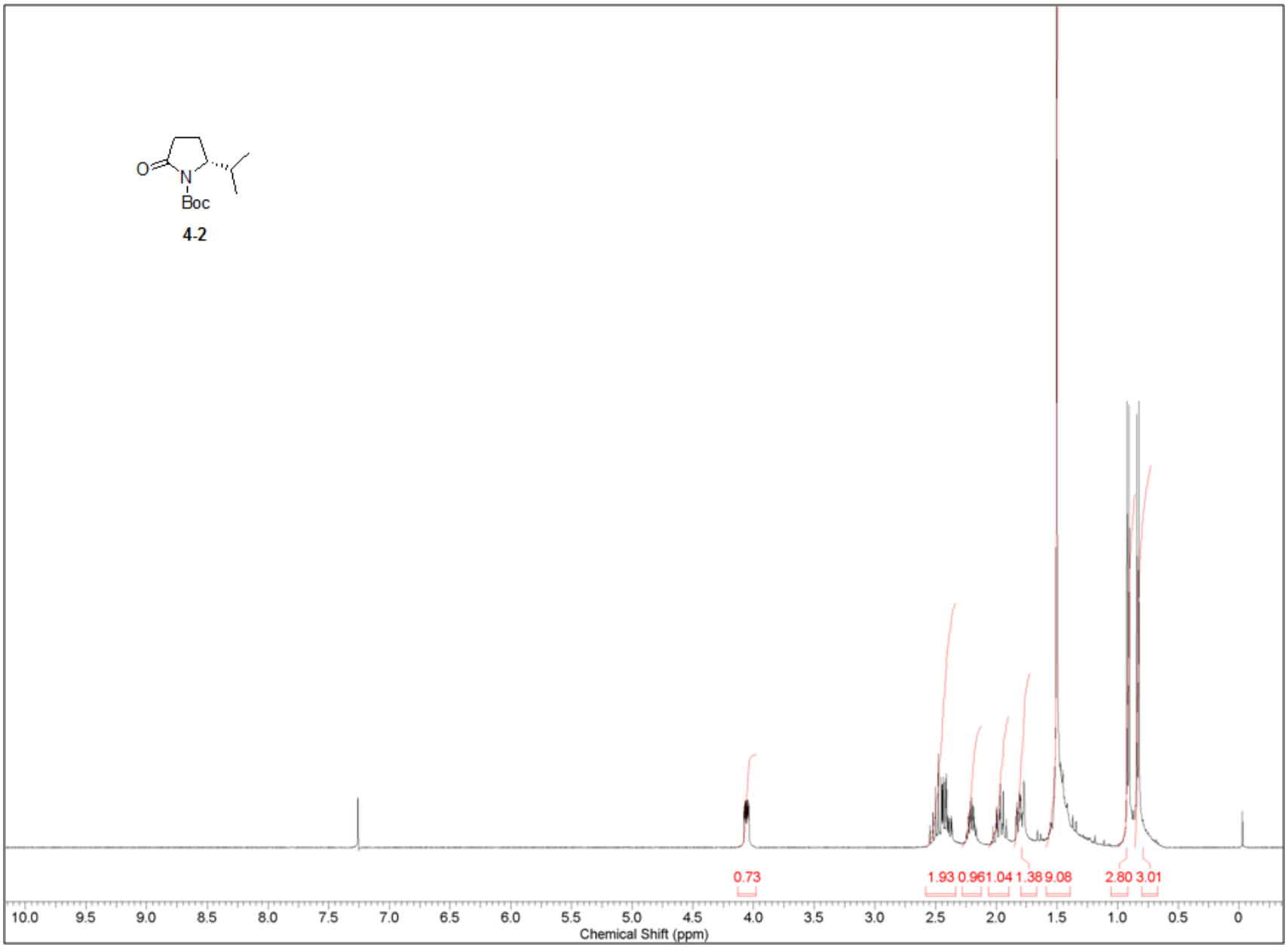
O
N
Boc
4-2
0.73
1.93
0.96
1.04
1.38
9.08
2.80
3.01
10.0
9.5
9.0
8.5
8.0
7.5
7.0
6.5
6.0
5.5
5.0
4.5
4.0
3.5
3.0
2.5
2.0
1.5
1.0
0.5
0
Chemical Shift (ppm)

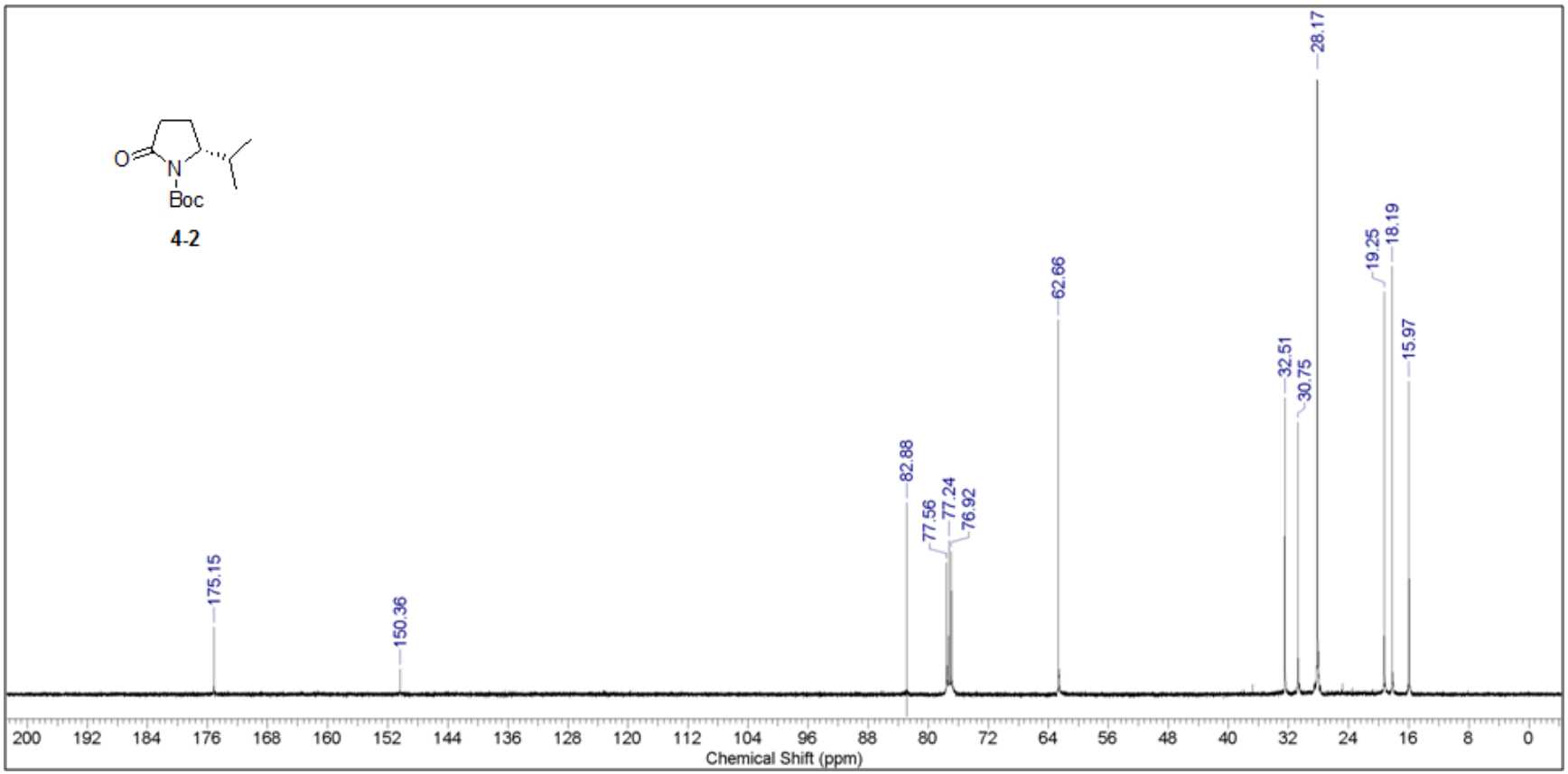
O
N
Boc
4-2
175.15
150.36
82.88
77.56
77.24
76.92
62.66
32.51
30.75
28.17
19.25
18.19
15.97
200 192 184 176 168 160 152 144 136 128 120 112 104 96 88 80 72 64 56 48 40 32 24 16 8 0
Chemical Shift (ppm)

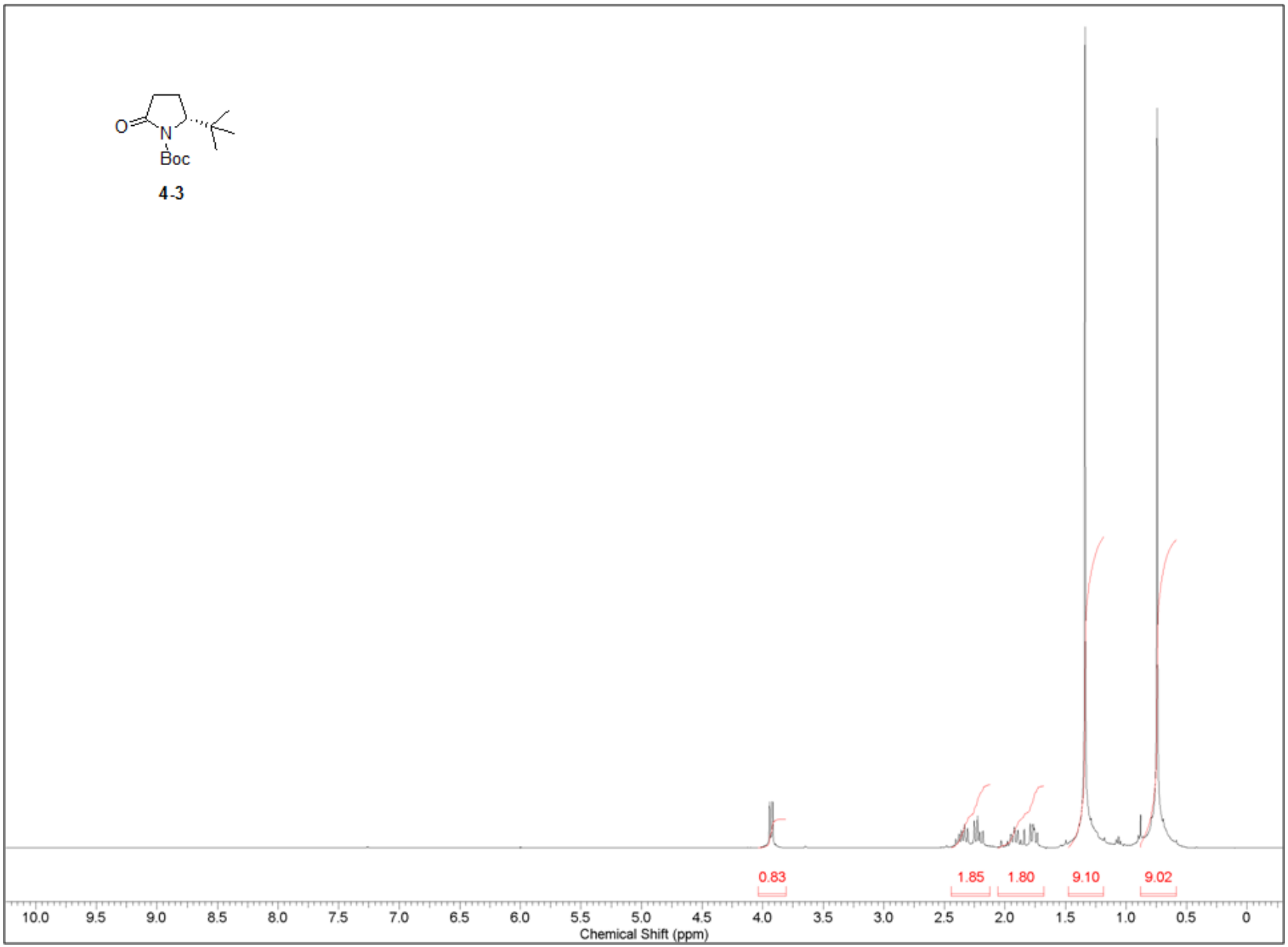
O
N
Boc
4-3
0.83
1.85
1.80
9.10
9.02
10.0
9.5
9.0
8.5
8.0
7.5
7.0
6.5
6.0
5.5
5.0
4.5
4.0
3.5
3.0
2.5
2.0
1.5
1.0
0.5
0
Chemical Shift (ppm)

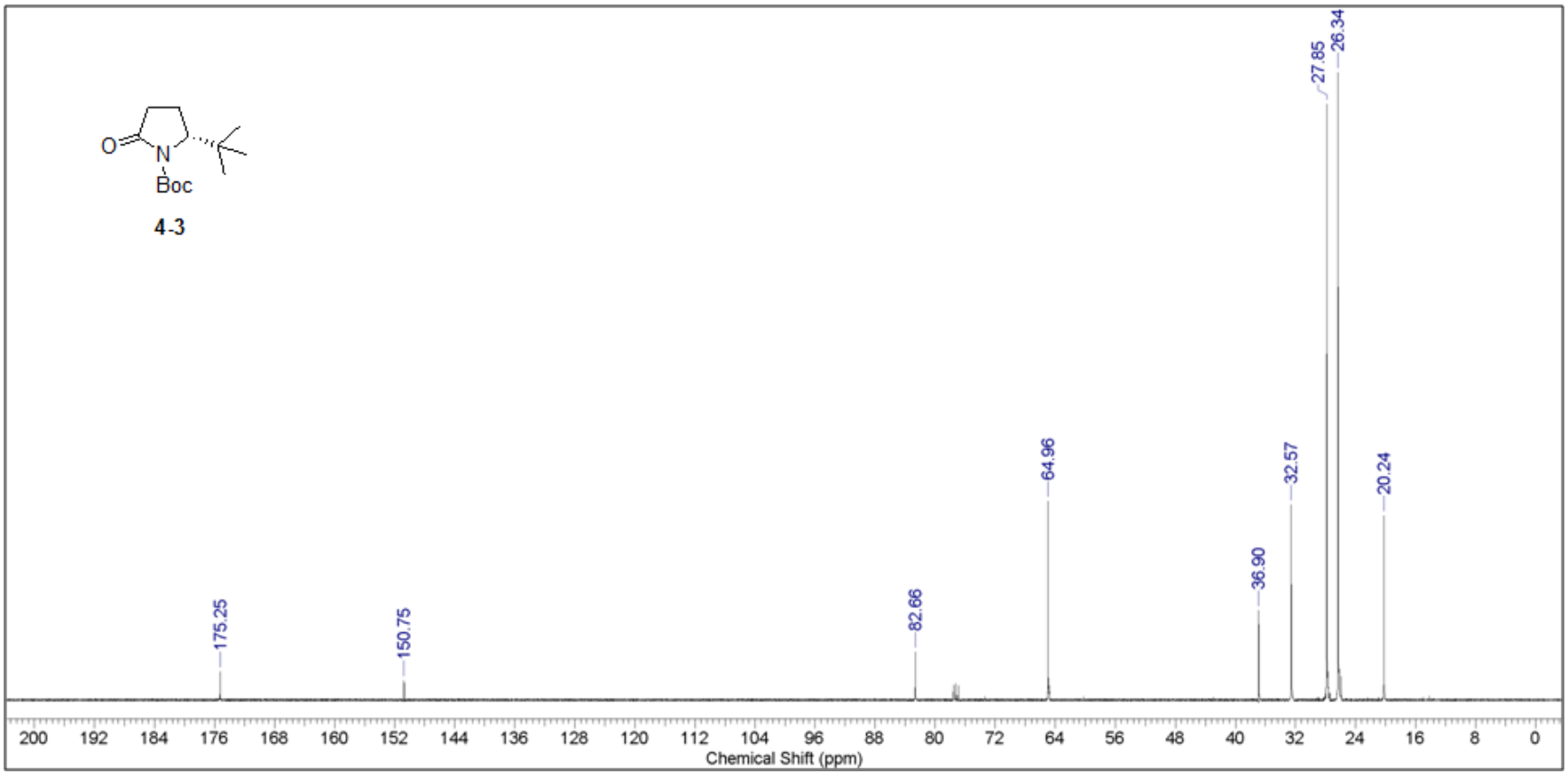
O
N
Boc
4-3
175.25
150.75
82.66
64.96
36.90
32.57
27.85
26.34
20.24
200 192 184 176 168 160 152 144 136 128 120 112 104 96 88 80 72 64 56 48 40 32 24 16 8 0
Chemical Shift (ppm)

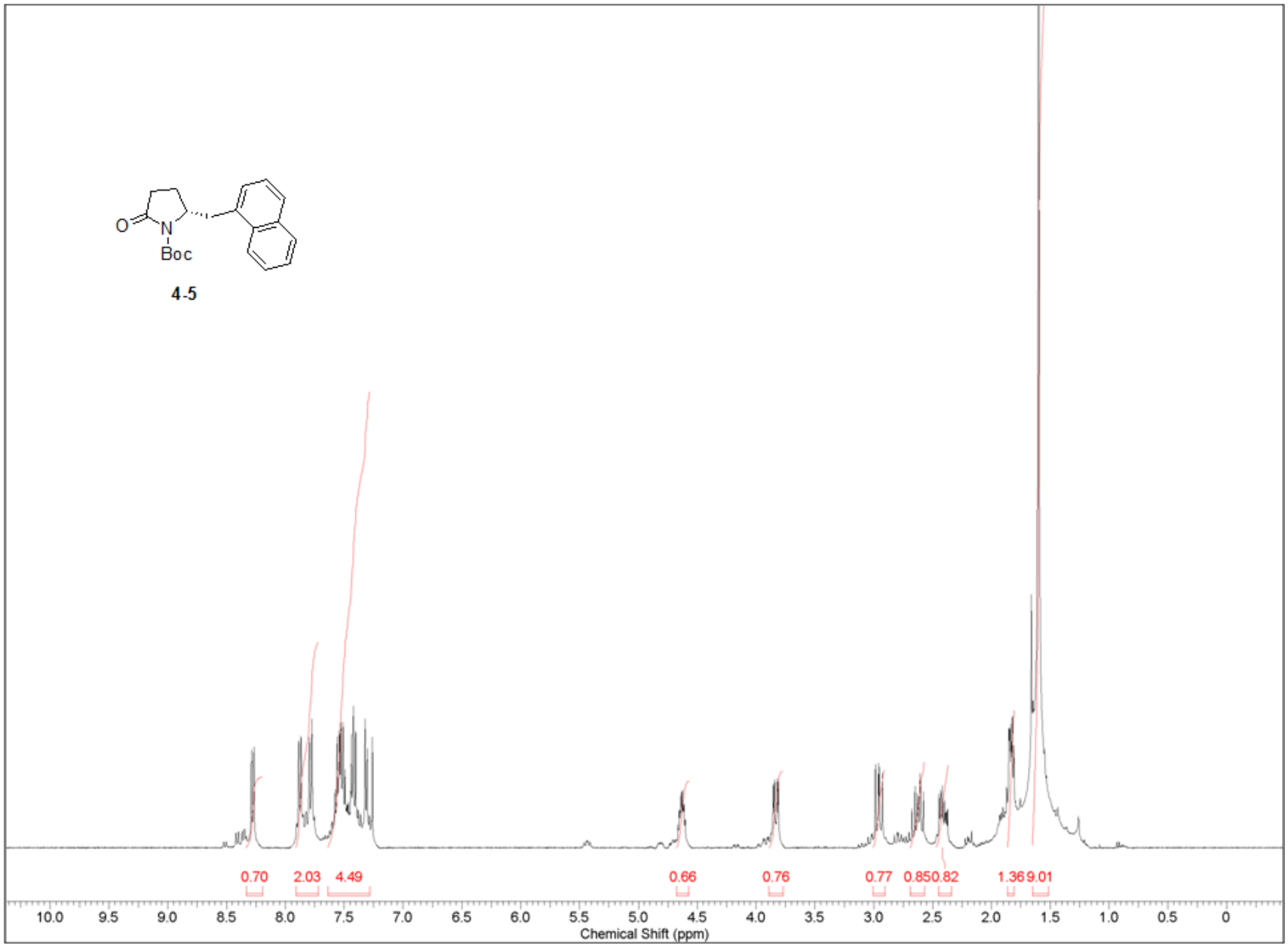
O
N
Boc
4-5
0.70
2.03
4.49
0.66
0.76
0.77
0.85
0.82
1.36
9.01
10.0
9.5
9.0
8.5
8.0
7.5
7.0
6.5
6.0
5.5
5.0
4.5
4.0
3.5
3.0
2.5
2.0
1.5
1.0
0.5
0
Chemical Shift (ppm)

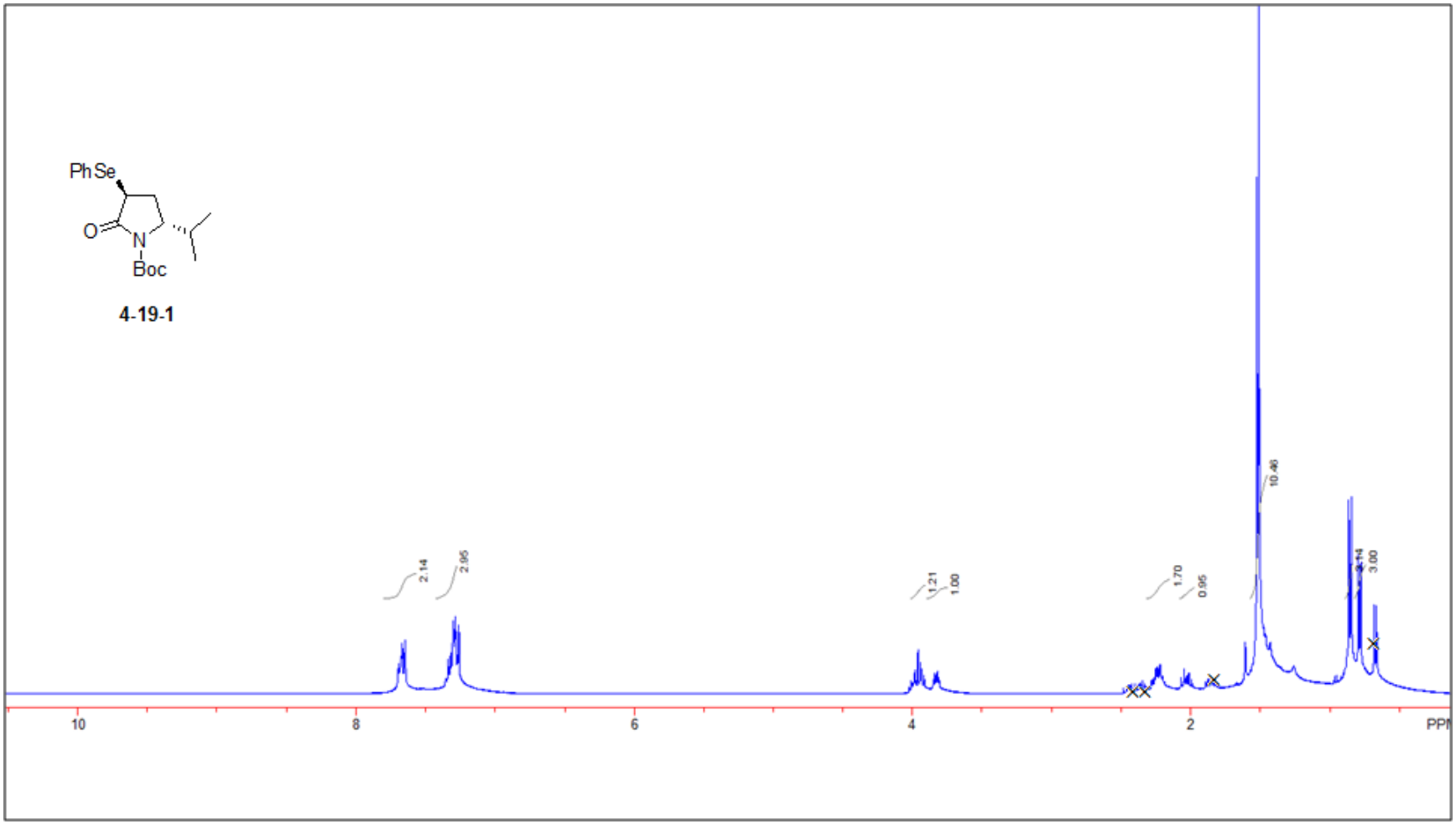
PhSe
O
N
Boc
4-19-1
2.14
2.95
1.21
1.00
1.70
0.95
10.46
3.00
10
8
6
4
2
PPM

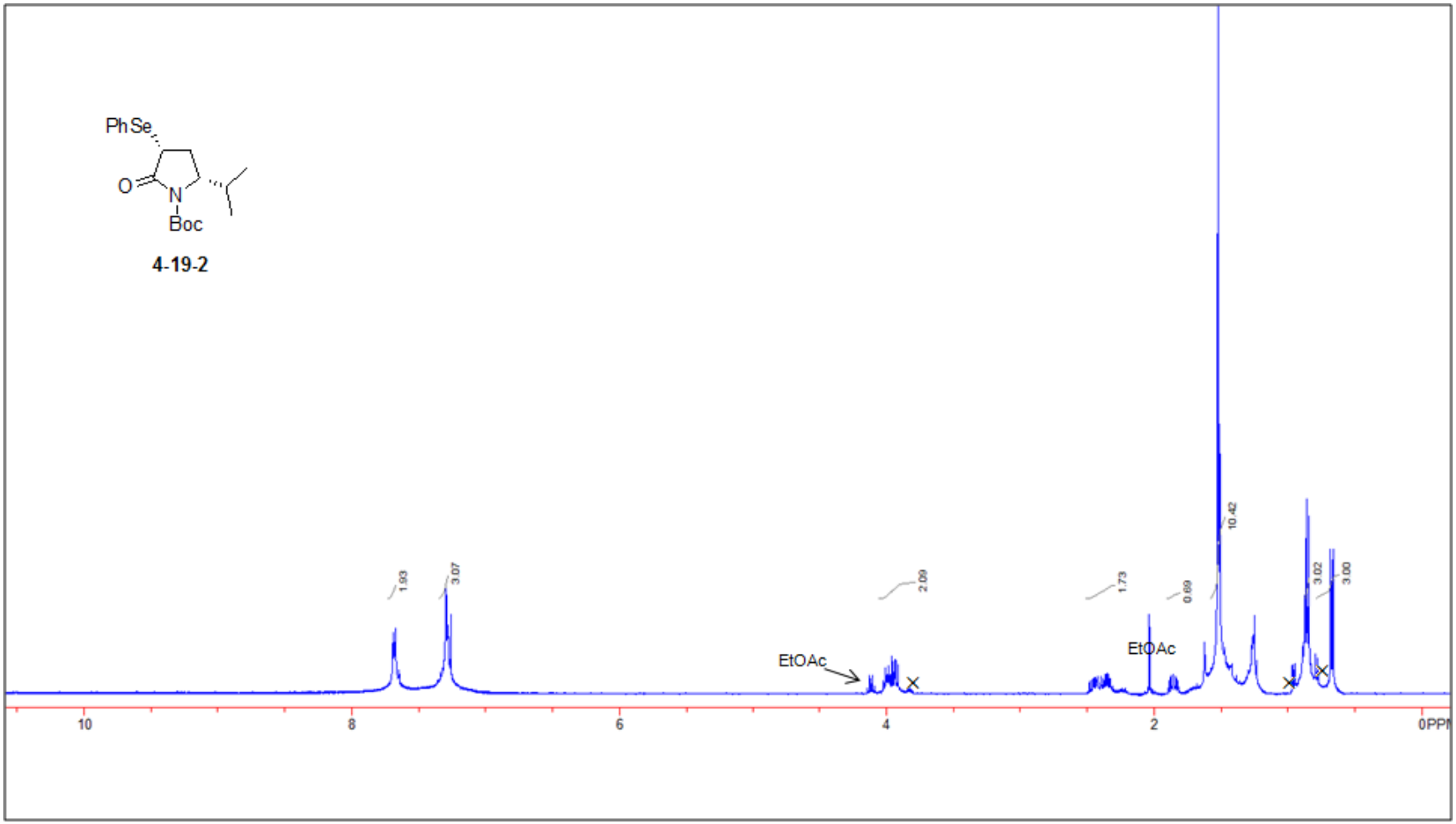
PhSe
O
N
Boc
4-19-2
1.93
3.07
2.09
1.73
0.69
10.42
3.02
3.00
EtOAc
EtOAc
10
8
6
4
2
0PPM

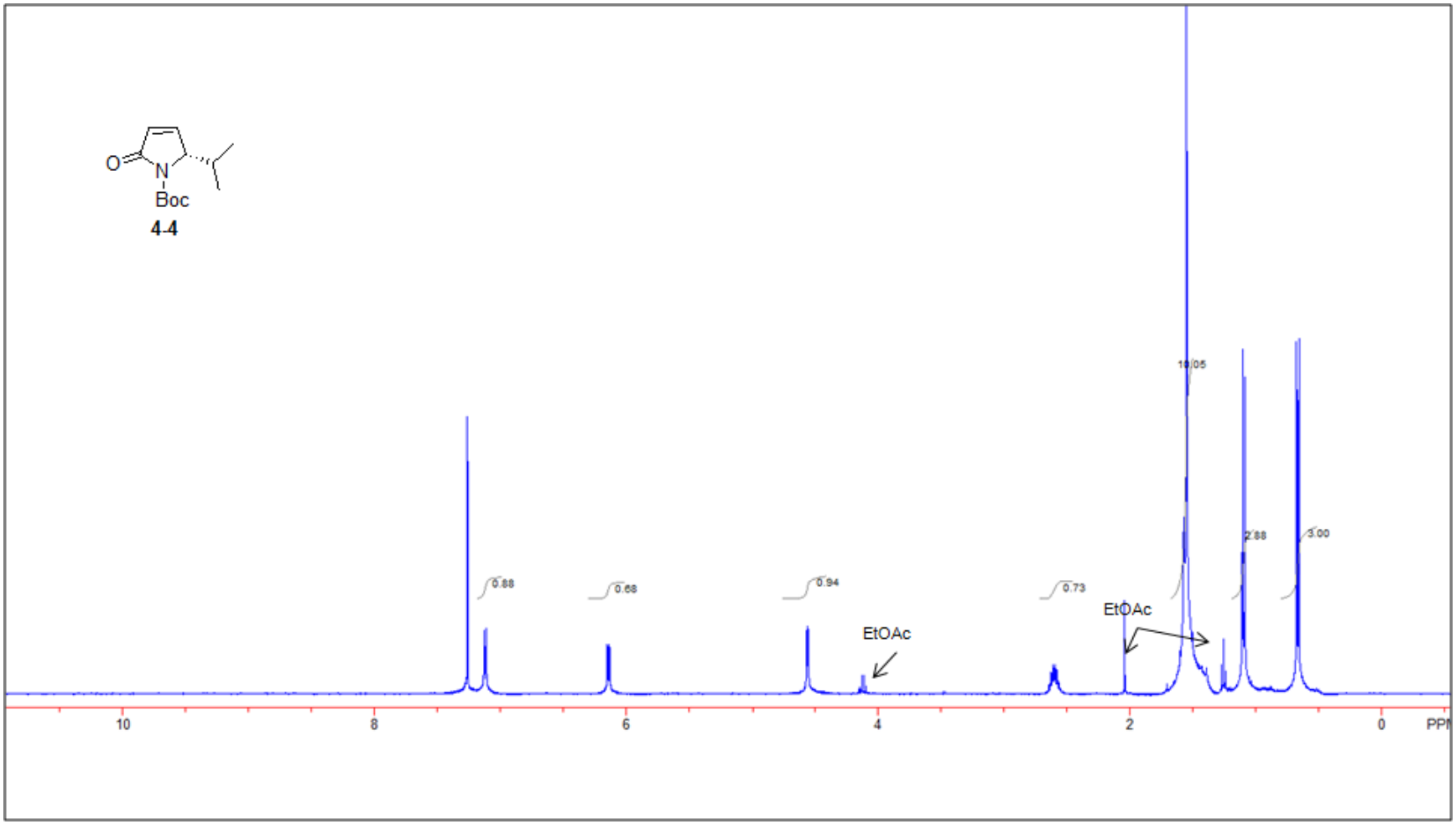
O
N
Boc
4-4
0.88
0.68
0.94
EtOAc
0.73
EtOAc
10.05
2.88
3.00
10
8
6
4
2
0
PPM

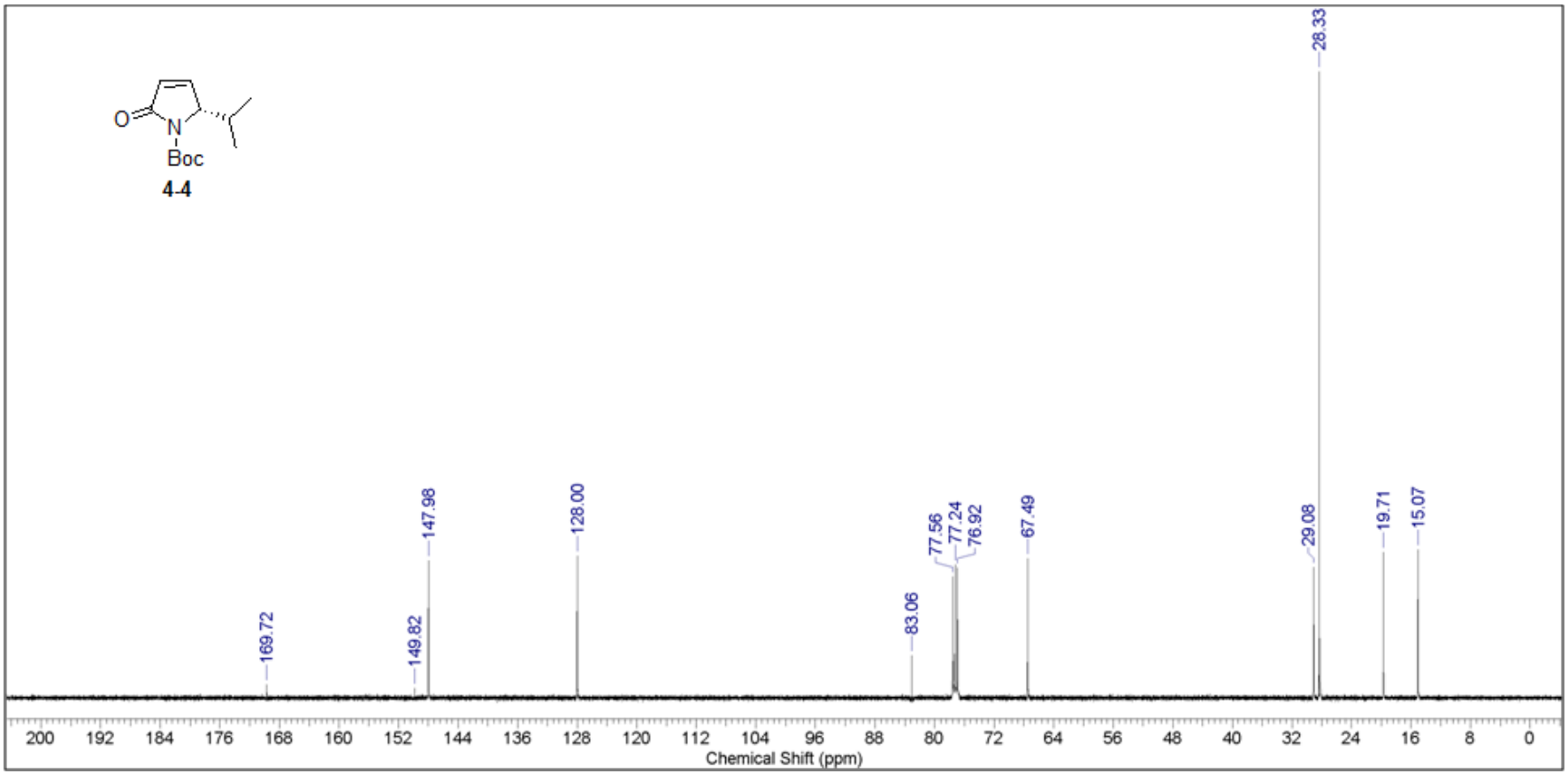
O
N
Boc
4-4
28.33
147.98
128.00
77.56
77.24
76.92
67.49
29.08
19.71
15.07
169.72
149.82
83.06
200 192 184 176 168 160 152 144 136 128 120 112 104 96 88 80 72 64 56 48 40 32 24 16 8 0
Chemical Shift (ppm)

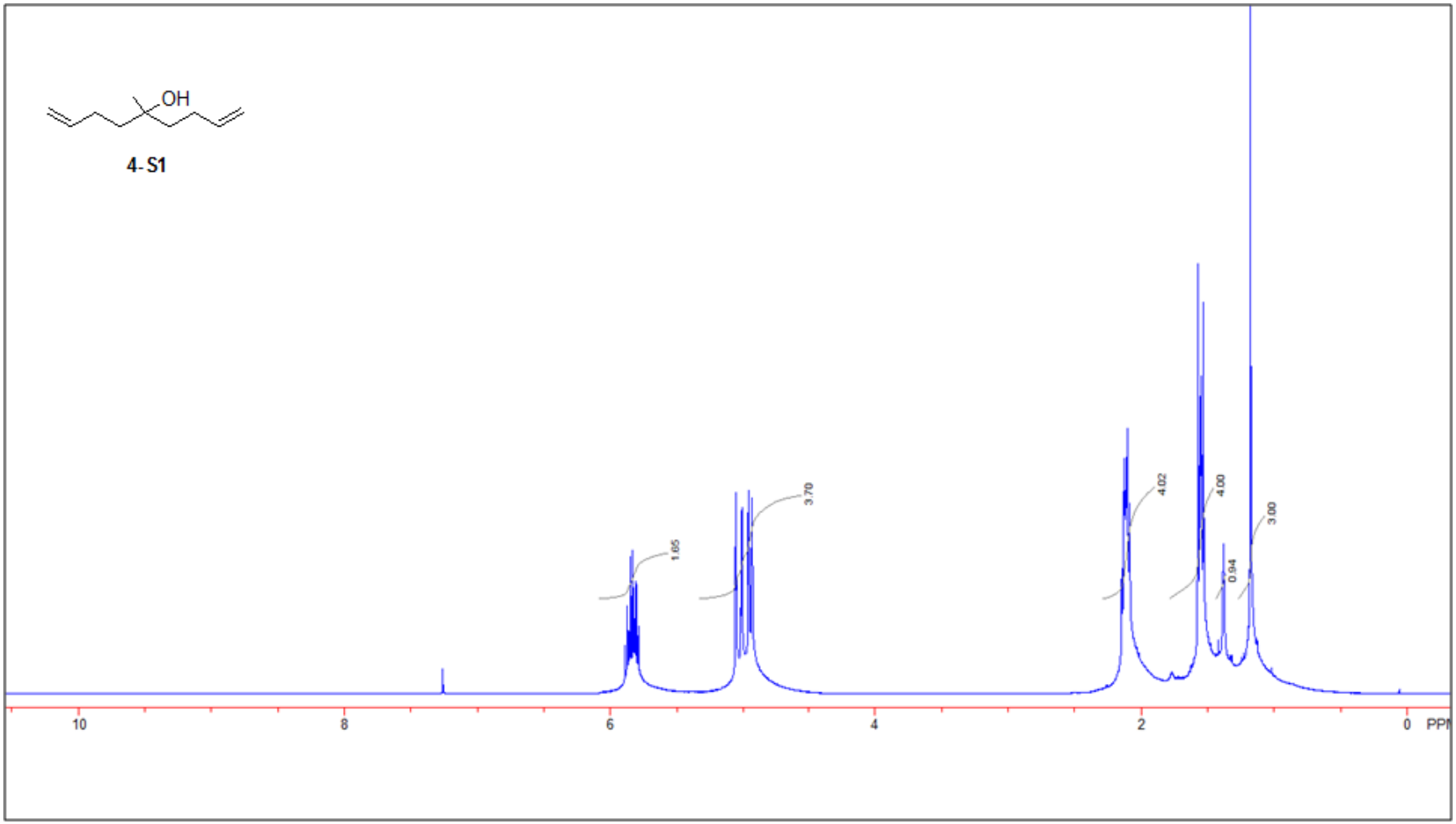
OH
4-S1
1.65
3.70
4.02
4.00
0.94
3.00
10
8
6
4
2
0
PPM

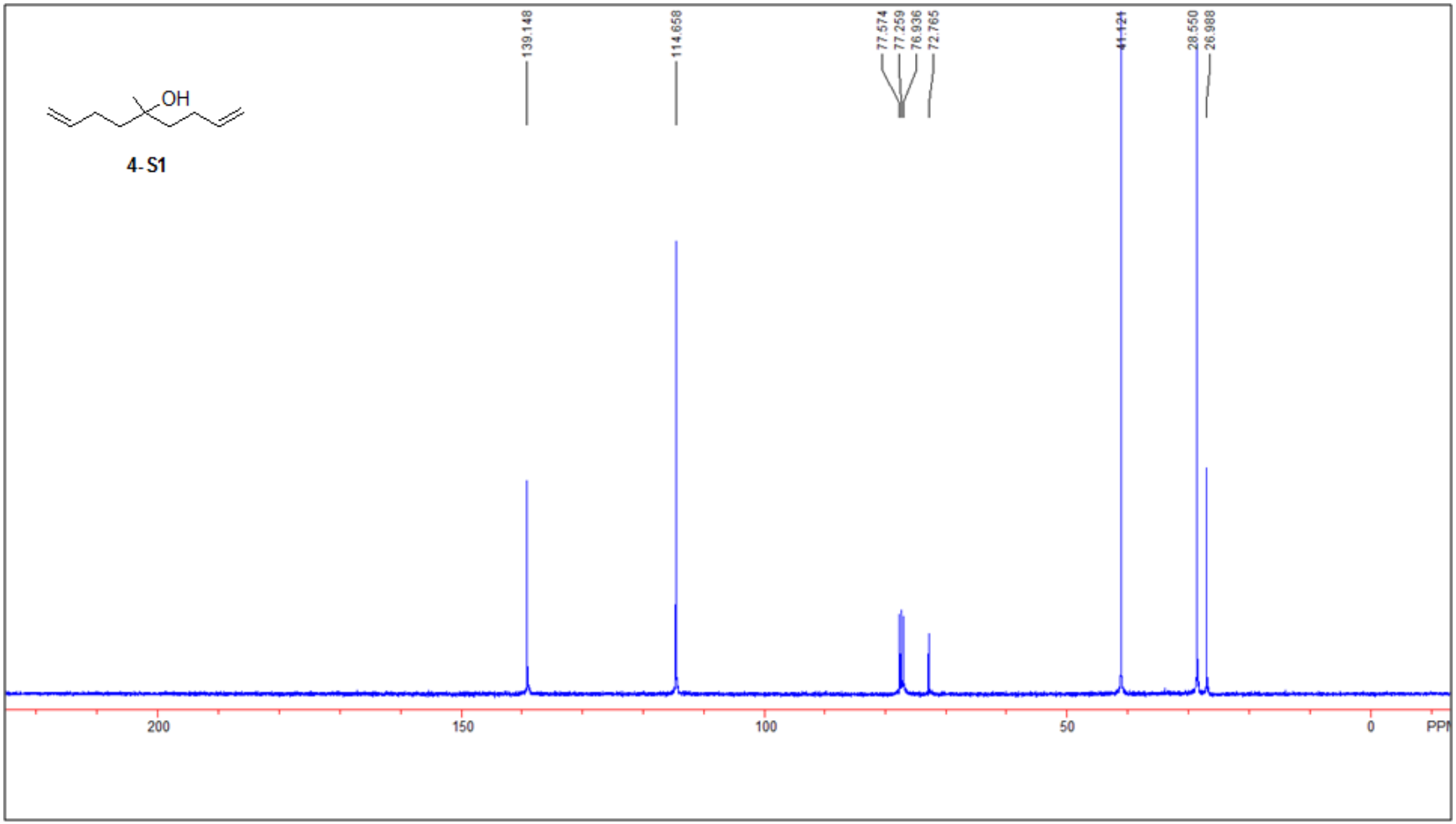
OH
4-S1
139.148
114.658
77.574
77.259
76.936
72.765
41.124
28.550
26.988
200
150
100
50
0
PPM

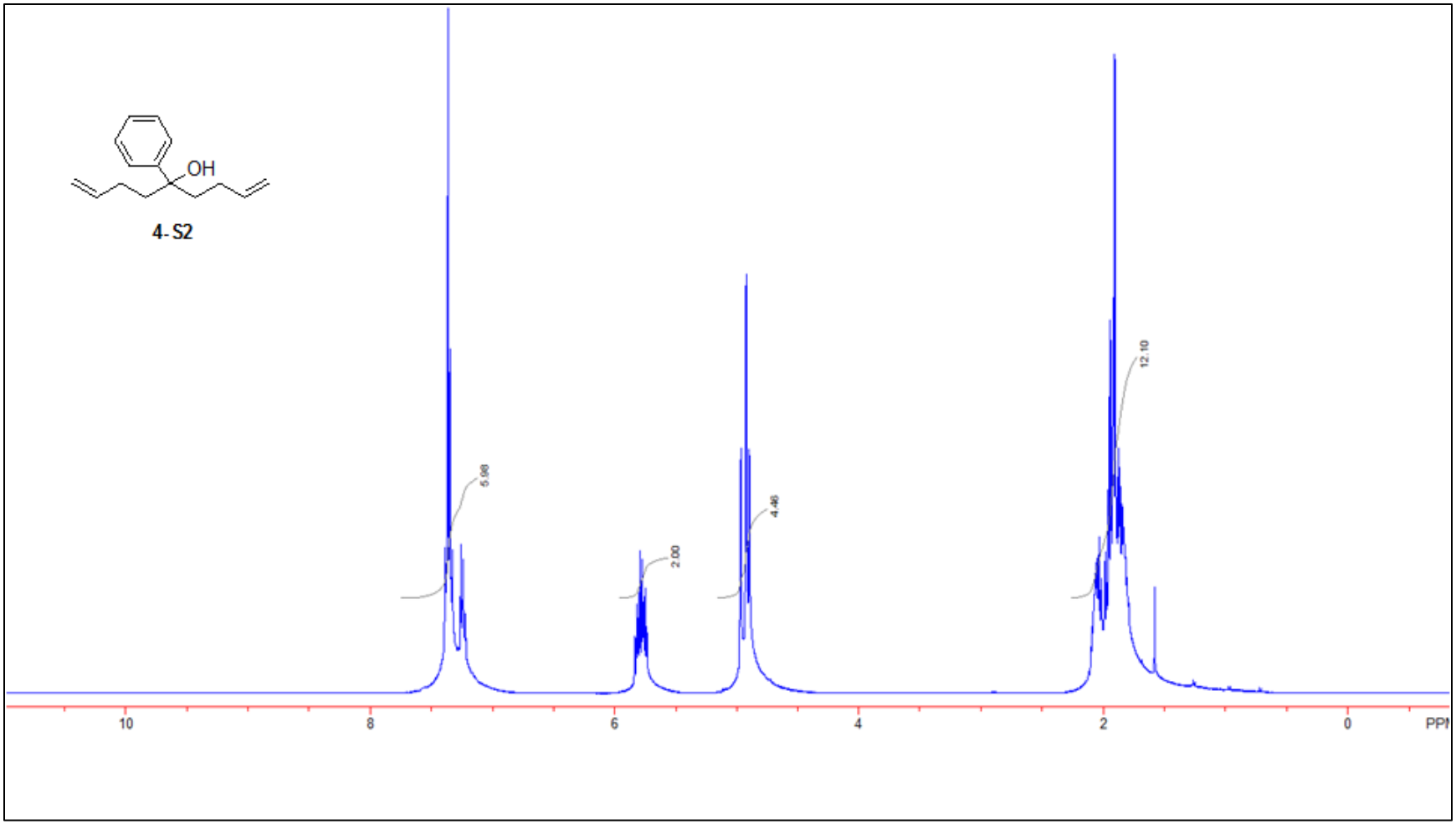
OH
4-S2
5.98
2.00
4.46
12.10
10
8
6
4
2
0
PPM

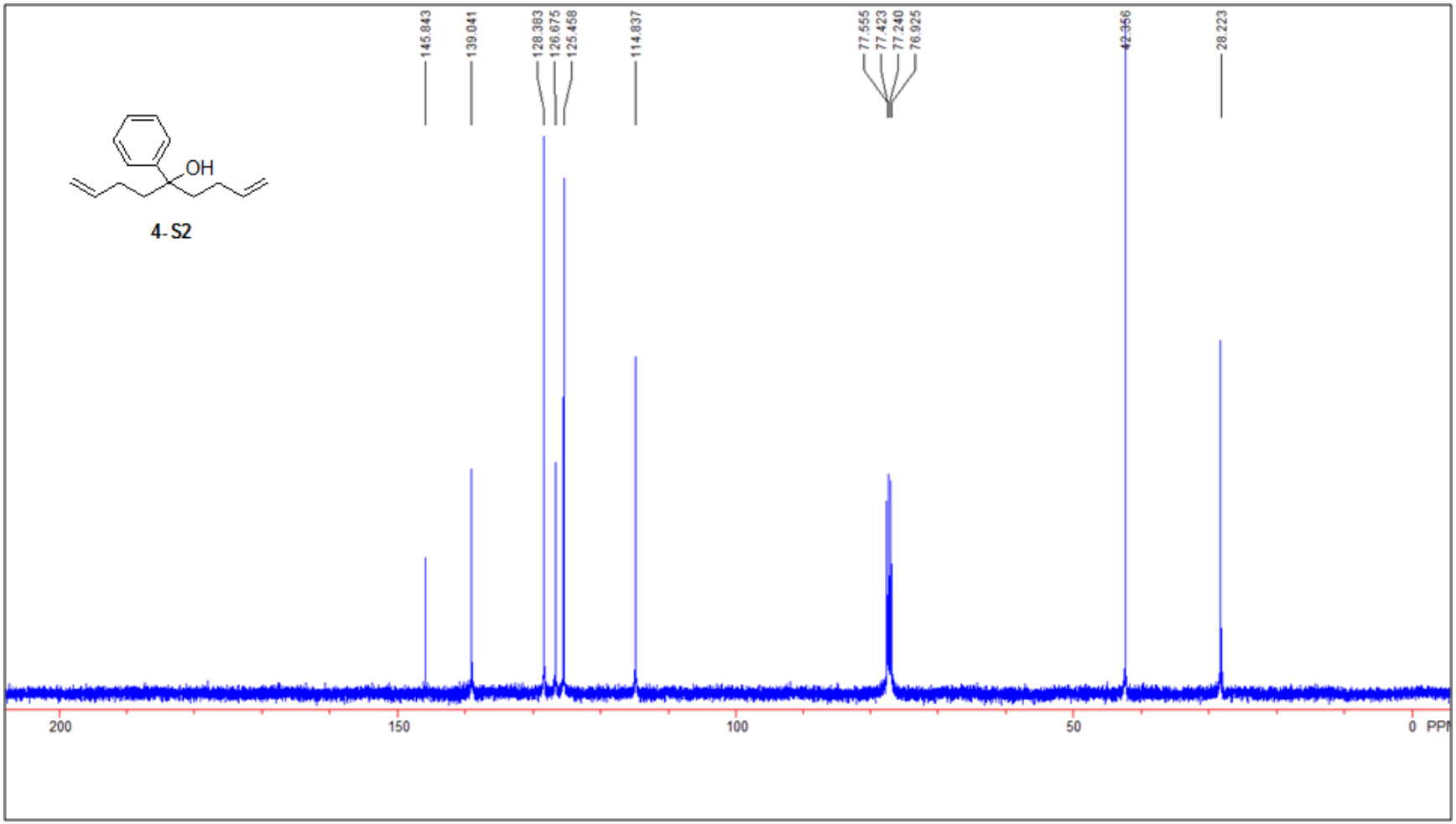
145.843
139.041
128.383
126.675
125.458
114.837
77.555
77.423
77.240
76.925
42.356
28.223
OH
4-S2
200
150
100
50
0 PPM

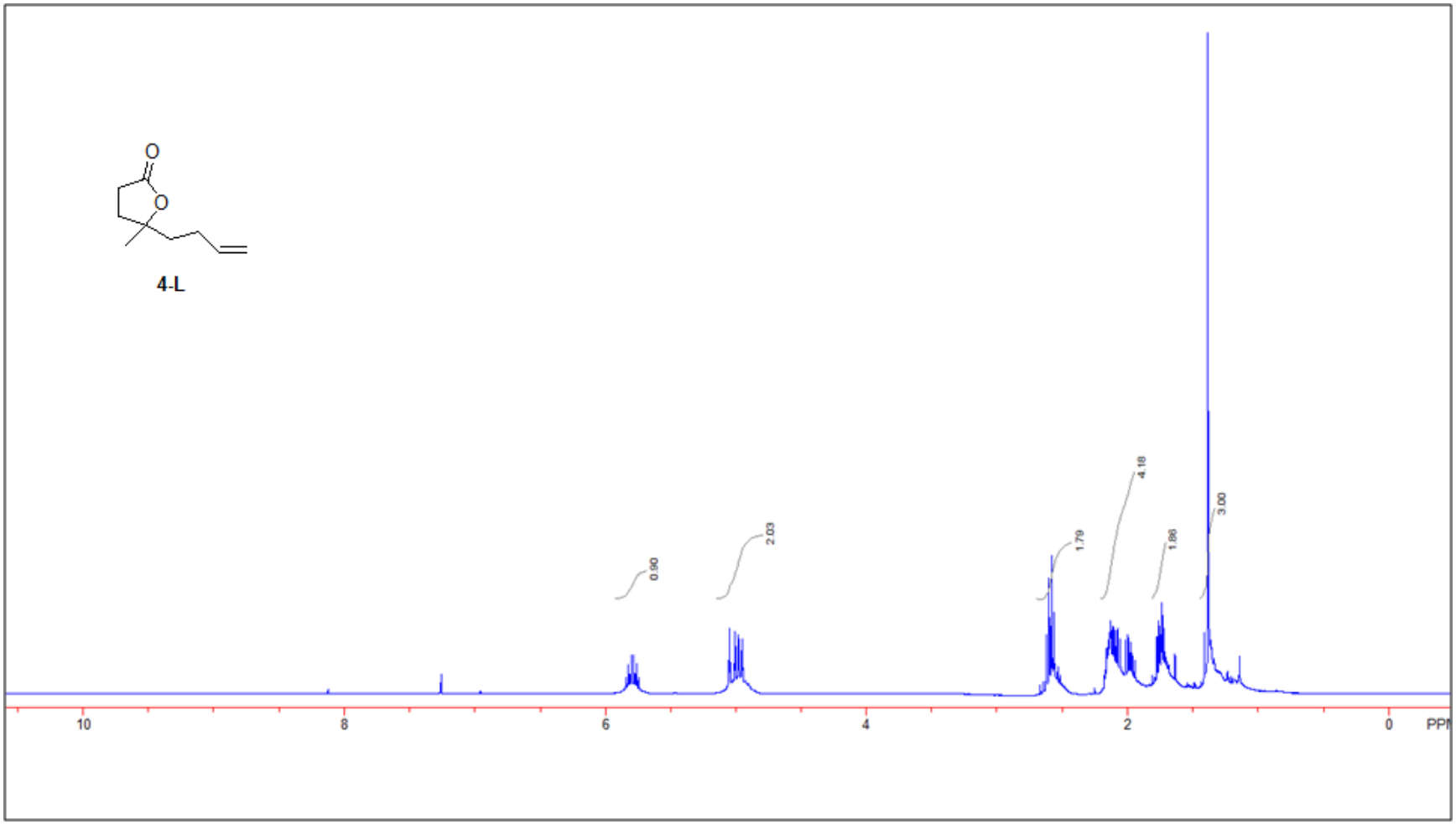
O
O
4-L
0.90
2.03
1.79
4.18
1.86
3.00
10
8
6
4
2
0
PPM

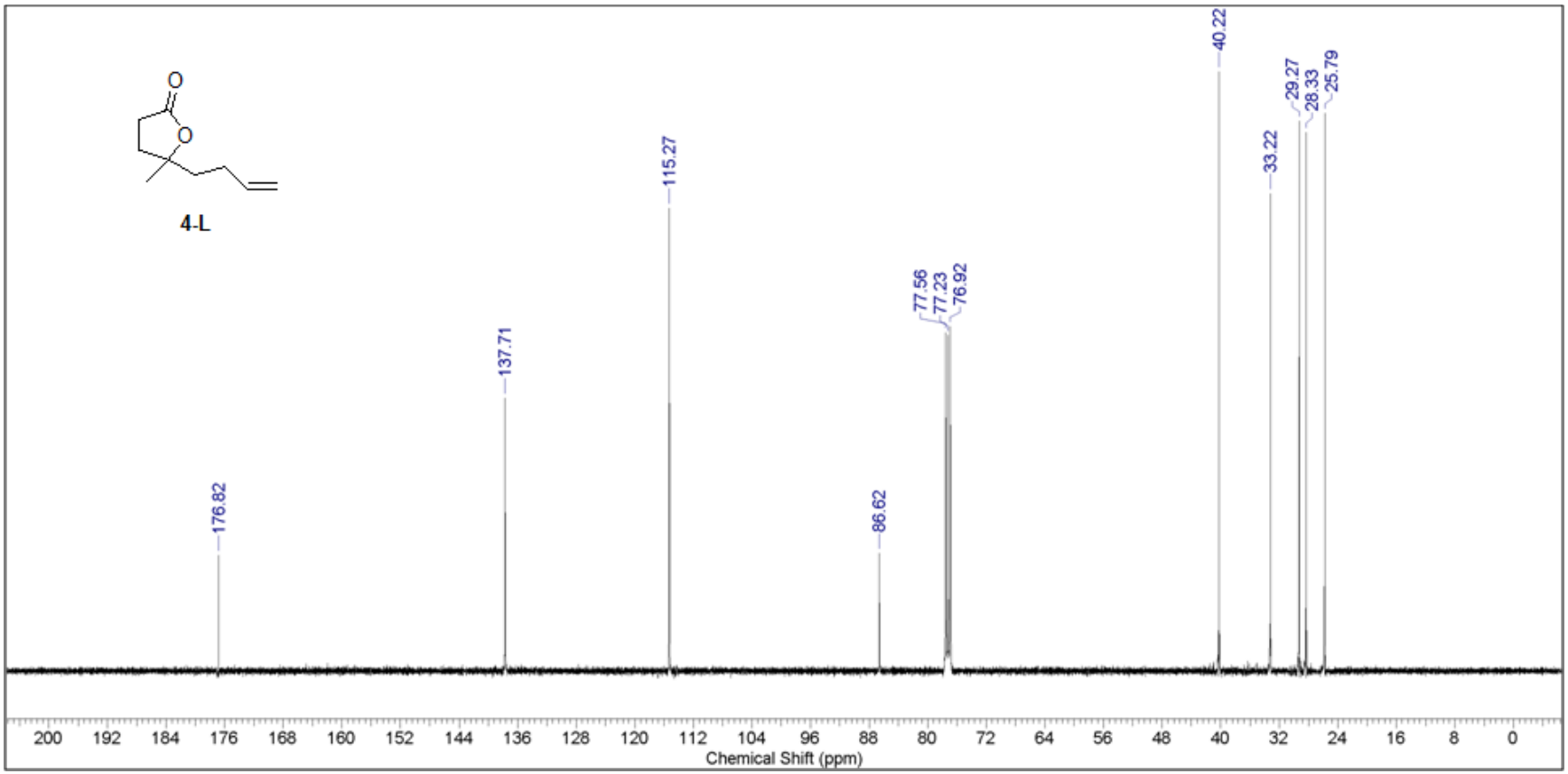
4-L
176.82
137.71
115.27
86.62
77.56
77.23
76.92
40.22
33.22
29.27
28.33
25.79
200 192 184 176 168 160 152 144 136 128 120 112 104 96 88 80 72 64 56 48 40 32 24 16 8 0
Chemical Shift (ppm)

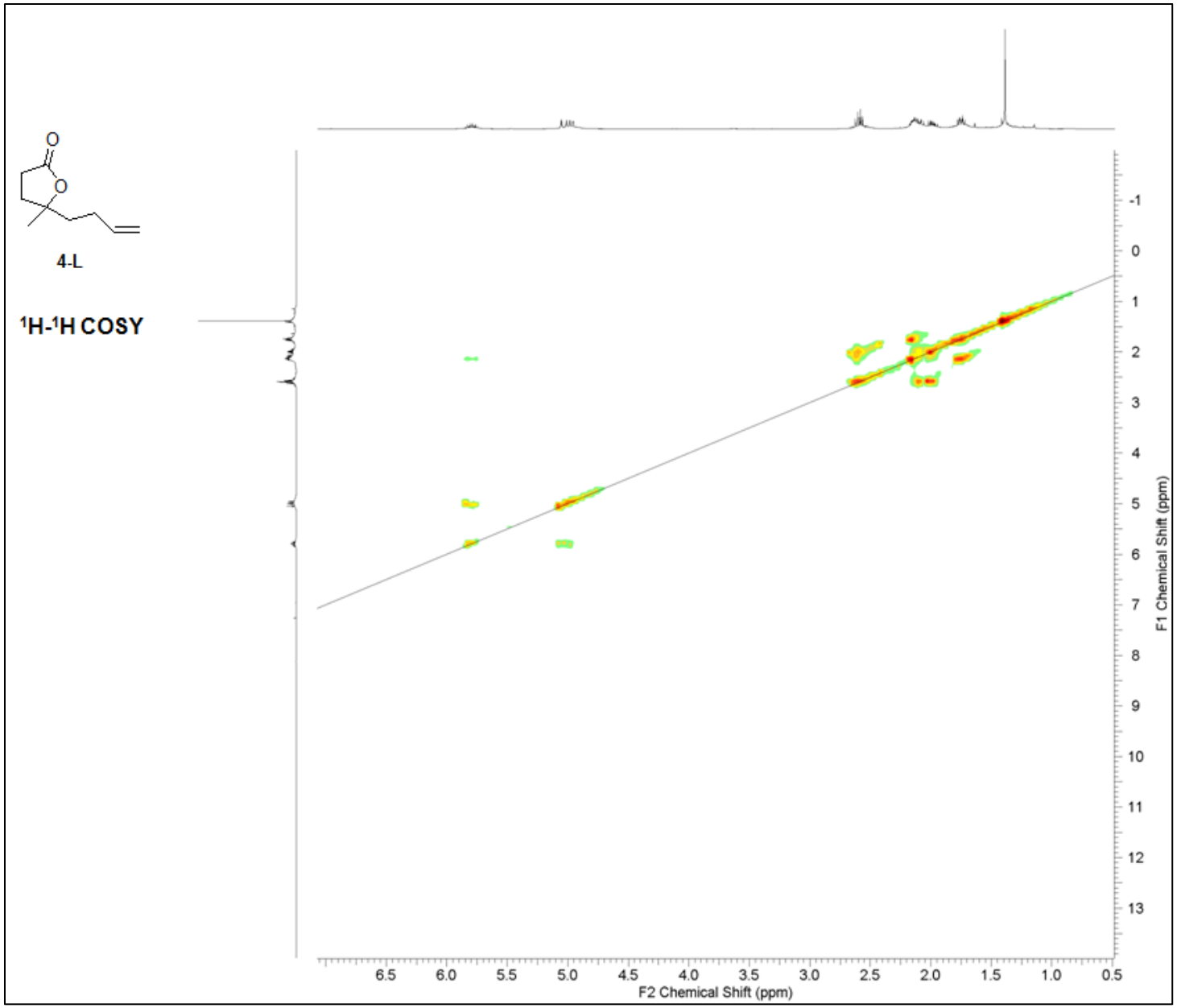
4-L
^{1}H-^{1}H COSY
F2 Chemical Shift (ppm)
F1 Chemical Shift (ppm)